

**INPUT TO STATE STABILIZING CONTROL LYAPUNOV FUNCTIONS FOR
HYBRID SYSTEMS**

A Dissertation
Presented to
The Academic Faculty

By

Shishir Nadubettu Yadukumar Kolathaya

In Partial Fulfillment
of the Requirements for the Degree
Doctor of Philosophy in the
School of Mechanical Engineering

Georgia Institute of Technology

December 2016

INPUT TO STATE STABILIZING CONTROL LYAPUNOV FUNCTIONS FOR HYBRID SYSTEMS

Approved by:

Dr. Aaron D. Ames
School of Mechanical Engineering
Georgia Institute of Technology

Dr. Jonathan Rogers
School of Mechanical Engineering
Georgia Institute of Technology

Dr. Jun Ueda
School of Mechanical Engineering
Georgia Institute of Technology

Dr. Patricio Antonio Vela
School of Electrical and Computer
Engineering
Georgia Institute of Technology

Dr. Magnus B. Egerstedt
School of Electrical and Computer
Engineering
Georgia Institute of Technology

Date Approved: November 04, 2016

He who can listen to music in the midst of noise can achieve great things

Vikram Sarabhai

To my father,

Dr. Yadukumar Nadubettu,

for being a great inspiration throughout my life.

ACKNOWLEDGMENTS

I would like to express my deepest gratitude to my committee chair and mentor, Dr. Aaron D. Ames, for his guidance and support throughout the course of my PhD. The amount of nonlinear control that I have learned from him is equivalent to one undergraduate degree on its own. I am extremely grateful to my committee members Dr. Jonathan Rogers, Dr. Jun Ueda, Dr. Patricio Antonio Vela, Dr. Magnus B. Egerstedt. Special thanks to Dr. Vela for the insightful comments during the one-on-one sessions, and Dr. Egerstedt for the critical feedback in several *GRITS-AMBER* lab meetings. I would like to thank my current and former lab mates Ryan, Matthew, Murali, Huihua, Eric Cousineau, Jordan, Michael, Wen-Loong, Ayonga, Eric Ambrose, Jake and Christian for all the glorious adventures we had together. I would also like to extend my gratitude to GRITS Lab members for the incredible support given to me for my proposal and also my final dissertation defense. Their comments and feedback were invaluable. Thanks should also go to my friends and the department faculty and staff for making my time at the Georgia Institute of Technology a great experience. I would like to acknowledge the support of National Science Foundation who funded my research. Lastly, my sincerest and heartfelt thank you to my entire family for being so supportive of my goals and aspirations and sticking with me all the way. I am deeply indebted to their sacrifices, patience and encouragement throughout my tenure as a PhD student.

TABLE OF CONTENTS

Acknowledgments	v
List of Tables	xii
List of Figures	xv
List of Videos	xvi
List of Abbreviations	xvii
Chapter 1: Introduction	1
1.1 Background	1
1.2 Main Contribution	4
1.3 Brief Outlines of Chapters	6
I Continuous Systems	10
Chapter 2: Preliminaries on Input to State Stability	11
2.1 Input to State Stability	14
2.2 Input to State Stable Lyapunov Functions	17
2.3 Input to State Stability of Affine Control Systems	19
2.4 Input to State Stability of Discrete Time Control Systems	20

Chapter 3: Input to State Stabilizing Control Lyapunov Functions	23
3.1 Control Lyapunov Functions	23
3.2 Input to State Stabilizing Control Lyapunov Functions	24
3.3 Rapidly Exponentially Stabilizing Control Lyapunov Functions	28
3.4 Extension of Artstein's Theorem	31
3.5 Discrete Time Systems	31
II Hybrid Systems	34
Chapter 4: Hybrid Systems	35
4.1 Basic Definition	35
4.2 Stability and Stabilizability of Hybrid Systems	41
4.3 Input to State Stability of Hybrid Systems	44
4.4 Systems with Impulse Effects	49
4.4.1 Exponentially Stabilizing CLFs of the Continuous Dynamics	53
4.4.2 Rapidly Exponential Input to State Stability and Minimum Dwell Time	57
4.4.3 Hybrid Periodic Orbits and Poincaré Maps	60
Chapter 5: Input to State Stabilizing Control Lyapunov Functions and Hybrid Zero Dynamics	65
5.1 Trajectory Tracking Control	65
5.1.1 Outputs	66
5.1.2 Feedback Linearization	67
5.1.3 Feedback Linearization of Time Dependent Outputs	69

5.2	Extension of Artstein’s Theorem	70
5.3	Partially Observable Systems	75
5.3.1	Partial and Full Zero Dynamics	77
5.3.2	Partial and Full Hybrid Zero Dynamics	79
5.4	Formal Results of Stability	84
5.4.1	Aperiodic systems	86
5.4.2	Periodic Systems	90
III	Bipedal Robots	95
Chapter 6:	Hybrid System Model of Bipedal Robots	96
6.1	Robot Model	96
6.1.1	Model of AMBER1	96
6.1.2	Model of AMBER2	103
6.1.3	Model of DURUS Humanoid	108
6.1.4	Model of DURUS-2D	112
6.2	Robot Tracking and Control	113
6.2.1	Computed Torque	114
6.2.2	Feedback Linearization \equiv Computed Torque	116
6.3	ISS-CLFs for Bipedal Walking	117
Chapter 7:	Dynamics of Uncertainty	122
7.1	Linear Feedback Laws	122
7.2	Proportional Voltage Control	126
7.3	Model Based Controllers	130

7.4	Torque Controllers	132
7.5	Parameter Uncertainty	133
7.6	Phase Uncertainty	134
Chapter 8: Parameter Uncertainty to State Stability	136
8.1	Unmodeled Dynamics and State Stability	138
8.2	Parameter Uncertainty Measure	141
8.3	Parameter to State Stability	142
8.4	Hybrid Dynamics	150
8.5	Main Theorem	156
8.6	Simulation Results	161
Chapter 9: Phase Uncertainty to State Stability	164
9.1	State Based vs. Time Based Control Laws	166
9.2	Phase to State Stability	169
9.3	Main Theorem	175
9.4	Simulation and Experimental Results	184
Chapter 10:Aperiodic Systems: Dynamic Dancing	189
10.1	Basic Definitions	189
10.1.1	Pose	189
10.1.2	Dynamic Transition	190
10.2	Single and Double Support Controllers	194
10.3	Configuration Zero Dynamics	197

10.4 Dynamic Robotic Dancing on AMBER2	199
10.5 Results	200
Conclusions and Future Work	202
References	214
Vita	215

LIST OF TABLES

- 6.1 Comparison of maximum recoverable push forces in lateral direction. The ISS based controller can handle greater pushes. Also reducing ε leads to instability due to the constraints on model uncertainty and torque limits. . . 119

LIST OF FIGURES

1.1	Pictorial representation of the classes of controllers that are input-to-state stabilizable. It can be observed that based on [11], all stabilizable affine control systems are input-to-state stabilizable. The blocks are not to scale.	3
1.2	Pictorial representation of a hybrid system with a single continuous and a single discrete event. The continuous event is affine in controls, and the discrete event does not have a control input in this case. This type of hybrid system belongs to a class called <i>systems with impulses</i> . x is the state, u is the control input.	4
1.3	Outline and flow of the thesis.	5
1.4	Progression of the walking controllers used on the robots over the years in AMBER Lab. From left to right: AMBER1, AMBER2, PROXI, DURUS humanoid, and the running robot DURUS-2D.	8
2.1	zero stability is achieved for a zero input, and asymptotic gain is achieved for a bounded input. We use these two important properties to prove input to state stability.	18
3.1	Venn diagram representation of the classes of controllers defined.	30
4.1	Graphical representation of hybrid systems. The edge set \mathbb{E} represents the discrete transitions from one domain to another. It should be noted that the designation of the edges is not restricted by the vertices. For example, e_2 is the edge from v_2 to v_1 .	38
4.2	Figure showing a simple hybrid system with affine controls in the continuous dynamics.	38

4.3	Representation of different possible domains for bipedal robotic dancing of AMBER2: double heel lift, front toe back heel lift, underactuated, front toe lift, front heel lift, flat footed, swing, back heel lift. There are eight possible vertices.	39
5.1	Figure showing a comparison between ES-CLF and RES-CLF. The impacts do not let $V(\eta)$ go to zero, while the ε term in $V_\varepsilon(\eta)$ allows for convergence to zero.	72
5.2	Figure showing the zero dynamics for a single domain, single reset map. The bipedal robot AMBER1 (see Fig. 6.2) will typically have this type of hybrid zero dynamics.	80
5.3	Figure showing a typical periodic orbit (\mathcal{O}) on the partial (full) hybrid zero dynamics. The figure shows a two dimensional partial zero dynamics manifold, which can vary based on the hybrid system chosen.	82
6.1	The biped AMBER1 on the treadmill.	97
6.2	The biped AMBER1 (left) and the stick figure showing the configuration angles (middle) and output constraints (right).	98
6.3	The bipedal robot AMBER2 (left) is constructed with the specific goal of multi-contact behavior as indicated by the design of the feet (right).	104
6.4	Robot configuration (left) and outputs (right).	104
6.5	Showing two domains: back heel lift (BHL) and the swing phase (S) with the two edges.	106
6.6	DURUS robot designed by SRI International.	109
6.7	The spring-legged planar running biped, DURUS-2D.	112
6.8	Hybrid system model for the walking robot DURUS (left) and for the running robot DURUS 2D (right).	114
6.9	Comparisons of the Lyapunov function for various values of $\bar{\varepsilon}$ for push recovery. The push force was 350N. The convergence is quicker for decreasing $\bar{\varepsilon}$. The jumps are due to discrete events (impacts).	119

6.10 Push recovery comparison via the Lyapunov functions for IO (a) and ISS (b) based controllers. $\varepsilon = \bar{\varepsilon} = 0.1$. The convergence rate is preserved for ISS-CLF.	120
6.11 Step over comparison via Lyapunov functions for IO (a) and ISS (b) based controllers. $\varepsilon = \bar{\varepsilon} = 0.1$. The convergence rate is preserved for ISS-CLF . . .	120
6.12 Walking over 5cm step height. Phase portraits for vertical z position of the torso base are shown here. The ISS based controller shows a much smaller deviation.	120
6.13 The top tiles show push recovery and the bottom tiles show stepping onto an unknown disturbance for an ISS controller. Push force of 350N is enforced (second tile) for 0.1s and the reactions are seen in tiles 3 and 4.	121
7.1 Figures showing the output errors going to zero for a zero disturbance. . . .	124
7.2 Figures showing the outputs showing boundedness under a bounded uncertainty.	125
7.3 Figures showing the progression of the outputs for zero disturbance.	126
7.4 Figures showing the progression of the outputs for a bounded disturbance. .	127
7.5 Figures showing the comparison between the voltage inputs obtained in simulation and experiment. The gap is less than 15V.	128
7.6 Figures showing the comparison between the simulated and the experimental joint angles. The maximum difference is close to 0.2rad.	129
8.1 Actual (solid lines) and desired (dashed lines) outputs as a function of time are shown here. Each figure corresponds to an output described to the left of the figures.	162
8.2 The RES-CLF (a), the measure (b) and the torque (c) as a function of time. \dot{V}_ε (slope of V_ε) crosses 0 in every step, but the CLF is still seen to be ultimately bounded. It can also be observed that $\ \nu\ $ increases when the torque inputs are high.	163
8.3 Progression of the measure, RES-CLF from the same initial point for different values of the auxiliary gain $\bar{\varepsilon}$ is shown in the figure. It appears that the ultimate bound decreases with the auxiliary gain $\bar{\varepsilon}$, thereby nullifying the effect of uncertain dynamics.	163

9.1	Figure showing the bound $b = b_\eta + b_z$ on the periodic orbit for a two domain hybrid system. Phase to state stability ensures that a bounded periodic orbit exists under a bounded uncertainty.	178
9.2	Progression of time vs. the phase variable shown for the walking simulation (left) and experiment (right).	185
9.3	Progression of time vs. the phase variable shown for the running simulation (left) and experiment (right).	186
9.4	Phase portraits of the ankle, knee, hip and waist pitch angles of the robot. Both simulation (S) and experimental (E) results are shown.	186
9.5	Limit cycles of simulations (left) and experiment (right), are shown for the running robot DURUS-2D. Both used the time based desired outputs: $y_2^d(t) = y_2^d(\tau(t), \alpha)$	187
9.6	Figure showing the walking tiles of DURUS humanoid for one step. Video link to the experiment is given in [5].	187
9.7	Running tiles of simulation vs experiment for the running robot DURUS-2D. Video link to the experiment is given in [6].	188
10.1	Representation of a meta-dynamical system for bipedal robotic dancing. Each vertex represents the pose, and the edges represent the transitions from one pose to another. This is an example of a nonperiodic hybrid system.	191
10.2	Figures showing the initial pose (left) and the final pose (right) for crouch respectively. The red arrows are the edges.	193
10.3	Tiles of a leg swing behavior consisting of a transition from back heel lift to swing pose. The top tiles illustrate the behavior of the robot achieved in simulation, and the bottom tiles show the same behavior realized experimentally on AMBER2.	194
10.4	Pictorial representation of the results obtained after the implementation of transitions and music synchronization for AMBER2 dancing.	200
10.5	Experimental data comparing the actual and desired angles for a sequence of steps extracted from a part of the dance sequence as realized on AMBER2. The vertical dashed lines indicate end points of the transitions.	201

LIST OF VIDEOS

- [1] *Robustness analysis of DURUS in simulation:*
<https://youtu.be/g5HzXRhcSQ>
- [2] *AMBER Walking:*
<https://youtu.be/SYXWoNU8QUE>
- [3] *AMBER robustness tests:*
<https://youtu.be/RgQ8atV1NW0>
- [4] *Bipedal walking of DURUS in 3D:*
<https://youtu.be/a-R4H8-8074>
- [5] *Bipedal robotic walking of DURUS humanoid:*
<https://youtu.be/5JugZGxZnqg>
- [6] *Bipedal robotic running of DURUS-2D:*
<https://youtu.be/3XQO06kvHFY>
- [7] *Dynamic Robotic Dancing on AMBER2:*
<https://youtu.be/IwR9XvojXWo>

LIST OF ABBREVIATIONS

CLF	control Lyapunov function
ZS	zero stability
AS	asymptotic stability
AG	asymptotic gain
ES	exponential stability
ES-CLF	exponentially stabilizing control Lyapunov function
RES-CLF	rapidly exponentially stabilizing control Lyapunov function
ISS	input-to-state stability
IOS	input-to-output stability
e-ISS	exponential-input-to-state stability
ISSability	input-to-state stabilizability
ISSabilizing ...	input-to-state stabilizing
ISSable	input-to-state stabilizable
ISS-CLF	input-to-state stabilizing control Lyapunov function
e-ISS-CLF	exponential-input-to-state stabilizing control Lyapunov function
Re-ISS-CLF ...	rapidly-exponential-input-to-state stabilizing control Lyapunov function
HZD	hybrid zero dynamics
EOM	equation of motion
DOF	degree of freedom
COM	center of mass
IO	input-output linearization

SUMMARY

The thesis analyzes the input-to-state stability (ISS) properties of control Lyapunov functions (CLFs) that stabilize hybrid systems. Systems that are input-to-state stable tend to be robust to modeling and sensing uncertainties. This dissertation will show that, given the class of control Lyapunov functions (CLFs), a subset of this class of control Lyapunov functions (CLFs) that input-to-state stabilize the given hybrid system, exists. These functions are called the input-to-state stabilizing control Lyapunov functions (ISS-CLFs). As an application, these ISS-CLFs are constructed for bipedal robots, which belong to a special class of hybrid systems: systems with impulsive effects. Bipedal robotic behaviors such as walking, running and dancing are implemented by utilizing variants of input-to-state stabilizing controllers both in simulations and experiments.

Controllers that are functions of the states and the model of the system are highly sensitive to imperfections in real world implementation, which leads to undesirable behaviors. These imperfections are captured by the notion of ISS in a way in which the deviation from the desired output is a function of the deviation from the stabilizing control input. The first step of this thesis is the stabilization of these imperfect nonlinear systems by identifying input-to-state stabilizing CLFs. This study analyzes general control systems and then further analyzes affine control systems. The second step of the thesis is the utilization of these ISS-CLFs in hybrid systems: a sequence of continuous and discrete events. Formulations derived for continuous systems do not always extend to general hybrid systems. The focus of this study, therefore, will shift to a special class of hybrid systems, systems with impulsive effects. This class of hybrid systems naturally model bipedal robots, which consist of high degrees of underactuation and impacts that are not just uncontrollable but also highly nonlinear. Under this class of hybrid systems, CLFs and the corresponding ISS-CLFs will be analyzed theoretically and experimentally. Controllers such as asymptotically stabilizing control Lyapunov functions (AS-CLFs), exponentially stabilizing control

Lyapunov functions (ES-CLFs), and rapidly exponentially stabilizing control Lyapunov functions (RES-CLFs) will be investigated. With these controllers, the ISS analysis will be mainly conducted on two kinds of input uncertainties, parameter and phase, which are frequently observed in bipedal robots. For completeness, this study will also include other uncertainties in a single chapter. The result of this analysis is the construction of input-to-state stabilizing controllers that are indeed robust to a wide array of uncertainties.

For parameter uncertainty, we first derive a nominal CLF-based controller that stabilizes a known model. Then, using the principles of ISS, we combine a computed torque term with a traditional PD term to derive a robust CLF-based controller that stabilizes the uncertain model. The goal of this implementation is to show that the robust CLF-based controller renders the system input-to-state stable with regard to a *measure* input, from which the parameter uncertainty is obtained. If traditional methods yield ultimate boundedness for a bounded parameter uncertainty, the proposed measure establishes *parameter-to-state stability* of the hybrid system, which is demonstrated on the bipedal robot AMBER with a modeling error of 30%, in which the stability of the proposed controller is verified in simulation. In a similar manner, to address the problem of implementing state-based parameterized trajectories on complex robotic systems, we first derive a class of state-based CLFs that render the ideal system stable, and then a class of ISS-CLFs, specifically a class of time+state-based CLFs, and show that the resulting hybrid system is *phase to state stable*. This property is demonstrated experimentally in the form of walking and running in the bipedal robots DURUS and DURUS-2D, respectively.

CHAPTER 1

INTRODUCTION

1.1 Background

Real-world implementations of controllers are always accompanied by imperfections such as input saturation, noisy sensing, inaccurate parameter estimation, and unmodeled disturbances, to name a few. A fitting argument that explains these imperfections/limitations is: *this imperfection does not lie in the system to be stabilized, but in the knowledge that is needed to stabilize*. The gap is in the implementation difficulties of the controller, due to uncertain states and model information. The theory of **input-to-state stability** (ISS) provides an elegant framework for capturing the effect of these imperfections/uncertainties on the control objective. As suggested by the name, the notion of input-to-state stability (ISS) studies the behavior of the output perturbations of a system as a function of the input perturbations.

The fact that *there is no equation in this world that represents a real world system*, is indeed, a profound statement. The whole concept of using *feedback* was born out of the necessity to overcome uncertainties [8]. George Zames and his successors did revolutionary work with regards to stabilization of input/output LTI systems. Some of the methods include H_2 , H_∞ , L_1 [9]. These are famously called as operator theory based approaches. Sontag combined this input/output approach and the Lyapunov based state space stability approach for nonlinear systems, calling it the notion of *input-to-state stability* [10]. Based on the formulations that followed, the idea was to capture all kinds of uncertainties in a unified framework, i.e., viewing the uncertainty as the deviation from a stabilizing control input. Hence, systems are called input-to-state stable (ISS), if a *small* input (perturbation) results in a *small* output (perturbation). With this understanding, it is claimed that systems

that are input-to-state stable tend to be robust to modeling and sensing uncertainties. This shift of focus from obtaining just a stabilizing controller to obtaining an input-to-state stabilizing controller that yields very low perturbations on the states had implications in the field of control theory.

For affine control systems, it is indeed possible to obtain an input-to-state stabilizing control law, given a stabilizing control law (see Fig. 1.1). This is a seminal work by Sontag [11] and has been extended to more complex forms of dynamical systems, namely **hybrid systems** [12, 13]. Hybrid systems are systems that can represent both the continuous and discrete events simultaneously. Large classes of systems can be represented as hybrid systems: systems with impulses, logic commands, continuous-time and discrete-time dynamics, jump phenomena, switching networks, switching power supplies and so on. Informally speaking, a hybrid system is an alternating sequence of continuous and discrete dynamics. Given a stabilizing control law, it is indeed possible to obtain control laws that input-to-state stabilize a hybrid system. [14] proved this result for linear switched systems. [15] proved the result for a general case and also derived Lyapunov functions that characterize *hybrid* input-to-state stability. In fact, [15] showed that under strengthened input-to-state stability conditions, one can show the existence of ISS-Lyapunov functions for hybrid systems.

Realization of stabilizing control laws (stabilizability in short) for hybrid systems has been studied extensively in literature [16]. Some of the problems addressed are finding a common Lyapunov function [17, 18], stability under fast switching [19, 20], stabilization via discrete events [21, 22]. Stabilization via Lyapunov functions, or rather, stabilization via **control Lyapunov functions** (CLFs) was mainly conceived and popularized by Artstein and Sontag [23, 24] during 1980's, and extended to hybrid systems during late 2000's [25]. CLFs enable the use of dynamic programming approaches to obtain optimal inputs in real-time controllers [26]. Some examples include [27, 28, 29]. This was a major step in optimal control theory due to the fact that the CLFs enabled the end user to be able to pick

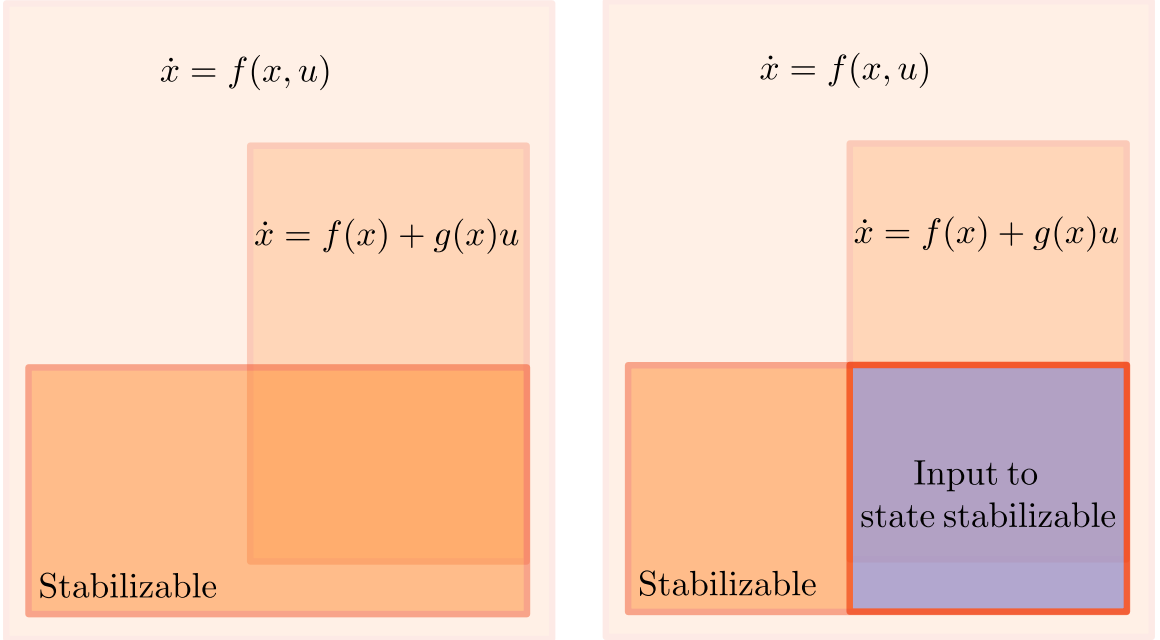


Figure 1.1: Pictorial representation of the classes of controllers that are input-to-state stabilizable. It can be observed that based on [11], all stabilizable affine control systems are input-to-state stabilizable. The blocks are not to scale.

from a choice of stabilizing control inputs. For real-time computations, one can choose a control law that satisfies a CLF based constraint along with other physical constraints such as input saturations, velocity/angle limits and also barrier certificates [30]; the end result being an optimal control strategy to drive the states of the system to the desired values.

As the complexity of the system increases, it is desirable to seek stabilization properties via control Lyapunov functions (CLFs). The complexity can grow in two folds: increase in the order of the system, and, increase in the dynamic behaviors. For example, for bipedal robots, adding more degrees of freedom and also achieving dynamic maneuvers like running add complexity to the control requirements. Implementation of stabilizing controllers gets harder with these systems due to under-actuations and extremely noisy impacts, bringing with itself a larger challenge. Coupled with the fact that as the complexity increases the uncertainty increases, we are presented with practical limitations of implementing a suitable control law. For complex hybrid systems such as these, investigating input-to-state stability (ISS), i.e., studying output perturbations for all kinds of input perturbations seems

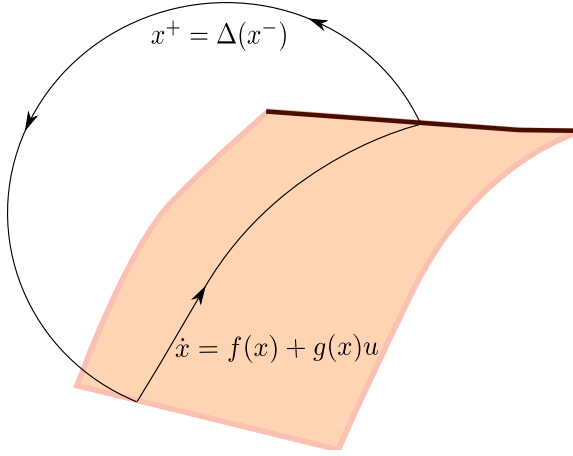


Figure 1.2: Pictorial representation of a hybrid system with a single continuous and a single discrete event. The continuous event is affine in controls, and the discrete event does not have a control input in this case. This type of hybrid system belongs to a class called *systems with impulses*. x is the state, u is the control input.

like an unavoidable task.

1.2 Main Contribution

The main contribution of this thesis is in the construction of a class of control Lyapunov functions (CLFs) that are input-to-state stabilizing. As such, a lot of the controllers examined in the thesis by default satisfy basic ISS properties, a major goal of constructing input-to-state stabilizing CLFs is to squeeze the best out of a given hybrid system. Example systems studied in the thesis are bipedal robots, one of the hardest hybrid system models to stabilize. Dynamics are highly nonlinear and under-actuated, and also undergo uncontrollable discrete transitions (impacts). Therefore, the ultimate objective is to achieve dynamic behaviors such as walking, running, dancing from these systems. It is important to note that bipedal locomotion is an example, while the proofs shown are for all kinds of hybrid systems. Fig. 1.2 is a pictorial representation for a hybrid system with a single continuous and a discrete event.

Through the use of constructions given by Sontag [11], it can be easily shown that, it is indeed possible to find a subset of input-to-state stabilizing CLFs from a given set of CLFs.

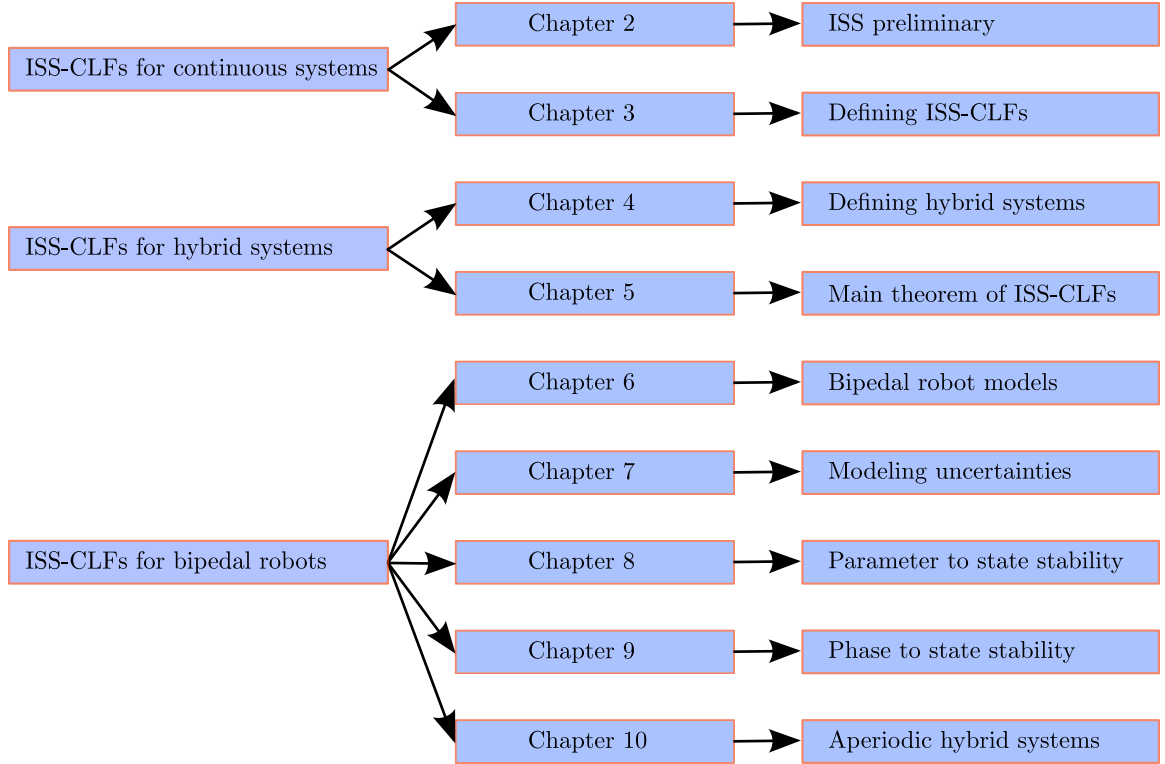


Figure 1.3: Outline and flow of the thesis.

The core advantage is the increase in the number of choices from just one to infinitely many, a necessity for optimal control approaches. This can be extended to hybrid systems, although, satisfying weak assumptions. In other words, for a general hybrid system, existence of a stabilizing controller implies existence of a weak input-to-state stabilizing controller. But, for a class of hybrid systems that contain continuous dynamics affine in controls, and uncontrollable discrete dynamics, strong input-to-state stability conditions can be satisfied. Note that there are conditions such as mean dwell time, rapid exponential convergence, hybrid invariance utilized for stabilizing hybrid systems via only the continuous dynamics. The first two parts of the thesis will focus on constructing ISS-CLFs for both continuous and hybrid systems and also determine conditions for hybrid invariance properties. The third and final part will discuss implementing these robust controllers in bipedal robots to realize walking, running and also dancing. Fig. 1.3 shows the brief outline of the thesis in block diagrams.

1.3 Brief Outlines of Chapters

Chapter 2: Preliminaries on Input-to-State Stability. This chapter contains a brief preliminary on input-to-state stability. It contains basic definitions of stability, exponential stability and other important properties that are required to define ISS and its properties.

Chapter 3: Control Lyapunov Functions. Obtained from the works of Artstein [23] and Sontag [24], this chapter contains the definitions of CLFs and the corresponding ISS-CLFs. It also defines the classes of asymptotically stabilizing control Lyapunov functions (AS-CLFs), exponentially stabilizing control Lyapunov functions (ES-CLFs), and the set of rapidly exponentially stabilizing control Lyapunov functions (RES-CLFs). Correspondingly, this chapter will also define the set of exponential-input-to-state stabilizing control Lyapunov functions (e-ISS-CLFs), rapidly-exponential-input-to-state stabilizing control Lyapunov functions (Re-ISS-CLFs). RES-CLFs and Re-ISS-CLFs are important for the exponential stabilization of hybrid periodic orbits (see [28]).

Chapter 4: Hybrid Systems. This chapter will introduce the definition of hybrid systems and the notion of input-to-state stability for hybrid systems. Informally speaking, hybrid system is an alternating sequence of continuous and discrete events. Category theory is used for the definition [12]. A wide variety of classes of hybrid systems can be described in this manner such as mechanical systems, networked control systems, switching power systems, embedded systems and so on.

Chapter 5: Input-to-State Stabilizing Control Lyapunov Functions and Hybrid Zero Dynamics. This chapter will construct CLF based controllers for the hybrid system models defined in Chapter 4. If trajectory tracking is involved, then output dynamics are computed for stability analysis. For bipedal robots, since some of the joints are not necessarily actuated, the notion of zero dynamics and partial zero dynamics are studied. In fact, it will be shown that the output coordinates and the zero coordinates form the transformed states-

pace for the original system. Therefore, the original statespace can be transformed into the corresponding transverse and zero coordinates via a diffeomorphism. This is an important step leading to analysis of stability of partially observable/controllable continuous dynamics of the hybrid systems. In fact, this chapter ends with Theorems 3 and 4, which use the property of exponential stabilizability of the continuous dynamics to realize exponential-input-to-state stabilizing control Lyapunov functions that input-to-state stabilize the entire hybrid system.

Chapter 6: Hybrid System Model of Bipedal Robots. This chapter will describe the hybrid system models for specific cases of bipedal robots such as AMBER1, AMBER2, DURUS, DURUS-2D. The main goal is to identify relative degree, under-actuations, outputs and also inputs for these systems. The objective is not just to drive the states of these robots to zero. Some applications require trajectory tracking of outputs (functions of the states), and the resulting output dynamics need to be investigated.

Chapter 7: Dynamics of Uncertainty. This chapter will describe how to model uncertainties and analyze the stability properties of the resulting uncertain system. A detailed list of controllers used is given in Fig. 1.4. ISS properties are shown for even traditional controllers like PD in this chapter. The kinds of uncertainties discussed are modeling, voltage inputs, unknown Coriolis-centrifugal effects and gravity effects. Two specific kinds of uncertainties, parameter and phase, will be picked and discussed in Chapters 8 and 9 and different variants of ISS-CLFs will be developed. Details of these two chapters are given next.

Chapter 8: Parameter Uncertainty to State Stability. This chapter will show that CLFs with a model mismatch can be shown to be parameter-to-state stable for the nonlinear hybrid system model of a robotic system undergoing impacts. In other words, despite the differences in the model, the model based CLF based controller will still yield a bounded output error for a bounded function of parameter uncertainty. To establish this fact, a

AMBER1	AMBER2	PROXI	DURUS	DURUS-2D
P Voltage Control	PD current control	PD current control	PD current control+Regulators, Time based parameterization	PD current control, Time+state based parameterization
2011	2013	2014	2015	2016

Figure 1.4: Progression of the walking controllers used on the robots over the years in AMBER Lab. From left to right: AMBER1, AMBER2, PROXI, DURUS humanoid, and the running robot DURUS-2D.

measure for parameter uncertainty for both the continuous and discrete map will be defined. This will be illustrated through the examination of a representative robotic system: the bipedal robot AMBER1 (shown in Fig. 6.1). There are other approaches like [31] that use control Lyapunov functions to achieve exponential convergence to zero under bounded uncertainty. Our objective is the same, i.e., utilize control Lyapunov functions to obtain exponential convergence, but, to an ultimate bound (in other words, convergence to small acceptable tracking errors). This formal construction helps in obtaining controllers that are not only highly convergent, but also robust to the model mismatch, getting the best from the two worlds. It will be shown with a CLF based controller, computed torque+PD, resulting in a stable walking gait for the robot in simulation.

Chapter 9: Phase Uncertainty to State Stability. Bipedal robotic walking (or running), at a fundamental level, uses a set of reference trajectories (gaits) that are modulated (parameterized) by a *phase* variable. The phase variable is usually a monotonic function of the configuration of the robot. Suitable candidates are calf angle, hip position that propagate

forward in time. The state dependency of the modulation of the desired trajectories forms the basis for realizing stable walking that show reactive behavior to pushing or pulling. As the complexity of the robot increases (in terms of both DOF and dynamic behaviors), the state dependency of the controller becomes more of a curse to the stability of the robot. Therefore, the goal of this chapter is to study phase based uncertainties of the system, and realize robust controllers via CLFs. Accordingly, controllers that rely on time instead of the phase are realized for smoother modulation. The end result is the construction of time dependent CLFs and the corresponding time dependent ISS-CLFs. Importantly, these results are verified both in simulation and experimentally on the walking robot DURUS and on the running robot DURUS-2D (left and right in Fig. 6.7 respectively).

Chapter 10: Aperiodic Systems: Dynamic Dancing. In this chapter, which is the final chapter, we will analyze input-to-state stability properties of aperiodic hybrid systems. The example picked is dynamic dancing of AMBER2. We will show that different dynamic behaviors can be combined together to form a meta-hybrid system. Again, the stability of this meta-hybrid system is ensured via the use of controllers that are input-to-state stable.

Part I

Continuous Systems

CHAPTER 2

PRELIMINARIES ON INPUT TO STATE STABILITY

In this chapter we will introduce basic definitions and results related to input to state stability (ISS) (henceforth, hyphen removed from *input-to-state*) for a general nonlinear system and then focus on robotic systems for experimental results; see [10] for a detailed survey on ISS. Most of the content here is taken from [11, 32, 33, 34, 35, 36]. A general nonlinear system with outputs is represented in the following fashion:

$$\dot{x} = f(x, u), \quad (2.1)$$

with x taking values in Euclidean space \mathbb{R}^n , the input $u \in \mathbb{R}^m$ for some positive integers n, m . We can also define the set of outputs $y : \mathbb{R}^n \rightarrow \mathbb{R}^k$ for some positive integer k . The mapping $f : \mathbb{R}^n \times \mathbb{R}^m \rightarrow \mathbb{R}^n$ is smooth and $f(0, 0) = 0$. We can define a set of outputs $y : \mathbb{R}^n \rightarrow \mathbb{R}^k$ that is continuous with $y(0) = 0$. We use a feedback control law

$$u = k(x), \quad k(0) = 0, \quad (2.2)$$

that makes the closed loop system

$$\dot{x} = f(x, k(x)) =: f^{cl}(x), \quad (2.3)$$

globally asymptotically stable about $x = 0$. We say that a controller, $k(x)$, is stabilizing if it makes the closed loop system (2.3) globally asymptotically stable. There are many variants of this general problem, which differ on the degree of smoothness required of k , as well as on the structure assumed of the original system. This type of problem is called a state space stabilization problem. We make a blanket assumption that f is smooth. We

can also use weaker conditions like Lipschitz continuity of f w.r.t. x and u . In fact, a large part of the proofs covered in the thesis uses this assumption. Mathematically, the notion of input/output stability arises from the need to find a feedback (2.2) with the property that the new control system

$$\dot{x} = f(x, k(x) + d), \quad (2.4)$$

be *input to state stable*. In essence, what is desired is that when the external perturbation input d in (2.4) is identically zero, the system (2.3) be globally asymptotically stable about $x = 0$ (so, this includes state-space stability) and that, in addition, a *nice* input $d \neq 0$ should produce a *nice* state trajectory $x(t)$ when starting at any initial state $x(0)$. We call this type of question an input/output stabilization problem. For partial observations of interest, we can be more precise about the stabilization of the states by referring to it as input d to state x stabilization problem.

It is a well known fact that the feedback control law $k(x)$ that achieves state-space stabilization does not necessarily produce input/output stabilization. Classes of systems that satisfy this property are of interest to us. We will state some basic definitions here. The field \mathbb{R} is the set of real numbers, \mathbb{R}^n denotes n dimensional Euclidean space, $\mathbb{R}_{\geq 0}$ denotes nonnegative real numbers. \mathbb{N} is the set of natural numbers, and \mathbb{N}_0 denotes the set of nonnegative integers, i.e., $\{0, 1, 2, \dots\}$. The vectors $y_1 \in \mathbb{R}^{k_1}, y_2 \in \mathbb{R}^{k_2}$, when combined together into one vector are denoted by $(y_1, y_2) = [y_1^T, y_2^T]^T$. $\mathbf{1}$ denotes an identity matrix, and $\mathbf{0}$ denotes a matrix of zeros. Also, $\mathbf{1}_{n \times n}$ denotes an $n \times n$ identity matrix (similarly for $\mathbf{0}_{n \times n}$). $|x|$ is the Euclidean vector norm. It is assumed that the disturbance d belongs to the space of all Lebesgue measurable functions, \mathbb{L}_∞^m . It is defined as

$$\|d\|_\infty := \text{ess sup}_{t \geq 0} \{|d(t)|\} < \infty. \quad (2.5)$$

So we have the set $\mathbb{L}_\infty^m = \{d \in \mathbb{R}^m \mid \|d\|_\infty < \infty\}$. The matrix norm is denoted by $\|P\|$,

which is its maximum eigenvalue.

Definition 1. *The equilibrium point, $x = 0$, of the system (2.3) is stable if $\forall \delta_1 > 0$, $\exists \delta_2 > 0$ such that $|x(t)| \leq \delta_1 \forall |x(0)| \leq \delta_2$, $t > 0$.*

$|x|$ denotes the usual Euclidean norm of a vector x .

Definition 2. *The equilibrium point, $x = 0$, of the system (2.3) is asymptotically stable if it is stable and attractive, i.e., $|x(t)| \rightarrow 0$ as $t \rightarrow \infty$.*

As mentioned before, if the controller (2.2) stabilizes the system (2.1), then the system (2.3) is asymptotically stable.

Definition 3. *The equilibrium point, $x = 0$, of the system (2.3) is exponentially stable if there are constants $\delta_1, \delta_2 > 0$ such that $|x(t)| \leq \delta_1 e^{-\delta_2 t} |x(0)|$.*

We can define stabilizability as follows.

Definition 4. *The system (2.1) is smoothly (continuously) stabilizable if there is a smooth (Lipschitz continuous) mapping $k : \mathbb{R}^n \rightarrow \mathbb{R}^m$ such that, under the control law $u = k(x)$, the closed loop system (2.3) is asymptotically stable.*

We also have other forms of stability such as the bounded input bounded output stability (BIBO), bounded input bounded state (BIBS) stability that are prominently used in linear systems. This notion is, in fact, extended to nonlinear systems via input to state stability.

Definition 5. *The system (2.4) is bounded input bounded state stable (BIBS) if for each $\delta_1 > 0$ $\exists \delta_2 > 0$ such that, for each bounded measurable control input d with $\|d\|_\infty < \delta_1$, and each initial condition $|x(0)| < \delta_1$, the solution satisfies $|x(t)| \leq \delta_2$ for all $t > 0$.*

We have the following theorem, for which the proof can be found in [32].

Lemma 1. Assume that

- f is globally Lipschitz, and
- the system (2.3) is globally exponentially stable. Then the system (2.4) is bounded input bounded stable (BIBS).

Somewhat weaker conditions on f would suffice, for instance that $f(x, u)$ be globally Lipschitz on u alone, but uniformly on x , or even that an estimate $|f(x, u) - f(x, 0)| \leq f'(u)$ holds, for some function f' . A good application of this lemma is for the class of controllers that yield exponential convergence, which are by default made ISS.

2.1 Input to State Stability

Class $\mathcal{K}, \mathcal{K}_\infty$ and \mathcal{KL} functions. A class \mathcal{K} function is a function $\alpha : [0, a) \rightarrow \mathbb{R}_{\geq 0}$, which is continuous, strictly increasing and satisfies $\alpha(0) = 0$. A class \mathcal{K}_∞ function is a function $\alpha : \mathbb{R}_{\geq 0} \rightarrow \mathbb{R}_{\geq 0}$, which is continuous, strictly increasing, unbounded, and satisfies $\alpha(0) = 0$, and a class \mathcal{KL} function is a function $\beta : \mathbb{R}_{\geq 0} \times \mathbb{R}_{\geq 0} \rightarrow \mathbb{R}_{\geq 0}$ such that $\beta(r, t) \in \mathcal{K}_\infty$ for each t and $\beta(r, t) \rightarrow 0$ as $t \rightarrow \infty$.

We can now define ISS for the entire dynamics of (2.4). It is important to note that the *input* treated for ISS is the disturbance d . Therefore, all ISS and related definitions are w.r.t. d . Let $x_0 = x(0)$.

Definition 6. The system (2.4) is input to state stable(ISS) if there exists $\beta \in \mathcal{KL}$, and $\iota \in \mathcal{K}_\infty$ such that

$$|x(t, x_0, d)| \leq \beta(|x_0|, t) + \iota(\|d\|_\infty), \quad \forall x_0, \forall t \geq 0, \forall d, \quad (2.6)$$

and (2.4) is locally ISS, if the inequality (2.6) is valid for an open ball of radius r , $x_0 \in \mathbb{B}_r(0)$.

Definition 7. *The system (2.4) is exponential input to state stable (e-ISS) if there exists $\beta \in \mathcal{KL}$, $\iota \in \mathcal{K}_\infty$ and a positive constant $\lambda > 0$ such that*

$$|x(t, x_0, d)| \leq \beta(|x_0|, t)e^{-\lambda t} + \iota(\|d\|_\infty), \quad \forall x_0, \forall t \geq 0, \forall d, \quad (2.7)$$

and (2.4) is locally e-ISS, if the inequality (2.7) is valid for an open ball of radius r , $x_0 \in \mathbb{B}_r(0)$.

It was mentioned in Lemma 1 that the exponential stability of f implies BIBS. This consequently implies ISS, based on the Definition 6.

Definition 8. *The system (2.4) is input to output stable(IOS) if there exists $\beta \in \mathcal{KL}$, and $\iota \in \mathcal{K}_\infty$ such that*

$$|y(t, x_0, d)| \leq \beta(|x_0|, t) + \iota(\|d\|_\infty), \quad \forall x_0, \forall t \geq 0, \forall d, \quad (2.8)$$

and (2.4) is locally ISS, if the inequality (2.6) is valid for an open ball of radius r , $x_0 \in \mathbb{B}_r(0)$.

Definition 9. *The system (2.4) is said to hold the asymptotic gain (AG) property if there exists $\iota \in \mathcal{K}_\infty$ such that*

$$\overline{\lim}_{t \rightarrow \infty} |x(t, x_0, d)| \leq \iota(\|d\|_\infty), \quad \forall x_0, \forall d, \quad (2.9)$$

where the $\overline{\lim}_{t \rightarrow \infty}$ denotes the supremum of the limit of x as $t \rightarrow \infty$ (the state x is not required to have a limit).

It is important to note that the AG property implies BIBS of the system (2.4), but the converse is not true. Based on the inequality (2.9) this becomes intuitively obvious, since

the boundedness on the right hand side of (2.9) is a function of the input d . This is not necessarily true for systems that are BIBS.

Definition 10. *The system (2.4) is said to be zero stable (ZS) for a zero input $d = 0$, if there exists $\beta \in \mathcal{KL}$ such that*

$$|x(t, x_0, 0)| \leq \beta(|x_0|, t), \quad \forall x_0, \forall t \geq 0. \quad (2.10)$$

By this definition, ZS \implies asymptotic stability of the system with a zero input. We can use the ZS (2.10) and AG property (2.9) to establish ISS.

Lemma 2. *The system (2.4) is ISS if and only if it is ZS and AG.*

Based on these definitions, we can define the notion of input to state stabilizability.

Definition 11. *A system of the form (2.1) is smoothly (continuously) input to state stabilizable if there exists a smooth (continuous) control law $k : \mathbb{R}^n \rightarrow \mathbb{R}^m$ such that, under the control law $u = k(x) + d$, the new system (2.4) is input to state stable.*

We also have special definitions that are not frequently used such as weak input to state stability, defined for controllers of the form:

$$u = k(x) + g'(x)d, \quad (2.11)$$

which has the continuously differentiable map $k : \mathbb{R}^n \rightarrow \mathbb{R}^m$, with $k(0) = 0$ and a matrix $g'(x) \in \mathbb{R}^{m \times m}$ with the mapping $g' : \mathbb{R}^n \rightarrow \mathbb{R}^{m \times m}$ consisting of continuously differentiable functions, invertible for each x , and d is the new input under consideration. The resulting control system is the following:

$$\dot{x} = f(x, k(x) + g'(x)d). \quad (2.12)$$

We have the following definition for weak input to state stability.

Definition 12. *The system (2.1) is weakly input to state stabilizable, if there exists a continuously differentiable map $k : \mathbb{R}^n \rightarrow \mathbb{R}^m$, with $k(0) = 0$ and a matrix $g' : \mathbb{R}^n \rightarrow \mathbb{R}^{m \times m}$ consisting of continuously differentiable functions, invertible for each x , such that under the control law (2.11) that system (2.12) is ISS.*

This type of stability is of less interest to us, since we are interested in systems where $g'(x) \equiv \mathbf{1}$ is an identity. But, a special property of these systems is that it is possible to obtain $g'(x)$ that makes the system (2.12) ISS given that there exists a stabilizing control law $k(x)$ (from (2.2)). More on this is given in [32].

2.2 Input to State Stable Lyapunov Functions

A direct consequence of using ISS concepts is the construction of input to state stable Lyapunov functions. In other words, we can develop Lyapunov functions that also satisfy a set of ISS conditions, and that results in ISS of the control system (2.4).

Definition 13. *A continuous function $V : \mathbb{R}^n \rightarrow \mathbb{R}_{\geq 0}$ is a storage function if it is positive definite and proper, that is, $V(x) \rightarrow \infty$ as $x \rightarrow \infty$. It is easy to show that $V(x)$ is a storage function if and only if there exist $\underline{\alpha}, \bar{\alpha} \in \mathcal{K}_{\infty}$ such that*

$$\underline{\alpha}(x) \leq V(x) \leq \bar{\alpha}(x), \quad \forall x \in \mathbb{R}^n. \quad (2.13)$$

Note that the lower bound amounts to properness and $V(x) > 0$ for $x \neq 0$, while the upper bound ensures $V(0) = 0$.

Definition 14. *An ISS-Lyapunov function for $\dot{x} = f(x, k(x) + d)$ is a smooth storage function $V : \mathbb{R}^n \rightarrow \mathbb{R}_{\geq 0}$, for which there exist functions $\iota, \alpha \in \mathcal{K}_{\infty}$ such that*

$$\dot{V}(x, d) \leq -\alpha(|x|) + \iota(\|d\|_{\infty}), \quad \forall x, d. \quad (2.14)$$

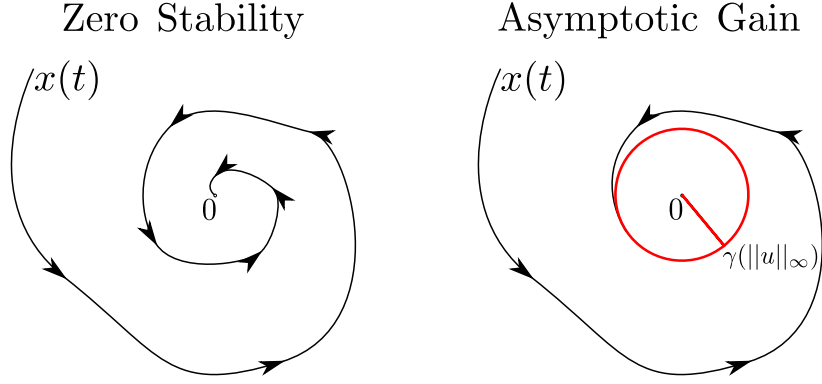


Figure 2.1: zero stability is achieved for a zero input, and asymptotic gain is achieved for a bounded input. We use these two important properties to prove input to state stability.

In other words, an ISS-Lyapunov function is a smooth solution of the inequality of the form (2.14).

The following lemma establishes the relationship between the ISS-Lyapunov function and the ISS of (2.4).

Lemma 3. *The system (2.4) is ISS if and only if it admits a smooth ISS-Lyapunov function.*

Proof of Lemma 3 is given in [10] and in [11]. In fact the inequality condition can be made stricter by using the exponential estimate for some $c > 0$:

$$\dot{V}(x, d) \leq -cV(x) + \iota(\|d\|_\infty), \quad \forall x, d, \quad (2.15)$$

which is then called the e-ISS-Lyapunov function. We also have the rapidly exponential estimate given by the following:

$$\dot{V}(x, d) \leq -\frac{c}{\varepsilon}V(x) + \iota(\|d\|_\infty), \quad \forall x, d, \quad (2.16)$$

where $0 < \varepsilon < 1$. The rapid exponential estimate is important in the context of hybrid systems (see Definition 27).

For systems of the form (2.12), weak-ISS-Lyapunov functions are used.

Definition 15. A weak-ISS-Lyapunov function for $\dot{x} = f(x, k(x) + g'(x)d)$ is a smooth storage function $V : \mathbb{R}^n \rightarrow \mathbb{R}_{\geq 0}$, for which there exist functions $\iota, \alpha \in \mathcal{K}_\infty$ such that

$$\dot{V}(x, d) \leq -\alpha(|x|) + \iota(\|d\|_\infty), \quad \forall x, d. \quad (2.17)$$

2.3 Input to State Stability of Affine Control Systems

We can pick affine control systems of the form

$$\dot{x} = f(x) + g(x)u, \quad f(0) = 0 \quad (2.18)$$

where $g(x) \in \mathbb{R}^{n \times m}$, a smooth function of x . Similar to (2.1), it is assumed that $f(0) = 0$ (to satisfy the requirement $u = k(0) = 0$), both f, g are Lipschitz in x . The main result of [11] was that systems of the type (2.18) can be made input to state stable. In other words, the affine system, (2.18), is smoothly input to state stabilizable, i.e., there exists a smooth map $k : \mathbb{R}^n \rightarrow \mathbb{R}^m$, with $k(0) = 0$, and the control law $k(x) + d$, such that the new system

$$\dot{x} = f(x) + g(x)k(x) + g(x)d \quad (2.19)$$

is ISS. This definition can be extended to almost smooth maps k as well, where almost smooth means that the controller is continuous at 0.

We can define the notion of ISSability (input to state stabilizability), which is a powerful tool to obtain controllers that satisfy the ISS conditions. A detailed analysis of stabilizability is given in [11]. We investigated weak stabilizability in Definition 12, which is obtained from [32]. Rephrasing this definition, Theorem 1 in [32] states that existence of a smooth stabilizing control law $k(x)$ implies weak input to state stabilizability. This notion of weak stabilizability gets stronger for affine systems of the form (2.18). This section will dwell more into this topic.

Definition 16. *The system (2.18) is smoothly stabilizable, if there is a smooth map $k : \mathbb{R}^n \rightarrow \mathbb{R}^m$ with $k(0) = 0$ such that the system (2.18) is GAS. It is smoothly input to state stabilizable if there is a k so that the system (2.19) becomes ISS.*

Based on this definition, we have this powerful Lemma that is taken from Theorem 1 of [11] and restated here.

Lemma 4. *For systems of the type (2.18) smooth stabilizability implies smooth input to state stabilizability.*

Proof of this lemma is given in [11]. The controller that is derived from this paper will be given in Chapter 3. As mentioned before, the smoothness conditions can be relaxed to construct Lipschitz continuous control laws for the latter part of the thesis.

2.4 Input to State Stability of Discrete Time Control Systems

We can pick discrete time systems of the form

$$x(i+1) = f(x(i), u(i)). \quad (2.20)$$

or affine discrete systems of the form

$$x(i+1) = f(x(i)) + g(x(i))u(i). \quad (2.21)$$

A stabilizing controller $u(i) = k(x(i))$ is applied such that the system

$$x(i+1) = f(x(i)) + g(x(i))k(x(i)) + g(x(i))d, \quad (2.22)$$

be bounded for small bounded perturbations d .

Definition 17. We say that (2.22) is input to state stable if $\beta \in \mathcal{KL}$, and $\iota \in \mathcal{K}_\infty$ such that

$$|x(i, x_0, d)| \leq \beta(|x_0|, i) + \iota(\|d\|_\infty), \quad \forall x_0, \forall i \in \mathbb{N}, \forall d \quad (2.23)$$

and we say that (2.22) is exponential input to state stable if for some $\lambda > 0$

$$|x(i, x_0, d)| \leq \beta(|x_0|, i)e^{-\lambda i} + \iota(\|d\|_\infty), \quad \forall x_0, \forall i \in \mathbb{N}, \forall d \quad (2.24)$$

Definition 18. A continuous function $V : \mathbb{R}^n \rightarrow \mathbb{R}_{\geq 0}$ is called an ISS-Lyapunov function for system (2.22) if there exist $\underline{\alpha}, \bar{\alpha}, \alpha, \iota \in \mathcal{K}_\infty$ such that

$$\underline{\alpha}(|x(i)|) \leq V(x(i)) \leq \bar{\alpha}(|x(i)|) \quad (2.25)$$

$$\text{and } V(x(i+1)) - V(x(i)) \leq -\alpha(|x(i)|) + \iota(\|d\|_\infty), \forall i \in \mathbb{N}, \forall x, d.$$

It can be observed that smoothness conditions can also be imposed on V , but not really necessary.

Lemma 5. As in the classic Lyapunov stability theory, the discrete-time system (2.22) is ISS if and only if it admits a discrete-time continuous ISS-Lyapunov function.

For continuous affine systems, continuous stabilization implies ISS stabilization according to Lemma 4. This is not the case any more for discrete systems, and the notion of weak input to state stabilizability is applied. See [37] for more details. The discrete time continuous controller $u(i) = k(x(i))$ is weak input to state stabilizing, if there is an invertible map $g' : \mathbb{R}^n \rightarrow \mathbb{R}^{m \times m}$ of continuous functions, such that the system

$$x(i+1) = f(x(i), k(x(i)) + g'(x(i))d) \quad (2.26)$$

is input to state stable. We therefore have weak-ISS-Lyapunov functions for discrete time

systems of the form (2.26).

Definition 19. A continuous function $V : \mathbb{R}^n \rightarrow \mathbb{R}_{\geq 0}$ is called a weak-ISS-Lyapunov function for system (2.26) if there exists $g'(x) \in \mathbb{R}^{m \times m}$ invertible and continuous, and $\underline{\alpha}, \bar{\alpha}, \alpha, \iota \in \mathcal{K}_\infty$ such that

$$\underline{\alpha}(|x(i)|) \leq V(x(i)) \leq \bar{\alpha}(|x(i)|) \quad (2.27)$$

$$\text{and } V(f(x(i), k(x(i)) + g'(x)d)) - V(x(i)) \leq -\alpha(|x(i)|) + \iota(\|d\|_\infty), \quad \forall i \in \mathbb{N}, \forall x, d.$$

Based on this definition of weak-ISS-Lyapunov functions, we have the following Lemma.

Lemma 6. For systems of the form (2.20), existence of a continuously stabilizing controller implies the existence of a weak input to state continuously stabilizing controller.

Proof of this Lemma can be found in [37]. Specifically, it is shown in Theorem 4 in the cited paper.

CHAPTER 3

INPUT TO STATE STABILIZING CONTROL LYAPUNOV FUNCTIONS

The goal of this chapter is to generalize and define the set of stabilizing controllers (i.e., not just one $k(x)$) via control Lyapunov functions (CLFs) that yield ISS. Specifically, in the context of ISS, we will derive a sub-class of control Lyapunov functions (CLF) that *input to state stabilize* the system (2.1). CLFs are obtained for the control input u , and the ISS conditions are satisfied for the disturbance input d . These types of CLFs are famously called *input to state stabilizing control Lyapunov functions* (ISS-CLFs). More details about the definition of these ISS-CLFs can be found in [38, 39]. Towards the end of this Chapter, we will derive this subclass for *rapidly exponentially stabilizing control Lyapunov functions* (RES-CLF) that are important leading into the next chapter (for hybrid systems).

3.1 Control Lyapunov Functions

We will define the CLF here.

Definition 20. *For the system (2.1), a continuously differentiable function $V : \mathbb{R}^n \rightarrow \mathbb{R}_{\geq 0}$ is an asymptotically stabilizing control Lyapunov function (CLF), if there exists a set of admissible controls $\mathbb{U} \subset \mathbb{R}^m$, and $\underline{\alpha}, \bar{\alpha}, \alpha \in \mathcal{K}_\infty$ such that for all x*

$$\begin{aligned} \underline{\alpha}(|x|) &\leq V(x) \leq \bar{\alpha}(|x|) \\ \inf_{u \in \mathbb{U}} [L_f V(x, u) + \alpha(|x|)] &\leq 0. \end{aligned} \tag{3.1}$$

We are interested in affine systems of the form (2.18), which represents a large class of systems (robotic systems are a prime example). So we can similarly define CLFs for such systems by replacing $L_f V(x)$ with $L_f V(x) + L_g V(x)u$.

We will define the *exponentially stabilizing control Lyapunov function* (ES-CLF), for affine systems here.

Definition 21. *For the system (2.18), a continuously differentiable function $V : \mathbb{R}^n \rightarrow \mathbb{R}_{\geq 0}$ is an exponentially stabilizing control Lyapunov function (ES-CLF) if there exists a set of admissible controls $\mathbb{U} \subset \mathbb{R}^m$ and positive constants $\underline{c}, \bar{c}, c > 0$ such that for all x*

$$\begin{aligned} \underline{c}\|x\|^2 &\leq V(x) \leq \bar{c}\|x\|^2 \\ \inf_{u \in \mathbb{U}} [L_f V(x) + L_g V(x)u + cV(x)] &\leq 0, \end{aligned} \quad (3.2)$$

L_f, L_g are the Lie derivatives. We can accordingly define a set of controllers that render exponential convergence of the states to 0

$$\mathbf{K}(x) = \{u \in \mathbb{U} : L_f V(x) + L_g V(x)u + cV(x) \leq 0\}, \quad (3.3)$$

which has the control values that result in $\dot{V} \leq -cV$.

3.2 Input to State Stabilizing Control Lyapunov Functions

We define here, a sub-class of CLFs, that are input to state stable. In other words, we define **input to state stabilizing control Lyapunov functions** (ISS-CLFs). We will use ISS-Lyapunov functions that are defined in Chapter 2. This definition is obtained from [38, 39] although different variants of this definition are possible (see [40]).

Definition 22. *For the system (2.1), an asymptotically stabilizing CLF, $V : \mathbb{R}^n \rightarrow \mathbb{R}_{\geq 0}$ (Definition 20), is an input to state stable stabilizing control Lyapunov function (ISS-CLF), if it satisfies the conditions of an ISS-Lyapunov function. In other words, a continuously differentiable function $V : \mathbb{R}^n \rightarrow \mathbb{R}_{\geq 0}$ is an ISS-CLF, if there exists a set of admissible*

controls $\mathbb{U} \subset \mathbb{R}^m$, and $\underline{\alpha}, \bar{\alpha}, \alpha, \iota \in \mathcal{K}_\infty$ such that

$$\begin{aligned}\underline{\alpha}(|x|) &\leq V(x) \leq \bar{\alpha}(|x|) \\ \inf_{u \in \mathbb{U}} [L_f V(x, u + d)] &\leq -\alpha(|x|) + \|d\|_\infty, \quad \forall x, d.\end{aligned}\tag{3.4}$$

We can use weak notions of ISS for systems of the form (2.1).

Definition 23. For the system (2.1), a continuously differentiable function $V : \mathbb{R}^n \rightarrow \mathbb{R}_{\geq 0}$ is a weak-ISS-CLF, if there exists a set of admissible controls $\mathbb{U} \subset \mathbb{R}^m$, a smooth invertible matrix $g' : \mathbb{R}^n \rightarrow \mathbb{R}^{m \times m}$, and $\underline{\alpha}, \bar{\alpha}, \alpha, \iota \in \mathcal{K}_\infty$ such that

$$\begin{aligned}\underline{\alpha}(|x|) &\leq V(x) \leq \bar{\alpha}(|x|) \\ \inf_{u \in \mathbb{U}} [L_f V(x) + L_g V(x, u + g'(x)d)] &\leq -\alpha(|x|) + \iota(\|d\|_\infty), \quad \forall x, d.\end{aligned}\tag{3.5}$$

We have a stronger definition for affine control systems of the form (2.18).

Definition 24. For the system (2.18), a continuously differentiable function $V : \mathbb{R}^n \rightarrow \mathbb{R}_{\geq 0}$ is an ISS-CLF, if there exists a set of admissible controls $\mathbb{U} \subset \mathbb{R}^m$, and $\underline{\alpha}, \bar{\alpha}, \alpha, \iota \in \mathcal{K}_\infty$ such that

$$\begin{aligned}\underline{\alpha}(|x|) &\leq V(x) \leq \bar{\alpha}(|x|) \\ \inf_{u \in \mathbb{U}} [L_f V(x) + L_g V(x)(u + d)] &\leq -\alpha(|x|) + \iota(\|d\|_\infty), \quad \forall x, d.\end{aligned}\tag{3.6}$$

Motivated by constructions of input to state stabilizable controllers developed by Sontag, specifically, equations (23) and (32) in [11], we can construct ISS-CLFs in the following manner. Parts of these are also derived from Artstein's theorem [23, 24]. Choosing the stabilizing controller $k(x)$ that resulted in the closed loop system (2.3) again, we have the Lie derivative w.r.t. the closed loop vector field f^{cl} as $L_{f^{cl}} V(x) = \frac{\partial V}{\partial x} f^{cl}(x)$. It was shown

in [11] that the controller

$$u = k(x) + \frac{1}{2m} L_{fcl} V(x) L_g V(x)^T, \quad (3.7)$$

input to state stabilizes the system (2.1). We can derive a simpler controller like the following, which also renders the system (2.4) ISS.

$$u = k(x) - \frac{1}{\bar{\varepsilon}} L_g V(x)^T, \quad (3.8)$$

for some $\bar{\varepsilon} > 0$. Based on this controller, we have the following Lemma, which defines a new set of CLFs that input to state stabilizes the system (2.1).

Lemma 7. *The continuously differentiable function $V : \mathbb{R}^n \rightarrow \mathbb{R}_{\geq 0}$ defined for $\underline{\alpha}, \bar{\alpha}, \alpha \in \mathcal{K}_\infty$ as*

$$\begin{aligned} \underline{\alpha}(|x|) &\leq V(x) \leq \bar{\alpha}(|x|) \\ \inf_{u \in \mathbb{U}} [L_f V(x) + L_g V(x)u + \alpha(|x|) + \frac{1}{\bar{\varepsilon}} L_g V(x) L_g V(x)^T] &\leq 0, \end{aligned} \quad (3.9)$$

is an ISS-CLF $\forall \bar{\varepsilon} > 0$.

Proof. We have the following expression after the derivative of the Lyapunov function:

$$\begin{aligned} \dot{V}(x, u + d) &= L_f V(x) + L_g V(x)(u + d) \\ &= L_f V(x) + L_g V(x)u + L_g V(x)d. \end{aligned} \quad (3.10)$$

After substituting the controller (3.9), we have

$$\dot{V}(x, u(x) + d) \leq -\alpha(|x|) - \frac{1}{\bar{\varepsilon}} L_g V(x) L_g V(x)^T + L_g V(x)d. \quad (3.11)$$

Since $L_g V(x) \in \mathbb{R}^{1 \times m}$, and any matrix multiplied with the transpose of itself results in a

nonnegative matrix, we have the following inequality after adding and subtracting $\bar{\varepsilon} \frac{\|d\|_\infty^2}{4}$:

$$\begin{aligned}\dot{V}(x, u(x) + d) &\leq -\alpha(|x|) - \frac{1}{\bar{\varepsilon}} \|L_g V(x)\|^2 + \|L_g V(x)\| \|d\|_\infty - \bar{\varepsilon} \frac{\|d\|_\infty^2}{4} + \bar{\varepsilon} \frac{\|d\|_\infty^2}{4} \\ &\leq -\alpha(|x|) - \left(\frac{1}{\sqrt{\bar{\varepsilon}}} \|L_g V(x)\| - \sqrt{\bar{\varepsilon}} \frac{\|d\|_\infty}{2} \right)^2 + \bar{\varepsilon} \frac{\|d\|_\infty^2}{4} \\ &\leq -\alpha(|x|) + \bar{\varepsilon} \frac{\|d\|_\infty^2}{4},\end{aligned}\tag{3.12}$$

which is in the form given by (2.14). It can be observed that an excellent way to drive the ultimate bound to a very small value is by decreasing $\bar{\varepsilon}$. \square

If we pick an exponentially stabilizing control Lyapunov function (ES-CLF), (3.2), we can modify (3.12) that results in exponential input to state stability (e-ISS) w.r.t. d .

Definition 25. For the system (2.18), an exponentially stabilizing CLF, $V : \mathbb{R}^n \rightarrow \mathbb{R}_{\geq 0}$ (Definition 20), is an exponential input to state stable stabilizing control Lyapunov function (e-ISS-CLF), if it satisfies the conditions of an e-ISS-Lyapunov function. In other words, a continuously differentiable function $V : \mathbb{R}^n \rightarrow \mathbb{R}_{\geq 0}$ is an e-ISS-CLF, if there exists a set of admissible controls $\mathbb{U} \subset \mathbb{R}^m$, and $\underline{c}, \bar{c}, c > 0$, and $\iota \in \mathcal{K}_\infty$ such that

$$\begin{aligned}\underline{c}\|x\|^2 &\leq V(x) \leq \bar{c}\|x\|^2 \\ \inf_{u \in \mathbb{U}} [L_f V(x) + L_g V(x)(u + d)] &\leq -cV(x) + \iota(\|d\|_\infty), \quad \forall x, d.\end{aligned}\tag{3.13}$$

We therefore have the following Lemma.

Lemma 8. The continuously differentiable function $V : \mathbb{R}^n \rightarrow \mathbb{R}_{\geq 0}$ defined for $\underline{c}, \bar{c}, c > 0$ as

$$\begin{aligned}\underline{c}\|x\|^2 &\leq V(x) \leq \bar{c}\|x\|^2 \\ \inf_{u \in \mathbb{U}} [L_f V(x) + L_g V(x)u + cV(x) + \frac{1}{\bar{\varepsilon}} L_g V(x)L_g V(x)^T] &\leq 0,\end{aligned}\tag{3.14}$$

is an e -ISS-CLF $\forall \bar{\varepsilon} > 0$.

Proof. Proof is straightforward from (3.12), where $\alpha(|x|)$ needs to be simply replaced with $cV(x)$. \square

Motivated by Lemma 7 we can create a subclass of controllers from ES-CLF that are e -ISS

$$\mathbf{K}_{\bar{\varepsilon}}(x) = \{u \in \mathbb{U} : L_f V(x) + L_g V(x)u + cV(x) + \frac{1}{\bar{\varepsilon}}L_g V(x)L_g V(x)^T \leq 0\}. \quad (3.15)$$

Since $\bar{\varepsilon}, L_g V(x)L_g V(x)^T$ are both ≥ 0 , it can be verified that $\mathbf{K}_{\bar{\varepsilon}} \subseteq \mathbf{K}$ (the set obtained from (3.3)).

3.3 Rapidly Exponentially Stabilizing Control Lyapunov Functions

If we need stronger bounds of convergences (especially used for hybrid systems like bipedal robots; more on this is discussed in Chapter 4), a *rapidly exponentially stabilizing control Lyapunov function* (RES-CLF) is constructed that stabilizes the output dynamics at a rapidly exponential rate (see [28] for more details) through a user defined $\varepsilon > 0$.

Definition 26. *The family of continuously differentiable functions $V_\varepsilon : \mathbb{R}^n \rightarrow \mathbb{R}_{\geq 0}$ is a rapidly exponentially stabilizing control Lyapunov function (RES-CLF) if there exist positive constants $c_1, c_2, c_3 > 0$ such that for all $0 < \varepsilon < 1$, x ,*

$$\begin{aligned} c_1\|x\|^2 &\leq V_\varepsilon(x) \leq \frac{c_2}{\varepsilon^2}\|x\|^2 \\ \inf_{u \in \mathbb{U}} [L_f V_\varepsilon(x) + L_g V_\varepsilon(x)u + \frac{c_3}{\varepsilon}V_\varepsilon(x)] &\leq 0. \end{aligned} \quad (3.16)$$

Therefore, we can define a class of controllers \mathbf{K}_ε :

$$\mathbf{K}_\varepsilon(x) = \{u \in \mathbb{U} : L_f V_\varepsilon(x) + L_g V_\varepsilon(x)u + \frac{\gamma}{\varepsilon} V_\varepsilon(x) \leq 0\}, \quad (3.17)$$

which yields the set of control values that satisfies the desired convergence rate. We accordingly have the definition for RES-CLFs that are input to state stabilizing. We have to use rapidly exponentially input to state stabilizing (Re-ISS)-Lyapunov functions as defined in (2.16). Based on this formulation, we have the following definition for *rapidly exponentially input to state stabilizing control Lyapunov function* (Re-ISS-CLF).

Definition 27. For the system (2.18), a RES-CLF, $V : \mathbb{R}^n \rightarrow \mathbb{R}_{\geq 0}$ (Definition 20), is a rapidly exponentially input to state stable stabilizing control Lyapunov function (Re-ISS-CLF), if it is satisfies the conditions of an Re-ISS-Lyapunov function (see 2.16). In other words, a continuously differentiable function $V : \mathbb{R}^n \rightarrow \mathbb{R}_{\geq 0}$ is an e-ISS-CLF, if there exists a set of admissible controls $\mathbb{U} \subset \mathbb{R}^m$, and $\underline{c}, \bar{c}, c > 0$, and $\iota \in \mathcal{K}_\infty$ such that

$$\begin{aligned} \underline{c}\|x\|^2 &\leq V(x) \leq \bar{c}\|x\|^2 \\ \inf_{u \in \mathbb{U}} [L_f V(x) + L_g V(x)(u + d)] &\leq -cV(x) + \iota(\|d\|_\infty), \quad \forall x, d. \end{aligned} \quad (3.18)$$

Similar to Lemma 8 we pick a subclass of controllers from RES-CLF in the following Lemma.

Lemma 9. The continuously differentiable function $V_\varepsilon : \mathbb{R}^n \rightarrow \mathbb{R}_{\geq 0}$ defined for $c_1, c_2, c_3 > 0$ as

$$\begin{aligned} c_1\|x\|^2 &\leq V_\varepsilon(x) \leq \frac{c_2}{\varepsilon^2}\|x\|^2 \\ \inf_{u \in \mathbb{U}} [L_f V_\varepsilon(x) + L_g V_\varepsilon(x)u + \frac{c_3}{\varepsilon} V_\varepsilon(x) + \frac{1}{\bar{\varepsilon}} L_g V_\varepsilon(x)L_g V_\varepsilon(x)^T] &\leq 0, \end{aligned} \quad (3.19)$$

is an Re-ISS-CLF $\forall 0 < \varepsilon < 1, \bar{\varepsilon} > 0$.

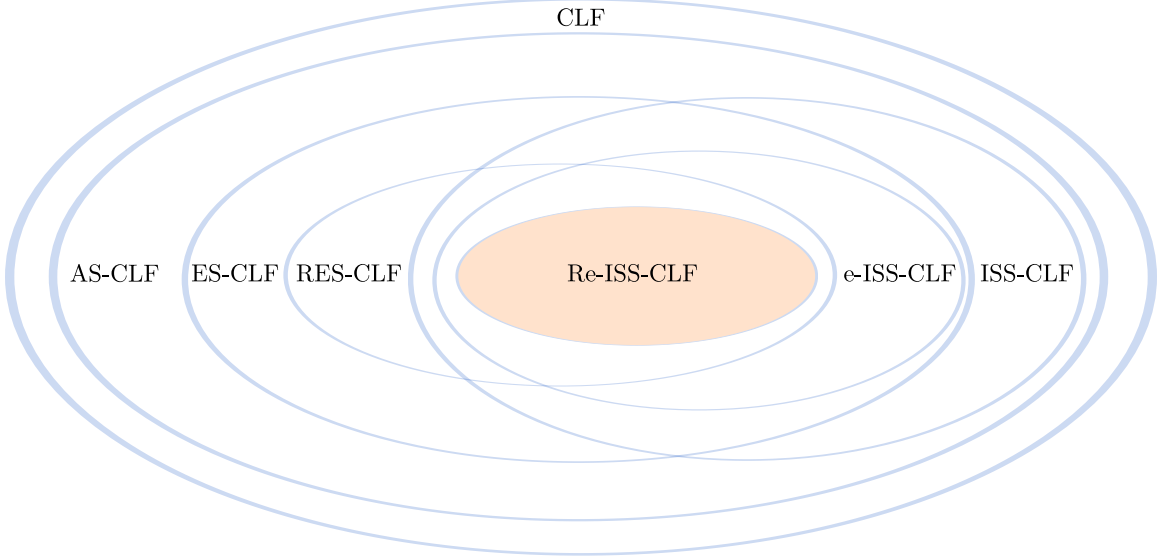


Figure 3.1: Venn diagram representation of the classes of controllers defined.

Proof. Proof of this Lemma is straightforward from (3.12), where $\alpha(|x|)$ needs to be simply replaced with $\frac{c_3}{\varepsilon} V_\varepsilon(x)$. \square

Motivated by Lemma 7 we can create a subclass of RES-CLFs that are Re-ISS

$$\mathbf{K}_{\varepsilon, \bar{\varepsilon}}(x) = \{u \in \mathbb{U} : L_f V(x) + L_g V(x)u + \frac{c_3}{\varepsilon} V_\varepsilon(x) + \frac{1}{\bar{\varepsilon}} L_g V_\varepsilon(x) L_g V_\varepsilon(x)^T \leq 0\}. \quad (3.20)$$

Similar to (3.15), $\bar{\varepsilon}, L_g V(x) L_g V(x)^T$ are both ≥ 0 , it can be verified that $\mathbf{K}_{\varepsilon, \bar{\varepsilon}} \subseteq \mathbf{K}_\varepsilon$ (the set obtained from (3.17)). In fact, $\mathbf{K}_{\varepsilon, \bar{\varepsilon}} \subseteq \mathbf{K}_{\bar{\varepsilon}} \subseteq \mathbf{K}$, and $\mathbf{K}_\varepsilon \subseteq \mathbf{K}$. See Fig. 3.1.

To summarize, for affine systems of the form (2.18), we showed that we can create a set of ISS controllers for the three types of classes: CLFs, ES-CLFs, RES-CLFs. We also defined two subclasses mathematically, e-ISS-CLF (3.15), and Re-ISS-CLF (3.20), which both yield e-ISS. The purpose of Re-ISS-CLF will be more clear in the context of hybrid systems in Chapter 4.

3.4 Extension of Artstein's Theorem

We can make use of Artstein's theorem [23], which states that existence of a smooth control Lyapunov function implies smooth stabilizability, which can be extended to include ISS-CLFs by using Lemma 4.

Lemma 10. *For systems of the form (2.18), existence of a smooth stabilizing control Lyapunov function implies the existence of a smooth input to state stabilizing control Lyapunov function.*

This, of course, can be extended to ES-CLFs and RES-CLFs and conclude that the corresponding ISS versions of these CLFs can be easily computed. Lemma 10 can be used to construct input to state stabilizing controllers, given a CLF. While constructing these robust controllers are possible, major challenge lies in obtaining a Lyapunov function for the given system. The most popular approach used is via feedback linearization (always used in robotic systems). Given the outputs, we can linearize the dynamics and obtain a Lyapunov function for the resulting linear system. More on this is explained in Chapter 6. If we pick only the outputs y then we can extend Lemma 10 to create *input to output stabilizing control Lyapunov functions* (IOS-CLF).

3.5 Discrete Time Systems

Similar to continuous systems, we can define CLFs for discrete systems here. We will omit the argument of the discrete time index i in this section, since, the inequalities presented here are all independent of time.

Definition 28. *For the system (2.20), a continuous function $V : \mathbb{R}^n \rightarrow \mathbb{R}_{\geq 0}$ is an **asymptotically stabilizing control Lyapunov function** (CLF), if there exists a set of admissible*

controls \mathbb{U} , and $\underline{\alpha}, \bar{\alpha}, \alpha \in \mathcal{K}_\infty$ such that for all x

$$\begin{aligned} \underline{\alpha}(|x|) &\leq V(x) \leq \bar{\alpha}(|x|) \\ \inf_{u \in \mathbb{U}} [V(f(x, u)) - V(x) + \alpha(|x|)] &\leq 0. \end{aligned} \quad (3.21)$$

We can also define a sub-class of CLFs that are input to state stable. In other words, we define **input to state stabilizing control Lyapunov functions** (ISS-CLFs) for discrete time systems of the form (2.20).

Definition 29. For the system (2.20), an asymptotically stabilizing CLF, $V : \mathbb{R}^n \rightarrow \mathbb{R}_{\geq 0}$ (Definition 28), is a **weak input to state stable stabilizing control Lyapunov function** (weak-ISS-CLF), if it satisfies the conditions of a weak ISS-Lyapunov function. In other words, a continuous function $V : \mathbb{R}^n \rightarrow \mathbb{R}_{\geq 0}$ is a weak-ISS-CLF, if there exists a set of admissible controls $\mathbb{U} \subset \mathbb{R}^m$, a smooth invertible map $g' : \mathbb{R}^n \rightarrow \mathbb{R}^{m \times m}$, and $\underline{\alpha}, \bar{\alpha}, \alpha, \iota \in \mathcal{K}_\infty$ such that

$$\begin{aligned} \underline{\alpha}(|x|) &\leq V(x) \leq \bar{\alpha}(|x|) \\ \inf_{u \in \mathbb{U}} [V(f(x, u + g'(x)d)) - V(x)] &\leq -\alpha(|x|) + \|d\|_\infty, \quad \forall x, d. \end{aligned} \quad (3.22)$$

We therefore have the following Lemma, which is the extension of Artstein's theorem for discrete time systems.

Lemma 11. For systems of the form (2.20), existence of a smooth stabilizing control Lyapunov function implies the existence of a smooth weak input to state stabilizing control Lyapunov function.

Since weak ISS conditions are of less importance to us, and also since these conditions are not a suitable reflection of the uncertainty effects observed in real systems, we will focus more attention toward input to state stabilization of continuous time affine control systems

only. The systems that are of interest to us are only those that yield strong ISS properties. The next chapter, which discusses hybrid systems, will analyze a general hybrid system and then study the class of systems where strong ISS properties can be realized.

Part II

Hybrid Systems

CHAPTER 4

HYBRID SYSTEMS

In this section, we will discuss a general hybrid model, and then discuss a class of hybrid systems that also naturally model bipedal robots: systems with impulse effects. Informally, a hybrid system is a sequence of continuous and discrete events. Formal definitions for hybrid systems can be found in [41, 42, 12, 43, 44]. The continuous events are called the flows, and the discrete events are called the jumps. A detailed account on robotic hybrid system models will be given in Chapter 6.

4.1 Basic Definition

We will study here a general nonlinear hybrid system consisting of states x of dimension n , and inputs u of dimension m . It will be assumed that the dimensions of the state and the control inputs do not change. Since the disturbances d (also of dimension m) studied in the thesis appear only along with the control inputs, the constant dimension of the control inputs is mandatory. For example, for robotic hybrid systems, the number of actuators remain the same irrespective of their behaviors. For systems with impulses, when the inputs do not appear in the discrete events, we will assume constant dimension of the inputs only in the continuous events.

Definition 30. *A hybrid control system is defined to be the tuple:*

$$\mathcal{HC} = (\Gamma, \mathbb{D}, \mathbb{S}, \mathbb{U}, \Delta, \mathbb{F}), \quad (4.1)$$

where each element in the set \mathcal{HC} is described below.

- *The directed graph: $\Gamma = (\mathbb{V}, \mathbb{E})$ consisting of vertices and edges,*

$$\mathbb{V} = \{v_1, v_2, \dots\}, \quad \mathbb{E} = \{e_1, e_2, \dots\} \subset \mathbb{V} \times \mathbb{V}. \quad (4.2)$$

Fig. 4.1 denotes a directed graph consisting of the vertices (circles) and edges (arrows). Therefore, if the edge, e_1 , denotes the arrow from v_1 to v_2 , then e_1 is the ordered pair: $e_1 = (v_1, v_2)$. We denote the source and target vertices as $\text{source}(e) = v_1$, $\text{target}(e) = v_2$. For a general case, we denote the ordered pair as

$$e = (\text{source}(e), \text{target}(e)).$$

- $\mathbb{D} = \{\mathbb{D}_{v_1}, \mathbb{D}_{v_2}, \dots\}$ is the set of domains. Each domain $\mathbb{D}_v \subset \mathbb{R}^n \times \mathbb{R}^m$, is a manifold with $v \in \mathbb{V}$ can be defined as the set of feasible states and admissible control inputs for the hybrid system. There could be kinematic and dynamic constraints that could limit the statespace. Note that all of the domains are assumed to have constant dimensions.
- $\mathbb{S} = \{\mathbb{S}_{e_1}, \mathbb{S}_{e_2}, \dots\}$ is the set of switching surfaces or guards, with each guard $\mathbb{S}_e \subset \mathbb{D}_{\text{source}(e)}$, is an embedded submanifold with $e \in \mathbb{E}$, representing the surface where the switch over to the next domain happens. A domain can have multiple guards. So the union of guards for each domain is denoted as $\mathbb{S}_v = \bigcup_{\{e \in \mathbb{E} | \text{source}(e) = v\}} \mathbb{S}_e$.
- $\mathbb{U} = \{\mathbb{U}_{v_1}, \mathbb{U}_{v_2}, \dots, \mathbb{U}_{e_1}, \mathbb{U}_{e_2}, \dots\} = \{\{\mathbb{U}_v\}_{v \in \mathbb{V}}, \{\mathbb{U}_e\}_{e \in \mathbb{E}}\}$, where each $\mathbb{U}_v \subset \mathbb{R}^m$ is the set of admissible control inputs. The set includes the control inputs for both the continuous and the discrete dynamics. It is assumed that the dimensions of the inputs do not change based on the domains or the guards. Given the set of admissible inputs, we denote the canonical projection as $\pi_x : \mathbb{D}_v \rightarrow \mathbb{R}^n$, that maps from the domain to

the corresponding states. It can be defined as

$$\pi_x(\mathbb{D}_v) = \{x \in \mathbb{R}^n : \exists u \in \mathbb{U}_v \cup (\cup_{\{e \in \mathbb{E} | \text{source}(e)=v\}} \mathbb{U}_e) \quad \text{s.t.} \quad (x, u) \in \mathbb{D}_v\}. \quad (4.3)$$

- $\Delta = \{\Delta_{e_1}, \Delta_{e_2}, \dots\}$, is the set of switching functions or reset maps or jump maps from one domain to the next domain. Each reset map $\Delta_e : \mathbb{S}_e \rightarrow \pi_x(\mathbb{D}_{\text{target}(e)})$, is computed at the end of every continuous event. We have

$$x^+ = \Delta_e(x^-, u), \quad (x^-, u) \in \mathbb{S}_e, x^+ \in \pi_x(\mathbb{D}_{\text{target}(e)}), e \in \mathbb{E}. \quad (4.4)$$

It is assumed that the reset maps are Lipschitz continuous in x .

- $\mathbb{F} = \{f_{v_1}, f_{v_2}, \dots\}$ provides the set of vector fields given by the equation

$$\dot{x} = f_v(x, u), \quad (x, u) \in \mathbb{D}_v \setminus \mathbb{S}_v, v \in \mathbb{V}. \quad (4.5)$$

$f_v : \mathbb{D}_v \setminus \mathbb{S}_v \rightarrow T_x \pi_x(\mathbb{D}_v \setminus \mathbb{S}_v)$ is assumed to be Lipschitz continuous in x .

If a feedback control law

$$u(x) = \begin{cases} k_v(x), & (x, k_v(x)) \in \mathbb{D}_v \setminus \mathbb{S}_v, \\ k_e(x), & (x, k_e(x)) \in \mathbb{S}_e, \end{cases} \quad v \in \mathbb{V}, e \in \mathbb{E}, \quad (4.6)$$

where each $k_v : \pi_x(\mathbb{D}_v \setminus \mathbb{S}_v) \rightarrow \mathbb{U}_v$, $k_e : \pi_x(\mathbb{S}_e) \rightarrow \mathbb{U}_e$, is implemented, the hybrid control system \mathcal{HC} reduces to a hybrid system

$$\mathcal{H} = (\Gamma, \mathbb{D}^{cl}, \mathbb{S}^{cl}, \Delta^{cl}, \mathbb{F}^{cl}), \quad \Delta^{cl} = \{\Delta_e^{cl}\}_{e \in \mathbb{E}}, \mathbb{F}^{cl} = \{f_v^{cl}\}_{v \in \mathbb{V}}, \quad (4.7)$$

with the omission of \mathbb{U} . $\mathbb{D}^{cl} = \{\pi_x(\mathbb{D}_v)\}_{v \in \mathbb{V}}$, $\mathbb{S}^{cl} = \{\pi_x(\mathbb{S}_e)\}_{e \in \mathbb{E}}$ and each $\Delta_e^{cl}(x) := \Delta_e(x, k_e(x))$, $f_v^{cl}(x) := f_v(x, k_v(x))$. By slight abuse of notations, we will remove the

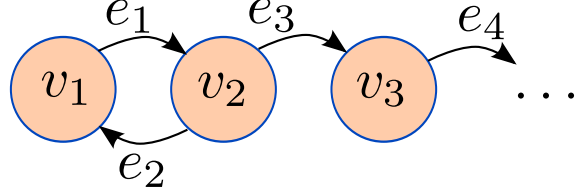


Figure 4.1: Graphical representation of hybrid systems. The edge set \mathbb{E} represents the discrete transitions from one domain to another. It should be noted that the designation of the edges is not restricted by the vertices. For example, e_2 is the edge from v_2 to v_1 .

superscript cl in some of the equations for convenience. The space of the sets defined can be easily distinguished based on the controllers and the model considered.

A system with a single domain and single reset map is called a simple hybrid control system. It can be represented in the form of (4.1) with the omission of the directed graph Γ :

$$\mathcal{SHC} = (\mathbb{D}, \mathbb{S}, \mathbb{U}, \Delta, \mathbb{F}). \quad (4.8)$$

A pictorial representation is given in Fig. 4.2. A wide variety of hybrid systems can be defined in the form of (4.1) such as mechanical systems, networked control systems, switching power systems, embedded systems and so on. This representation is derived from category theory used in [12]. A pictorial representation of the hybrid system is shown in Fig. 4.1. Fig. 4.3 shows a pictorial representation for different domains of a dancing model

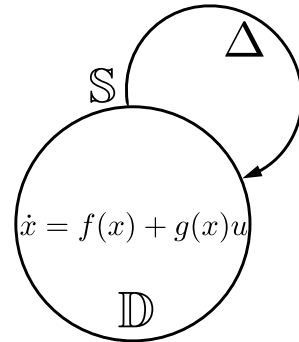


Figure 4.2: Figure showing a simple hybrid system with affine controls in the continuous dynamics.

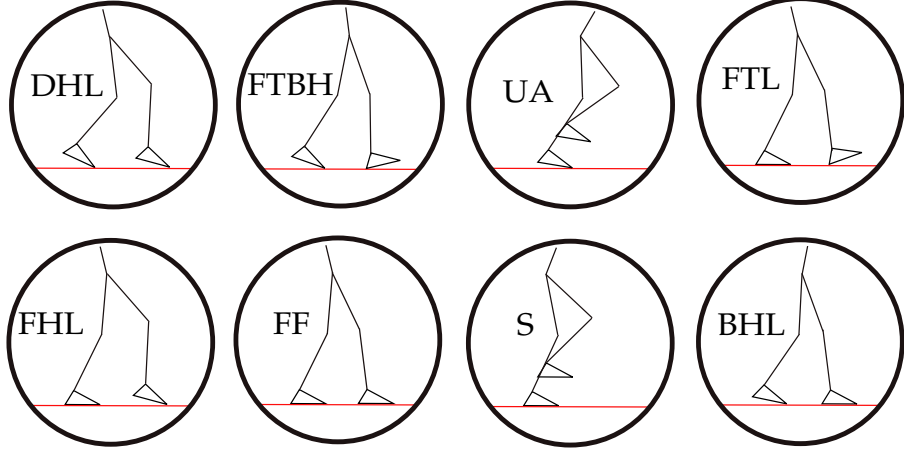


Figure 4.3: Representation of different possible domains for bipedal robotic dancing of AMBER2: double heel lift, front toe back heel lift, underactuated, front toe lift, front heel lift, flat footed, swing, back heel lift. There are eight possible vertices.

for AMBER2. Since we are specifically interested in affine systems, we will eventually deviate from the vector fields of the form (4.5). We will show basic stability and input to state stability properties for a general hybrid system, and then shift our focus on systems that are more interesting to us: systems with impulse effects.

For the hybrid control system (4.1), we substitute the control laws defined by (4.6) and the resulting closed loop dynamics are given by

$$\begin{aligned} f_v^{cl}(x) &= f_v(x, k_v(x)), \quad (x, k_v(x)) \in \mathbb{D}_v \setminus \mathbb{S}_v, v \in \mathbb{V} \\ \Delta_e^{cl}(x^-) &= \Delta_e(x^-, k_e(x^-)), \quad (x^-, k_e(x^-)) \in \mathbb{S}_e, e \in \mathbb{E}. \end{aligned} \quad (4.9)$$

Evolution of this closed loop dynamics over time is of interest to us. This evolution is called an execution of the hybrid system \mathcal{H} (4.7). The definition of execution is taken from [45, 46, 47].

Execution. The execution of the hybrid system, \mathcal{H} , is a tuple

$$(\Xi, \mathbf{I}, \rho, \mathbf{C}), \quad (4.10)$$

- $\Xi \subseteq \mathbb{N}_0$ is the indexing set.
- $\mathbf{I} = \{\mathbf{I}_i\}_{i \in \Xi}$ is the collection of intervals, e.g., $\mathbf{I}_i = [t_i, t_{i+1}]$ if $i, i+1 \in \Xi$ and $\mathbf{I}_{N-1} = [t_{N-1}, t_N]$ or $[t_{N-1}, t_N)$ or $[t_{N-1}, \infty)$ if $|\Xi| = N$, N is finite. Here $t_i, t_{i+1}, t_N \in \mathbb{R}_{\geq 0}$ and $t_i \leq t_{i+1}$.
- $\rho : \Xi \rightarrow \mathbb{V}$ is a map such that for all $i, i+1 \in \Xi$, $(\rho(i), \rho(i+1)) \in \mathbb{E}$.
- \mathbf{C} is the set of trajectories, $\{\mathbf{C}_i\}_{i \in \Xi}$, where each $\mathbf{C}_i : \mathbb{R}_{\geq 0} \rightarrow \pi_x(\mathbb{D}_{\rho(i)})$. They must satisfy $\dot{\mathbf{C}}_i(t) = f_{\rho(i)}^{cl}(\mathbf{C}_i(t))$ on \mathbf{I}_i along with some consistency conditions for all $i, i+1 \in \Xi$:
 - $\mathbf{C}_i(t_{i+1}) \in \pi_x(\mathbb{S}_{(\rho(i), \rho(i+1))})$.
 - $\Delta_{(\rho(i), \rho(i+1))}^{cl}(\mathbf{C}_i(t_{i+1})) = \mathbf{C}_{i+1}(t_{i+1})$.
 - $t_{i+1} = \min\{t \in \mathbf{I}_i : \mathbf{C}_i(t) \in \pi_x(\mathbb{S}_{(\rho(i), \rho(i+1))})\}$.

The closed loop dynamics $f_{\rho(i)}^{cl}, \Delta_{(\rho(i), \rho(i+1))}^{cl}$ are obtained from (4.9).

The execution is finite, if $\Xi \subset \mathbb{N}_0$ and all the intervals are closed $\mathbf{I}_i = [t_i, t_{i+1}]$ with $t_N < \infty$, it is infinite if $\Xi = \mathbb{N}_0$ or if $\sum_{i \in \Xi} t_{i+1} - t_i = \infty$. The thesis will not discuss finite executions, zeno executions and also consecutive jumps. Therefore, if $\Xi \subset \mathbb{N}_0$, then we have that $t_N = \infty \implies \mathbf{I}_{N-1} = [t_{N-1}, t_N)$, and if $\Xi = \mathbb{N}_0$, we have that $\lim_{i \rightarrow \infty} t_i = \infty$. Consecutive jumps are excluded for satisfying minimum dwell time conditions (required in 4.4.2). Therefore $\exists T > 0$ such that $t_{i+1} - t_i \geq T$, for all $i \in \Xi$.

Hybrid time domains. We can also define a *hybrid time domain* that is the union of the intervals, given by $\mathbf{T} := \bigcup_{i \in \Xi} (\mathbf{I}_i, i)$. Therefore, the execution of a hybrid system can also be given in terms of solutions that are functions of hybrid time domain (see [48] for a detailed analysis on hybrid time domains). The hybrid arc is nothing but the trajectory $\mathbf{C}_i(t)$, where $(t, i) \in \mathbf{T}$. The hybrid arc is the solution in the hybrid time domain $(t, i) \in \mathbf{T}$.

The hybrid control input for each $i \in \Xi$ can be obtained as

$$u_i(t) = \begin{cases} k_{\rho(i)}(\mathbf{C}_i(t)), & t \in [t_i, t_{i+1}) \\ k_{(\rho(i), \rho(i+1))}(\mathbf{C}_i(t)), & t = t_{i+1} \end{cases} \quad i, i+1 \in \Xi, \quad (4.11)$$

and if $\Xi \subset \mathbb{N}_0$

$$u_{\mathbf{N}-1}(t) = k_{\rho(\mathbf{N}-1)}(\mathbf{C}_{\mathbf{N}-1}(t)), \quad t \in [t_{\mathbf{N}-1}, t_{\mathbf{N}}]. \quad (4.12)$$

The hybrid control input is a function of the hybrid time domain, and for each $i \in \Xi$ the mapping from t to $u_i(t) = u(t, i)$ is Lebesgue measurable, locally essentially bounded on the interval $\{t : (t, i) \in \mathbf{T}\}$. It must be noted that there is a natural ordering of the hybrid intervals in the hybrid time domain, i.e., $i' \leq i \implies t_{i'} \leq t_i$. Therefore, we have the ordering for the hybrid intervals $(t', i') \leq (t, i)$, and $(t, i) \rightarrow \infty$ can be defined as either $t \rightarrow \infty$ or $i \rightarrow \infty$ or both $t, i \rightarrow \infty$. If Ξ is a proper subset of \mathbb{N}_0 , $(t, i) \rightarrow \infty$ implies $t \rightarrow \infty$. If $\Xi = \mathbb{N}_0$, $(t, i) \rightarrow \infty$ implies $i \rightarrow \infty$. For periodic orbits $(t, i) \rightarrow \infty$ implies $t \rightarrow \infty, i \rightarrow \infty$. Since zeno executions and chattering phenomena (also treated as zeno [45]) are not discussed, the case when $\lim_{i \rightarrow \infty} t_i < \infty$, for $\Xi = \mathbb{N}_0$, is not included in the thesis.

4.2 Stability and Stabilizability of Hybrid Systems

There is a significant amount of work done on the problem of stabilizing hybrid systems and switched systems. Some of the work include [21, 17, 18, 49, 22]. We will define basic notions of stability and then introduce the notion of stabilizability. Execution of the hybrid system yields the set of trajectories, \mathbf{C} . We will denote $x_i := \mathbf{C}_i$ for ease of notation. Therefore, $x_i(t) = \mathbf{C}_i(t), (t, i) \in \mathbf{T}$. Also denote $x(0) := x_0(t_0)$, where $t_0 = 0$.

Definition 31. *The origin, $x = 0$, of the hybrid system, \mathcal{H} , is stable if $\forall \delta_1 > 0, \exists \delta_2 > 0$ such that $|x_i(t)| \leq \delta_1, \forall (t, i) \in \mathbf{T}, \forall |x(0)| \leq \delta_2$.*

Definition 32. *The origin, $x = 0$, of the hybrid system, \mathcal{H} , is asymptotically stable, if it is stable and $\lim_{(t,i) \rightarrow \infty} |x_i(t)| = 0$.*

Definition 33. *The origin, $x = 0$, of the hybrid system, \mathcal{H} , is exponentially stable, if there are constants $\delta_1, \delta_2 > 0$ such that $|x_i(t)| \leq \delta_1 e^{-\delta_2(t+i)} |x(0)|$.*

For the hybrid system of the form (4.1), we have the following definition of a Lyapunov function.

Definition 34. *A continuously differentiable function $V : \mathbb{R}^n \rightarrow \mathbb{R}_{\geq 0}$ is a Lyapunov function for the hybrid system \mathcal{H} , (4.7), if there exist $\underline{\alpha}, \bar{\alpha}, \alpha \in \mathcal{K}_\infty$ such that for all v, e, x*

$$\begin{aligned} \underline{\alpha}(|x|) &\leq V(x) \leq \bar{\alpha}(|x|) \\ L_{f_v^{cl}} V(x) + \alpha(|x|) &\leq 0, \quad \text{if } (x, k_v(x)) \in \mathbb{D}_v \setminus \mathbb{S}_v \\ V(\Delta_e^{cl}(x)) - V(x) + \alpha(|x|) &\leq 0, \quad \text{if } (x, k_e(x)) \in \mathbb{S}_e. \end{aligned} \tag{4.13}$$

Converse Lyapunov theorems are valid even for hybrid systems under mild regularity conditions as given by [50, 51, 25, 52].

Lemma 12. *For hybrid systems of the form (4.7), asymptotic stability \iff existence of a Lyapunov function.*

The notion of stabilizability for hybrid systems in general has been dealt with in [17, 18, 16, 21, 22]. Note that stabilizability in this context means asymptotic stabilizability. The general stabilizability (Lyapunov stability criterion) notion presented in the thesis will be always asymptotic stability.

Definition 35. *The origin $x = 0$ of the hybrid system \mathcal{HC} is stabilizable if there are control laws $k_v : \mathbb{R}^n \rightarrow \mathbb{U}_v, v \in \mathbb{V}, k_e : \mathbb{R}^n \rightarrow \mathbb{U}_e, e \in \mathbb{E}$ such that the closed loop hybrid system \mathcal{H} is asymptotically stable.*

Similar definition can be obtained for exponential stability of hybrid systems. Since the interest is more on the existence of control Lyapunov functions for hybrid systems \mathcal{HC} , we will utilize the definitions obtained from [25]. Define

$$\pi_u(x, \mathbb{D}_v) := \{u \in \mathbb{U}_v \cup_{\{e \in \mathbb{E} | \text{source}(e)=v\}} \mathbb{U}_e | (x, u) \in \mathbb{D}_v\}. \quad (4.14)$$

We therefore have the set valued mappings $\pi_u^v : \mathbb{R}^n \rightrightarrows \mathbb{U}_v$, $\pi_u^e : \mathbb{R}^n \rightrightarrows \mathbb{U}_e$ as

$$\pi_u^v(x) := \pi_u(x, \mathbb{D}_v \setminus \mathbb{S}_v), \quad \pi_u^e(x) := \pi_u(x, \mathbb{S}_e). \quad (4.15)$$

We have the following definition of CLFs for hybrid systems.

Definition 36. A continuously differentiable function $V : \mathbb{R}^n \rightarrow \mathbb{R}_{\geq 0}$ is a control Lyapunov function for the hybrid control system \mathcal{HC} if there exist $\underline{\alpha}, \bar{\alpha}, \alpha \in \mathcal{K}_{\infty}$ such that for all $v \in \mathbb{V}, e \in \mathbb{E}$ and for all x

$$\begin{aligned} \underline{\alpha}(|x|) &\leq V(x) \leq \bar{\alpha}(|x|) \\ \inf_{u \in \pi_u^v(x)} [L_{f_v} V(x, u) + \alpha(|x|)] &\leq 0, \quad \text{if } (x, u) \in \mathbb{D}_v \setminus \mathbb{S}_v \\ \inf_{u \in \pi_u^e(x)} [V(\Delta_e(x, u)) - V(x) + \alpha(|x|)] &\leq 0, \quad \text{if } (x, u) \in \mathbb{S}_e \end{aligned} \quad (4.16)$$

Given the control Lyapunov function for the hybrid system, it is imperative that the hybrid control system is stabilizable. Based on these definitions, we therefore have the following Lemma obtained from [25].

Lemma 13. For hybrid systems of the form (4.1), existence of a smooth control Lyapunov function \iff stabilizability.

The Lemma is, of course, Artstein's theorem [23] applied for hybrid systems. The proof of this Lemma is given in [25], wherein the regularity conditions are applied.

4.3 Input to State Stability of Hybrid Systems

Input to state stability for hybrid systems is defined similar to continuous systems, with the norm on the disturbance inputs being the maximum value of the suprema of the inputs of individual events,

$$\|d\|_\infty = \sup_{i \in \Xi} \left\{ \max \left\{ \text{ess sup}_{t \in [t_{i-1}, t_i)} |d(t)|, |d(t_i)| \right\} \right\}. \quad (4.17)$$

Therefore d takes values in the space of all Lebesgue measurable functions $d \in \mathbb{L}_\infty^m$. With this norm, all the definitions from Definition 6 to 14 are valid with minor modifications. We define the \mathcal{KLL} function as the function with three arguments $\beta(|x|, t, i)$, where $\beta(|x|, t, i) \in \mathcal{KL}$ for a fixed i and $\beta(|x|, t, i) \in \mathcal{L}$ for a fixed $|x|, t$. Assume that the control law given by (4.6) is a stabilizing control law for the hybrid control system \mathcal{HC} , we are interested in studying the stability properties for control inputs of the form

$$u(x, d) = \begin{cases} k_v(x) + g'_v(x)d, & v \in \mathbb{V} \\ k_e(x) + g'_e(x)d, & e \in \mathbb{E} \end{cases}, \quad (4.18)$$

where $g' : \mathbb{R}^n \rightarrow \mathbb{R}^{m \times m}$ is a smooth invertible matrix. Based on this control law, we have a new hybrid control system

$$\begin{aligned} \mathcal{HC}^d &= (\Gamma, \mathbb{D}^d, \mathbb{S}^d, \mathbb{U}^d, \Delta^d, \mathbb{F}^d) \\ \mathbb{D}^d &= \{\mathbb{D}_v^d\}_{v \in \mathbb{V}} \\ \mathbb{S}^d &= \{\mathbb{S}_e^d\}_{e \in \mathbb{E}} \\ \mathbb{U}^d &= \{\{\mathbb{U}_v^d\}_{v \in \mathbb{V}}, \{\mathbb{U}_e^d\}_{e \in \mathbb{E}}\} \\ \Delta^d &= \{\Delta_e^d\}_{e \in \mathbb{E}} \\ \mathbb{F}^d &= \{f_v^d\}_{v \in \mathbb{V}}, \end{aligned} \quad (4.19)$$

where each $\mathbb{U}_\square^d \subset \mathbb{L}_\infty^m$ is the set of Lebesgue measurable disturbance inputs. The domains and the guards are given by $\mathbb{D}_v^d \subset \mathbb{R}^n \times \mathbb{L}_\infty^m$, $\mathbb{S}_e^d \subset \mathbb{D}_{\text{source}(e)}^d$, Δ^d is the set of switching functions specifically described as

$$\Delta_e^d(x^-, d) = \Delta_e(x^-, k_e(x^-) + g'_e(x^-)d), \quad (x^-, d) \in \mathbb{S}_e, \quad (4.20)$$

and \mathbb{F}^d provides the set of vector fields that yield the continuous dynamics

$$\dot{x} = f_v^d(x, d) = f_v(x, k_v(x) + g'_v(x)d), \quad (x, d) \in \mathbb{D}_v \setminus \mathbb{S}_v. \quad (4.21)$$

Note that the disturbance d has dependency on the states of the system. This requirement is mandatory to avoid cases not included in the model. For example, for bipedal robots, slipping conditions are not included and the control input applied should be in the domain of admissibility. We therefore have the following sets

$$\begin{aligned} \mathbb{S}_e^d &:= \{(x, d) \in \mathbb{R}^n \times \mathbb{L}_\infty^m | (x, k_e(x) + g'_e(x)d) \in \mathbb{S}_e\}, \quad e \in \mathbb{E} \\ \mathbb{S}_v^d &:= \bigcup_{\{e \in \mathbb{E} | \text{source}(e) = v\}} \mathbb{S}_e^d \\ \mathbb{D}_v^d &:= \{(x, d) \in \mathbb{R}^n \times \mathbb{L}_\infty^m | (x, k_v(x) + g'_v(x)d) \in \mathbb{D}_v \setminus \mathbb{S}_v\} \cup \mathbb{S}_v^d, \quad v \in \mathbb{V}, \end{aligned} \quad (4.22)$$

where k_v, k_e are obtained after applying a feedback controller (see (4.18)) that also satisfy $(x, k_v(x)) \in \mathbb{D}_v \setminus \mathbb{S}_v$, $(x, k_e(x)) \in \mathbb{S}_e$.

Therefore, for hybrid control systems of the form (4.19), we have the following definitions of input to state stability. Let $x_0 := x(0) = x_0(t_0)$. Similar to \mathcal{KL} functions, there are also \mathcal{KLL} functions that are utilized here for defining ISS. If $\beta \in \mathcal{KLL}$, then $\beta(|x|, t, i) \rightarrow 0$ as $i \rightarrow 0$.

Definition 37. *The system \mathcal{HC}^d is input to state stable w.r.t. the input d if there exist*

$\beta \in \mathcal{KLL}$, $\iota \in \mathcal{K}_\infty$ such that

$$|x_i(t, x_0, d)| \leq \beta(|x_0|, t, i) + \iota(\|d\|_\infty), \quad \forall x_0, \forall (t, i) \in \mathbf{T}, \forall d. \quad (4.23)$$

Definition 38. The system \mathcal{HC}^d is exponential input to state stable w.r.t. the input d if there exist $\beta \in \mathcal{KLL}$, $\iota \in \mathcal{K}_\infty$, and $\lambda > 0$ such that

$$|x_i(t, x_0, d)| \leq \beta(|x_0|, t, i)e^{-\lambda(t+i)} + \iota(\|d\|_\infty), \quad \forall x_0, \forall (t, i) \in \mathbf{T}, \forall d. \quad (4.24)$$

Definition 39. A continuously differentiable function $V : \mathbb{R}^n \rightarrow \mathbb{R}_{\geq 0}$ is an ISS-Lyapunov function for the hybrid control system \mathcal{HC}^d if there exist $\underline{\alpha}, \bar{\alpha}, \iota \in \mathcal{K}_\infty$ such that for all $v \in \mathbb{V}, e \in \mathbb{E}$ and for all x, d

$$\begin{aligned} \underline{\alpha}(|x|) &\leq V(x) \leq \bar{\alpha}(|x|) \\ L_{f_v^d} V(x, d) &\leq -\alpha(|x|) + \iota(\|d\|_\infty), \quad \text{if } (x, d) \in \mathbb{D}_v^d \setminus \mathbb{S}_v^d \\ V(\Delta_e^d(x, d)) - V(x) &\leq -\alpha(|x|) + \iota(\|d\|_\infty), \quad \text{if } (x, d) \in \mathbb{S}_e^d. \end{aligned} \quad (4.25)$$

We have the following definition of an input to state stabilizing control Lyapunov function for hybrid systems. For more details on the definition of ISS-CLFs for hybrid systems, see [53]. Similar to the weak ISSability notion introduced in Chapters 2, 3, we will study a weak form of ISS-CLF here.

Definition 40. A continuously differentiable function $V : \mathbb{R}^n \rightarrow \mathbb{R}_{\geq 0}$ is a weak input to state stabilizing control Lyapunov function (weak-ISS-CLF) for the hybrid control system \mathcal{HC} if there exist $\underline{\alpha}, \bar{\alpha}, \alpha, \iota \in \mathcal{K}_\infty$, and an invertible $g' : \mathbb{R}^n \rightarrow \mathbb{R}^{m \times m}$ such that for all

$v \in \mathbb{V}, e \in \mathbb{E}$ and for all x, d

$$\underline{\alpha}(|x|) \leq V(x) \leq \bar{\alpha}(|x|)$$

$$\begin{aligned} \inf_{u \in \pi_u^v(x)} [L_{f_v} V(x, u + g'_v(x)d) + \alpha(|x|)] &\leq \iota(\|d\|_\infty), \quad \text{if } (x, d) \in \mathbb{D}_v^d \setminus \mathbb{S}_v^d \\ \inf_{u \in \pi_u^e(x)} [V(\Delta_e^f(x, u + g'_e(x)d)) - V(x) + \alpha(|x|)] &\leq \iota(\|d\|_\infty), \quad \text{if } (x, d) \in \mathbb{S}_e^d. \end{aligned} \quad (4.26)$$

Note that the set valued maps π_u^v, π_u^e are obtained from (4.15) which always satisfy $(x, u) \in \mathbb{D}_v$. The allowable disturbance is restricted by the control law (see (4.22)). A more detailed discussion on ISS notion for hybrid systems can be found in [15, 54, 55, 56].

Definition 41. *The hybrid control system \mathcal{HC} , (4.1), is weak input to state stabilizable, if there is a control law of the form (4.6), such that the resulting hybrid control system, \mathcal{HC}^d (4.19) is input to state stable. The system is strong input to state stabilizable, if $g' \equiv \mathbf{1}_{m \times m}$.*

We have the following Lemma that is obtained from [15].

Lemma 14. *For hybrid control systems of the form (4.1), smooth stabilizability implies smooth weak input to state stabilizability.*

It can be observed that Lemma 14 only yields input to state stability for controllers of the form (4.18) for both discrete and continuous time systems. This can be indeed re-framed in the form of CLFs.

Lemma 15. *For hybrid control systems of the form (4.1), existence of a smooth CLF implies the existence of a smooth weak-ISS-CLF.*

Proof. By Lemma 13, CLF \Rightarrow stabilizability. By Lemma 14 stabilizability \Rightarrow input to state stabilizability. Therefore given any stabilizing controller, we can always find an input to state stabilizing controller $k_\square(x) \in \mathbb{U}_\square$, and an invertible $g'_\square(x) \in \mathbb{R}^{m \times m}$ such

that for the control law (4.18), the new resulting hybrid control system (4.19) is input to state stable w.r.t. the disturbance d . Therefore, for each controller belonging to the set defined by the CLFs, an ISSable (input to state stabilizable) controller can be picked, with the resulting CLF satisfying the conditions of an ISS-Lyapunov function. \square

As mentioned in 2.3, we are more interested in strong input to state stability conditions in hybrid systems. The weak ISS conditions become strong if the hybrid system is globally Lipschitz with respect to the control input u . With the interest of including only those classes of systems that satisfy strong ISS properties, we analyze continuous dynamics that are affine in controls. Therefore, we have a hybrid control system consisting of the tuple

$$\mathcal{AHC} = (\Gamma, \mathbb{D}, \mathbb{S}, \mathbb{U}, \Delta^{fg}, \mathbb{FG}), \quad (4.27)$$

where now all the notations have the usual definitions except Δ^{fg} , \mathbb{FG} , which is represented as follows $\mathbb{FG} = \{(f_{v_1}, g_{v_1}), (f_{v_2}, g_{v_2}), \dots\}$ provides the set of vector fields given by the equation

$$\dot{x} = f_v(x) + g_v(x)u, \quad (x, u) \in \mathbb{D}_v \setminus \mathbb{S}_v, v \in \mathbb{V}. \quad (4.28)$$

The switching functions are also redefined to have affinity properties, but has no significant advantage over the non-affine representation. $\Delta^{fg} = \{\Delta_{e_1}^{fg}, \Delta_{e_2}^{fg}, \dots\}$, where each $\Delta_{e_i}^{fg} = (\Delta_{e_i}^f, \Delta_{e_i}^g)$ is the set of switching functions or reset maps from one domain to the next domain. We have

$$x^+ = \Delta_e^f(x^-) + \Delta_e^g(x^-)u, \quad (x^-, u) \in \mathbb{S}_e, e \in \mathbb{E}. \quad (4.29)$$

The hybrid control system representation (4.27) is not unique, and can be done in the form

of equations as

$$\mathcal{AHC} = \begin{cases} \dot{x} = f_{v_1}(x) + g_{v_1}(x)u, & (x, u) \in \mathbb{D}_{v_1} \setminus \mathbb{S}_{v_1}, \\ \dot{x} = f_{v_2}(x) + g_{v_2}(x)u, & (x, u) \in \mathbb{D}_{v_2} \setminus \mathbb{S}_{v_2}, \\ \dot{x} = f_{v_3}(x) + g_{v_3}(x)u, & (x, u) \in \mathbb{D}_{v_3} \setminus \mathbb{S}_{v_3}, \\ \vdots \\ x^+ = \Delta_{e_1}^f(x^-) + \Delta_{e_1}^g(x^-)u, & (x^-, u) \in \mathbb{S}_{e_1}, \\ x^+ = \Delta_{e_2}^f(x^-) + \Delta_{e_2}^g(x^-)u, & (x^-, u) \in \mathbb{S}_{e_2}, \\ x^+ = \Delta_{e_3}^f(x^-) + \Delta_{e_3}^g(x^-)u, & (x^-, u) \in \mathbb{S}_{e_3}, \\ \vdots \end{cases} \quad (4.30)$$

(4.30) is an alternate form of an affine hybrid control system, where the controls are affine in both continuous and discrete dynamics.

4.4 Systems with Impulse Effects

If we include only those hybrid systems with affine controls in the continuous dynamics, and no controls in the discrete dynamics, then we have a special class of hybrid systems. These types of systems are typical of bipedal robots, where the discrete dynamics is the impact dynamics. In other words, the discrete dynamics cannot be controlled (which is a much harder problem to solve). These systems are generally called *systems with impulsive effects* or *systems with impulse effects* or even *systems with impulses*. Hybrid mechanical systems can be modeled in this fashion.

This class of systems can be modeled as a tuple:

$$\mathcal{IHC} = (\Gamma, \mathbb{D}, \mathbb{S}, \mathbb{U}, \Delta, \mathbb{FG}), \quad (4.31)$$

which is the redefinition of (4.30). The jump map (or the reset map) Δ is redefined to not

have control inputs as arguments:

$$x^+ = \Delta_e(x^-), \quad x^- \in \pi_x(\mathbb{S}_e), x^+ \in \pi_x(\mathbb{D}_{\text{target}(e)}), e \in \mathbb{E}, \quad (4.32)$$

(4.31) can also be represented in the form of equations as

$$\mathcal{IHC} = \begin{cases} \dot{x} = f_{v_1}(x) + g_{v_1}(x)u, & (x, u) \in \mathbb{D}_{v_1} \setminus \mathbb{S}_{v_1}, \\ \dot{x} = f_{v_2}(x) + g_{v_2}(x)u, & (x, u) \in \mathbb{D}_{v_2} \setminus \mathbb{S}_{v_2}, \\ \dot{x} = f_{v_3}(x) + g_{v_3}(x)u, & (x, u) \in \mathbb{D}_{v_3} \setminus \mathbb{S}_{v_3}, \\ \vdots \\ x^+ = \Delta_{e_1}(x^-), & x^- \in \pi_x(\mathbb{S}_{e_1}), \\ x^+ = \Delta_{e_2}(x^-), & x^- \in \pi_x(\mathbb{S}_{e_2}), \\ x^+ = \Delta_{e_3}(x^-), & x^- \in \pi_x(\mathbb{S}_{e_3}), \\ \vdots \end{cases} \quad (4.33)$$

More details on the definition of systems with impulse effects can be found in [57]. Based on constructions of converse Lyapunov theorems for hybrid systems, we know that if there is a closed loop control law $u(x) = k_v(x)$, $(x, k_v(x)) \in \mathbb{D}_v \setminus \mathbb{S}_v$, $v \in \mathbb{V}$ that stabilizes the new hybrid control system (4.31), then there is a Lyapunov function of the form

$$\begin{aligned} \underline{\alpha}(|x|) &\leq V(x) \leq \bar{\alpha}(|x|) \\ L_{f_v}V(x) + L_{g_v}V(x)k_v(x) + \alpha(|x|) &\leq 0, \quad \text{if } (x, k_v(x)) \in \mathbb{D}_v \setminus \mathbb{S}_v \\ V(\Delta_e(x)) - V(x) + \alpha(|x|) &\leq 0, \quad \text{if } x \in \pi_x(\mathbb{S}_e), \end{aligned} \quad (4.34)$$

for all e, v, x . We can also study control inputs with disturbances: $u(x) = k_v(x) + d$, $(x, k_v(x) + d) \in \mathbb{D}_v \setminus \mathbb{S}_v$. We therefore, have the resulting hybrid control system with the

input being the disturbances:

$$\mathcal{IHC}^d = (\Gamma, \mathbb{D}^d, \mathbb{S}^d, \mathbb{U}^d, \Delta^d, \mathbb{F}\mathbb{G}^d), \quad (4.35)$$

where the notations are similar to the derivations used for (4.19) with the only difference being the omission of the control input for the reset map. The stabilizing controllers k_v for the continuous dynamics can be obtained via CLFs.

Definition 42. A continuously differentiable function $V : \mathbb{R}^n \rightarrow \mathbb{R}_{\geq 0}$ is a control Lyapunov function for the hybrid control system \mathcal{IHC} if there exist $\underline{\alpha}, \bar{\alpha}, \alpha \in \mathcal{K}_\infty$ such that for all for all $x, v \in \mathbb{V}, e \in \mathbb{E}$

$$\begin{aligned} \underline{\alpha}(|x|) &\leq V(x) \leq \bar{\alpha}(|x|) \\ \inf_{u \in \pi_u^v(x)} [L_{f_v} V(x) + L_{g_v} V(x)u + \alpha(|x|)] &\leq 0, \quad \text{if } (x, u) \in \mathbb{D}_v \setminus \mathbb{S}_v \\ V(\Delta_e(x)) - V(x) + \alpha(|x|) &\leq 0, \quad \text{if } x \in \pi_x(\mathbb{S}_e). \end{aligned} \quad (4.36)$$

The set valued map, compared to (4.15), has a slightly different formulation: $\pi_u^v(x) := \{u \in \mathbb{U}_v | (x, u) \in \mathbb{D}_v \setminus \mathbb{S}_v\}$. A similar definition for ISS-CLFs is given below. See [53] for more details and for a more generic definition of ISS-CLFs for hybrid systems.

Definition 43. A continuously differentiable function $V : \mathbb{R}^n \rightarrow \mathbb{R}_{\geq 0}$ is an input to state stabilizing control Lyapunov function for the hybrid control system \mathcal{IHC} if there exist $\underline{\alpha}, \bar{\alpha}, \alpha, \iota \in \mathcal{K}_\infty$ such that $\forall v, e, x, d$

$$\begin{aligned} \underline{\alpha}(|x|) &\leq V(x) \leq \bar{\alpha}(|x|) \\ \inf_{u \in \pi_u^v(x)} [L_{f_v} V(x) + L_{g_v} V(x)u + L_{g_v} V(x)d + \alpha(|x|)] &\leq \iota(\|d\|_\infty), \quad \text{if } (x, d) \in \mathbb{D}_v^d \setminus \mathbb{S}_v^d \\ V(\Delta_e(x)) - V(x) + \alpha(|x|) &\leq 0, \quad \text{if } x \in \pi_x(\mathbb{S}_e^d). \end{aligned} \quad (4.37)$$

We can also study exponentially stabilizing CLFs for these types of systems in the following manner.

Definition 44. A continuously differentiable function $V : \mathbb{R}^n \rightarrow \mathbb{R}_{\geq 0}$ is an exponentially stabilizing control Lyapunov function for the hybrid control system \mathcal{IHC} if there exist $\underline{c}, \bar{c}, c > 0$ such that for all for all v, e, x

$$\begin{aligned} \underline{c}\|x\|^2 &\leq V(x) \leq \bar{c}\|x\|^2 \\ \inf_{u \in \pi_u^v(x)} [L_{f_v}V(x) + L_{g_v}V(x)u + cV(x)] &\leq 0, \quad \text{if } (x, u) \in \mathbb{D}_v \setminus \mathbb{S}_v \\ V(\Delta_e(x)) - V(x) + e^{-c}V(x) &\leq 0, \quad \text{if } x \in \pi_x(\mathbb{S}_e). \end{aligned} \tag{4.38}$$

A similar definition for e-ISS-CLFs is given below.

Definition 45. A continuously differentiable function $V : \mathbb{R}^n \rightarrow \mathbb{R}_{\geq 0}$ is an exponential input to state stabilizing control Lyapunov function for the hybrid control system \mathcal{IHC} if there exist $\underline{c}, \bar{c}, c > 0$ such that $\forall v, e, x, d$

$$\begin{aligned} \underline{c}\|x\|^2 &\leq V(x) \leq \bar{c}\|x\|^2 \\ \inf_{u \in \pi_u^v(x)} [L_{f_v}V(x) + L_{g_v}V(x)u + L_{g_v}V(x)d + cV(x)] &\leq \iota(\|d\|_\infty), \quad \text{if } (x, d) \in \mathbb{D}_v^d \setminus \mathbb{S}_v^d \\ V(\Delta_e(x)) - V(x) + e^{-c}V(x) &\leq 0, \quad \text{if } x \in \pi_x(\mathbb{S}_e^d). \end{aligned} \tag{4.39}$$

We have the following Lemma, which guarantees existence of ISS-CLFs for hybrid systems.

Lemma 16. For systems of the form \mathcal{IHC} , existence of a CLF of the form (4.36) implies the existence of an ISS-CLF of the form (4.37).

Proof. Based on the constructions of CLF obtained from (4.36), we pick a CLF V that

satisfies the following form for all v, e, x :

$$\begin{aligned} \underline{\alpha}(|x|) &\leq V(x) \leq \bar{\alpha}(|x|) \\ \inf_{u \in \pi_u^v(x)} [L_{f_v}V(x) + L_{g_v}V(x)u + L_{g_v}V(x)L_{g_v}V(x)^T + \alpha(|x|)] &\leq 0, \quad \text{if } (x, u) \in \mathbb{D}_v \setminus \mathbb{S}_v \\ V(\Delta_e(x)) - V(x) + \alpha(|x|) &\leq 0, \quad \text{if } x \in \pi_x(\mathbb{S}_e), \end{aligned} \quad (4.40)$$

for some $\underline{\alpha}, \bar{\alpha}, \alpha \in \mathcal{K}_\infty$. It can be verified that (4.40) is indeed a CLF. For a control law of this type, we know that

$$\begin{aligned} \dot{V}(x, u + d) &= L_{f_v}V(x) + L_{g_v}V(x)u + L_{g_v}V(x)d \\ &\leq -\alpha(|x|) - L_{g_v}V(x)L_{g_v}V(x)^T + L_{g_v}V(x)d, \end{aligned} \quad (4.41)$$

and based on results from (3.12), we have

$$L_{f_v}V(x) + L_{g_v}V(x)u + L_{g_v}V(x)d \leq -\alpha(|x|) + \bar{\varepsilon} \frac{\|d\|_\infty^2}{4}, \quad (4.42)$$

which satisfies the conditions of ISS-CLF for hybrid systems. \square

Due to the difficulty in obtaining the common CLFs for hybrid systems in general, we will study CLFs that render exponential stability of the continuous dynamics. As was shown in [28], RES-CLFs (of the form (3.16)) also render exponential stability of the entire hybrid system, by just rapidly exponentially stabilizing the continuous dynamics. Input to state stabilizing controllers inspired by these RES-CLFs will be discussed now.

4.4.1 Exponentially Stabilizing CLFs of the Continuous Dynamics

Given a stable hybrid system, converse Lyapunov theorems guarantee existence of Lyapunov functions (see [51, 58]) that are decreasing along solutions of the system. Similar results for control Lyapunov functions can also be easily established (see [25]). Existence

of these functions are a powerful result, but not enough for finding Lyapunov functions in general. On the other hand, it can be shown that it is possible to stabilize these classes of hybrid systems by just stabilizing the continuous dynamics under certain conditions. This is based on the work on RES-CLF based controllers from [28]. Some of the conditions that are included are hybrid invariance, i.e., for all $e \in \mathbb{E}$, $\Delta_e(0) = 0$, average dwell time (explained further in (4.46)). These types of controllers exponentially stabilize the continuous dynamics. In other words, the systems included are the classes that have exponentially stabilizable continuous dynamics. These kinds of systems naturally model hybrid mechanical systems like bipedal robots, which are feedback linearizable under certain conditions (partially feedback linearizable systems are studied in Chapter 5). Given the hybrid system, \mathcal{IHC} (4.31), we use the stabilizing control law (obtained from (3.3))

$$u(x) = k_v(x) \in \mathbf{K}_v(x), \quad (x, k_v(x)) \in \mathbb{D}_v \setminus \mathbb{S}_v, \quad v \in \mathbb{V}, \quad (4.43)$$

for the continuous dynamics. \mathbf{K}_v is the set of controllers obtained from (3.3) that is domain dependent:

$$\mathbf{K}_v(x) = \{u \in \pi_u^v(x) | L_{f_v} V(x) + L_{g_v} V(x)u + cV(x) \leq 0\}, \quad v \in \mathbb{D}_v. \quad (4.44)$$

Applying the control law (4.43) yields the closed loop hybrid system: $\mathcal{IHC} = (\Gamma, \mathbb{D}, \mathbb{S}, \Delta, \mathbb{F}_k)$.
 $\mathbb{F}_k = \{f_{v_1} + g_{v_1}k_{v_1}, f_{v_2} + g_{v_2}k_{v_2}, \dots\}$.

We have the result from [54, 55, 59, 60], which shows that for systems of the form (4.31), e-ISS of the continuous dynamics with average dwell time implies ISS of the entire system. We will define the dwell time condition as follows. Let $N(s_1, s_2)$ denote the number of impulse times in the semi-open interval $[s_1, s_2)$. Therefore, if $i, i+1, \dots, i+j \in \Xi$ is the indexing, such that $t_i, t_{i+1}, \dots, t_{i+j} \in [s_1, s_2)$, then $N(s_1, s_2) = j$. With this number, we can define a candidate e-ISS Lyapunov function for systems with impulses in the following manner:

Definition 46. A continuously differentiable function $V : \mathbb{R}^n \rightarrow \mathbb{R}_{\geq 0}$ is a candidate exponential ISS-Lyapunov function for the hybrid system \mathcal{IH} if there exist $\underline{c}, \bar{c}, c_1, c_2 > 0$, and $\iota \in \mathcal{K}_\infty$ such that $\forall v, e, x, d$

$$\begin{aligned} \underline{c}\|x\|^2 &\leq V(x) \leq \bar{c}\|x\|^2 \\ \dot{V}(x, d) &\leq -c_1 V(x) + \iota(\|d\|_\infty), \quad \text{if } (x, d) \in \mathbb{D}_v^d \setminus \mathbb{S}_v^d \\ V(\Delta_e(x)) &\leq e^{c_2} V(x) + \iota(\|d\|_\infty), \quad \text{if } x \in \pi_x(\mathbb{S}_e^d). \end{aligned} \quad (4.45)$$

We have the following Lemma that is obtained from [59] and reformulated to correctly represent the systems that are of interest to us, i.e., stabilizing continuous dynamics but destabilizing impulse effects. This Lyapunov function is a suitable candidate for representing the dynamics of (4.31).

Lemma 17. Let V be a candidate e -ISS-Lyapunov function for \mathcal{IH} with $c > 0$ specifying the convergence rate. Then for arbitrary constants $a_1, a_2 > 0$, let the set of impulsive time sequences $\{t_i\}_{i \in \Xi}$ satisfy

$$c_2 N(s_1, s_2) + (c_1 + a_1)(s_1 - s_2) \leq a_2 \quad \forall s_2 \geq s_1 \geq t_0. \quad (4.46)$$

Then the system (4.31) is ISS.

Proof of the above Lemma is found in [59]. It is important to note that the expression for the number of impulse times can be simplified as

$$N(s_1, s_2) \leq \frac{c_1 + a_1}{c_2}(s_2 - s_1) + a_2, \quad (4.47)$$

which shows a linear relationship between the time interval and the number of discrete transitions. This is called the average-dwell-time (ADT), which was first introduced in [61].

We can now introduce the main contribution that establishes the existence of an input to state stabilizing CLF given the stabilizing CLF.

Theorem 1. *If there exists an ES-CLF for the continuous dynamics that exponentially stabilizes the hybrid control system, \mathcal{IHC} (4.31), and if the ADT condition (4.46) is satisfied, then there exists an e-ISS-CLF for the continuous dynamics that input to state stabilizes this hybrid control system.*

Proof. Similar to the construction of e-ISS-CLFs for continuous systems (3.9), we construct the ISS based controllers based on the constructions from CLF. Therefore, given the CLF for the continuous dynamics, we have the e-ISS-CLF from (3.14):

$$\begin{aligned} \underline{c}\|x\|^2 &\leq V(x) \leq \bar{c}\|x\|^2 \\ \inf_{u \in \pi_u^v(x)} [L_{f_v}V(x) + L_{g_v}V(x)u + cV(x) + \frac{1}{\bar{\varepsilon}}L_{g_v}V(x)L_{g_v}V(x)^T] &\leq 0, \quad (x, u) \in \mathbb{D}_v \setminus \mathbb{S}_v, \end{aligned} \quad (4.48)$$

for each $v \in \mathbb{V}$ with the constants $\underline{c}, \bar{c}, c$ having the usual meaning from (3.14). We know that this equation satisfies the ISS-Lyapunov function inequality for all d for the continuous dynamics. Therefore assuming that the impulse maps are Lipschitz, we can have the following two inequalities:

$$\begin{aligned} \dot{V}(x, d) &\leq -cV(x) + \iota(\|d\|_\infty), \quad \text{if } (x, d) \in \mathbb{D}_v^d \setminus \mathbb{S}_v^d \\ V(\Delta_e(x)) &\leq \frac{\bar{c}}{\underline{c}}L_\Delta^2 V(x), \quad \text{if } x \in \pi_x(\mathbb{S}_e^d), \end{aligned} \quad (4.49)$$

which is in the form given by (4.45). L_Δ is the maximum of the Lipschitz constants of all the impact maps. It is assumed that $\Delta_e(0) = 0$. The average dwell time condition (4.46) can be used by substituting for $c_1 = c$ and $e^{c_2} = \frac{\bar{c}}{\underline{c}}L_\Delta^2$. Satisfying this condition yields ISS. \square

Note that Theorem 1 requires the ADT conditions to be satisfied to yield sufficient conditions that results in ISS. An alternative is also to use RES-CLFs (from (3.16)) and use

the user defined $\varepsilon > 0$ to manually adjust the ADT conditions to yield both stabilization and input to state stabilization results.

Non-hybrid invariance conditions. Assuming $\Delta_e(0) \neq 0$. We can rewrite the impact equations

$$\|\Delta_e(x) - \Delta_e(0) + \Delta_e(0)\| \leq L_\Delta \|x\| + \|\Delta_e(0)\|. \quad (4.50)$$

We therefore have

$$V(\Delta_e(x)) \leq \frac{\bar{c}}{\underline{c}} L_\Delta^2 V(x) + 2L_\Delta \|x\| \|\Delta_e(0)\| + \|\Delta_e(0)\|^2, \quad x \in \pi_x(\mathbb{S}_e), \quad (4.51)$$

The last two terms can be termed the disturbance input that appears in the impact dynamics. Therefore, the inequality for the Lyapunov candidate (4.49) will take the following form

$$\begin{aligned} \dot{V}(x, d) &\leq -cV(x) + \iota(\|d\|_\infty), \quad \text{if } (x, d) \in \mathbb{D}_v^d \setminus \mathbb{S}_v^d \\ V(\Delta_e(x)) &\leq \frac{\bar{c}}{\underline{c}} L_\Delta^2 V(x) + \|d_i\|_\infty, \quad \text{if } x \in \pi_x(\mathbb{S}_e^d), \end{aligned} \quad (4.52)$$

where $d_i = 2L_\Delta \|x\| \|\Delta_e(0)\| + \|\Delta_e(0)\|^2$. As was shown in [54], hybrid systems with the dynamics of this type can also exhibit ISS under the bounded disturbances d, d_i . The boundedness assumption is reasonable locally.

4.4.2 Rapidly Exponential Input to State Stability and Minimum Dwell Time

Exponential stability conditions for these classes of hybrid systems can be realized by the choice of appropriate controllers. We analyze stabilizing controllers that rapidly exponentially stabilize the continuous dynamics. The advantage is with the increase in convergence rate, the destabilizing affect of discrete dynamics gets minimized under a hybrid invariance, and the ADT condition (see (4.46)) can be automatically satisfied. We know the discrete map is locally Lipschitz in the states, i.e., $\|\Delta_e(x) - \Delta_e(y)\| \leq L_{\Delta_e} \|x - y\|$. Lipschitz

continuity and hybrid invariance yields $\|\Delta_e(x)\| \leq L_{\Delta_e}\|x\|$. Let $\Xi = \mathbb{N}_0$. Therefore by applying the control law

$$u(x) = k_{v,\varepsilon}(x) \in \mathbf{K}_{v,\varepsilon}(x), \quad (x, k_{v,\varepsilon}(x)) \in \mathbb{D}_v \setminus \mathbb{S}_v, v \in \mathbb{V}, \quad (4.53)$$

we obtain the RES-CLF for the continuous dynamics, $V_\varepsilon : \mathbb{R}^n \rightarrow \mathbb{R}_{\geq 0}$, of the form given by (3.16). $\mathbf{K}_{v,\varepsilon}$ is obtained from (3.17):

$$\mathbf{K}_{v,\varepsilon}(x) = \{u \in \pi_u^v(x) | L_{f_v} V(x) + L_{g_v} V(x)u + cV(x) \leq 0\}, \quad v \in \mathbb{D}_v \setminus \mathbb{S}_v. \quad (4.54)$$

Applying this controller results in the closed loop hybrid system: $\mathcal{IH}^\varepsilon = (\Gamma, \mathbb{D}, \mathbb{S}, \Delta, \mathbb{F}^\varepsilon)$. $\mathbb{F}^\varepsilon = \{f_{v_1} + g_{v_1}k_{v_1,\varepsilon}, f_{v_2} + g_{v_2}k_{v_2,\varepsilon}, \dots\}$. By slight abuse of notations again, we denote the trajectories (or flow) of the system as $x_i(t) = \mathbf{C}_i(t)$ (from the execution (4.10) of this closed loop hybrid system).

$$\begin{aligned} V_\varepsilon(x_{i+1}(t_{i+1})) &= V_\varepsilon(\Delta_{(\rho(i), \rho(i+1))}(x_i(t_{i+1}))) \leq \frac{c_2}{\varepsilon} L_\Delta^2 \|x_i(t_{i+1})\|^2 \leq \frac{c_2}{\varepsilon c_1} L_\Delta^2 V_\varepsilon(x_i(t_{i+1})) \\ V_\varepsilon(x_i(t_{i+1})) &\leq e^{-\frac{c_3}{\varepsilon}(t_{i+1}-t_i)} V_\varepsilon(x_i(t_i)) \\ \implies V_\varepsilon(x_{i+1}(t_{i+1})) &\leq \frac{c_2}{\varepsilon c_1} L_\Delta^2 e^{-\frac{c_3}{\varepsilon}(t_{i+1}-t_i)} V_\varepsilon(x_i(t_i)). \end{aligned} \quad (4.55)$$

L_Δ is the maximum of the Lipschitz constants of all the jump maps of the hybrid system. If there is a finite $T > 0$ s.t. $t_{i+1} - t_i \geq T, \forall i \in \Xi$, we know that $V_\varepsilon \rightarrow 0$, as $\varepsilon \rightarrow 0$. We have the following Lemma, which shows that stability of the hybrid system can be realized via RES-CLFs (3.17).

Lemma 18. *Let the hybrid control system \mathcal{IH}^ε be of the form (4.31). For all classes of Lipschitz continuous feedback, $u(x) = k_{v,\varepsilon} \in \mathbf{K}_\varepsilon(x)$, if the minimum dwell time T for the continuous dynamics is nonzero, i.e., $t_{i+1} - t_i \geq T > 0, \forall i \in \Xi$, and if $\Delta_e(0) = 0, \forall e \in \mathbb{E}$, then for a sufficiently small $\varepsilon > 0$, the hybrid system \mathcal{IH}^ε , is exponentially stable.*

Proof. Proof is straightforward from (4.55). Since $t_{i+1} - t_i \geq T > 0, \forall i \in \Xi$, we have

$$V_\varepsilon(x_{i+1}(t_{i+1})) \leq \frac{c_2}{\varepsilon c_1} L_\Delta^2 e^{-\frac{c_3}{\varepsilon} T} V_\varepsilon(x_i(t_i)), \quad \forall i \in \Xi. \quad (4.56)$$

Let ε be small enough such that $\frac{c_2}{\varepsilon c_1} L_\Delta^2 e^{-\frac{c_3}{\varepsilon} T} < 1$ (a contraction). Therefore, we have $V_\varepsilon(x_i(t_i)) \rightarrow 0$ as $(t, i) \rightarrow \infty$, and $x \rightarrow 0$ as $V_\varepsilon \rightarrow 0$. \square

This minimum dwell time assumption was also used to prove stabilizability of linear switched systems in [14]. Given that a hybrid system is stabilizable, the interest is now refocused on the input to state stability property.

Given the hybrid system, \mathcal{IHC} , we use the control law from (3.20) that input to state stabilizes the continuous dynamics. We have

$$\begin{aligned} \mathbf{K}_{v,\varepsilon,\bar{\varepsilon}}(x) &= \{u \in \pi_u^v(x) \mid L_{f_v} V(x) + L_{g_v} V(x)u + \frac{1}{\bar{\varepsilon}} L_{g_v} V(x)L_{g_v} V(x)^T + \frac{c}{\varepsilon} V(x) \leq 0\}, \\ u(x) = k_{v,\varepsilon,\bar{\varepsilon}}(x) &\in \mathbf{K}_{v,\varepsilon,\bar{\varepsilon}}(x), \quad (x, k_{v,\varepsilon,\bar{\varepsilon}}(x)) \in \mathbb{D}_v \setminus \mathbb{S}_v, v \in \mathbb{V}. \end{aligned} \quad (4.57)$$

It can be shown that controllers from (4.57) yield exponential input to state stability for hybrid systems \mathcal{IHC} .

Theorem 2. *Given the RES-CLF of the continuous dynamics, $u(x) = k_{v,\varepsilon}(x) \in \mathbf{K}_{v,\varepsilon}(x)$ (4.53), that exponentially stabilizes the hybrid control system (4.31), then the Re-ISS-CLF of the continuous dynamics, $u(x) = k_{v,\varepsilon,\bar{\varepsilon}} \in \mathbf{K}_{v,\varepsilon,\bar{\varepsilon}}(x)$ (4.57), exponentially input to state stabilizes the hybrid control system (4.31).*

Proof. After substituting (4.53) in the derivative of V_ε , we have

$$\begin{aligned}
\dot{V}_\varepsilon(x, u + d) &\leq -\frac{\gamma}{\varepsilon}V_\varepsilon - \frac{1}{\bar{\varepsilon}}\|L_{g_v}V_\varepsilon\|^2 + L_{g_v}V_\varepsilon\|d\|_\infty \\
&\leq -\frac{\gamma}{\varepsilon}V_\varepsilon - \frac{1}{\bar{\varepsilon}}\|L_{g_v}V_\varepsilon\|^2 + L_{g_v}V_\varepsilon\|d\|_\infty - \bar{\varepsilon}\frac{\|d\|_\infty^2}{4} + \bar{\varepsilon}\frac{\|d\|_\infty^2}{4} \\
&\leq -\frac{\gamma}{\varepsilon}V_\varepsilon - \left(\frac{1}{\sqrt{\bar{\varepsilon}}}\|L_{g_v}V_\varepsilon\| - \sqrt{\bar{\varepsilon}}\frac{\|d\|_\infty}{2}\right)^2 + \bar{\varepsilon}\frac{\|d\|_\infty^2}{4} \\
&\leq -\frac{\gamma}{\varepsilon}V_\varepsilon + \bar{\varepsilon}\frac{\|d\|_\infty^2}{4} \\
&\leq -\frac{\gamma}{2\varepsilon}V_\varepsilon - \frac{\gamma}{2\varepsilon}c_1|x|^2 + \bar{\varepsilon}\frac{\|d\|_\infty^2}{4}.
\end{aligned} \tag{4.58}$$

Therefore, for $|x| \geq \sqrt{\frac{\bar{\varepsilon}\varepsilon}{2\gamma c_1}}\|d\|_\infty$ we get exponential convergence $\dot{V}_\varepsilon \leq -\frac{\gamma}{2\varepsilon}V_\varepsilon$. Therefore we have

$$V_\varepsilon(x_{i+1}(t_{i+1})) \leq \frac{c_2}{2\varepsilon c_1}L_\Delta^2 e^{-\frac{c_3}{2\varepsilon}T}V_\varepsilon(x_i(t_i)), \quad \forall i \in \Xi, |x_i| \geq \sqrt{\frac{\bar{\varepsilon}\varepsilon}{2\gamma c_1}}\|d\|_\infty. \tag{4.59}$$

We finish the proof by picking a sufficiently small ε . \square

4.4.3 Hybrid Periodic Orbits and Poincaré Maps

If the solutions are periodic, we can realize controllers that render periodic solutions for the hybrid system and the notion of input to stability of these periodic solutions can be established. Consequently, for the solutions that are periodic with period T^* , we can define Poincaré maps that motivate the construction of discrete time Lyapunov functions, from which the notion of input to stability for such periodic orbits can be established.

We will analyze periodic orbits for hybrid systems that have a directed cycle. We therefore have the set of l vertices

$$\mathbb{V}_c = \{v_1, v_2, \dots, v_l\}, \tag{4.60}$$

and the set of l edges

$$\mathbb{E}_c = \{e_1 = (v_1, v_2), e_2 = (v_2, v_3), \dots, e_l = (v_l, v_1)\}. \quad (4.61)$$

Therefore, the directed cycle is $\Gamma_c = (\mathbb{V}_c, \mathbb{E}_c)$. Accordingly, we have the set of domains, guards, vector fields and switching functions to yield a tuple:

$$\mathcal{IHC}_c = (\Gamma_c, \mathbb{D}_c, \mathbb{U}_c, \mathbb{S}_c, \Delta_c, \mathbb{FG}_c). \quad (4.62)$$

Application of a control law (say $u(x) = k_v(x)$, $(x, k_v(x)) \in \mathbb{D}_v \setminus \mathbb{S}_v$, $v \in \mathbb{V}$) yields the closed loop hybrid system

$$\mathcal{IHC}_c = (\Gamma_c, \mathbb{D}_c, \mathbb{S}_c, \Delta_c, \mathbb{F}_c), \quad \mathbb{F}_c := \{f_{v_1} + g_{v_1}k_{v_1}, f_{v_2} + g_{v_2}k_{v_2}, \dots\}. \quad (4.63)$$

A periodic orbit for this directed cycle can be defined below.

Definition 47. Let $(\Xi, \mathbf{I}, \rho, \mathbf{C})$, as obtained from (4.10), be the execution of the hybrid system with the directed cycle (4.63). The periodic orbit of this hybrid system is the execution satisfying the following:

- $\Xi = \mathbb{N}_0$.
- $\lim_{i \rightarrow \infty} t_i - t_0 = \infty$.
- $\rho(i) = \begin{cases} v_1 & \text{if } i = 0, 1, 2l, \dots \\ v_2 & \text{if } i = 1, l+1, 2l+1, \dots \\ \vdots & \\ v_l & \text{if } i = l-1, 2l-1, \dots \end{cases}$
- $\mathbf{C}_{li}(t_{li}) = \mathbf{C}_{l(i+1)}(t_{l(i+1)})$.

The period of this periodic orbit is $t_l - t_0$. A detailed account on executions for periodic orbits can be found in [46].

Definition 48. The flow of the closed loop vector field $f_{\rho(i)}^{cl}$ is the mapping $\varphi^{\rho(i)} : \mathbb{R}_{\geq 0} \times \mathbb{B} \rightarrow \pi_x(\mathbb{D}_{\rho(i)})$, where $\mathbb{B}(\mathbf{C}_i(t_i))$ is the neighborhood of $\mathbf{C}_i(t_i)$. The flow satisfies the following properties:

- $\mathbf{C}_i(t_i) = \varphi^{\rho(i)}(0, \mathbf{C}_i(t_i))$.
- $\mathbf{C}_i(t_i + t + s) = \varphi^{\rho(i)}(t, \varphi^{\rho(i)}(s, \mathbf{C}_i(t_i)))$.
- $\varphi^{\rho(i)}(-s, \varphi^{\rho(i)}(s, x)) = x, x \in \mathbb{B}(\mathbf{C}_i(t_i))$.

For convenience, we will use the notation for the flow: $\varphi_t^{\rho(i)}(x) := \varphi^{\rho(i)}(t, x)$. We can define the periodic orbit (from Definition 48) in terms of the flows

$$\mathcal{O} = \bigcup_{i=0,1,\dots,l-1} \{\varphi_t^{\rho(i)}(\mathbf{C}_i(t_i)) \in \mathbb{D}_{\rho(i)} : 0 \leq t \leq t_{i+1} - t_i\}. \quad (4.64)$$

We also have the time-to-switching function, i.e., time until the next discrete transition:

$$T_i = \min\{t \in \mathbf{I}_i : \varphi_t^{\rho(i)}(x) \in \mathbb{S}_{(\rho(i), \rho(i+1))}\}, \quad x \in \mathbb{B}(\mathbf{C}_i(t_i)) \cap \pi_x(\mathbb{S}_{(\rho(i), \rho(i+1))}). \quad (4.65)$$

The Poincaré map can be defined as the first return map:

$$\mathbb{P}_{\text{source}(e)} : \pi_x(\mathbb{S}_e) \rightarrow \pi_x(\mathbb{S}_e), \quad e \in \mathbb{E}, \quad (4.66)$$

or in terms of the indexing set Ξ :

$$\mathbb{P}_{\rho(i)} : \pi_x(\mathbb{S}_{(\rho(i), \rho(i+1))}) \rightarrow \pi_x(\mathbb{S}_{(\rho(i+l), \rho(i+l+1))}), \quad (4.67)$$

which can be obtained from the following:

$$\begin{aligned} \mathbb{P}_{\rho(i)}(x) &= \varphi_{T_{i+l}}^{\rho(i+l)} \circ \Delta_{(\rho(i+l), \rho(i+l-1))} \circ \dots \\ &\quad \circ \varphi_{T_{i+2}}^{\rho(i+2)} \circ \Delta_{(\rho(i+2), \rho(i+1))} \circ \varphi_{T_{i+1}}^{\rho(i+1)} \circ \Delta_{(\rho(i+1), \rho(i))}(x), \quad x \in \mathbb{S}_{(\rho(i), \rho(i+1))}. \end{aligned} \quad (4.68)$$

For this Poincaré map, we have the fixed point $x^* \in \mathbb{S}_{(\rho(i),\rho(i+1))}$ that satisfies $\mathbb{P}_{\rho(i)}(x^*) = x^*$.

Stability and ISS properties of periodic orbits can be studied by using Poincaré maps, in which the sequence of continuous and discrete events can be combined into one discrete event. This discrete event can be analyzed by using discrete-time Lyapunov functions. Therefore, we have the following formulations for the discrete-time ISS-Lyapunov function, $V : \mathbb{R}^n \rightarrow \mathbb{R}_{\geq 0}$, for some $\underline{\alpha}, \bar{\alpha}, \alpha, \iota \in \mathcal{K}_\infty$:

$$\underline{\alpha}(|x - x^*|) \leq V(x - x^*) \leq \bar{\alpha}(|x - x^*|) \quad (4.69)$$

$$V(\mathbb{P}_{\rho(i)}(x) - x^*) - V(x - x^*) \leq -\alpha(|x|) + \iota(\|d\|_\infty), \forall x \in \mathbb{B}(x^*) \cap \pi_x(\mathbb{S}_{(\rho(i),\rho(i+1))}), \forall d.$$

This motivates using the ISS criterion for hybrid systems as shown in the following Lemma.

Lemma 19. *If the Poincaré map $\mathbb{P}_{\text{source}(e)} : \pi_x(\mathbb{S}_e) \rightarrow \pi_x(\mathbb{S}_e)$ admits a continuous discrete ISS-Lyapunov function, then the periodic orbit \mathcal{O} of the cycle (4.63) is ISS.*

We can make use of this Lemma to show stability of bipedal robotic walking in AMBER1 (as shown in Fig. 6.1) and DURUS (as shown in Fig. 6.6), and also show running in DURUS (as shown in Fig. 6.7). In particular, we will focus on two kinds of uncertainty: parameter and phase uncertainty, that are prominent in bipedal walking robots. Under the assumption that the bipedal robot is zero stable when the model is perfectly known (parameter measure being identically zero), the notion of ISS motivates the introduction of a measure that is a function of the uncertainty in the robot model parameters, and show that the hybrid walking model of the robot is parameter to state stable. In a similar fashion, the modulation of the desired trajectories (gaits) are usually done through the phase variable, which is a function of the configuration of the robot. Joint angle estimation errors add together leading to inaccurate determination of the phase variable. This phase uncertainty results in unstable walking gaits, which is solved by choosing from a set of controllers that are phase to state stable.

Single domain hybrid systems. For single domain hybrid systems (simple hybrid systems), the subscript (or superscript) notations for the vertices and edges can be dropped to yield only one Poincaré map and flow with reference to the guard. For this type of hybrid system, the Poincaré map $\mathbb{P} : \pi_x(\mathbb{S}) \rightarrow \pi_x(\mathbb{S})$ (no subscript because of only one guard), can be defined as: $\mathbb{P}(x) = \varphi_T(\Delta(x))$, $x \in \pi_x(\mathbb{S})$, T is the time until the state returns to the guard \mathbb{S} . If $x^* \in \pi_x(\mathbb{S})$ is the fixed point of this Poincaré map, we have $\mathbb{P}(x^*) = x^*$. Therefore, we have a periodic orbit with period T^* , i.e., $\varphi_{T^*}(\Delta(x^*)) = x^*$. Therefore, in the neighborhood of the periodic solution, the Poincaré map allows for the reformulation of the hybrid event into a single discrete event. Assume that $\mathcal{O} = \{\varphi_t(\Delta(x^*)) \in \pi_x(\mathbb{D}) : 0 \leq t \leq T\}$ is the periodic orbit of the single domain hybrid system. If this periodic orbit is locally zero stable, then there is a constant $r > 0$ such that if x starts in a ball of radius r defined around \mathcal{O} , $\mathbb{B}_r(\mathcal{O})$, then $x(t) \rightarrow \mathcal{O}$ as $t \rightarrow \infty$. We can construct a discrete time ISS-Lyapunov function that has the following dissipation:

$$\begin{aligned} V(\mathbb{P}(x) - x^*) &\leq e^{-c}V(x - x^*) + \iota(\|d\|_\infty), \quad \forall x \in \pi_x(\mathbb{S}) \cap \mathbb{B}_r(x^*), \forall d, \\ \implies V(\mathbb{P}(x) - x^*) - V(x - x^*) &\leq -(1 - e^{-c})V(x - x^*) + \iota(\|d\|_\infty), \end{aligned} \quad (4.70)$$

for some $c > 0$, and $\iota \in \mathcal{K}_\infty$. This motivates using the ISS criterion for hybrid systems as shown in the following Lemma.

Lemma 20. *If the Poincaré map \mathbb{P} admits a smooth discrete ISS-Lyapunov function, then the periodic orbit \mathcal{O} of the simple version of the hybrid system (4.63) (one domain and one guard) is ISS.*

CHAPTER 5

INPUT TO STATE STABILIZING CONTROL LYAPUNOV FUNCTIONS AND HYBRID ZERO DYNAMICS

The goal of this chapter is to construct controllers, specifically control Lyapunov functions, and input to state stabilizing control Lyapunov functions on partially observable systems. The focus will be specifically on partially feedback linearizable systems. In this framework, bipedal robots can be modeled (shown in Chapter 6) that exhibit under-actuations and full actuations (and even overactuations). Inspired by feedback linearization, which is the most popular way of obtaining Lyapunov functions for robotic systems, we will construct CLFs that drive a set of outputs to zero. As a consequence of stabilizing these systems via CLFs, is the possibility of constructing the corresponding ISS-CLFs.

5.1 Trajectory Tracking Control

We will utilize trajectory tracking control laws and establish ISS versions of these control laws in this section. Multiple relative degrees are observed usually in the trajectory tracking of outputs (functions of states) in several hybrid system models. We will study outputs that are relative degrees one and two, and (as a side note) state extensibility to higher relative degrees. Therefore, for rigid body manipulators, we have the configuration space $\mathbb{Q} \subset \mathbb{R}^{n_R}$, with n_R the DOF of the manipulator, the joint positions/angles $q \in \mathbb{Q}$, joint velocities $\dot{q} \in T_q \mathbb{Q}$. Therefore, for systems such as these, we define the state $x \in T\mathbb{Q} \subset \mathbb{R}^{2n_R}$. In general, we are interested in stable trajectory tracking in hybrid systems with the continuous dynamics of the form (4.28), and discrete dynamics of the form (4.32). They are provided

here again for convenience:

$$\begin{aligned}\dot{x} &= f_v(x) + g_v(x)u, & (x, u) \in \mathbb{D}_v \setminus \mathbb{S}_v, v \in \mathbb{V}, \\ x^+ &= \Delta_e(x^-), & x^- \in \pi_x(\mathbb{D}_{\text{source}(e)}), e \in \mathbb{E},\end{aligned}\quad (5.1)$$

where the reset map is (4.4) with the omission of the control input. In brief, we will analyze hybrid systems of the form (4.31) with the only noticeable difference being the notation for the dimensions of the state $x \in \mathbb{R}^{2n_R}$, where $2n_R = n$ for a robot.

It is important to note that the continuous dynamics can have under-actuations (typically observed in bipedal robots). Therefore, the systems of interest are hybrid systems with partially observable continuous dynamics and uncontrollable discrete dynamics. It was shown in [28] how to stabilize such systems via a RES-CLF (3.17).

5.1.1 Outputs

The goal of this section is to define the set of outputs given the state x . In order to achieve robot walking/running, a periodic orbit is constructed (gait design) and a suitable controller is applied that tracks this reference periodic orbit. In other words, realization of a limit cycle in the bipedal robot results in stable walking/running. Periodicity of the trajectories is strictly not necessary, and it will be shown that stability of hybrid systems can still be achieved with milder assumptions: hybrid invariance, and minimum dwell time.

The problem formulation is such that the objective is to drive the robot states to the desired values by a tracking control law. We have the set of actual outputs of the robot as $y^a : T\mathbb{Q} \rightarrow \mathbb{R}^k$, and the desired outputs as $y^d : \mathbb{R}_{\geq 0} \rightarrow \mathbb{R}^k$. y^d is modulated by a phase (or time) variable $\tau : T\mathbb{Q} \rightarrow \mathbb{R}_{\geq 0}$ (or $\tau : \mathbb{R}_{\geq 0} \rightarrow \mathbb{R}_{\geq 0}$ for time based). By adapting a feedback linearizing controller, we can drive the relative degree one outputs (velocity outputs)

$$y_{1,v}(q, \dot{q}) = y_{1,v}^a(q, \dot{q}) - y_{1,v}^d(\tau_v, \alpha_v) \in \mathbb{R}^{k_{1,v}}, \quad (5.2)$$

and relative degree two outputs (pose outputs)

$$y_{2,v}(q) = y_{2,v}^a(q) - y_{2,v}^d(\tau_v, \alpha_v) \in \mathbb{R}^{k_{2,v}}, \quad (5.3)$$

to zero, with the subscript $v \in \mathbb{V}$ denoting the domain, α_v denoting the parameters of the desired trajectory. $k_{1,v} + k_{2,v} = k_v$. These outputs are generally called *virtual constraints* [62]. Normally, the phase variable, τ_v , for relative degree two outputs is a function of the configuration $\tau_v(q)$. Walking gaits, viewed as a set of desired periodic trajectories, are modulated as functions of a phase variable to eliminate the dependence on time [63]. In this case, the velocity (relative degree one) outputs are: $y_{1,v}(q, \dot{q}) = y_{1,v}^a(q, \dot{q}) - y_{1,v}^d(\alpha_v)$, where modulation is absent. In terms of the states, x , we can define the outputs as follows:

$$\begin{aligned} y_{1,v}(x) &= y_{1,v}^a(x) - y_{1,v}^d(\alpha_v) \\ y_{2,v}(x) &= y_{2,v}^a(x) - y_{2,v}^d(\tau_v, \alpha_v). \end{aligned} \quad (5.4)$$

5.1.2 Feedback Linearization

The feedback linearizing controller that drives the purely state dependent outputs $y_{1,v} \rightarrow 0$, $y_{2,v} \rightarrow 0$ is given by:

$$u = \begin{bmatrix} L_{g_v} y_{1,v} \\ L_{g_v} L_{f_v} y_{2,v} \end{bmatrix}^{-1} \left(- \begin{bmatrix} L_{f_v} y_{1,v} \\ L_{f_v}^2 y_{2,v} \end{bmatrix} + \mu \right), \quad (5.5)$$

where L_{f_v}, L_{g_v} denote the Lie derivatives and μ denotes the auxiliary input applied after the feedback linearization.

Note that any effective tracking controller will theoretically suffice (the experimental implementation uses PD control [64]). We therefore employ a control Lyapunov function

(CLF) based controller that can drive the following outputs to zero

$$\eta_v = \begin{bmatrix} y_{1,v} \\ y_{2,v} \\ \dot{y}_{2,v} \end{bmatrix}. \quad (5.6)$$

If the system has outputs with more relative degrees of freedom, then η_v can be accordingly modified. Applying the controller (5.5) results in the following output dynamics:

$$\dot{\eta}_v = \underbrace{\begin{bmatrix} 0 & 0 & 0 \\ 0 & 0 & 1_{k_{2,v} \times k_{2,v}} \\ 0 & 0 & 0 \end{bmatrix}}_{F_v} \eta_v + \underbrace{\begin{bmatrix} 1_{k_{1,v} \times k_{1,v}} & 0 \\ 0 & 0 \\ 0 & 1_{k_{2,v} \times k_{2,v}} \end{bmatrix}}_{G_v} \mu, \quad k_{1,v} + k_{2,v} = k_v. \quad (5.7)$$

$k_{1,v}$ is the size of the velocity outputs $y_{1,v}$, and $k_{2,v}$ is the size of the relative degree two outputs $y_{2,v}$. The dimension of the outputs

$$k_{1,v} + k_{2,v} = k_v$$

is typically equal to the number of actuators m_R . Therefore, based on the actuation type, we have the following three cases:

- Full-actuation (for rigid body manipulators $k_v = m_R = n_R$).
- Under-actuation (for rigid body manipulators $k_v = m_R \leq n_R$).
- For over-actuation (for rigid manipulators $k_v = m_a$, the number of actuating inputs that is equal to the DOF, $m_R > m_a = n_R$).

We will not explicitly analyze the case of over-actuation (even though used for the case of AMBER2 dancing) due to the fact that the outputs over constrain the given system. A convenient way to include over-actuation is by picking some of the desired outputs as the

actual outputs the system. Henceforth, we will assume that the number of the outputs is always equal to the number of inputs, $k_v = m_R = m, \forall v \in \mathbb{V}$. Accordingly, the auxiliary input $\mu \in U \subset \mathbb{R}^m$.

The auxiliary control input μ is chosen via control Lyapunov functions (CLFs) that drives $\eta_v \rightarrow 0$. More on CLFs is explained toward the end of this section.

5.1.3 Feedback Linearization of Time Dependent Outputs

Here we will pick the time based modulation $\tau(t)$ instead of the phase based modulation shown in 5.1.2. Given (5.3), if the desired outputs are modulated by the time instead of the state dependent phase, we have the following output representation

$$y_{1,v}^t(t, x) = y_{1,v}^a(x) - y_{1,v}^d(\tau_v(t), \alpha_v), \quad (5.8)$$

for velocity outputs and

$$y_{2,v}^t(t, x) = y_{2,v}^a(x) - y_{2,v}^d(\tau_v(t), \alpha_v), \quad (5.9)$$

for relative degree two (pose) outputs. The outputs are derived from (5.2),(5.3) where the phase is now dependent on time $\tau(t)$. With the absence of modulation for the velocity outputs, we have : $y_{1,v}^t = y_{1,v}$. The resulting output dynamics is obtained by taking the derivative

$$\begin{aligned} \dot{y}_{1,v}^t(t, x) &= L_{f_v} y_{1,v}^a(x) + L_{g_v} y_{1,v}^a(x) u - \dot{y}_{1,v}^d(\tau_v(t), \alpha) \\ \ddot{y}_{2,v}^t(t, x) &= L_{f_v}^2 y_{2,v}^a(x) + L_{g_v} L_{f_v} y_{2,v}^a(x) u - \ddot{y}_{2,v}^d(\tau_v(t), \alpha). \end{aligned} \quad (5.10)$$

Therefore, we have a time based feedback linearization for time based relative degree one and two outputs

$$u(t, x) = \begin{bmatrix} L_{g_v} y_{1,v}^a(x) \\ L_{g_v} L_{f_v} y_{2,v}^a(x) \end{bmatrix}^{-1} \left(- \begin{bmatrix} L_f y_{1,v}^a(x) \\ L_{f_v}^2 y_{2,v}^a(x) \end{bmatrix} + \begin{bmatrix} \dot{y}_{1,v}^d(\tau_v(t), \alpha) \\ \ddot{y}_{2,v}^d(\tau_v(t), \alpha) \end{bmatrix} + \mu_t \right), \quad (5.11)$$

where $\mu_t \in U \subset \mathbb{R}^m$ is the new time dependent linear output that can be properly constructed to yield convergence of the time based outputs. Applying the controller (5.11) results in the following output dynamics:

$$\dot{\eta}_{t,v} = \underbrace{\begin{bmatrix} 0 & 0 & 0 \\ 0 & 0 & 1_{k_{2,v} \times k_{2,v}} \\ 0 & 0 & 0 \end{bmatrix}}_{F_v} \eta_{t,v} + \underbrace{\begin{bmatrix} 1_{k_{1,v} \times k_{1,v}} & 0 \\ 0 & 0 \\ 0 & 1_{k_{2,v} \times k_{2,v}} \end{bmatrix}}_{G_v} \mu_t, \quad k_{1,v} + k_{2,v} = k_v, \quad (5.12)$$

where

$$\eta_{t,v} = \begin{bmatrix} y_{1,v}^t \\ y_{2,v}^t \\ \dot{y}_{2,v}^t \end{bmatrix}. \quad (5.13)$$

5.2 Extension of Artstein's Theorem

We will omit the subscript v for simpler representation. Given the output η , we have the following candidate Lyapunov function: $V(\eta) = \eta^T P \eta$, where P is the solution to the continuous-time algebraic Riccati equation (CARE):

$$F^T P + P F - P G G^T P + Q = 0, \quad Q = Q^T > 0. \quad (5.14)$$

V is positive definite and can be described as:

$$\lambda_{\min}(P)\|\eta\|^2 \leq V \leq \lambda_{\max}(P)\|\eta\|^2, \quad (5.15)$$

where $\lambda_{\min}(P), \lambda_{\max}(P) > 0$ are the minimum and maximum eigenvalues of P respectively. Taking the derivative of V yields:

$$\dot{V}(\eta) = \eta^T(F^T P + P F)\eta + 2\eta^T P G \mu. \quad (5.16)$$

To find a specific value of μ , we can utilize a minimum norm controller (see [65]) that minimizes $\mu^T \mu$ subject to the inequality constraint:

$$\dot{V}(\eta, \mu) = \eta^T(F^T P + P F)\eta + 2\eta^T P G \mu \leq -\gamma V(\eta), \quad (5.17)$$

where $\gamma := \frac{\lambda_{\min}(Q)}{\lambda_{\max}(P)}$ is a constant obtained from CARE. Satisfying (5.17) implies exponential convergence. This implies that $V(\eta)$ is an output stabilizing CLF based on Definition 21. By representing $V(x) = \eta(x)^T P \eta(x)$, we have a set of controllers that exponentially stabilizes the outputs η .

$$\mathbf{K}(x) = \{u \in \mathbb{U} : L_f V(x) + L_g V(x)u + \gamma V(x) \leq 0\}, \quad (5.18)$$

where $L_f V(x) = \frac{\partial V}{\partial x} f(x)$, $L_g V(x) = \frac{\partial V}{\partial x} g(x)$.

By choosing $\varepsilon > 0$ so that we have the following matrix:

$$P_\varepsilon := \begin{bmatrix} \mathbf{1}_{k_{1,v} \times k_{1,v}} & \mathbf{0} & \mathbf{0} \\ \mathbf{0} & \frac{1}{\varepsilon} \mathbf{1}_{k_{2,v} \times k_{2,v}} & \mathbf{0} \\ \mathbf{0} & \mathbf{0} & \mathbf{1}_{k_{2,v} \times k_{2,v}} \end{bmatrix} P \begin{bmatrix} \mathbf{1}_{k_{1,v} \times k_{1,v}} & \mathbf{0} & \mathbf{0} \\ \mathbf{0} & \frac{1}{\varepsilon} \mathbf{1}_{k_{2,v} \times k_{2,v}} & \mathbf{0} \\ \mathbf{0} & \mathbf{0} & \mathbf{1}_{k_{2,v} \times k_{2,v}} \end{bmatrix}, \quad (5.19)$$

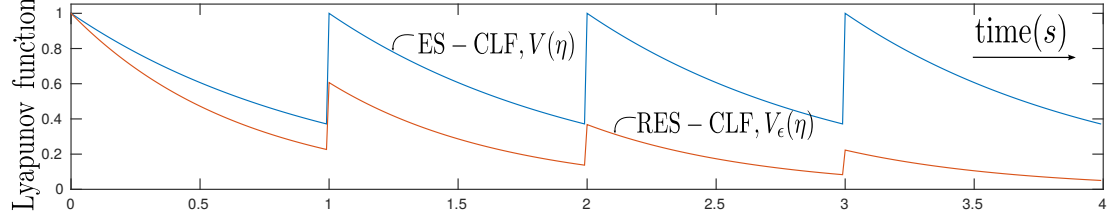


Figure 5.1: Figure showing a comparison between ES-CLF and RES-CLF. The impacts do not let $V(\eta)$ go to zero, while the ε term in $V_\varepsilon(\eta)$ allows for convergence to zero.

that is in fact solution to the following CARE:

$$F^T P_\varepsilon + P_\varepsilon F - \frac{1}{\varepsilon} P_\varepsilon G G^T P_\varepsilon + \frac{1}{\varepsilon} Q_\varepsilon = 0, \quad (5.20)$$

where

$$Q_\varepsilon = \begin{bmatrix} \mathbf{1}_{k_{1,v} \times k_{1,v}} & \mathbf{0} & \mathbf{0} \\ \mathbf{0} & \frac{1}{\varepsilon} \mathbf{1}_{k_{2,v} \times k_{2,v}} & \mathbf{0} \\ \mathbf{0} & \mathbf{0} & \mathbf{1}_{k_{2,v} \times k_{2,v}} \end{bmatrix} Q \begin{bmatrix} \mathbf{1}_{k_{1,v} \times k_{1,v}} & \mathbf{0} & \mathbf{0} \\ \mathbf{0} & \frac{1}{\varepsilon} \mathbf{1}_{k_{2,v} \times k_{2,v}} & \mathbf{0} \\ \mathbf{0} & \mathbf{0} & \mathbf{1}_{k_{2,v} \times k_{2,v}} \end{bmatrix} = 0, \quad (5.21)$$

which satisfies a stronger convergence rate condition for $\dot{V}_\varepsilon \leq -\frac{\gamma}{\varepsilon} \eta^T P_\varepsilon \eta$. Accordingly, we can construct the following Lyapunov function:

$$V_\varepsilon(\eta) = \eta^T P_\varepsilon \eta, \quad (5.22)$$

which satisfies the conditions for a *rapidly exponentially stabilizing control Lyapunov function* (RES-CLF), (3.16).

It is verified that V_ε is a RES-CLF. Fig. 5.1 shows the use of having rapid convergence, which is to compensate for the destabilizing impacts in order to realize exponential convergence for a hybrid system model. By (3.16), $c_1, c_2 > 0$ take the minimum and maximum

eigenvalues of P , respectively. Differentiating (5.22) yields:

$$\dot{V}_\varepsilon(\eta) = L_F V_\varepsilon(\eta) + L_G V_\varepsilon(\eta)\mu, \quad (5.23)$$

where

$$L_F V_\varepsilon(\eta) = \eta^T (F^T P_\varepsilon + P_\varepsilon F)\eta, \quad L_G V_\varepsilon(\eta) = 2\eta^T P_\varepsilon G. \quad (5.24)$$

We can define a minimum norm controller that minimizes $\mu^T \mu$ subject to the inequality constraint:

$$L_F V_\varepsilon(\eta) + L_G V_\varepsilon(\eta)\mu \leq -\frac{\gamma}{\varepsilon} V_\varepsilon(\eta), \quad (5.25)$$

which when satisfied implies exponential convergence. Therefore, we can define a set of controllers

$$\mathbf{K}_\varepsilon(\eta) = \{\mu \in \mathbb{U} : L_F V_\varepsilon(\eta) + L_G V_\varepsilon(\eta)\mu + \frac{\gamma}{\varepsilon} V_\varepsilon(\eta) \leq 0\}, \quad (5.26)$$

which yields the set of control values that satisfies the desired convergence rate. Since $V_\varepsilon(\eta(x)) = \eta(x)^T P_\varepsilon \eta(x)$, we now have the class of output stabilizing controllers defined for this robotic system

$$\mathbf{K}_\varepsilon(x) = \{u \in \mathbb{U} : L_f V_\varepsilon(x) + L_g V_\varepsilon(x)u + \frac{\gamma}{\varepsilon} V_\varepsilon(x) \leq 0\}, \quad (5.27)$$

which is obtained by substituting (6.37) in the derivative of the Lyapunov function \dot{V}_ε

$$\begin{aligned} L_f V_\varepsilon(x) &= \eta(x)^T P_\varepsilon \frac{\partial \eta(x)}{\partial x} f(x) + f^T(x) \frac{\partial \eta(x)}{\partial x}^T P_\varepsilon \eta(x) \\ L_g V_\varepsilon(x) &= 2\eta(x)^T P_\varepsilon \frac{\partial \eta(x)}{\partial x} g(x). \end{aligned} \quad (5.28)$$

This is a valid RES-CLF for the output dynamics (of η) by feedback linearization. Therefore, by extension of Artstein's theorem (Lemma 10), there exists an IOS-CLF (rather Re-IOS-CLF) given by the set

$$\mathbf{K}_{\varepsilon, \bar{\varepsilon}}(x) = \{u \in \mathbb{U} : L_f V_\varepsilon(x) + L_g V_\varepsilon(x)u + \frac{\gamma}{\varepsilon} V_\varepsilon(x) + \frac{1}{\bar{\varepsilon}} L_g V(x) L_g V(x)^T \leq 0\}. \quad (5.29)$$

It is important to note that CLF used here is to control what are called the transverse dynamics, which are not specifically described here. 5.3 will explain more about stabilizing the dynamics of the entire state space, i.e., the transverse dynamics (or normal dynamics) and the uncontrolled dynamics (or zero dynamics). The zero dynamics arise due to under-actuations in robotic systems.

In a similar fashion, for time based outputs η_t , we can obtain the set for time based RES-CLFs and the corresponding time based Re-IOS-CLFs in the following manner

$$\mathbf{K}^t(\eta_t) = \{\mu \in \mathbb{U} : L_F V_\varepsilon^t(\eta_t) + L_G V_\varepsilon^t(\eta_t)\mu + \frac{\gamma}{\varepsilon} V_\varepsilon^t(\eta_t) \leq 0\}. \quad (5.30)$$

We denote $V_\varepsilon^t(\eta_t(t, x)) = \eta_t(t, x)^T P_\varepsilon \eta_t(t, x)$. Therefore

$$\mathbf{K}_\varepsilon^t(x) = \{u \in \mathbb{U} : L_f V_\varepsilon^t(t, x) + L_g V_\varepsilon^t(t, x)u + \frac{\gamma}{\varepsilon} V_\varepsilon^t(t, x) \leq 0\}, \quad (5.31)$$

$$\begin{aligned} \text{where } L_f V_\varepsilon^t(t, x) &= \frac{\partial V_\varepsilon^t(t, x)}{\partial t} + \eta_t(t, x)^T P_\varepsilon \frac{\partial \eta_t(t, x)}{\partial x} f(x) + f^T(x) \frac{\partial \eta_t(t, x)}{\partial x}^T P_\varepsilon \eta_t(t, x) \\ L_g V_\varepsilon^t(t, x) &= 2\eta_t^T(t, x) P_\varepsilon \frac{\partial \eta_t(t, x)}{\partial x} g(x), \end{aligned} \quad (5.32)$$

which yields the class of controllers

$$\begin{aligned} \mathbf{K}_{\varepsilon, \bar{\varepsilon}}^t(x) = \{u \in \mathbb{U} : L_f V_\varepsilon^t(t, x) + L_g V_\varepsilon^t(t, x)u + \frac{\gamma}{\varepsilon} V_\varepsilon^t(t, x) \dots \\ + \frac{1}{\bar{\varepsilon}} L_g V^t(t, x) L_g V^t(t, x)^T \leq 0\}, \end{aligned} \quad (5.33)$$

that is Re-IOS-CLF.

5.3 Partially Observable Systems

It was shown in 5.2 that given the set of RES-CLFs, it is possible to obtain Re-IOS-CLFs that input to state stabilize systems with impulses. We are interested in how the zero dynamics and the RES-CLF allow us to obtain stable tracking (or periodic orbits) for the full order system. It was shown in [28] that an *exponential* stability assumption is not sufficient for ensuring stability of hybrid periodic orbits due to the discrete dynamics (impacts). Further, [28] proposed a solution that realizes *stronger* exponential convergences for the continuous dynamics that compensates for the destabilizing impacts (see Fig. 5.1). Specifically the systems were of the form:

$$\begin{aligned}\dot{\eta} &= \psi_f(\eta, z) + \psi_g(\eta, z)u \\ \dot{z} &= \psi_z(\eta, z),\end{aligned}\tag{5.34}$$

$\psi_f(0, z) = 0$ and ψ_f, ψ_g, ψ_z are all Lipschitz continuous w.r.t. η, z . $\eta \in \mathbb{R}^{k_1+2k_2}$ is the set of observable states, $z \in \mathbb{R}^{n-k_1-2k_2}$ is the set of unobservable states. η are also called the transverse coordinates. Accordingly, z are called the zero coordinates, due to the fact that $\dot{z} = \psi_z(0, z)$ are the zero dynamics. Given the continuous dynamics of a general system, (4.28), we can reformulate the dynamics to represent in the form (5.34). This reformulation is achieved by representing the disturbance inputs along with the transverse and zero dynamics in the following fashion

$$\begin{aligned}\dot{\eta} &= \underbrace{F\eta}_{\psi_f} + G \begin{bmatrix} L_g y_1 \\ L_g L_f y_2 \end{bmatrix} \left(u + \underbrace{\begin{bmatrix} L_g y_1 \\ L_g L_f y_2 \end{bmatrix}}_d^{-1} \begin{bmatrix} L_f y_1 \\ L_f^2 y_2 \end{bmatrix} \right) \\ \dot{z} &= \psi_z(\eta, z),\end{aligned}\tag{5.35}$$

which satisfy the standing assumptions required for constructing input to state stabilizing controllers for the continuous dynamics (see (2.18) for conditions on the vector fields). It is also possible to have simpler representations by substituting a feedback linearizing controller and investigate the perturbations w.r.t. μ : $\dot{\eta} = F\eta + G\mu + Gd$. Therefore, for such types of controllers, the systems will be of the form:

$$\begin{aligned}\dot{\eta} &= F\eta + G\mu \\ \dot{z} &= \Psi(\eta, z),\end{aligned}\tag{5.36}$$

which is obtained from (5.7). Main objective is to study ISS properties of partially exponentially stabilizing controllers for systems of the form (5.34), and formulation of the transverse (η) dynamics is dependent on the types of controllers used. More on modeling the uncertainties in these types of systems will be studied in a separate chapter (specifically Chapter 7). Similar to the continuous dynamics, the impact dynamics can also be represented in transformed coordinates:

$$\Delta(\eta^-, z^-) = (\eta^+, z^+),\tag{5.37}$$

where the $\Delta = \Delta_e$, $e \in \mathbb{E}$, has the subscripts omitted for convenience. Henceforth, in this chapter, it will be assumed that the impact maps Δ_e always transform the coordinates (η, z) from one domain to another.

To summarize, the goal of this section is to determine stabilizing controllers for hybrid systems of the type (4.31), where the dynamics is of the form (5.34). This section will also identify the unobservable/uncontrollable states of robotic hybrid systems and then determine stabilizing controllers for these partially observable/controllable systems.

5.3.1 Partial and Full Zero Dynamics

As an example, we will study an underactuated robot model and show how the transverse and zero dynamics evolve based on the implementation of the CLFs.

Example 1. *The EOM (which is also provided in (6.36)) for an n_R -DOF robotic system,*

$$D(q)\ddot{q} + C(q, \dot{q})\dot{q} + G(q) = Bu, \quad (5.38)$$

consisting of inertia, Coriolis-centrifugal and gravity matrices (more details can be found in (6.36)). B is the mapping from the input $u \in \mathbb{R}^{m_R}$ to the joints. We assume that there are $n_R - m_R$ rows of that do not have the input u (corresponding rows of B are zeros). We can realize the state $x = (q, \dot{q}) \in \mathbb{R}^{2n_R}$. Therefore, we can pick the first $n_R - m_R$ rows of the inertia matrix multiplied with \dot{q} : $D_1(q)\dot{q}$, which yields

$$\frac{d}{dt}(D_1(q)\dot{q}) = \dot{D}_1(q)\dot{q} + D_1(q)\ddot{q} = \dot{D}_1(q)\dot{q} - H_1(q, \dot{q}) \quad (5.39)$$

The input u does not appear in (5.39). Given a portion of the configuration space $q_1 \in \mathbb{R}^{n_R - m_R}$, we can have the following set of zero coordinates

$$z = \begin{bmatrix} q_1 \\ D_1(q)\dot{q} \end{bmatrix} \in \mathbb{R}^{2n_R - 2m_R}. \quad (5.40)$$

The configuration q consists of both actuated and unactuated variables. We are interested in the stability of the zero dynamics i.e., stability of (5.40). Normally, for walking/running, the optimization problem is formulated such that the zero dynamics has a stable periodic orbit. For hybrid systems, the problem is formulated such that the hybrid zero dynamics has a stable periodic orbit (see [66]). Theorem 1 from [28] shows that an exponentially stable periodic orbit in the zero dynamics implies exponentially stable periodic of the full dynamics if the controller of the form (5.18) is used.

Since the goal is to also include systems that do not show periodicity, we will study stabilization and input to state stabilization of trajectory tracking controllers in general. The assumption is that the continuous dynamics are input to state stable (for both the transverse and the zero dynamics). In addition, in order to practically represent a real world model, the hybrid invariance conditions are also relaxed (more details given in 5.3.2).

When the control objective is met such that $\eta = 0$ for all time then the system is said to be operating on the zero dynamics surface [67]

$$\mathbb{Z} = \{x \in \pi_x(\mathbb{D}) | \eta = 0\}, \quad (5.41)$$

for the domain $\mathbb{D} = \mathbb{D}_v$ (the subscript notation v is suppressed for convenience). Further, by relaxing the zeroing of the velocity output $y_1 : T\mathbb{Q} \rightarrow \mathbb{R}^{k_1}$, we can realize partial zero dynamics:

$$\mathbb{PZ} = \{x \in \pi_x(\mathbb{D}) | y_2 = 0, L_f y_2 = 0\}. \quad (5.42)$$

We can describe this condition w.r.t. every domain, \mathbb{D}_v , as

$$\mathbb{PZ}_v = \{x \in \pi_x(\mathbb{D}_v) | y_{2,v} = 0, L_{f_v} y_{2,v} = 0\}, \quad v \in \mathbb{V}. \quad (5.43)$$

To illustrate, the humanoid robot, DURUS (see Fig. 6.6), has feet and employs ankle actuation to propel the hip forward during the continuous dynamics. The relaxation assumption is implemented on the hip velocity, resulting in *partial zero dynamics*. For the running robot DURUS-2D (see Fig. 6.7), since the feet are underactuated, purely relative degree two outputs are picked that result in *full zero dynamics* of the system

$$\mathbb{Z}_v = \{x \in \pi_x(\mathbb{D}_v) | y_{2,v} = 0, L_f y_{2,v} = 0\}, \quad v \in \mathbb{V}, \quad (5.44)$$

which is similar to (5.43) except for the change of notation from $\mathbb{P}\mathbb{Z}_v$ to \mathbb{Z}_v . In the case of AMBER2 (see Fig. 6.3), there are certain domains that use relative degree one and two outputs, and also domains that are modeled as purely relative degree two outputs. Therefore, based on the domain, the dancing of AMBER2 is going to exhibit either pure zero dynamics or partial zero dynamics.

5.3.2 Partial and Full Hybrid Zero Dynamics

The controller u given by (5.18) or (5.27) or (5.29), being domain specific, guarantees partial (or full) zero dynamics only in the continuous dynamics. Therefore, for a hybrid control system \mathcal{IHC} , partial (full) hybrid zero dynamics can be guaranteed if and only if the discrete maps $\{\Delta_e\}_{e \in \mathbb{E}}$ are invariant of the partial (or full) zero dynamics in each domain. As a result, the parameters α_v of the outputs must be chosen in a way that renders the surface invariant through impacts. This condition can be represented mathematically as

$$\Delta_e(\mathbb{P}\mathbb{Z}_{\text{source}(e)} \cap \mathbb{S}_{\text{source}(e)}) \subset \mathbb{P}\mathbb{Z}_{\text{target}(e)}, \quad e = \{\text{source}(e) \rightarrow \text{target}(e)\} \in \mathbb{E}, \quad (5.45)$$

for transitions from partial zero dynamics to partial zero dynamics, and

$$\Delta_e(\mathbb{Z}_{\text{source}(e)} \cap \mathbb{S}_{\text{source}(e)}) \subset \mathbb{Z}_{\text{target}(e)}, \quad e = \{\text{source}(e) \rightarrow \text{target}(e)\} \in \mathbb{E}, \quad (5.46)$$

for the transitions from full zero dynamics to full zero dynamics. We have other variants of this formulation based on the type of the zero dynamics that the source and the target domains contain

$$\begin{aligned} \Delta_e(\mathbb{Z}_{\text{source}(e)} \cap \mathbb{S}_{\text{source}(e)}) &\subset \mathbb{P}\mathbb{Z}_{\text{target}(e)}, \quad e = \{\text{source}(e) \rightarrow \text{target}(e)\} \in \mathbb{E}, \\ \Delta_e(\mathbb{P}\mathbb{Z}_{\text{source}(e)} \cap \mathbb{S}_{\text{source}(e)}) &\subset \mathbb{Z}_{\text{target}(e)}, \quad e = \{\text{source}(e) \rightarrow \text{target}(e)\} \in \mathbb{E}. \end{aligned} \quad (5.47)$$

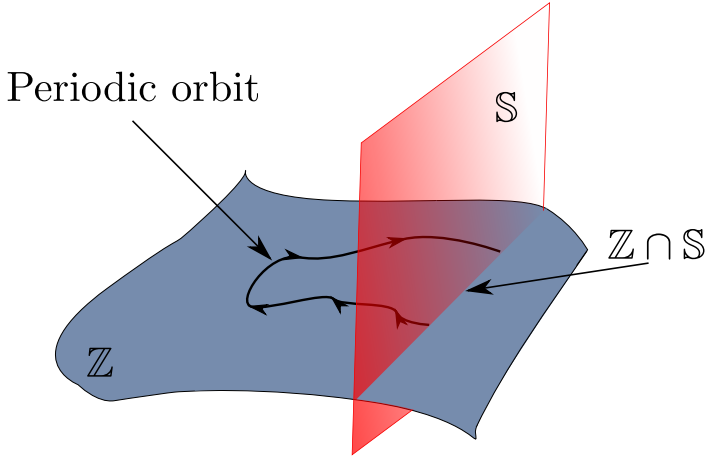


Figure 5.2: Figure showing the zero dynamics for a single domain, single reset map. The bipedal robot AMBER1 (see Fig. 6.2) will typically have this type of hybrid zero dynamics.

Fig. 5.2 shows a single domain hybrid system (simple hybrid system) consisting of 2-dimensional zero dynamics for the bipedal robot AMBER1 (see Fig. 6.2). Fig. 5.3 depicts the dynamics of a two domain hybrid system with 2-dimensional partial zero dynamics. The best way to ensure hybrid invariance under a discrete transition is by a careful selection of the desired trajectories (desired gait) via the parameterization: α_v . Hence if the desired trajectories are a function of Bezier polynomials, the parameters α_v are the coefficients. These coefficients are chosen by using a direct collocation based walking gait optimization problem, which is explained in [64, 68].

Given the transverse coordinates η_v and the zero coordinates z_v , we have the diffeomorphism $\Phi_v : \pi_x(\mathbb{D}_v) \rightarrow \mathbb{R}^n$ that maps from x to (η_v, z_v) . The diffeomorphism can be divided into parts

$$\Phi_v(x) = \begin{bmatrix} \Phi_{1,v}(x) \\ \Phi_{2,v}(x) \\ \Phi_{3,v}(x) \end{bmatrix} = \begin{bmatrix} y_{1,v}(x) \\ y_{2,v}(x) \\ \dot{y}_{2,v}(x) \\ z_v(x) \end{bmatrix}. \quad (5.48)$$

Similarly, the outputs can also be divided into two parts

$$\eta_v = \begin{bmatrix} y_{1,v} \\ y_{2,v} \end{bmatrix}, \quad \eta_{2,v} = \begin{bmatrix} y_{2,v} \\ \dot{y}_{2,v} \end{bmatrix}. \quad (5.49)$$

We can also derive the tangent map, $d\Phi_v : T_x\pi_x(\mathbb{D}_v) \rightarrow T_{(\eta_v, z_v)}\Phi_v(\pi_x(\mathbb{D}_v))$, which can also be divided into parts $d\Phi_v^\eta, d\Phi_v^z$, for the reduced order coordinates obtained from (5.48). The diffeomorphism and the tangent map for the coordinates $(y_{1,v}, z_v)$ are given by

$$\Phi_v^z = \begin{bmatrix} \Phi_{1,v} \\ \Phi_{3,v} \end{bmatrix}, \quad d\Phi_v^z = \begin{bmatrix} d\Phi_{1,v} \\ d\Phi_{3,v} \end{bmatrix}. \quad (5.50)$$

Similar to the state based transformation, the time based output dynamics can also be written in normal form as

$$\begin{aligned} \dot{\eta}_t &= F\eta_t + G\mu_t, \\ \dot{z}_t &= \Psi_t(\eta_t, z_t). \end{aligned} \quad (5.51)$$

z_t are the set of zero dynamic coordinates normal to η_t and has the invariant dynamics $\dot{z}_t = \Psi_t(0, z_t)$. For these time based states, we have the diffeomorphism: $\Phi_t(t, x) = (\eta_t, z_t)$.

Similarly to (5.49), the time based coordinates outputs can also be divided into two parts

$$\eta_t = \begin{bmatrix} y_1^t \\ \eta_{t,2} \end{bmatrix}, \quad \eta_{t,2} = \begin{bmatrix} y_2^t \\ \dot{y}_2^t \end{bmatrix}, \quad (5.52)$$

where the domain v is ignored for ease of representation.

We can now define the classes of controllers that stabilize the hybrid system (4.31).

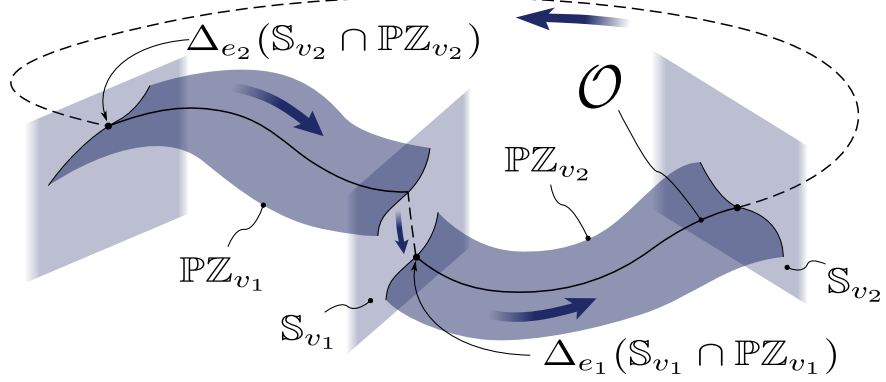


Figure 5.3: Figure showing a typical periodic orbit (\mathcal{O}) on the partial (full) hybrid zero dynamics. The figure shows a two dimensional partial zero dynamics manifold, which can vary based on the hybrid system chosen.

Again, we will ignore the subscript v for ease of reading. We have the class of controllers:

$$\mathbf{K}(\eta) = \{\mu \in \mathbf{U} : L_F V(\eta) + L_G V(\eta)\mu + \gamma V(\eta) \leq 0\}, \quad (5.53)$$

where $L_f V(\eta) = \eta^T (F^T P + PF)\eta$, $L_g V(\eta) = 2\eta^T PG$, and

$$\mathbf{K}(\eta, z) = \{u \in \mathbb{U} : L_f V(\eta, z) + L_g V(\eta, z)u + \gamma V(\eta) \leq 0\}, \quad (5.54)$$

where $L_f V(\eta, z) = \frac{\partial V}{\partial x} f(x)$, $L_g V(\eta, z) = \frac{\partial V}{\partial x} g(x)$, with $x = \Phi^{-1}(\eta, z)$. We have the class of controllers from RES-CLF as

$$\mathbf{K}_\varepsilon(\eta) = \{\mu \in \mathbf{U} : L_F V_\varepsilon(\eta) + L_G V_\varepsilon(\eta)\mu + \frac{\gamma}{\varepsilon} V_\varepsilon(\eta) \leq 0\}, \quad (5.55)$$

where $L_F V_\varepsilon(\eta) = \eta^T (F^T P_\varepsilon + P_\varepsilon F)\eta$, $L_G V_\varepsilon(\eta) = 2\eta^T P_\varepsilon G$, and

$$\mathbf{K}_\varepsilon(\eta, z) = \{u \in \mathbb{U} : L_f V_\varepsilon(\eta, z) + L_g V_\varepsilon(\eta, z)u + \frac{\gamma}{\varepsilon} V_\varepsilon(\eta) \leq 0\}, \quad (5.56)$$

which is obtained by substituting (4.28) in the derivative of the Lyapunov function \dot{V}_ε

$$\begin{aligned} L_f V_\varepsilon(\eta, z) &= \eta^T P_\varepsilon \frac{\partial \eta}{\partial x} f(x) + f^T(x) \frac{\partial \eta^T}{\partial x} P_\varepsilon \eta \\ L_g V_\varepsilon(\eta, z) &= 2\eta^T P_\varepsilon \frac{\partial \eta}{\partial x} g(x), \quad x = \Phi^{-1}(\eta, z) \end{aligned} \quad (5.57)$$

and finally the class from Re-ISS-CLF as

$$\begin{aligned} \mathbf{K}_{\varepsilon, \bar{\varepsilon}}(\eta, z) = \{u \in \mathbb{U} : L_f V_\varepsilon(\eta, z) + L_g V_\varepsilon(\eta, z) u + \frac{\gamma}{\varepsilon} V_\varepsilon(\eta) + \dots \\ \frac{1}{\bar{\varepsilon}} L_g V_\varepsilon(\eta, z) L_g V_\varepsilon(\eta, z)^T \leq 0\}. \end{aligned} \quad (5.58)$$

For time based outputs η_t we have the following formulation for the RES-CLF and Re-ISS-CLF

$$\mathbf{K}_\varepsilon^t(\eta_t) = \{\mu \in \mathbb{U} : L_F V_\varepsilon^t(\eta_t) + L_G V_\varepsilon^t(\eta_t) \mu + \frac{\gamma}{\varepsilon} V_\varepsilon^t(\eta_t) \leq 0\}, \quad (5.59)$$

where $L_F V_\varepsilon^t(\eta_t) = \eta_t^T (F^T P_\varepsilon + P_\varepsilon F) \eta_t$, $L_G V_\varepsilon^t(\eta_t) = 2\eta_t^T P_\varepsilon G$, and

$$\mathbf{K}_\varepsilon^t(\eta_t, z_t) = \{u \in \mathbb{U} : L_f V_\varepsilon^t(\eta_t, z_t) + L_g V_\varepsilon^t(\eta_t, z_t) u + \frac{\gamma}{\varepsilon} V_\varepsilon^t(\eta_t) \leq 0\}, \quad (5.60)$$

which is obtained by substituting (6.37) in the derivative of the Lyapunov function \dot{V}_ε

$$\begin{aligned} L_f V_\varepsilon^t(\eta_t, z_t) &= \frac{\partial V_\varepsilon^t}{\partial t} \eta_t^T P_\varepsilon \frac{\partial \eta_t}{\partial x} f(x) + f^T(x) \frac{\partial \eta_t^T}{\partial x} P_\varepsilon \eta_t \\ L_g V_\varepsilon^t(\eta_t, z_t) &= 2\eta_t^T P_\varepsilon \frac{\partial \eta_t}{\partial x} g(x), \quad x = \Phi^{-1}(\eta_t, z_t) \end{aligned} \quad (5.61)$$

and finally the class for Re-ISS-CLF as

$$\begin{aligned} \mathbf{K}_{\varepsilon, \bar{\varepsilon}}^t(\eta_t, z_t) = \{u \in \mathbb{U} : L_f V_\varepsilon^t(\eta_t, z_t) + L_g V_\varepsilon^t(\eta_t, z_t) u + \frac{\gamma}{\varepsilon} V_\varepsilon^t(\eta_t) + \dots \\ \frac{1}{\bar{\varepsilon}} L_g V_\varepsilon^t(\eta_t, z_t) L_g V_\varepsilon^t(\eta_t, z_t)^T \leq 0\}. \end{aligned} \quad (5.62)$$

For limiting the use of notations, the classes of controllers defined in (5.59) and (5.60) are both denoted by \mathbf{K}_ε^t with the difference being the dependency on the number of arguments. Therefore, for a standard time based RES-CLF, the class, without substituting (5.11), would be denoted by $\mathbf{K}_\varepsilon^t(\eta_t, z_t)$, and for the time dependent RES-CLF, the class that utilizes the auxiliary input μ_t after substituting (5.11) would be denoted by $\mathbf{K}_\varepsilon^t(\eta_t)$. Similarly, for a state based RES-CLF without the substitution of (5.5), the class of controllers is denoted by $\mathbf{K}_\varepsilon(\eta, z)$, and with the substitution would be denoted by $\mathbf{K}_\varepsilon(\eta)$. To summarize, the main control input u is a function of two arguments, while the auxiliary control input μ is a function of only one, the normal coordinates η .

5.4 Formal Results of Stability

In this section, we will investigate the stability and robustness of hybrid systems for controllers of the form (5.56) first and then analyze stability of input to state stabilizing controllers of the form (5.58). Theorem 2 in [28] showed for hybrid periodic orbits and can be easily extended to aperiodic hybrid systems to realize behaviors like dancing (discussed more in Chapter 10). By viewing walking as periodic orbits that are hybrid in nature, we check for conditions that result in attractive and forward invariant periodic orbits. We analyze the robustness by modeling the uncertainties of the system in Chapter 7.

Applying the controller $k_{v,\varepsilon}(\eta_v, z_v) \in \mathbf{K}_{v,\varepsilon}(\eta_v, z_v)$ (from the set (5.56) along with the inclusion of the domain dependency $v \in \mathbb{V}$) on the hybrid control system \mathcal{IHC} (4.31) yields the following hybrid system

$$\mathcal{IHC}^\varepsilon = (\Gamma, \mathbb{D}, \mathbb{S}, \Delta, \mathbb{F}^\varepsilon), \quad (5.63)$$

where the only difference is the set of vector fields $\mathbb{F}^\varepsilon = \{f_{v_1} + g_{v_1} k_{v_1,\varepsilon}, f_{v_2} + g_{v_2} k_{v_2,\varepsilon}, \dots\}$ which are obtained after the substitution of (5.56). Similarly, applying $k_{v,\bar{\varepsilon}}(\eta_v, z_v) \in$

$\mathbf{K}_{v,\varepsilon,\bar{\varepsilon}}(\eta_v, z_v)$ (5.58) instead of (5.56) results in the hybrid system

$$\mathcal{IH}^{\varepsilon,\bar{\varepsilon}} = (\Gamma, \mathbb{D}, \mathbb{S}, \Delta, \mathbb{F}^{\varepsilon,\bar{\varepsilon}}). \quad (5.64)$$

Similar to the construction of (4.19), we have the following hybrid control system that models the disturbances, given the closed loop hybrid system (5.64):

$$\mathcal{IHC}^{\varepsilon,\bar{\varepsilon},d} = (\Gamma, \mathbb{D}^d, \mathbb{S}^d, \Delta^d, \mathbb{F}^{\varepsilon,\bar{\varepsilon}}\mathbb{G}), \quad (5.65)$$

where the collection of vector fields $\mathbb{F}^{\varepsilon,\bar{\varepsilon}}\mathbb{G}$ is obtained after the substitution of (5.58).

Since the same controller (5.56) drives the relative degree two outputs $y_{2,v} \rightarrow 0$, as specified by (5.42),(5.44), the result is (partial) zero dynamics. Hybrid invariance (5.45)-(5.47) and convergence of outputs $y_{2,v} \rightarrow 0$ results in a reduced order hybrid system consisting of only the coordinates $y_{1,v}, z_v$.

$$\mathcal{IH}|_z = (\Gamma, \mathbb{D}|_z, \mathbb{S}|_z, \Delta|_z, \mathbb{F}|_z), \quad (5.66)$$

$$\text{where } \mathbb{D}|_z = \{\mathbb{PZ}_{v_1}, \mathbb{PZ}_{v_2}, \dots\},$$

$$\mathbb{S}|_z = \{\mathbb{S}_{e_1} \cap \mathbb{PZ}_{\text{source}(e_1)}, \mathbb{S}_{e_2} \cap \mathbb{PZ}_{\text{source}(e_2)}, \dots\},$$

$$\Delta|_z = \{\Delta_{e_1}|_z, \Delta_{e_2}|_z, \dots\},$$

$$\mathbb{F}|_z = \{f_{v_1}|_z, f_{v_2}|_z, \dots\}.$$

This definition of reduced order hybrid system applies to both bipedal walking and running with the difference being the omission of y_1 resulting in purely zero dynamic coordinates. It will be inherently implied that all formal stability results established for walking (\mathbb{PZ}) are also applicable for running (\mathbb{Z}).

Canonical embedding. The partial (full) hybrid zero dynamics can be embedded into the full order system via the canonical embedding, for which the states of the partial zero

dynamics get mapped into the states of the full order system: $\Pi_0^v : \Phi_v^z(\mathbb{P}\mathbb{Z}_v) \rightarrow \Phi_v(\mathbb{D}_v)$.

Therefore the canonical embedding yields $\Pi_0^v(y_{1,v}, z_v) = (y_{1,v}, 0, z_v)$.

5.4.1 Aperiodic systems

Here, in this subsection, we will study non-periodic systems and then study input to state stability properties of the continuous time controllers (developed so far) for hybrid systems. We will assume that each continuous event satisfies the minimum dwell time assumption ($T > 0$), similar to what was constructed in 4.4.2.

Theorem 3. *For systems with impulse effects of the form (5.65), assume that the zero dynamics is exponential input to state stable (e-ISS) in the continuous dynamics. Also assume that the minimum dwell time conditions are satisfied. Applying the Lipschitz continuous feedback law, $u(\eta_v, z_v) \in \mathbf{K}_{v,\varepsilon,\bar{\varepsilon}}(\eta_v, z_v)$, $v \in \mathbb{V}$ that partially rapidly exponentially ISSabilizes the continuous dynamics implies that the system (5.65) is ISS.*

Proof. The transverse dynamics is rapidly exponentially-ISS in the continuous dynamics.

Therefore, for the Lyapunov function $V_{\varepsilon,v} = \eta_v^T P_{\varepsilon,v} \eta_v$, we have for some $\iota_\eta \in \mathcal{K}_\infty$

$$\begin{aligned} p_{1,v} \|\eta_v\|^2 &\leq V_{\varepsilon,v}(\eta_v) \leq \frac{p_{2,v}}{\varepsilon^2} \|\eta_v\|^2 \\ \dot{V}_{\varepsilon,v} &\leq -\frac{\gamma}{\varepsilon} V_{\varepsilon,v} + \iota_\eta(\|d\|_\infty). \end{aligned} \tag{5.67}$$

Generic versions for $V_{\varepsilon,v}$ (i.e., not just $\eta_v^T P_{\varepsilon,v} \eta_v$) is also possible by converse theorems for exponential stability. We will choose equal convergence rates across all continuous dynamics for η_v (possible because they are controllable). The perturbation $\iota_\eta(\|d\|_\infty)$ is the maximum of the disturbances across all continuous events. Similarly, zero dynamics is also exponential input to state stable (e-ISS) in the continuous dynamics, and by converse ISS-Lyapunov theorem (see [34] for a detailed account on converse Lyapunov theorems for

ISS systems)

$$\begin{aligned}
& p_{3,v} \|z_v\|^2 \leq V_{z,v} \leq p_{4,v} \|z_v\|^2 \\
& \frac{\partial V_{z,v}}{\partial z_v} \Psi_v(0, z_v) \leq -p_{5,v} \|z_v\|^2 + \iota_z(\|d_z\|_\infty) \\
& \left| \frac{\partial V_{z,v}}{\partial z_v} \right| \leq p_{6,v} \|z_v\|
\end{aligned} \tag{5.68}$$

for some $\iota_z \in \mathcal{K}_\infty$. We therefore have the following Lyapunov candidate for the full order dynamics for each domain $v \in \mathbb{V}$:

$$V_v = \sigma_v V_{\varepsilon,v} + V_{z,v} \tag{5.69}$$

Taking the derivative of V_v , we have the following

$$\begin{aligned}
\dot{V}_v &= \sigma_v \dot{V}_{\varepsilon,v} + \frac{\partial V_{z,v}}{\partial z_v} \Psi_v(\eta_v, z_v) \\
&\leq -\sigma_v \frac{\gamma}{\varepsilon} V_{\varepsilon,v} + \frac{\partial V_{z,v}}{\partial z_v} \Psi_v(0, z_v) + \frac{\partial V_{z,v}}{\partial z_v} (\Psi_v(\eta_v, z_v) - \Psi_v(0, z_v)) + \sigma_v \iota_\eta(\|d\|_\infty) \\
&\leq -\sigma_v \frac{\gamma}{\varepsilon} V_{\varepsilon,v} - p_{5,v} \|z_v\|^2 + \frac{\partial V_{z,v}}{\partial z_v} (\Psi_v(\eta_v, z_v) - \Psi_v(0, z_v)) + \sigma_v \iota_\eta(\|d\|_\infty) \dots \\
&\quad + \sigma_v \iota_z(\|d_z\|_\infty) \\
&\leq -\sigma_v \frac{\gamma}{\varepsilon} V_{\varepsilon,v} + L_{\eta,v} p_{6,v} \|z_v\| \|\eta_v\| - p_{5,v} \|z_v\|^2 + \max\{2\sigma_v \iota_\eta(\|d\|_\infty), 2\iota_z(\|d_z\|_\infty)\},
\end{aligned} \tag{5.70}$$

and by picking a sufficiently large $\sigma_v > 0$, we have that the Lyapunov candidate V_v is indeed an e-ISS Lyapunov function. Similar to the results obtained in (4.45) we have the following inequality for each domain and its corresponding set of guards.

$$\begin{aligned}
\dot{V}_v(\eta_v, z_v, d) &\leq -c_1 V_v(\eta_v, z_v) + \max\{2\sigma_v \iota_\eta(\|d\|_\infty), 2\iota_z(\|d_z\|_\infty)\}, \\
V_v(\Delta_e(\eta_v^-, z_v^-)) &\leq e^{c_2} V_v(\eta_v^-, z_v^-) \quad \text{for each source}(e) = v.
\end{aligned} \tag{5.71}$$

Note that $V_{\text{source}(e)}(\Delta_e(\eta_v^-, z_v^-)) \neq V_{\text{target}(e)}(\Delta_e(\eta_v^-, z_v^-))$. Assume $\sigma = \max_{v \in \mathbb{V}} \sigma_v$. We

can also assume that c_1, c_2 are the worst case values giving the worst case convergence rates for both the continuous and discrete dynamics across all domains and guards. It is difficult to stabilize hybrid systems that have multiple Lyapunov functions based on the continuous dynamics of the system. A convenient way to establish input to state stability for systems of this type is by assuming a minimum dwell time condition, which was also used in Theorem 2.

Given the disturbance $\|d_\sigma\|_\infty := \|(d, d_z)\|_\infty$, we can find $\iota_\sigma \in \mathcal{K}_\infty$, such that

$$\iota_\sigma(\|d_\sigma\|_\infty) = \max\{2\sigma\iota_\eta(\|d\|_\infty), 2\iota_z(\|d_z\|_\infty)\}.$$

Let $p_1 := \min_{v \in \mathbb{V}} p_{1,v}, p_2 := \max_{v \in \mathbb{V}} p_{2,v}$. Given the hybrid control system of the form (4.31) and feedback controller of the form, $u \in \mathbf{K}_{\epsilon, \bar{\epsilon}}$, given by (5.58), we have the execution $(\Xi, \mathbf{I}, \rho, \mathbf{C})$. The execution of the closed loop system with impulse effects, is similar to the execution defined in Chapter 4. We therefore, have that under sufficiently large enough dwell time T , states $(\eta_v, z_v) \rightarrow 0, v \in \mathbb{V}$ as $t \rightarrow \infty$.

Under a constant bounded disturbance, $\|d\|_\infty$, the exponential ultimate bound for the states b_c for each continuous event can be explicitly computed

$$\begin{aligned} \dot{V}_v(\eta_v, z_v, d) &\leq -\frac{c_1}{2} V_v(\eta_v, z_v), \quad \text{for } \|\eta_v, z_v\| \geq \frac{c_1}{p_1} \iota_\sigma(\|d_\sigma\|_\infty) \\ \implies b_c &:= \left(\frac{2c_1}{p_1} \iota_\sigma(\|d_\sigma\|_\infty) \right)^{\frac{1}{2}}. \end{aligned} \tag{5.72}$$

By assuming hybrid invariance of the impact map $\Delta_e(0, 0) = (0, 0)$, we have

$$\|\Delta_e(\eta_v, z_v)\| \leq L_{\Delta,e} \|(\eta_v, z_v)\|, \quad v = \text{source}(e), \tag{5.73}$$

$L_{\Delta,e}$ is the Lipschitz constant. Let $L_\Delta = \max_{e \in \mathbb{E}} L_{\Delta,e}$. We therefore have the bounds for the post impact map for each guard $b_i := L_\Delta b_c$. Therefore, given these bounds, the minimum dwell time can be explicitly computed. If $b_i \geq \|(\eta_v(0), z_v(0))\| \geq b_c$, in each

continuous event, then following inequality should be satisfied:

$$\begin{aligned}
\|(\eta_v(T), z_v(T))\| &\leq b_c \\
\|(\eta_v(T), z_v(T))\| &\leq \frac{p_2}{\varepsilon} e^{-\frac{\gamma}{4\varepsilon}T} \|(\eta_v(0), z_v(0))\| \leq \frac{p_2}{\varepsilon} e^{-\frac{\gamma}{2\varepsilon}T} b_i \\
&\leq \frac{p_2}{\varepsilon} e^{-\frac{\gamma}{4\varepsilon}T} L_\Delta b_c.
\end{aligned} \tag{5.74}$$

Therefore the dwell time T should be large enough so that $\|(\eta_v(T), z_v(T))\| \leq b_c$. This ensures that the states always remain in the ultimate bound. It can be observed that as $\|d_\sigma\|_\infty$ gets smaller and smaller, the states go to zero. \square

Non-hybrid invariance conditions. Assuming $\Delta_e(0, 0) \neq (0, 0)$. We can rewrite the impact equations

$$\|\Delta_e(\eta_v, z_v) - \Delta_e(0, 0) + \Delta_e(0, 0)\| \leq L_\Delta \|(\eta_v, z_v)\| + \|\Delta_e(0, 0)\| \tag{5.75}$$

Therefore, by taking $d_i = L_\Delta \|(\eta_v, z_v)\| \|\Delta_e(0, 0)\| + \|\Delta_e(0, 0)\|^2$, we have the following inequalities for the Lyapunov candidate

$$\begin{aligned}
\dot{V}_v(\eta_v, z_v, d) &\leq -c_1 V_v(\eta_v, z_v) + \max\{2\sigma\iota_\eta(\|d\|_\infty), 2\iota_z(\|d_z\|_\infty)\}, \\
V_v(\Delta_e(\eta_v^-, z_v^-)) &\leq e^{c_2} V_v(\eta_v^-, z_v^-) + d_i \quad \text{for each source(e) = v.}
\end{aligned} \tag{5.76}$$

Due to non-hybrid invariance, the bound on the post impact states is larger $b_i = L_\Delta b_c + \|\Delta_e(0, 0)\|$. Therefore, for $b_i \leq \|(\eta_v, z_v)\| \leq b_c$, we need to satisfy the dwell time condition to allow sufficient time for the states to reach the ultimate bound. In other words, for non-hybrid invariance conditions, the time required to come back to the ultimate bound is larger.

5.4.2 Periodic Systems

By transforming x into the coordinates (η_v, z_v) , $v \in \mathbb{V}$ by using the diffeomorphism (5.48), we can define the flow for the transformed coordinates similar to Definition 48. For ease of notations, we will re-denote the flow of the transformed coordinates (η_v, z_v) as φ^v .

Definition 49. *Given the execution (4.10) of the hybrid system (5.64), the flow of the closed loop vector field $f_{\rho(i)} + g_{\rho(i)} k_{\rho(i), \varepsilon, \bar{\varepsilon}}$ is the mapping $\varphi^{\rho(i)} : \mathbb{R}_{\geq 0} \times \mathbb{B} \rightarrow \Phi_{\rho(i)}(\pi_x(\mathbb{D}_{\rho(i)}))$, where $\mathbb{B}(\Phi_{\rho(i)}(\mathbf{C}_i(t_i)))$ is the neighborhood of the diffeomorphism of $\mathbf{C}_i(t_i)$. The flow satisfies the following properties:*

- $\Phi_{\rho(i)}(\mathbf{C}_i(t_i)) = \varphi^{\rho(i)}(0, \Phi_{\rho(i)}(\mathbf{C}_i(t_i))).$
- $\Phi_{\rho(i)}(\mathbf{C}_i(t_i + t + s)) = \varphi^{\rho(i)}(t, \varphi^{\rho(i)}(s, \Phi_{\rho(i)}(\mathbf{C}_i(t_i)))).$
- $\varphi^{\rho(i)}(-s, \varphi^{\rho(i)}(s, (\eta_{\rho(i)}, z_{\rho(i)}))) = (\eta_{\rho(i)}, z_{\rho(i)}), \quad (\eta_{\rho(i)}, z_{\rho(i)}) \in \mathbb{B}(\Phi_{\rho(i)}(\mathbf{C}_i(t_i))).$

For convenience, denote $\varphi^{\rho(i)}(t, (\eta_{\rho(i)}, z_{\rho(i)})) = \varphi_t^{\rho(i)}(\eta_{\rho(i)}, z_{\rho(i)}).$

If the hybrid system (5.63) contains a directed cycle, i.e., if the hybrid system (5.63) is of the form (4.63), we can obtain formulations for periodic orbits. Therefore, we have the hybrid control system of the form (4.62). Similarly, under hybrid invariance conditions, we have the following tuple for the reduced order hybrid system with the directed cycle:

$$\mathcal{IH}_c|_z = (\Gamma_c, \mathbb{D}_c|_z, \mathbb{S}_c|_z, \Delta_c|_z, \mathbb{F}_c|_z), \quad (5.77)$$

The outputs of the system are picked such that a stable periodic orbit in the hybrid zero dynamics is realized.

We apply $k_{v,\varepsilon}(x) \in \mathbf{K}_{v,\varepsilon}$ (5.56) for the continuous dynamics on the hybrid control system (4.62) to yield the closed loop hybrid system:

$$\mathcal{IH}_c^\varepsilon = (\Gamma_c, \mathbb{D}_c, \mathbb{S}_c, \Delta_c, \mathbb{F}_c^\varepsilon). \quad (5.78)$$

We apply $k_{v,\varepsilon,\bar{\varepsilon}}(x) \in \mathbf{K}_{v,\varepsilon,\bar{\varepsilon}}$ (5.58) for the continuous dynamics on the hybrid control system (4.62) to yield the following closed loop hybrid system:

$$\mathcal{IH}_c^{\varepsilon,\bar{\varepsilon}} = (\Gamma_c, \mathbb{D}_c, \mathbb{S}_c, \Delta_c, \mathbb{F}_c^{\varepsilon,\bar{\varepsilon}}). \quad (5.79)$$

Under disturbances, we will have the following hybrid control system formulation:

$$\mathcal{IHC}_c^{\varepsilon,\bar{\varepsilon},d} = (\Gamma_c, \mathbb{D}_c^d, \mathbb{S}_c^d, \mathbb{U}_c^d, \Delta_c^d, \mathbb{F}_c^{\varepsilon,\bar{\varepsilon}} \mathbb{G}_c). \quad (5.80)$$

Assume that there is a periodic execution in the partial (full) hybrid zero dynamics of the reduced order hybrid system with the directed cycle (5.77). The periodic orbit is the execution $(\Xi, \mathbf{I}, \rho, \mathbf{C}^z)$ satisfying the following:

- $\Xi = \mathbb{N}_0$.
- $\lim_{i \rightarrow \infty} t_i - t_0 = \infty$.
- $\rho(i) = \begin{cases} v_1 & \text{if } i = 0, 1, 2l, \dots \\ v_2 & \text{if } i = 1, l+1, 2l+1, \dots \\ \vdots & \\ v_l & \text{if } i = l-1, 2l-1, \dots \end{cases}$
- $\mathbf{C}_{li}^z(t_{li}) = \mathbf{C}_{l(i+1)}^z(t_{l(i+1)})$.

Here each $\mathbf{C}_i^z(t) \in \mathbb{PZ}_{\rho(i)}$, $t \in \mathbf{I}_i$. Similar to Definition 49, we can define the flow of the partial zero dynamics in terms of the transformed coordinates. Denote the flow of the partial zero dynamics as $\varphi_t^{z,v} : \mathbb{R}_{\geq 0} \times \mathbb{B} \rightarrow \Phi_v^z(\mathbb{PZ}_v)$

\mathcal{O}_z denotes the periodic execution in terms of the transformed coordinates

$$\mathcal{O}_z := (\Xi, \mathbf{I}, \rho, \Phi \mathbf{C}^z), \quad \Phi \mathbf{C}^z := \{\Phi_{\rho(i)}^z \mathbf{C}_i^z\}_{i \in \Xi}, \quad \Phi_{\rho(i)}^z \mathbf{C}_i^z(t) := \Phi_{\rho(i)}^z(\mathbf{C}_i^z(t)). \quad (5.81)$$

Since we know that by applying a control law via the RES-CLF for the transverse dynamics (5.56), we can render the outputs $\eta_{2,v} \rightarrow 0$ in the continuous dynamics. Therefore, if the outputs are rendered zero, the periodic orbit in the hybrid zero dynamics can be embedded into the full order dynamics to yield the periodic orbit \mathcal{O} of the full order dynamics. This periodic orbit is obtained via the canonical embedding: $\Pi_0^v(y_{1,v}, z_v) = (y_{1,v}, 0, z_v)$:

$$\mathcal{O} := \Pi_0(\mathcal{O}_z) := (\Xi, \mathbf{I}, \rho, \Pi_0 \Phi \mathbf{C}^z), \quad \Pi_0 \Phi \mathbf{C}^z := \{\Pi_0^{\rho(i)}(\Phi_{\rho(i)}^z \mathbf{C}_i^z)\}_{i \in \Xi}. \quad (5.82)$$

Fig. 5.3 shows a periodic orbit for illustration.

By defining the norm $\|(\eta_v, z_v)\| = \|y_{1,v}\| + \|\eta_{2,v}\| + \|z_v\|$, we can define the distance from the periodic orbit as

$$\begin{aligned} \|(\eta_v, z_v)\|_{\mathcal{O}} &= \inf_{(\eta'_v, z'_v) \in \mathcal{O}} \|(\eta_v, z_v) - (\eta'_v, z'_v)\| \\ &= \inf_{(y'_{1,v}, z'_v) \in \mathcal{O}_z} \|(z_v - z'_v)\| + \|(y_{1,v} - y'_{1,v})\| + \|\eta_{2,v}\|. \end{aligned} \quad (5.83)$$

The continuous dynamics is exponentially stable in each domain if there are constants $r, \delta_1, \delta_2 > 0$ such that if

$$(\eta_v, z_v) \in \{(\eta_v, z_v) \in \Phi_v(\pi_x(\mathbb{D}_v)) : \|(\eta_v, z_v)\|_{\mathcal{O}} < r\},$$

it follows that $\|\varphi_t^v(\eta_v, z_v)\|_{\mathcal{O}} \leq \delta_1 e^{-\delta_2 t} \|(\eta_v, z_v)\|_{\mathcal{O}}$. Exponential stability of \mathcal{O} is obtained via Poincaré maps, (4.66). Hereafter, we redefine the Poincaré maps in terms of the transformed coordinates (similar to the redefinition done for the flow φ_t^v and the reset map Δ_e):

$$\mathbb{P}_{\text{source}(e)} : \Phi_{\text{source}(e)}(\pi_x(\mathbb{S}_e)) \rightarrow \Phi_{\text{source}(e)}(\pi_x(\mathbb{S}_e)), \quad e \in \mathbb{E}. \quad (5.84)$$

The fixed point is denoted by $(\eta^*, z^*) \in \mathbb{S}_{\text{source}(e)}$ such that $\mathbb{P}_{\text{source}(e)}(\eta^*, z^*) = (\eta^*, z^*)$ for some $e \in \mathbb{E}$. The periodic orbit \mathcal{O} is exponentially stable if $\|\mathbb{P}_v(\eta_v, z_v) - (\eta^*, z^*)\| \leq$

$e^{-c}\|(\eta_v - \eta^*, z_v - z^*)\|$, $c > 0$, $(\eta_v, z_v) \in \mathbb{B}(\eta^*, z^*) \cap \mathbb{S}_e$. Poincaré map of the partial (full) hybrid zero dynamics \mathbb{P}_z and the corresponding exponentially stability of the periodic orbit \mathcal{O}_z can also be similarly defined.

Analysis of the stability of $\mathcal{IH}_c^\varepsilon$ under the assumption that the (partial) hybrid zero dynamics $\mathcal{IH}_c|_z$ has a stable periodic orbit has been studied in [28]; the main theorem from this article will be stated here. The proof was shown for a single domain hybrid system, which is easily extensible to multi-domain hybrid systems.

Lemma 21. *Let \mathcal{O}_z be an exponentially stable periodic orbit for the (partial) hybrid zero dynamics $\mathcal{IH}_c|_z$ (5.77) transverse to $\mathbb{S}|_z$. If there exists a domain dependent RES-CLF $V_{\varepsilon,v}$ for the continuous dynamics, then there exists an $\hat{\varepsilon} > 0$ such that for all $0 < \varepsilon < \hat{\varepsilon}$ and for all Lipschitz continuous feedback $u(\eta_v, z_v) \in \mathbf{K}_{v,\varepsilon}(\eta_v, z_v)$, $v \in \mathbb{V}$, $\mathcal{O} = \iota_0(\mathcal{O}_z)$ is an exponentially stable periodic orbit of the full order hybrid system $\mathcal{IH}_c^\varepsilon$ (5.78).*

To put in simple words, Theorem 21 says that for small enough $\varepsilon > 0$, the set of controllers (5.56) renders the full order periodic orbit \mathcal{O} exponentially stable. Since $\mathbf{K}_{v,\varepsilon,\bar{\varepsilon}} \subset \mathbf{K}_{v,\varepsilon}$, Theorem 21 naturally extends to controllers of the form (5.58). Therefore, we need to show that $\mathbf{K}_{v,\varepsilon,\bar{\varepsilon}}$ for each $v \in \mathbb{V}$ is indeed an input to state stabilizing controller for the full order periodic orbit \mathcal{O} .

We have the following theorem, which is the extension of Lemma 10 to hybrid systems of the form (5.80).

Theorem 4. *Let \mathcal{O}_z be an exponentially stable periodic orbit for the hybrid zero dynamics $\mathcal{IH}_c|_z$ transverse to $\mathbb{S}|_z$. Existence of a Lipschitz continuous control law, $u(\eta_v, z_v) \in \mathbf{K}_{v,\varepsilon}(\eta_v, z_v)$, $v \in \mathbb{V}$, that exponentially stabilizes $\mathcal{O} = \iota_0(\mathcal{O}_z)$ in the hybrid system (4.62), implies the existence of a Lipschitz continuous control law, $u(\eta_v, z_v) \in \mathbf{K}_{v,\varepsilon,\bar{\varepsilon}}(\eta_v, z_v)$, $v \in \mathbb{V}$, that exponentially input to state stabilizes \mathcal{O} in the hybrid control system (4.62).*

Proof of the above theorem will be shown for two specific kinds of uncertainties in

Chapters 8 (parameter uncertainty) and 9 (phase uncertainty). In Chapter 7 we will pick other kinds of uncertainties encountered in bipedal walking robots in detail and analyze the ISS properties.

Part III

Bipedal Robots

CHAPTER 6

HYBRID SYSTEM MODEL OF BIPEDAL ROBOTS

In this chapter, we will discuss a general hybrid model for a bipedal robot. We will also show methods to obtain control Lyapunov functions via feedback linearization. The walking robot DURUS, and the running robot DURUS-2D are shown in Fig. 6.7. The robot with pointed feet AMBER1 is shown in Fig. 6.1. The robot with feet used to realize dynamically stable dancing (see Fig. 10.1) is shown in Fig. 6.3. AMBER1 is modeled as a simple hybrid system (single domain, single vector field and a single impact map), while AMBER2 is modeled as a multi-domain hybrid system that consists of 10 vertices and 20 edges. The footed robot, DURUS, switches between double support (ds) and single support (ss) phases, and in the case of running, the robot model consists of stance (s) and flight (f) phases. Therefore, both DURUS and DURUS-2D are modeled as two domain hybrid systems, as shown by Fig. 6.8. From Fig. 6.7, the DURUS humanoid has feet that are always assumed to be flat on ground, while the running robot DURUS-2D has pointed feet rendering the feet unactuated. More complex versions of locomotion can also be adopted in DURUS, such as multi contact heel and toe behaviors, which have been studied in [69].

6.1 Robot Model

We will study robot models AMBER1, AMBER2, DURUS 2D and finally the 3D humanoid DURUS.

6.1.1 Model of AMBER1

AMBER1 is a 2D bipedal robot with five links (two calves, two thighs and a torso, see Fig. 6.1). AMBER1 is 61 cm tall with a total mass of 3.3 kg. The robot has point feet, and is thus under-actuated at the ankle. In addition, this robot is built for only 2D walk-

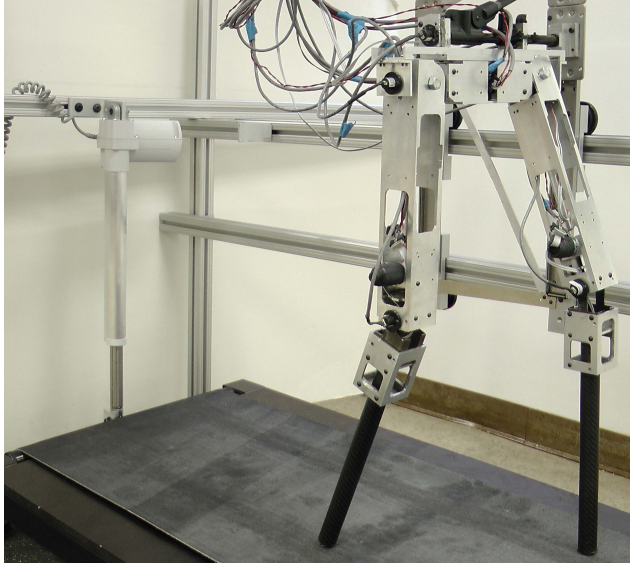


Figure 6.1: The biped AMBER1 on the treadmill.

ing. Since we are modeling walking in AMBER1, the legs alternate between swing (non-stance) and stance phases. So if the left leg is stance, then the right leg becomes the swinging (nonstance) leg. For this robot, $\mathbb{Q} \subset \mathbb{R}^{n_R}$ denotes the configuration space with $q = (q_{sf}, q_{sk}, q_{sh}, q_{nsh}, q_{nsk})^T \in \mathbb{Q}$ containing the relative angles between the links as shown in Fig. 6.2. The model constraints are also shown in Fig. 6.2. $h(q)$ is the unilateral constraint, which is effectively the height of the swinging foot from ground. When the foot hits the ground, the stance and nonstance legs are swapped. The hybrid model for this robot can (see [70, 71] for details) be represented by (4.8), which is exactly the formulation shown in (4.1) except for the absence of the directed graph Γ . This directed graph representation via vertices and edges is omitted since only one domain and one guard is required. In other words, there is only one continuous phase and one discrete dynamics (nonstance foot strike).

For this hybrid system, the domain, guard, reset map and the vector field are given here. The domain and switching surfaces (guards) are defined w.r.t. $h : \mathbb{Q} \rightarrow \mathbb{R}$, the height of the

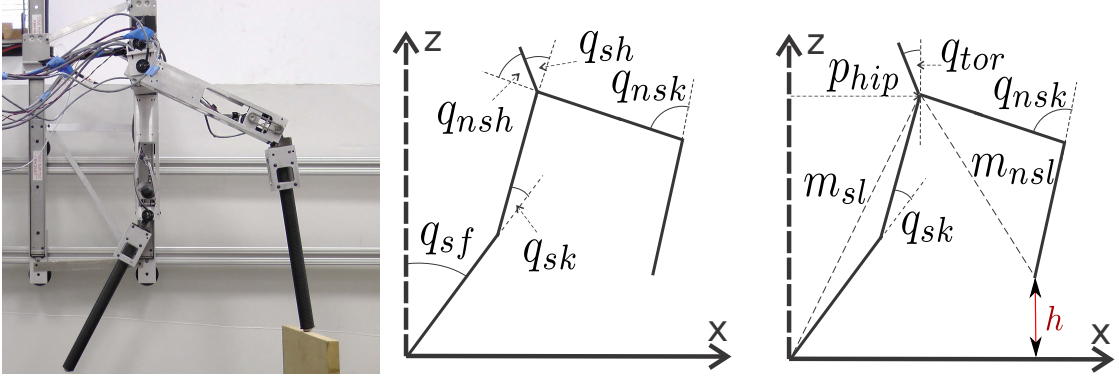


Figure 6.2: The biped AMBER1 (left) and the stick figure showing the configuration angles (middle) and output constraints (right).

swing foot from ground (see Fig. 6.2).

$$\begin{aligned}\mathbb{D} &= \{(q, \dot{q}) \in T\mathbb{Q} : h(q) \geq 0\} \\ \mathbb{S} &= \{(q, \dot{q}) \in T\mathbb{Q} : h(q) = 0, \dot{h}(q) < 0\}\end{aligned}\tag{6.1}$$

$\Delta(x)$ represents the impact map obtained from the discrete dynamics, and $\mathbb{FG} = (f, g)$ forms the vector field that is obtained from the continuous dynamics. Both the continuous and discrete dynamics are described below.

Continuous Dynamics. Calculating the inertial properties of each link of the robot (Fig. 6.1) yields the Lagrangian,

$$\mathcal{L}(q, \dot{q}) = \frac{1}{2} \dot{q}^T D(q) \dot{q} - \mathcal{V}(q).\tag{6.2}$$

Explicitly, this is done symbolically through the method of exponential twists (see [72]). $D(q) \in \mathbb{R}^{n \times n}$ is the inertia matrix, and \mathcal{V} is the potential energy. The inertias of the motors and boom are also included. Let I_r , I_g , I_m be the rotational inertias of the rotor (reflected), gearbox, and motor, respectively. Then, $I_m = I_r + I_g$. Because I_r is large, I_g can be ignored. Each joint is connected to a motor through a metal chain. Therefore, the axis of rotation of the rotor has an offset w.r.t. that of the link. Using the parallel axis theorem:

$I_p = I_m + m_m d_m^2$, where I_p is the motor inertia shifted to the joint axis, m_m is the mass of the rotating motor parts, and d_m is the distance between axes. Again, since $m_m = 0.011 \text{ kg}$, $I_p \approx I_m$.

The combined inertia matrix, D_{com} , used in the Lagrangian is

$$D_{com}(q) = D(q) + \text{diag}(0, I_{m,sk}, I_{m,sh}, I_{m,nsh}, I_{m,nsk}), \quad (6.3)$$

where $I_{m,sk}$, $I_{m,sh}$, $I_{m,nsh}$, $I_{m,nsk}$ represent the motor inertias of the links. The Euler-Lagrange equation yields a dynamic model

$$D_{com}(q)\ddot{q} + C(q, \dot{q})\dot{q} + G(q) = Bu, \quad (6.4)$$

where the control, $u \in \mathbb{R}^{m_R}$, is a vector of torque inputs. $C(q, \dot{q}) \in \mathbb{R}^{n_R \times n_R}$ is the matrix of Coriolis-centrifugal terms, $G(q) \in \mathbb{R}^{n_R}$ is the gravity vector. $B \in \mathbb{R}^{n_R \times m}$ is the torque mapping consisting of 1's and 0's with $B(1, 1) = 0$. Without loss of generality, it can be assumed that the mapping B is one to one from the torque input u to the corresponding joints. Since AMBER1 has DC motors, we need to derive equations with voltage inputs. Since the motor inductances are small, we can realize the electromechanical system

$$v_{in} = R_a i_a + K_\omega \omega, \quad (6.5)$$

where v_{in} is the vector of voltage inputs to the motors, i_a is the vector of currents through the motors, and R_a is the resistance matrix. Since the motors are individually controlled, R_a is a diagonal matrix. K_ω is the motor velocity constant matrix and ω is a vector of angular velocities of the motors. Representing (6.5) in terms of currents, the applied torque is $u = K_\varphi R_a^{-1}(v_{in} - K_\omega \omega)$, with K_φ the torque constant matrix. Thus, the Euler-Lagrange

equation takes the form

$$D_{com}(q)\ddot{q} + C(q, \dot{q})\dot{q} + G(q) = BK_\varphi R_a^{-1}(v_{in} - K_\omega \omega). \quad (6.6)$$

Converting this model to first order ODEs yields the affine control system (f, g) with inputs v_{in} :

$$\begin{aligned} f(q, \dot{q}) &= \begin{bmatrix} \dot{q} \\ -D_{com}^{-1}(q)(C(q, \dot{q})\dot{q} + G(q) + BK_\varphi R_a^{-1}K_\omega \dot{q}) \end{bmatrix}, \\ g(q) &= \begin{bmatrix} \mathbf{0} \\ D_{com}^{-1}(q)BK_\varphi R_a^{-1} \end{bmatrix}. \end{aligned} \quad (6.7)$$

Discrete Dynamics. When the nonstance foot impacts the ground, the angular velocities change. Hence we define a reset map (switching map), $\Delta : \mathbb{S} \rightarrow \mathbb{D} \setminus \mathbb{S}$, which maps the pre-impact state to the post-impact state. This reset map has two components: one is the impact velocity map, $\Delta_{\dot{q}}$ (given the pre-impact velocities, the post-impact velocities will be $\Delta_{\dot{q}}(q)\dot{q}$), and the other one is the relabeling matrix, Δ_q , which swaps the “stance” and “nonstance” legs. The reset map Δ is given by

$$\Delta : \mathbb{S} \rightarrow \mathbb{D}, \quad \Delta(q, \dot{q}) = \begin{bmatrix} \Delta_q q \\ \Delta_q \Delta_{\dot{q}}(q)\dot{q} \end{bmatrix}. \quad (6.8)$$

Δ_q updates the configuration q at impact (by appropriately changing the labels). $\Delta_{\dot{q}}$ is obtained as follows. Let $(p_x(q), p_z(q))$ be the position of the nonstance foot. p_x^{ns} denotes the x horizontal distance from stance foot, and p_z^{ns} denotes the vertical distance from stance

foot. We have the Jacobian of these positions as

$$\mathcal{J} = \begin{bmatrix} \frac{\partial p_x^{ns}}{\partial q} \\ \frac{\partial p_z^{ns}}{\partial q} \end{bmatrix}. \quad (6.9)$$

Given the pre-impact velocity \dot{q}^- , the post-impact velocity \dot{q}^+ is obtained from the following

$$\begin{bmatrix} D_{com} & -\mathcal{J}^T \\ \mathcal{J} & 0 \end{bmatrix} \begin{bmatrix} \dot{q}^+ \\ \delta F_{imp} \end{bmatrix} = \begin{bmatrix} D_{com}\dot{q}^- \\ 0 \end{bmatrix}, \quad (6.10)$$

where δF_{imp} is the set of impulsive forces acting from the ground, \mathcal{J} is obtained from (6.9). After obtaining the \dot{q}^+ , relabeling is done to obtain the switching (reset) map. More details are provided in [73].

Trajectory tracking. Walking is generally achieved by realizing a set of reference trajectories for each joint actuator. We can define the desired trajectories for a set of k outputs $y : \mathbb{Q} \rightarrow \mathbb{R}^k$ for AMBER1.

- The linearization of the x -position of the hip, p_{hip} , given by:

$$\delta p_{\text{hip}}(q) = L_c(-q_{sf}) + L_t(-q_{sf} - q_{sk}), \quad (6.11)$$

where L_c , L_t are the calf and thigh lengths, respectively.

- Linearized slope of the nonstance leg, m_{nsl} (the tangent of the angle between the z-axis and the line on the nonstance leg connecting the ankle and hip), given by:

$$\delta m_{nsl}(q) = -q_{sf} - q_{sk} - q_{sh} + q_{nsh} + q_{nsk}L_c/(L_c + L_t). \quad (6.12)$$

- q_{sk} , the stance knee angle.

- q_{nsk} , the nonstance knee angle.
- $q_{tor}(q)$, the torso angle from vertical

$$q_{tor}(q) = q_{sf} + q_{sk} + q_{sh}. \quad (6.13)$$

These outputs are shown in Fig. 6.2.

Since, AMBER1 is under-actuated, we have only four motors to control. Therefore, the number of outputs that we can control is limited by the degree of under-actuation. Of course, in the case of robots like AMBER2 where the under-actuation also depends on the domain the robot is operating (for example, double support has over actuation in AMBER2), the outputs picked change in every phase. Therefore, we pick four relative degree outputs ($k = 4$) of AMBER1 and drive them to a set of desired functions.

$$y^d(\tau, \alpha) = \begin{bmatrix} y_H(\tau, \alpha_{sk}) \\ y_H(\tau, \alpha_{nsk}) \\ y_H(\tau, \alpha_{nsl}) \\ y_H(\tau, \alpha_{tor}) \end{bmatrix}, \quad y^a(q) = \begin{bmatrix} q_{sk} \\ q_{nsk} \\ \delta m_{nsl}(q) \\ q_{tor}(q) \end{bmatrix} \quad (6.14)$$

where $y_H(t, \alpha_i)$, $i \in \{sk, nsk, nsl, tor, nsf\}$ contains the parameters α_i specific to the output. They are obtained from an offline optimization problem to obtain a realizable reference walking gait. See [74] for more details. y_H are called human functions, obtained via the human-inspired gait optimization [70], and consist of sines and cosines

$$y_H(t, \alpha) = e^{-\alpha_4 t} (\alpha_1 \cos(\alpha_2 t) + \alpha_3 \sin(\alpha_2 t)) + \alpha_5. \quad (6.15)$$

The modulation of the desired trajectories are modulated by the phase variable τ , either

via time or via the under-actuated coordinates. Specifically, we use the following

$$\tau(q) = \frac{\delta p_{\text{hip}}(q) - \delta p_{\text{hip}}(q^+)}{v_{\text{hip}}}, \quad (6.16)$$

where $\delta p_{\text{hip}}(q^+)$ is the linearized position of the hip at the beginning of a step. q^+ is the configuration where the height of the nonstance foot is zero, i.e., $h(q^+) = 0$. v_{hip} is some constant. Using (6.16), we define the final form of the outputs, which is the difference between the actual and desired outputs

$$y(q) = y^a(q) - y^d(\tau(q), \alpha). \quad (6.17)$$

We use feedback linearizing controller to drive these outputs to zero. More on the trajectory tracking control law and its ensuing uncontrolled dynamics will be discussed in Chapter 6, Section 5.1 and Chapter 5.

6.1.2 Model of AMBER2

AMBER2 is a 2D bipedal robot with seven links (two calves, two thighs, two feet and a torso, see Fig. 6.3) primarily built for obtaining multi-contact walking behavior (see [69]). This thesis shows work on achieving dynamically stable dancing in AMBER2, as a deviation from the traditional walking i.e., nonperiodic behaviors. AMBER2 is the second generation of robots that was built in AMBER Lab and is an expansion upon its predecessor, AMBER1 (Fig. 6.1). Unlike AMBER1, AMBER2 was designed to walk in a circle around a pivot connected by a boom. Each of the joints are actuated by brushless DC (BLDC) motors. The drives are remotely connected to the stationary power supply with the help of slip rings. The joint angles of the robot are measured by absolute incremental optical encoders.

Due to the changes of contact points on the foot throughout the course of the dance, generalized coordinates are naturally used to characterize the robot. Specifically, the con-

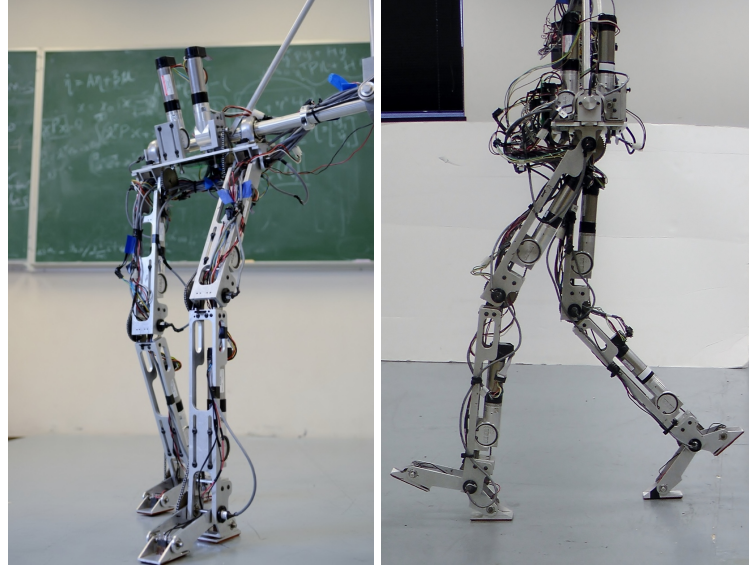


Figure 6.3: The bipedal robot AMBER2 (left) is constructed with the specific goal of multi-contact behavior as indicated by the design of the feet (right).

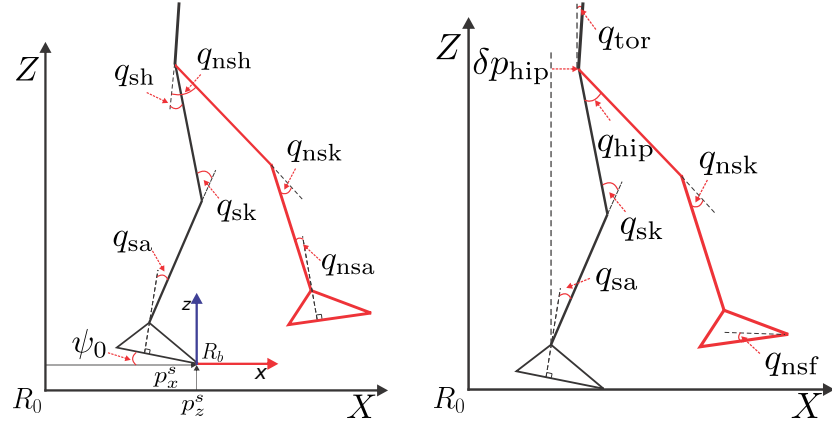


Figure 6.4: Robot configuration (left) and outputs (right).

figuration space $\mathbb{Q} = \mathbb{R}^2 \times SO(2) \times \mathbb{Q}_b \in \mathbb{R}^{n_R}$ is represented in coordinates as $q = (q_0, q_b)$, where the extended coordinate q_0 represent the rotation angle of the body fixed frame R_b with respect to a fixed inertial frame R_0 ; here $q_b = (q_{sa}, q_{sk}, q_{sh}, q_{nsh}, q_{nsk}, q_{nsa})$ denotes the body coordinates of the robot as shown in Fig. 6.4. Note that the translational coordinates p_x^s, p_z^s are also shown, which are not included in the dynamics since the stance toe is assumed to be pinned to ground throughout the course of dancing. For AMBER2, $n_R = 9$, $\mathbb{Q}_b \subset \mathbb{R}^6$ and $q \in \mathbb{R}^9$, and the number of actuators $k = 6$.

Similar to AMBER1, we can model AMBER2 as a hybrid system, but with more than one domain, vector field and reset map. The directed graph Γ will have 8 vertices and 42 edges based on Fig. 4.3. We have the set of vertices

$$\mathbb{V} = \{\text{DHL}, \text{FTBH}, \text{UA}, \text{FTL}, \text{FHL}, \text{FF}, \text{S}, \text{BHL}\} \quad (6.18)$$

We will pick only two domains (see Fig. 6.5) will be described here to give the basic notion. We can define the contact points $\mathcal{C} = \{\text{st}, \text{sh}, \text{nst}, \text{nsh}\}$ corresponding to stance toe, stance heel, nonstance toe and nonstance heel respectively. The heights $h_c, c \in \mathcal{C}$ will correspond to the heights of the respective contact points. By fixing the contact point st to ground the number of possible contact conditions for the remaining three is 2^3 (that is why 8 domains in Fig. 4.3). For the two domains in Fig. 6.5: back hell lift (BHL) and swing (S), we have the following representation

$$\begin{aligned} \mathbb{D}_{\text{BHL}} &= \{(q, \dot{q}) \in \mathbb{R}^{2n_R} \mid h_{\text{nsh}} \geq 0, \begin{bmatrix} h_{\text{st}} \\ h_{\text{sh}} \\ h_{\text{nst}} \end{bmatrix} = 0\}, \\ \mathbb{D}_{\text{S}} &= \{(q, \dot{q}) \in \mathbb{R}^{2n_R} \mid \begin{bmatrix} h_{\text{nst}} \\ h_{\text{nsh}} \end{bmatrix} \geq 0, \begin{bmatrix} h_{\text{st}} \\ h_{\text{sh}} \end{bmatrix} = 0\}, \end{aligned} \quad (6.19)$$

and the guards (switching surfaces) determine the states of the robot where the transitions take place. It is important to note that in the original hybrid model switching happens in multiple directions, and therefore the guard of each domain is the union of the individual switching surfaces for each transition. Guard of $\text{BHL} \rightarrow \text{S}$ and $\text{S} \rightarrow \text{BHL}$ are defined as follows

$$\mathbb{S}_{\text{BHL} \rightarrow \text{S}} = \{(q, \dot{q}) \in \mathbb{R}^{2n_R} \mid h_{\text{nst}} = 0, h_{\text{nst}} > 0, h_{\text{nsh}} \geq 0, \begin{bmatrix} h_{\text{st}} \\ h_{\text{sh}} \end{bmatrix} = 0\}, \quad (6.20)$$

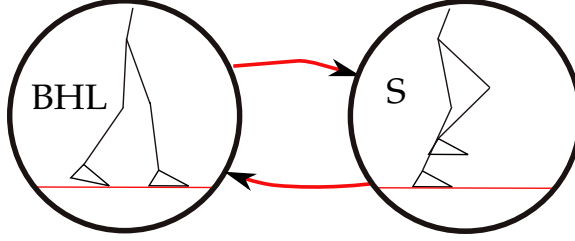


Figure 6.5: Showing two domains: back heel lift (BHL) and the swing phase (S) with the two edges.

$$\mathbb{S}_{S \rightarrow BHL} = \{(q, \dot{q}) \in \mathbb{R}^{2n_R} | h_{nst} = 0, \dot{h}_{nst} < 0, h_{nsh} \geq 0, \begin{bmatrix} h_{st} \\ h_{sh} \end{bmatrix} = 0\}. \quad (6.21)$$

Union of the source of the individual edges emanating from each domain is $\mathbb{S}_S = \bigcup_{v \in V} \mathbb{S}_{S \rightarrow v}$, where the set of vertices are given by (6.18). Note that the execution of this hybrid system is done by using a time based control law (see [75]). More on this is discussed in Chapter 10.

Continuous Dynamics. The Lagrangian dynamics for this n_R -DOF robot is similar to that of AMBER1 (6.4) with the inclusion of floating base degrees of freedom. With the multiple foot behaviors that can be realized, we know that the feet cannot go below ground. The dynamics need to be realized through the use of holonomic constraints, which constrain both heel and toe of the nonstance foot whenever they are in contact with ground. These holonomic constraints are enforced in the following manner.

$$D(q)\ddot{q} + C(q, \dot{q})\dot{q} + G(q) = B(q)u + \mathcal{J}_{sh}^T F_{sh} + \mathcal{J}_{nst}^T F_{nst} + \mathcal{J}_{nsh}^T F_{nsh}, \quad (6.22)$$

where $\mathcal{J}_i(q)$ is the Jacobian of specific contact points $i \in \mathcal{C}$ corresponding stance heel, nonstance toe and nonstance heel respectively. $F_i(q, \dot{q})$, which are the reaction forces due to the holonomic constraints, are defined for each domain based on the contact conditions of the heel and toe. Note that $F_i = 0$ if there is no contact with ground. F_i can be explicitly derived from the states x and the controller u by differentiating the holonomic constraints

twice. The details are omitted here and can be found in [72]. If $F_{\text{nst}} = 0$ and $F_{\text{nsh}} = 0$, then a fully actuated condition of the robot is realized. Otherwise, an over-actuated condition is

$$\text{achieved. We will denote } \mathcal{J}_A = \begin{bmatrix} \mathcal{J}_{\text{sh}} \\ \mathcal{J}_{\text{nst}} \\ \mathcal{J}_{\text{nsh}} \end{bmatrix} \text{ and } F_A = \begin{bmatrix} F_{\text{sh}} \\ F_{\text{nst}} \\ F_{\text{nsh}} \end{bmatrix}.$$

Discrete Dynamics. The discrete dynamics is obtained similar to AMBER1. See (6.10) for more details.

Trajectory tracking. The trajectories achieved to realize dynamic dancing are time based in nature. Therefore, we will choose time based desired trajectories for this application. Due to presence of feet, AMBER2 has more actuators compared to AMBER1. In addition, the behavior of the feet are affected by interactions with ground. Therefore, we have outputs designed based on if both the feet are on ground (double support ds) or just one foot (single support ss). We have outputs defined separately for single support and double support domains.

$$y_{\text{ss}}^a(q) = \begin{bmatrix} q_{sk} \\ q_{nsk} \\ q_{hip}(q) \\ q_{tor}(q) \\ q_{nsf}(q) \end{bmatrix}, \quad y_{\text{ss}}^d(\tau, \alpha_{\text{ss}}) = \begin{bmatrix} y_H(\tau, \alpha_{sk}) \\ y_H(\tau, \alpha_{nsk}) \\ y_H(\tau, \alpha_{hip}) \\ y_H(\tau, \alpha_{tor}) \\ y_H(\tau, \alpha_{nsf}) \end{bmatrix}, \quad (6.23)$$

where the actual outputs are redefined with the inclusion of ψ_0 (Fig. 6.4)

$$\begin{aligned} \delta p_{\text{hip}}(q) &= -(L_c + L_t)(\psi_0 + q_{sk} + q_{sa}) - L_t q_{sk}, \\ q_{hip}(q) &= q_{nsh} - q_{sh}, \\ q_{tor}(q) &= \psi_0 + q_{sa} + q_{sk} + q_{sh}, \\ q_{nsf}(q) &= \psi_0 + q_{sa} + q_{sk} + q_{sh} - q_{nsh} - q_{nsk} - q_{nsa}. \end{aligned} \quad (6.24)$$

The outputs for the double support domain are

$$y_{\text{ds}}^a(q) = \begin{bmatrix} q_{sa} \\ y_{\text{ss}}^a(q) \end{bmatrix}, \quad y_{\text{ds}}^d(\tau, \alpha_{\text{ds}}) = \begin{bmatrix} y_H(\tau, \alpha_{sa}) \\ y_{\text{ss}}^d(\tau, \alpha_{\text{ds}}) \end{bmatrix}. \quad (6.25)$$

The phase variable, which modulates the walking functions y_H (from (6.15)), is a function of time $\tau(t)$. To drive the outputs y^a to y^d , we use time based feedback linearization.

6.1.3 Model of DURUS Humanoid

DURUS is a 23 DOF robot, consisting of fifteen actuated joints throughout the body. There is one linear passive spring at the end of each leg. The generalized coordinates of the robot are described in Fig. 6.6 (see [64]); the continuous dynamics of the bipedal robot is given by the following:

$$D(q)\ddot{q} + C(q, \dot{q})\dot{q} + G(q) = Bu + \mathcal{J}_W^T(q)F_W, \quad (6.26)$$

$$\mathcal{J}_W(q)\ddot{q} + \dot{\mathcal{J}}_W(q, \dot{q})\dot{q} = 0, \quad (6.27)$$

where $\mathcal{J}_W(q)$ are the Jacobian of the contact constraints of the feet, and F_W are the associated contact wrenches. The constraints are on the position of the feet and their angles with ground. Other terms in the EOM have the usual meaning as in (6.22). Assumptions on the model are the same as that for AMBER1,AMBER2, such as $D(q)$ is invertible, B is one-to-one mapping from the actuators to joints. The nonsingulariry assumption of $D(q)$ can be utilized to obtain Lipschitz continuity property of the vector fields, which will be important to prove stability results in Chapters 7-9. Due to the presence of passive springs, the double-support domain becomes more prominent compared to AMBER1. A two-domain hybrid system model is utilized to model DURUS walking, where a transition from double support (ds) to single support (ss) domain takes place when the normal force on nonstance foot reaches zero, and a transition from single support to double support domain occurs

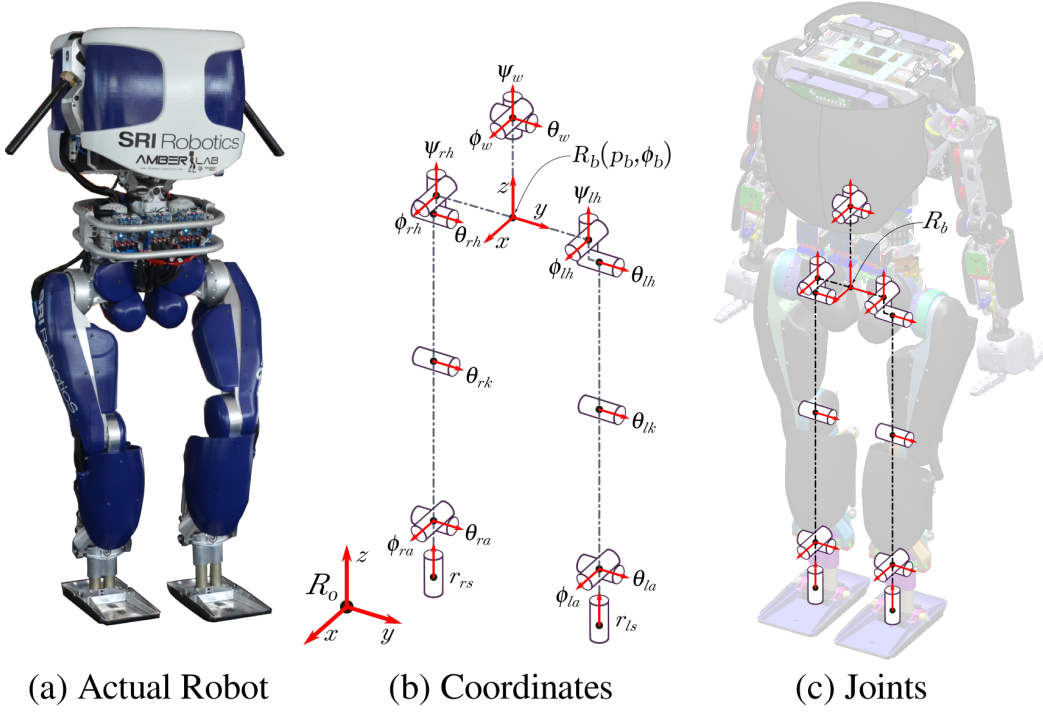


Figure 6.6: DURUS robot designed by SRI International.

when the nonstance foot strikes the ground [64]. Since there is no impact while transitioning from double-support to single-support, the discrete map is an identity. The holonomic constraints are defined in such a way that feet are flat on the ground when they are in contact with the ground. In addition, DURUS is supported by a linear boom, which restricts the motion of the robot to the sagittal plane. The contacts with the boom are also modeled as holonomic constraints.

The hybrid control system model (in the form of (4.1)) for this robot is described here.

- We can define two vertices and edges as: $\mathbb{V}_W = \{\text{ss}, \text{ds}\}$, $\mathbb{E}_W = \{\text{ss} \rightarrow \text{ds}, \text{ds} \rightarrow \text{ss}\}$ forming the directed graph $\Gamma_W = (\mathbb{V}_W, \mathbb{E}_W)$. A pictorial representation of Γ for DURUS humanoid is provided with the directed graph for DURUS-2D in Fig. 6.8.

- The domains are described below:

$$\mathbb{D}_{ss} = \{(q, \dot{q}, u) \in \mathbb{R}^{2n_R} \times \mathbb{R}^{m_R} | h_s = 0, h_{ns} \geq 0\},$$

$$\mathbb{D}_{ds} = \{(q, \dot{q}, u) \in \mathbb{R}^{2n_R} \times \mathbb{R}^{m_R} | h_s = 0, h_{ns} = 0, F_W^{ns} \geq 0\}. \quad (6.28)$$

Here h_{\square} denotes the height of the contact points specified by $\square \in \mathcal{C}_W = \{s, ns\}$. F_W^{ns} is the vertical ground reaction force acting on the nonstance foot.

- By selecting the domains as in (6.28), we have the guards

$$\mathbb{S}_{ss \rightarrow ds} = \{(q, \dot{q}, u) \in \mathbb{R}^{2n_R} \times \mathbb{R}^{m_R} | h_s = 0, h_{ns} = 0, \dot{h}_{ns} < 0\},$$

$$\mathbb{S}_{ds \rightarrow ss} = \{(q, \dot{q}, u) \in \mathbb{R}^{2n_R} \times \mathbb{R}^{m_R} | h_s = 0, h_{ns} = 0, F_W^{ns} = 0\}. \quad (6.29)$$

- \mathbb{U} is the set of admissible controls, and is generally the set of allowable torque inputs for the robot. CLFs are defined from this set and it is assumed that this set is large enough for feasibility.
- There is no impact from double support to single support phase, so $\Delta_{ds \rightarrow ss}$ is an identity map as mentioned before. The map $\Delta_{ss \rightarrow ds} : \mathbb{S}_{ss \rightarrow ds} \rightarrow \mathbb{D}_{ds}$ is obtained by using the impact model obtained from the discrete dynamics.

$$\Delta_{ss \rightarrow ds}(q, \dot{q}) = \begin{bmatrix} \Delta_q & 0 \\ 0 & \Delta_q \Delta_{\dot{q}}(q) \end{bmatrix} \begin{bmatrix} q \\ \dot{q} \end{bmatrix}. \quad (6.30)$$

- \mathbb{FG} is obtained from (6.26) by representing $x = (q, \dot{q})$.

Trajectory tracking. We pick joint angles that are normal to the sagittal plane, e.g., commanding zero position to all roll and yaw joints. In particular, we define a relative degree

one output as

$$y_1(q) = \delta\dot{p}_{hip}(q) - v_{\text{hip}}, \quad (6.31)$$

where v_{hip} is a constant (typically a desired hip velocity), $\delta p_{hip}(q)$ is the linearized hip position picked similar to (6.24),

$$\delta p_{hip}(q) = L_a\theta_{ra} + (L_a + L_c)\theta_{rk} + (L_a + L_c + L_t)\theta_{rh}, \quad (6.32)$$

with L_a , L_c , and L_t the length of ankle, calf, and thigh link of the robot respectively. The relative degree two outputs are defined in the following (assuming right leg is the stance leg)

- stance knee pitch: $y_2^{a,\text{skp}} = \theta_{rk}$,
- stance torso pitch: $y_2^{a,\text{stp}} = -\theta_{ra} - \theta_{rk} - \theta_{rh}$,
- waist pitch: $y_2^{a,\text{wp}} = \theta_w$,
- non-stance knee pitch: $y_2^{a,\text{nskp}} = \theta_{lk}$,
- non-stance foot pitch: $y_2^{a,\text{nsfp}} = p_z^{nst}(q) - p_z^{nsh}(q)$,
- non-stance slope:

$$y_2^{a,\text{nsl}} = -\theta_{ra} - \theta_{rk} - \theta_{rh} + \frac{L_c}{L_c + L_t}\theta_{lk} + \theta_{lh},$$

where $p_z^{nst}(q)$ and $p_z^{nsh}(q)$ are the height of nonstance toe and heel respectively. To guarantee that the non-stance foot remains flat, the desired non-stance foot pitch output should be zero. Correspondingly, the desired outputs $y_d^2(\tau, \alpha)$ are defined as 6th-order Bézier polynomials, where τ is the phase variable, which can be either time based or state based. The state based phase variable $\tau(q)$ is the same as (6.16). The combined outputs of the system are defined as $y^a(q) = [y_1^a, y_2^{aT}]^T$ and $y^d(\tau, \alpha) = [v_{\text{hip}}, y_2^d(\tau, \alpha)^T]^T$. We use time based feedback linearization to drive the actual outputs to the desired outputs.

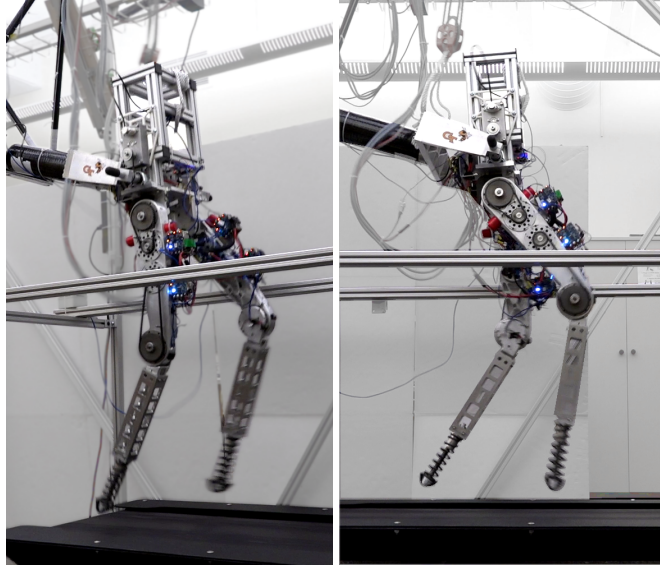


Figure 6.7: The spring-legged planar running biped, DURUS-2D.

6.1.4 Model of DURUS-2D

DURUS-2D is a 11 DOF planar bipedal robot (Fig. 6.7) a predecessor of the DURUS humanoid robot. The primary goal of this robot was to realize stable walking gaits with compliance. After successively achieving walking [76], the next natural step was to achieve more complex behaviors. With the objective of achieving running, the hybrid system running model is developed. DURUS-2D has two springs on the feet that are pointed. Therefore, DURUS-2D has a high degree of under-actuation with two phases: stance s and flight f. Besides, since the objective is to achieve running, the actuators need to operate at high velocities to get the desired high speed. The continuous dynamics for DURUS-2D is the same as for DURUS humanoid (as given by (6.26)) except for the Jacobian of the constraints

$$\mathcal{J}_R = \begin{bmatrix} \mathcal{J}_s \\ \mathcal{J}_{ns} \end{bmatrix}, \quad (6.33)$$

where $\mathcal{J}_s, \mathcal{J}_{ns}$ corresponds to the Jacobian of the stance and nonstance foot respectively.

The hybrid system model of DURUS-2D is described here

- The directed graph has the vertices and edges as: $\mathbb{V}_R = \{s, f\}$, $\mathbb{E}_R = \{s \rightarrow f, f \rightarrow s\}$.

A pictorial representation of this directed graph is given in Fig. 6.8.

- The domains are described below.

$$\begin{aligned}\mathbb{D}_s &= \{(q, \dot{q}) \in \mathbb{R}^{2n_R} \mid h_s = 0, h_{ns} > 0\}, \\ \mathbb{D}_f &= \{(q, \dot{q}) \in \mathbb{R}^{2n_R} \mid h_s > 0, h_{ns} \geq 0\}. \end{aligned}\quad (6.34)$$

Here h_\square denotes the height of the contact points specified by $\square \in \mathcal{C}_R = \{s, ns\}$.

An alternative definition of the domain can also be obtained by using the holonomic constraints $h_v : \mathbb{Q} \rightarrow \mathbb{R}^l$ wherein the position and orientation of the contact points \mathcal{C} are fixed.

- By choosing the domains as in (6.34),

$$\begin{aligned}\mathbb{S}_{s \rightarrow f} &= \{(q, \dot{q}) \in \mathbb{R}^{2n_R} \mid h_s = 0, h_{ns} > 0, \dot{h}_s > 0\}, \\ \mathbb{S}_{f \rightarrow s} &= \{(q, \dot{q}) \in \mathbb{R}^{2n_R} \mid h_s > 0, h_{ns} = 0, \dot{h}_{ns} < 0\}. \end{aligned}\quad (6.35)$$

- Similar to the DURUS humanoid, there is no impact from double support to single support phase, so $\Delta_{s \rightarrow f}$ is an identity map. The map $\Delta_{f \rightarrow s} : \mathbb{S}_f \rightarrow \mathbb{D}_s$ is obtained by using the impact model obtained from the discrete dynamics.

Other elements of (4.1) are obtained similar to that of DURUS.

6.2 Robot Tracking and Control

We now can describe the trajectory tracking controllers for AMBER1, AMBER2, DURUS and finally the running robot DURUS-2D here. Assuming $v \in \mathbb{V}$ with the vertex set taking the specific forms for each robot, we can define the feedback control laws for each vertex

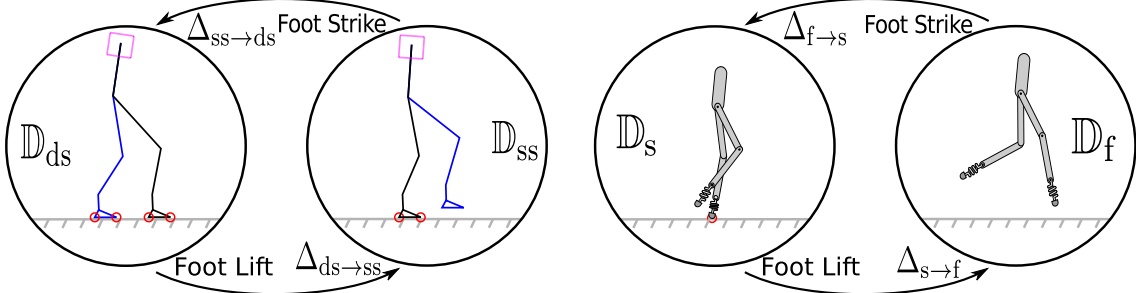


Figure 6.8: Hybrid system model for the walking robot DURUS (left) and for the running robot DURUS 2D (right).

(domain). We choose a general EOM of the form

$$D(q)\ddot{q} + C(q, \dot{q})\dot{q} + G(q) = B(q)u + \mathcal{J}_{\square}^T F_{\square}, \quad (6.36)$$

where $\square \in \{A, W, R\}$, which corresponds to the holonomic constraints of AMBER2 (6.22) or DURUS or DURUS-2D (6.26). Accordingly, we have the dynamics represented in terms of the state $x = (q, \dot{q})$.

$$\begin{aligned} \dot{x} &= f(x) + g(x)u \\ f(x) &= \begin{bmatrix} \dot{q} \\ D^{-1}(q)(-C(q, \dot{q})\dot{q} - G(q) + \mathcal{J}_{\square}^T F_{\square}) \end{bmatrix}, \quad g(x) = \begin{bmatrix} 0 \\ D^{-1}(q)B \end{bmatrix}. \end{aligned} \quad (6.37)$$

6.2.1 Computed Torque

We will utilize the method of computed torque since it is highly effective for robotic systems [77]. It is also convenient in the context of uncertain models, which will be studied in Chapter 8. Given relative degree one and two outputs y_1, y_2 , we have the following

derivatives

$$\begin{aligned}\dot{y}_1 &= \frac{\partial y_1}{\partial \dot{q}} \ddot{q} + \frac{\partial y_1}{\partial q} \dot{q} \\ \ddot{y}_2 &= \frac{\partial L_f y_2}{\partial \dot{q}} \ddot{q} + \frac{\partial L_f y_2}{\partial q} \dot{q}.\end{aligned}\tag{6.38}$$

we therefore denote the Jacobians

$$\mathcal{J}_y := \begin{bmatrix} \frac{\partial y_1}{\partial \dot{q}} \\ \frac{\partial L_f y_2}{\partial \dot{q}} \end{bmatrix}, \quad \dot{\mathcal{J}}_y := \begin{bmatrix} \frac{\partial y_1}{\partial q} \\ \frac{\partial L_f y_2}{\partial q} \end{bmatrix}.\tag{6.39}$$

It can be observed that for relative degree two outputs $\frac{\partial L_f y_2}{\partial \dot{q}} = \frac{\partial y_2}{\partial q}$.

Since the number of outputs is less than the degrees of freedom, $k < n_R$, we add $n_R - k$ rows to \mathcal{J}_y and $\dot{\mathcal{J}}_y$ to make the co-efficient matrix of \ddot{q} in (6.38) full rank. These rows correspond to the configuration that are under-actuated resulting in

$$\begin{bmatrix} 0 \\ \dot{y}_1 \\ \ddot{y}_2 \end{bmatrix} = \begin{bmatrix} D_1 \\ \mathcal{J}_y \end{bmatrix} \ddot{q} + \begin{bmatrix} H_1 \\ \dot{\mathcal{J}}_y \dot{q} \end{bmatrix},\tag{6.40}$$

where H_1 is the first $n_R - k$ rows of $H(q, \dot{q}) = C(q, \dot{q})\dot{q} + G(q) + \mathcal{J}_{\square}^T F_{\square}$, $\square \in \{A, W, R\}$, and D_1 is the first $n_R - k$ rows of the inertia matrix, $D(q)$. These rows correspond to the under-actuated degrees of freedom of the robot (corresponding to zero rows of the torque map B). It should be observed that since the under-actuated degrees of freedom have zero torque being applied, the resulting EOM of the robot leads to zero on the left hand side of (6.40), and hence the choice of rows. Accordingly, we can define the desired acceleration

for the robot to be:

$$\ddot{q}_d = \begin{bmatrix} D_1 \\ \mathcal{J}_y \end{bmatrix}^{-1} \left(\begin{bmatrix} 0 \\ \mu \end{bmatrix} - \begin{bmatrix} H_1 \\ \dot{\mathcal{J}}_y \dot{q} \end{bmatrix} \right), \quad (6.41)$$

where μ is a linear control input. The resulting torque controller that realizes this desired acceleration in the robot can be defined as:

$$Bu = D(q)\ddot{q}_d + C(q, \dot{q})\dot{q} + G(q). \quad (6.42)$$

6.2.2 Feedback Linearization \equiv Computed Torque

Here we will show that the controllers feedback linearization and computed torque are both equivalent even for under-actuated systems. For partially observable systems, there are ways to apply feedback linearization as long as the number of outputs is equal to the number of actuators ($m = k$). It is also possible to extend this I/O control approach even for non-square systems via control Lyapunov functions.

Lemma 22. *Substituting (6.42) and (6.41) in (6.36) results in linear dynamics*

$$\begin{bmatrix} \dot{y}_1 \\ \ddot{y}_2 \end{bmatrix} = \mu \quad (6.43)$$

Proof. Substituting (6.42), (6.41) in (6.36) results in

$$\begin{aligned} D(q)\ddot{q} + C(q, \dot{q})\dot{q} + G(q) &= D(q)\ddot{q}_d + C(q, \dot{q})\dot{q} + G(q) \\ \implies \ddot{q} &= \begin{bmatrix} D_1 \\ \mathcal{J}_y \end{bmatrix}^{-1} \left(\begin{bmatrix} 0 \\ \mu \end{bmatrix} - \begin{bmatrix} H_1 \\ \dot{\mathcal{J}}_y \dot{q} \end{bmatrix} \right). \end{aligned} \quad (6.44)$$

Therefore, we have the following

$$\begin{aligned} \begin{bmatrix} D_1 \\ \mathcal{J}_y \end{bmatrix} \ddot{q} + \begin{bmatrix} H_1 \\ \dot{\mathcal{J}}_y \dot{q} \end{bmatrix} &= \begin{bmatrix} 0 \\ \mu \end{bmatrix} \\ \implies \begin{bmatrix} \dot{y}_1 \\ \ddot{y}_2 \end{bmatrix} &= \mu. \end{aligned} \tag{6.45}$$

□

μ can be chosen to therefore stabilize the y dynamics. We will utilize a CLF based controller to achieve this goal.

6.3 ISS-CLFs for Bipedal Walking

In this section we will analyze the classes of RES-CLFs and Re-ISS-CLFs constructed from Chapter 5 on the bipedal robot DURUS (see Fig. 6.6). For verification of the improved stabilizing results presented by input to state stabilizing controllers, we simulate a humanoid robot under various disturbances and observe improvements of the stability of the gait. The robot under study is DURUS, a 23 DOF robot, consisting of fifteen actuated joints and one linear passive spring at the end of each leg. The generalized coordinates of the robot are described in Fig. 6.6 (see [64]) and the continuous dynamics of the bipedal robot is given by (6.26). The nominal walking gait in this simulation study has two phases: single support, and double support, as shown in Fig. 6.8. A stable reference walking gait is obtained and verified via an offline optimization algorithm. Therefore, based on Theorem 2 of [28], there is a small enough ε (observed to be ≤ 0.2) that makes the hybrid periodic orbit exponentially stable. It is important to note that the torque requirements increase with the decrease in ε .

The main objective of performing a perturbation analysis is to test the stability of the walking gait under uncertainties that are as realistic as possible. Therefore, we set torque

limits of 250Nm for each joint and apply a modeling error of 10% to the mass-inertial properties of the robot. Specifically the modeling error was enforced on the mass, center of mass and inertial properties of each link. It is assumed that other properties such as links lengths and spring constants are accurate. The stabilizing controller chosen for simulation is IO linearization (as given by (5.5))

$$u_{\text{IO}} = \begin{bmatrix} L_g y_{1,v} \\ L_g L_f y_{2,v} \end{bmatrix}^{-1} \left(- \begin{bmatrix} L_f y_{1,v} \\ L_f^2 y_{2,v} \end{bmatrix} + \begin{bmatrix} -\frac{1}{\varepsilon} y_{1,v} \\ -\frac{2}{\varepsilon} L_f y_{2,v} - \frac{1}{\varepsilon^2} y_{2,v} \end{bmatrix} \right).$$

The input to state stabilizing controller chosen was (as given by (3.8))

$$u_{\text{ISS}} = u_{\text{IO}} - \frac{1}{\bar{\varepsilon}} L_g V^T.$$

where the Lyapunov function $V(\eta_v) = \eta_v^T P_{\varepsilon,v} \eta_v$. P_ε , depends on ε , is the solution to the CARE: $F^T P_\varepsilon + P_\varepsilon F - \frac{1}{\varepsilon} P_\varepsilon G G^T P_\varepsilon + \frac{1}{\varepsilon} Q_\varepsilon$ (see equation (47) of [28]).

Two test cases were chosen: lateral push force to the hip for a duration of 0.1s at the beginning of the single support domain, and stepping onto an unknown ground height. Table 6.1 shows the comparison for the push force recovery between u_{IO} and u_{ISS} for different values of $\varepsilon, \bar{\varepsilon}$. It can be observed that with u_{ISS} the robot can handle greater push forces. With lower ε , the stability of the robot is affected (due to 10% model error and torque saturations) resulting in poorer performance for $\varepsilon = 0.05$. On the other hand, Fig. 6.9 shows that the convergence improves as $\bar{\varepsilon}$ is lowered. Fig. 6.10 shows the Lyapunov function comparisons for the push recovery. Fig. 6.11 and Fig. 6.12 show the comparisons for unknown step over different heights. Fig. 6.13 shows tiles of push recovery (top) and stepping over (bottom) for an ISS controller. A video link demonstrating the simulations performed on the robot is given in [1].

Table 6.1: Comparison of maximum recoverable push forces in lateral direction. The ISS based controller can handle greater pushes. Also reducing ε leads to instability due to the constraints on model uncertainty and torque limits.

Controller	IO Gain (ε)	Maximum Allowable Push (N)
IO	0.2	380
	0.1	420
	0.05	395
ISS ($\bar{\varepsilon} = 0.1$)	0.2	380
	0.1	435
	0.05	410
ISS ($\bar{\varepsilon} = 0.01$)	0.2	435
	0.1	435
	0.05	405

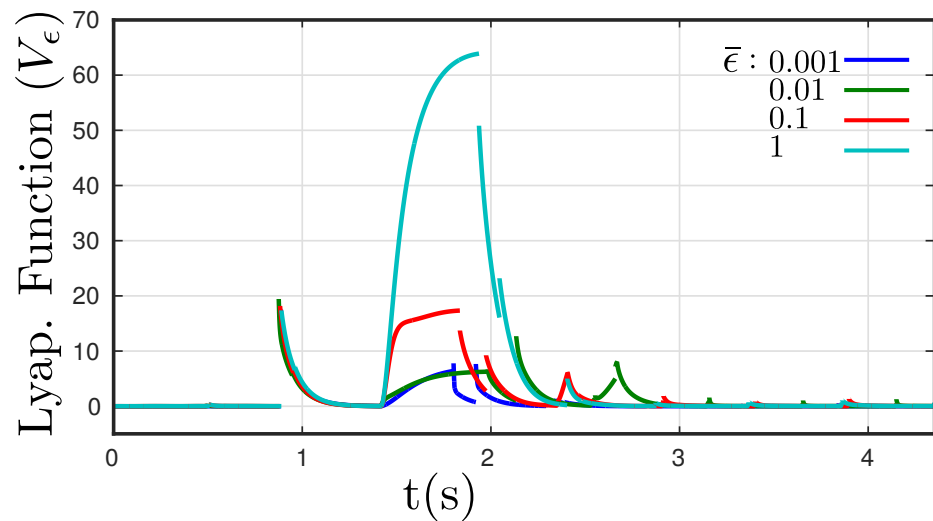


Figure 6.9: Comparisons of the Lyapunov function for various values of $\bar{\varepsilon}$ for push recovery. The push force was 350N. The convergence is quicker for decreasing $\bar{\varepsilon}$. The jumps are due to discrete events (impacts).

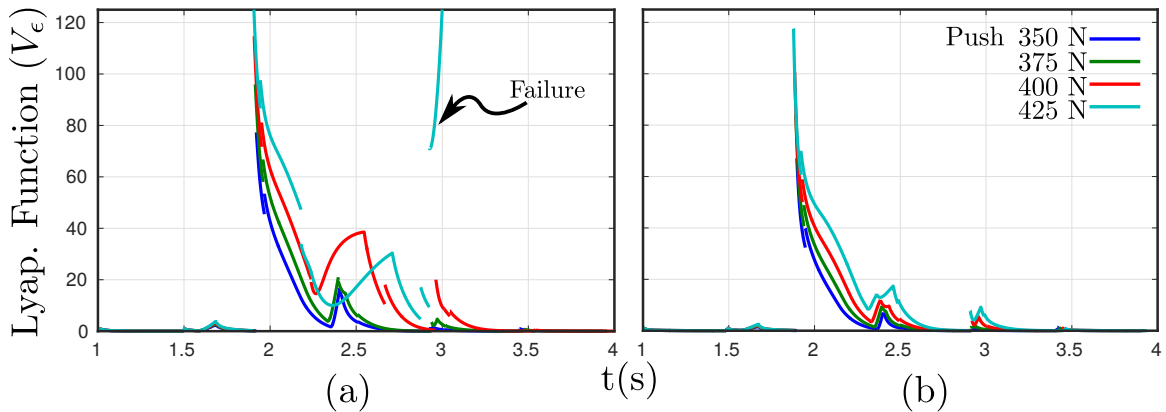


Figure 6.10: Push recovery comparison via the Lyapunov functions for IO (a) and ISS (b) based controllers. $\varepsilon = \bar{\varepsilon} = 0.1$. The convergence rate is preserved for ISS-CLF.

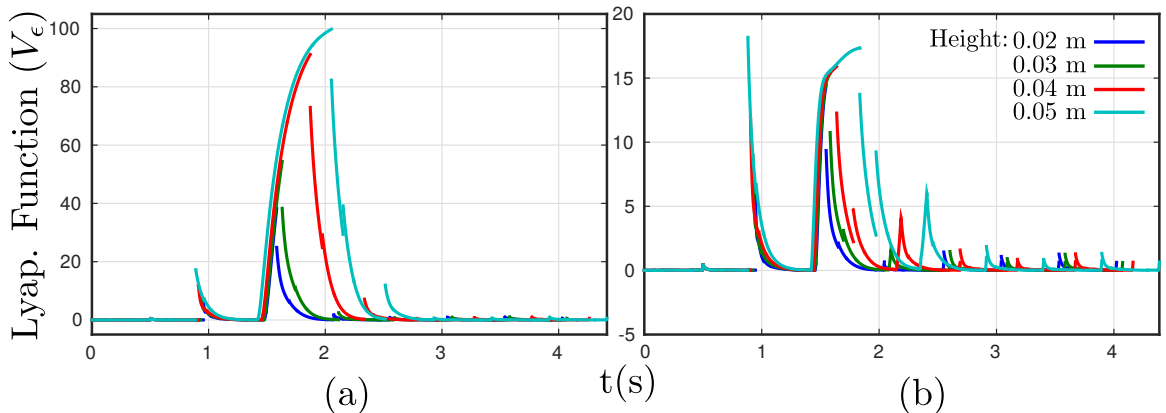


Figure 6.11: Step over comparison via Lyapunov functions for IO (a) and ISS (b) based controllers. $\varepsilon = \bar{\varepsilon} = 0.1$. The convergence rate is preserved for ISS-CLF.

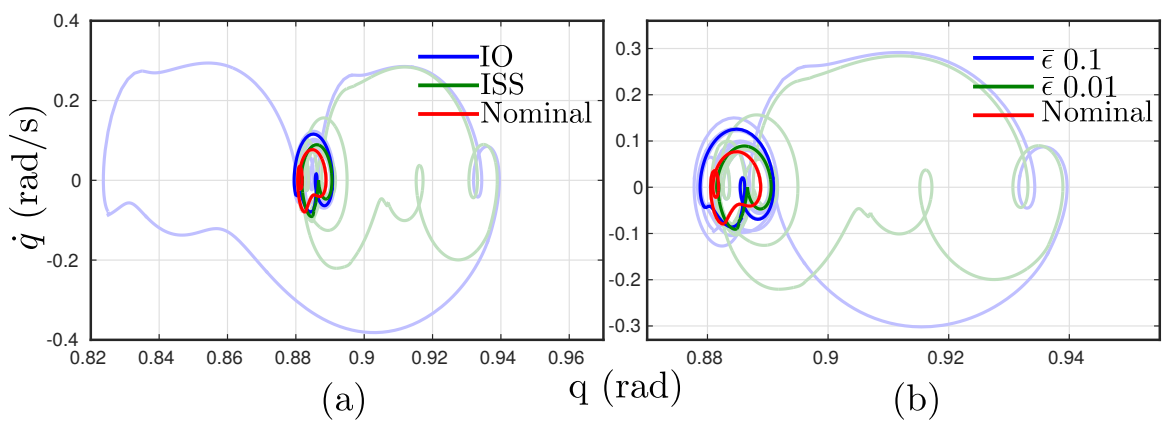


Figure 6.12: Walking over 5cm step height. Phase portraits for vertical z position of the torso base are shown here. The ISS based controller shows a much smaller deviation.

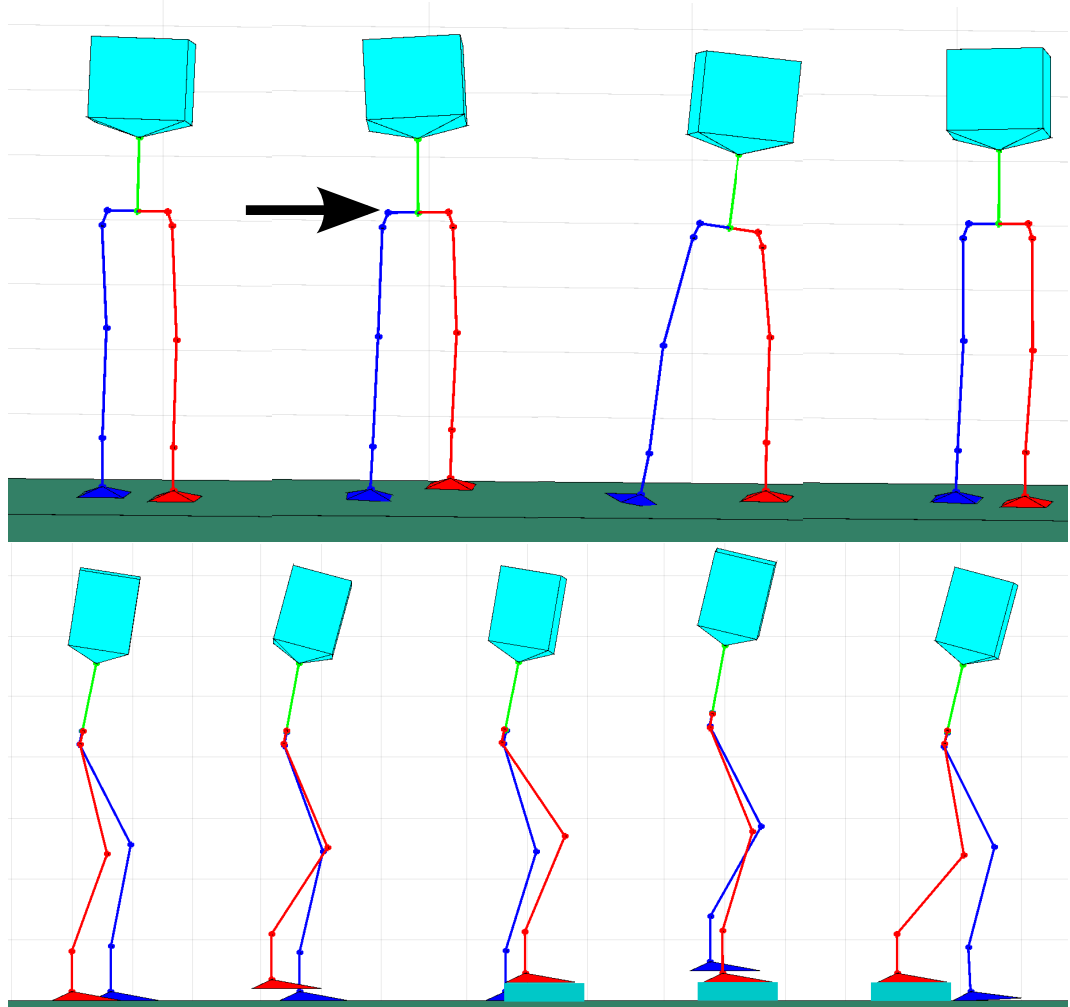


Figure 6.13: The top tiles show push recovery and the bottom tiles show stepping onto an unknown disturbance for an ISS controller. Push force of 350N is enforced (second tile) for 0.1s and the reactions are seen in tiles 3 and 4.

CHAPTER 7

DYNAMICS OF UNCERTAINTY

In this chapter, we will study how to model some of uncertainties in the dynamics of the system. In other words, we will analyze some of the prominent input uncertainties d in detail and find ways to explicitly represent them in a case by case basis. We will analyze hybrid systems with a single domain and single resetmap for convenience (they can all be easily extended to multi-domain hybrid systems) except for the last section of this chapter (Section 7.6), which includes multiple domains.

7.1 Linear Feedback Laws

We will use some of the ideas taken from [78], which showed that PD control renders a robotic system integral input to state stable. By assuming full actuation (B to be square and full rank, $n_R = m_R$), we will choose a particular control law

$$u = -K_p(q - q_d) - K_d(\dot{q} - \dot{q}_d), \quad (7.1)$$

K_p, K_d are constant gain matrices, and q_d, \dot{q}_d are constant desired velocities. Substituting for this control input in the EOM (6.22) yields

$$\begin{aligned} D(q)\ddot{q} + C(q, \dot{q})\dot{q} + G(q) &= -BK_p(q - q_d) - BK_d(\dot{q} - \dot{q}_d) \\ \implies \ddot{q} &= -D^{-1}(q)(C(q, \dot{q})\dot{q} + G(q)) - D^{-1}(q)BK_p(q - q_d) - D^{-1}(q)BK_d(\dot{q} - \dot{q}_d), \end{aligned} \quad (7.2)$$

where the inertia matrix $D(q)$ is assumed to be positive definite.

By denoting the disturbance input $d(q, \dot{q}) := -C(q, \dot{q})\dot{q} - G(q)$, we have the following

outputs

$$y = q - q_d, \quad (7.3)$$

and the following output dynamics

$$\begin{aligned} L_f y &= \dot{q} - \dot{q}_d \\ L_f^2 y &= -\frac{\partial \dot{q}_d}{\partial q} \dot{q} + \left(\mathbf{1} - \frac{\partial \dot{q}_d}{\partial \dot{q}} \right) (-D^{-1}(C\dot{q} + G)) \\ L_g L_f y &= D^{-1}B - \frac{\partial \dot{q}_d}{\partial \dot{q}} (D^{-1}B). \end{aligned} \quad (7.4)$$

Denoting $\mathcal{J} = \frac{\partial y}{\partial q} = \mathbf{1} - \frac{\partial \dot{q}_d}{\partial \dot{q}}$, we have

$$\begin{bmatrix} \dot{y} \\ \ddot{y} \end{bmatrix} = \underbrace{\begin{bmatrix} \mathbf{0} & \mathbf{1} \\ -\mathcal{J}D^{-1}BK_p & -\mathcal{J}D^{-1}BK_p \end{bmatrix}}_A \begin{bmatrix} y \\ \dot{y} \end{bmatrix} + \begin{bmatrix} \mathbf{0} \\ 1 \end{bmatrix} \underbrace{L_f^2 y}_{=:d}. \quad (7.5)$$

Since the inertia matrix D is positive definite, its maximum and minimum eigenvalues are both positive. Therefore, if we assume \mathcal{J} is bounded, it is possible to tune the matrices K_p, K_d such that the matrix A is Hurwitz. It can be easily seen that the signs of $q - q_d$ do not change even after the multiplication of the matrices $K_p, D^{-1}(q)$. Under a zero disturbance, it can be observed that (7.12) results in an *almost* linear dynamics (subject to perturbations of $\mathcal{J}(q), D^{-1}(q)$). By appropriately tuning K_p, K_d and also appropriately selecting q_d , it is possible to realize stability of this *almost* linear system.

This can be easily extended to under-actuated systems, in which the number of outputs

reduces to equal the number of actuators $y : \mathbb{R}^{n_R} \rightarrow \mathbb{R}^{m_R}$:

$$\begin{aligned}
y(q) &= y_a(q) - y_d(q) \\
L_f y(q, \dot{q}) &= \mathcal{J}(q)\dot{q} \\
L_f^2 y(q, \dot{q}) &= \frac{\partial \mathcal{J}\dot{q}}{\partial q}(q, \dot{q})\dot{q} + \mathcal{J}(q)(-D^{-1}(q)(C(q, \dot{q})\dot{q} + G(q))) \\
L_g L_f y(q, \dot{q}) &= \mathcal{J}(q)D^{-1}(q)B.
\end{aligned} \tag{7.6}$$

A convenient feedback control law that can be applied is $u = -K_p y - K_d L_f y$, where the gain matrices $K_p, K_d \in \mathbb{R}^{m \times m}$ are appropriately tuned. Note that extension to underactuated systems is possible as long as the zero dynamics is stable. An application is AMBER1 where $n = 5$, $k = 4$. Simulation results are shown in Fig. 7.1 and Fig. 7.2. Fig. 7.1 shows the results for $d = 0$ and Fig. 7.2 shows the results for $d \approx 0$, a bounded disturbance. It can easily checked that the resulting implementation is d to y stable. In other

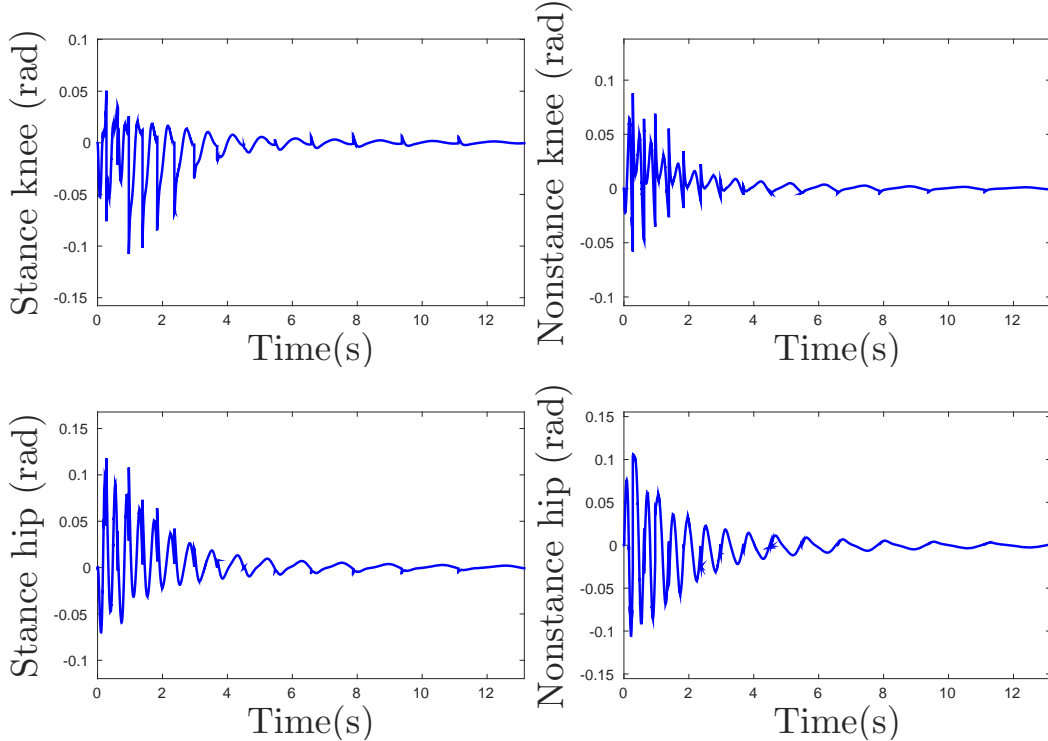


Figure 7.1: Figures showing the output errors going to zero for a zero disturbance.

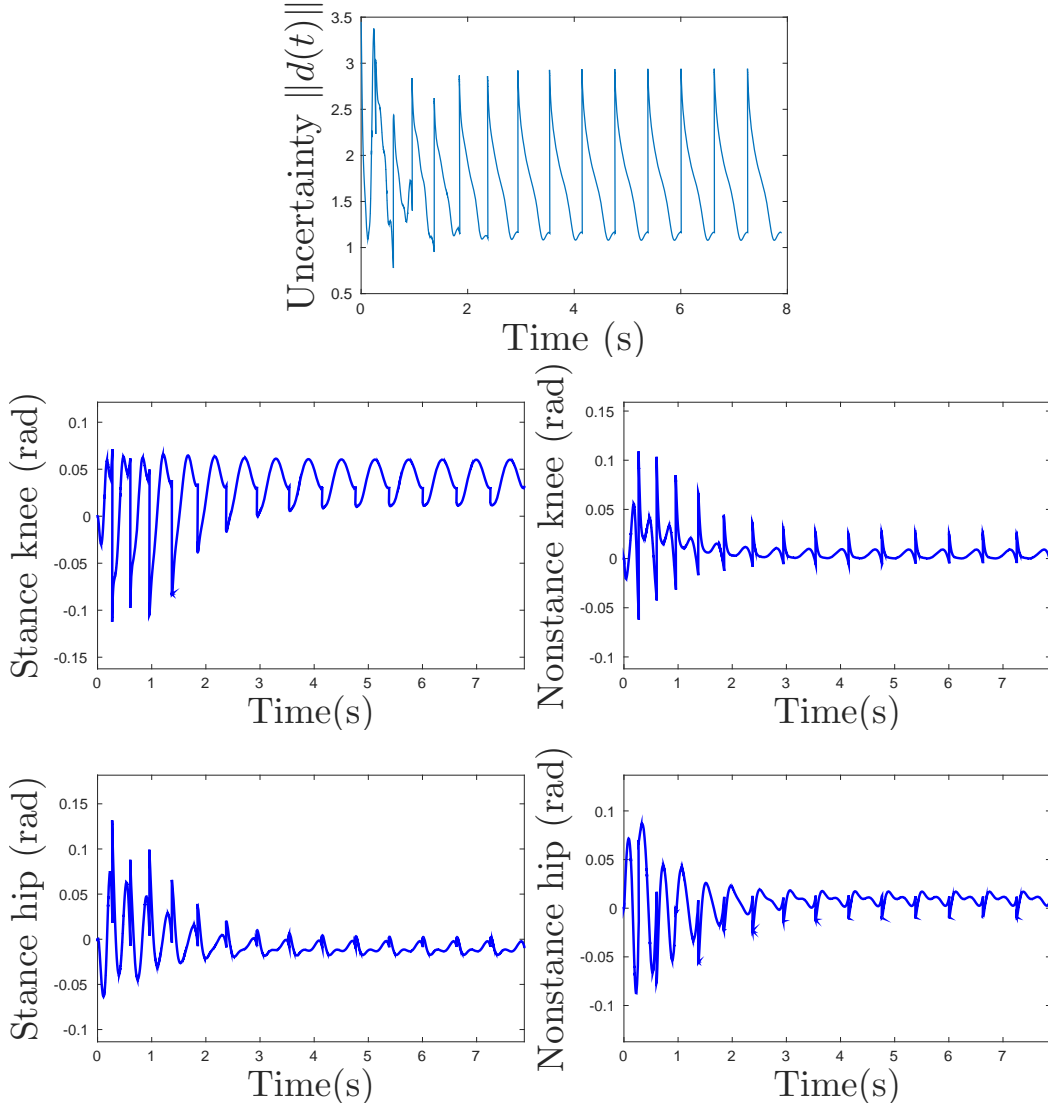


Figure 7.2: Figures showing the outputs showing boundedness under a bounded uncertainty.

words, if $d = 0$, then $|y| \rightarrow 0$, and if $\|d\|_\infty$ is bounded, the outputs y are also bounded. Linear feedback laws laws are implemented in all the robots shown in Fig. 1.4. Walking was implemented in AMBER1, PROXI, DURUS humanoid, running was implemented in DURUS-2D, and dynamic robotic dancing was implemented in AMBER2. It is important to note that this construction is extensible to under-actuated hybrid systems under hybrid invariance conditions (satisfied because the impact dynamics are solely dependent on the inertia matrix $D(q)$). Hybrid invariance conditions and the resulting hybrid zero dynamics

were discussed in detail in 5.3.2.

7.2 Proportional Voltage Control

We choose the vector fields f, g of the form (6.7) and based on the control law used in [79], we construct the EOM. Assume that the robot is fully actuated ($n_R = m_R$), i.e., B is full rank. We therefore have

$$\dot{x} = f(x) + g(x)(-K_p(q - q_d)) \quad (7.7)$$

$$\begin{bmatrix} \dot{q} \\ \ddot{q} \end{bmatrix} = \begin{bmatrix} \dot{q} \\ -D_{com}^{-1}(C\dot{q} + G + BK_\varphi R_a^{-1}K_\omega \dot{q}) - D_{com}^{-1}BK_\varphi R_a^{-1}K_p(q - q_d) \end{bmatrix}$$

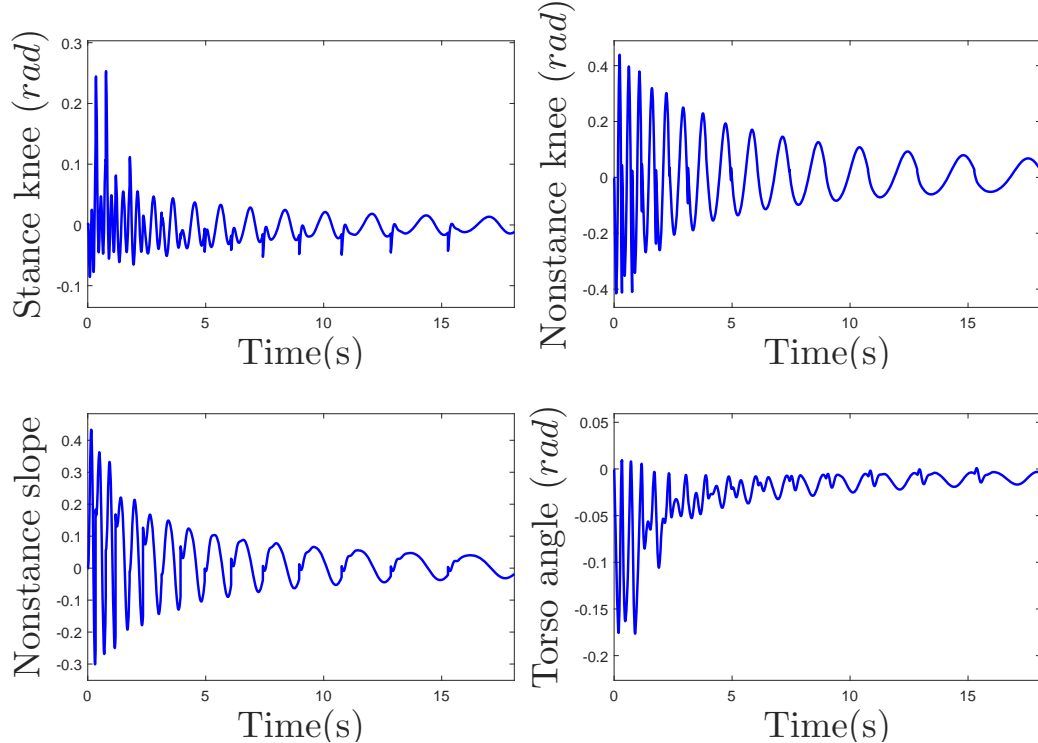


Figure 7.3: Figures showing the progression of the outputs for zero disturbance.

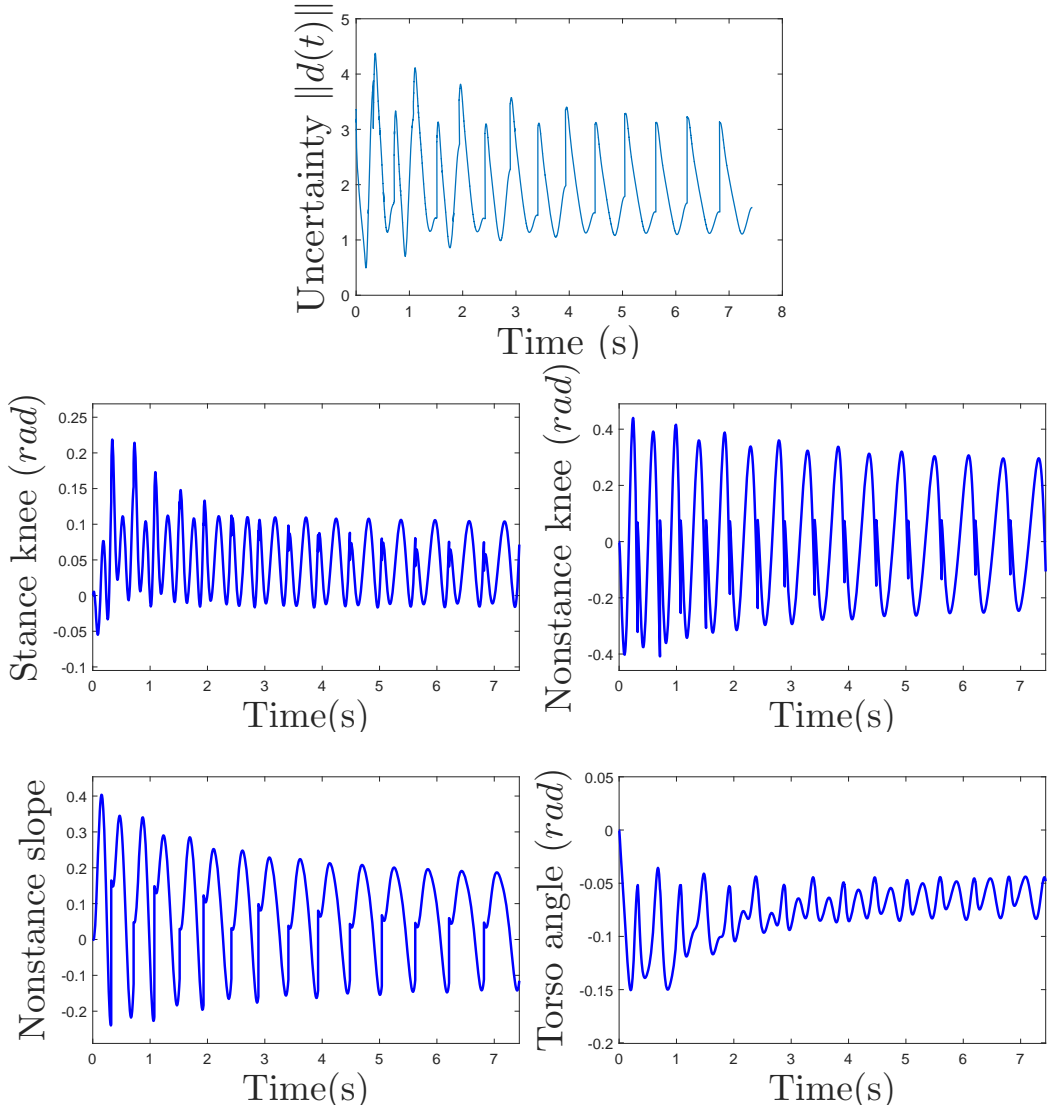


Figure 7.4: Figures showing the progression of the outputs for a bounded disturbance.

Consider the following output

$$y = q - q_d$$

$$L_f y = \dot{q} - \dot{q}_d$$

$$\begin{aligned} L_f^2 y &= -\frac{\partial \dot{q}_d}{\partial q} \dot{q} + \left(\mathbf{1} - \frac{\partial \dot{q}_d}{\partial \dot{q}} \right) (-D_{com}^{-1}(C\dot{q} + G + BK_\varphi R_a^{-1} K_\omega \dot{q})) \\ L_g L_f y &= D^{-1} BK_\varphi R_a^{-1} - \frac{\partial \dot{q}_d}{\partial \dot{q}} (D^{-1} BK_\varphi R_a^{-1}). \end{aligned} \quad (7.8)$$

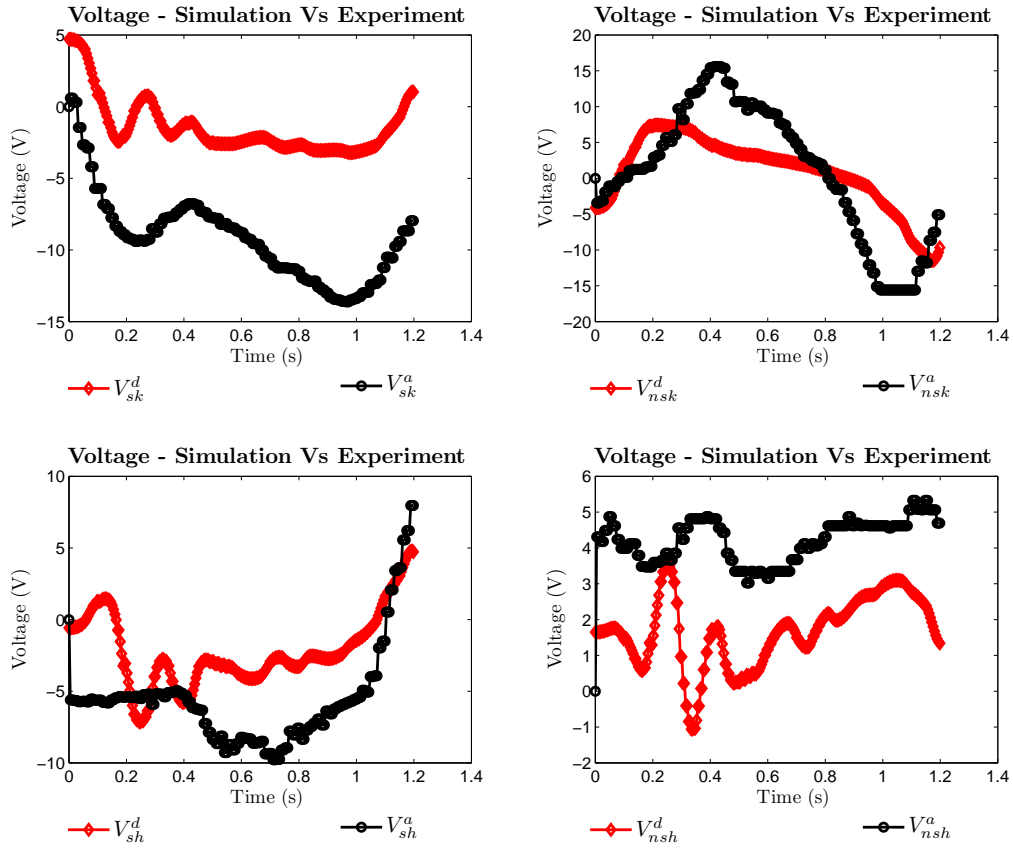


Figure 7.5: Figures showing the comparison between the voltage inputs obtained in simulation and experiment. The gap is less than $15V$.

This construction is similar to the construction shown in 7.1, in which the input is the torque instead of the voltage with an extra term that stabilizes the joint velocities.

Denoting again

$$\mathcal{J} = \mathbf{1} - \frac{\partial \dot{q}_d}{\partial \dot{q}}, \quad (7.9)$$

which is a function of q_d , we have the following resulting equation after applying $u =$

$-K_p y$:

$$\begin{bmatrix} \dot{y} \\ \ddot{y} \end{bmatrix} = \underbrace{\begin{bmatrix} \mathbf{0} & \mathbf{1} \\ -\mathcal{J}D_{com}^{-1}BK_\varphi R_a^{-1}K_p & \mathbf{0} \end{bmatrix}}_A \begin{bmatrix} y \\ \dot{y} \end{bmatrix} + \underbrace{\begin{bmatrix} \mathbf{0} \\ \mathbf{1} \end{bmatrix}}_{=:d} L_f^2 y \quad (7.10)$$

By reformulating the disturbance d , we can include the term $\mathcal{J}D_{com}^{-1}BK_\varphi R_a^{-1}rK_\omega \dot{q}$ (from the expression $L_f^2 y$ in (7.8)) in the matrix A to yield

$$d := -\frac{\partial \dot{q}_d}{\partial q} \dot{q} + \mathcal{J}(-D_{com}^{-1}(C\dot{q} + G + BK_\varphi R_a^{-1}K_\omega \dot{q}_d)), \quad (7.11)$$

where $\mathcal{J}D_{com}^{-1}BK_\varphi R_a^{-1}K_\omega \dot{q}_d$ is added and subtracted. Therefore, (7.10) can be rewritten

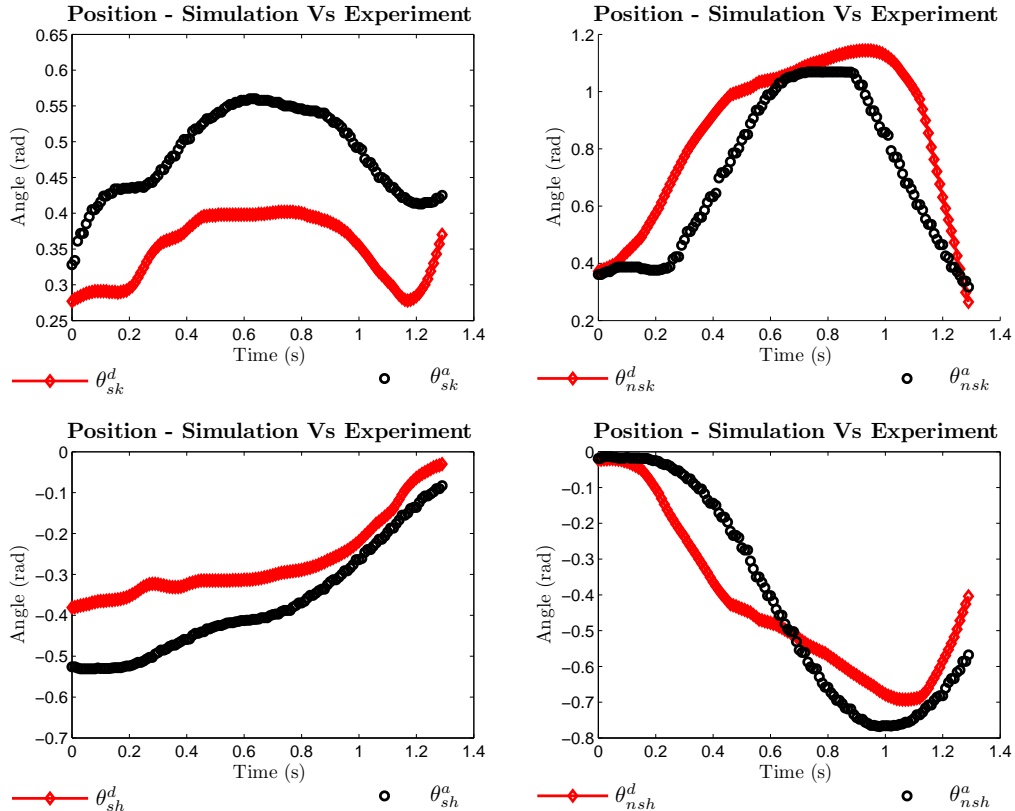


Figure 7.6: Figures showing the comparison between the simulated and the experimental joint angles. The maximum difference is close to 0.2rad.

as

$$\begin{bmatrix} \dot{y} \\ \ddot{y} \end{bmatrix} = \underbrace{\begin{bmatrix} 0 & \mathbf{1} \\ -\mathcal{J}D^{-1}BK_\varphi R_a^{-1}K_p & -\mathcal{J}D^{-1}BK_\varphi R_a^{-1}K_\omega \end{bmatrix}}_A \begin{bmatrix} y \\ \dot{y} \end{bmatrix} + \begin{bmatrix} \mathbf{0} \\ \mathbf{1} \end{bmatrix} d. \quad (7.12)$$

The proportional voltage controller used resulted in the dynamics of the form (7.12). As long as the matrix A is Hurwitz, the resulting system under hybrid invariance is d to y stable.

A similar formulation can be implemented for under-actuated systems. This proportional voltage control formulation, $u = -K_p y$, was implemented in AMBER1. The simulation results are shown in Fig. 7.3 and Fig. 7.4. Hurwitz property is achieved by appropriately adjusting the gains of K_p . Experimental results are shown in Fig. 7.5 and Fig. 7.6, in which the maximum input difference was close to $15V$ and the resulting maximum tracking error was close to 0.2rad . Videos of AMBER1 walking are given in [2, 3].

7.3 Model Based Controllers

For fully actuated systems ($n_R = m_R$), if we assume that the parameters of the robot such as COM position, mass, inertia, are unknown, then the computed torque controller (6.42) yields

$$D(q)\ddot{q} + C(q, \dot{q})\dot{q} + G(q) = \hat{D}(q)\ddot{q}_d + \hat{C}(q, \dot{q})\dot{q} + \hat{G}(q), \quad (7.13)$$

where the $\hat{\cdot}$ over the symbols indicate that the assumed model was used. Therefore, we can study the resulting dynamics under parameter uncertainty as follows.

$$\begin{aligned} D(q)\ddot{q} + C(q, \dot{q})\dot{q} + G(q) &= \underbrace{(\hat{D}(q) - D(q))\ddot{q}_d + (\hat{C}(q, \dot{q}) - C(q, \dot{q}))\dot{q} + (\hat{G}(q) - G(q))}_{=:d} \\ &\quad \cdots + D(q)\ddot{q}_d + C(q, \dot{q})\dot{q} + G(q), \end{aligned} \quad (7.14)$$

which results in the following:

$$D(q)\ddot{q} = D(q)\ddot{q}_d + d. \quad (7.15)$$

The objective is to drive the configuration q and velocity \dot{q} of the robot to some desired values via CLFs. We know that if $d \equiv 0$, we can construct CLFs via feedback linearization. Representing the dynamics in terms of the outputs, we have

$$\begin{aligned} y(q) &= q - q_d(q) \\ \dot{y}(q, \dot{q}) &= \mathcal{J}(q)\dot{q}, \quad \mathcal{J}(q) = \frac{\partial y}{\partial q} \\ \ddot{y}(q, \dot{q}) &= \mathcal{J}(q)(\ddot{q}_d + D^{-1}(q)d(q, \dot{q})) + \dot{\mathcal{J}}(q, \dot{q})\dot{q} \end{aligned} \quad (7.16)$$

The desired acceleration, \ddot{q}_d , can be appropriately chosen: $\ddot{q}_d = \mathcal{J}^{-1}(\mu - \dot{\mathcal{J}}\dot{q})$. $\mu \in \mathbb{R}^{n_R}$ is the auxiliary control input. Note that \ddot{q}_d is not dependent on the model. The following linear dynamics can be obtained

$$\begin{bmatrix} \dot{y} \\ \ddot{y} \end{bmatrix} = \underbrace{\begin{bmatrix} 0 & \mathbf{1}_{n \times n} \\ 0 & 0 \end{bmatrix}}_F \begin{bmatrix} y \\ \dot{y} \end{bmatrix} + \underbrace{\begin{bmatrix} 0 \\ \mathbf{1}_{n \times n} \end{bmatrix}}_G \mu. \quad (7.17)$$

Consider the following candidate Lyapunov function:

$$V(q, \dot{q}) := \begin{bmatrix} q - q_d(q) \\ \dot{q} - \dot{q}_d(q, \dot{q}) \end{bmatrix}^T P \begin{bmatrix} q - q_d(q) \\ \dot{q} - \dot{q}_d(q, \dot{q}) \end{bmatrix}, \quad (7.18)$$

where P is the solution to the continuous algebraic Riccati equation (CARE): $F^T P + PF - PGG^T P + Q = 0$, where $Q > 0$ is some positive definite matrix. It can be verified that V is a valid CLF if μ is picked accordingly. In fact, it is an ES-CLF because of the linearized

system. It can be explicitly written as

$$\begin{aligned} \lambda_{\min}(P)|(q - q_d, \dot{q} - \dot{q}_d)|^2 &\leq V(q, \dot{q}) \leq \lambda_{\max}(P)|(q - q_d, \dot{q} - \dot{q}_d)|^2, \\ \inf_{\mu \in \mathbb{R}^n} [L_F V(q, \dot{q}) + L_G V(q, \dot{q})\mu + \frac{\lambda_{\min}(Q)}{\lambda_{\max}(P)} V(q, \dot{q})] &\leq 0. \end{aligned} \quad (7.19)$$

Based on Lemma 10, we have the corresponding ISS-CLF as

$$\begin{aligned} \lambda_{\min}(P)|(q - q_d, \dot{q} - \dot{q}_d)|^2 &\leq V(q, \dot{q}) \leq \lambda_{\max}(P)|(q - q_d, \dot{q} - \dot{q}_d)|^2, \\ \inf_{\mu \in \mathbb{R}^n} [L_F V(q, \dot{q}) + L_G V(q, \dot{q})\mu + \frac{\lambda_{\min}(Q)}{\lambda_{\max}(P)} V(q, \dot{q}) + \frac{1}{\bar{\varepsilon}} L_G V(q, \dot{q}) L_G V(q, \dot{q})^T] &\leq 0. \end{aligned} \quad (7.20)$$

It must be noted that the resulting dynamics is e-ISS with the input being the uncertainty d , which is also a function of the desired acceleration \ddot{q}_d . It is even more important to note that $L_F V$, $L_G V$ are Lie derivatives w.r.t the fields obtained from (7.15), which have no bearing on the model.

7.4 Torque Controllers

Practical implementation of feedback linearization has several challenges, since it requires model inversion. There are examples of applications where an approximate feedback linearization was implemented [80]. There is work on applying a feedforward torque input modulated by the phase variable [73]. The idea is to use the simulated trajectories and fit a curve to the the torques used on the assumed model. Consider the following feedback linearizing controller obtained from the nominal model with the assumption that the outputs are identically zero. In other words, it is assumed that robot is exhibiting partial hybrid

zero dynamics (5.42).

$$\begin{aligned}
y(q) &= y_a(q) - y_d(q) \\
L_f y(q, \dot{q}) &= \dot{y}(q, \dot{q}) \\
L_f^2 y(q, \dot{q}) &= \frac{\partial L_f y}{\partial q}(q, \dot{q}) \dot{q} - \frac{\partial L_f y}{\partial \dot{q}}(q)(C(q, \dot{q}) \dot{q} + G(q)) \\
L_g L_f y(q, \dot{q}) &= \frac{\partial L_f y}{\partial \dot{q}}(q) D^{-1}(q) B,
\end{aligned} \tag{7.21}$$

which can be used to compute the following control law

$$\hat{u} = L_g L_f y(q_d, \dot{q}_d)^{-1} (-L_f^2 y(q_d, \dot{q}_d)) - \frac{1}{\varepsilon} L_g V(q, \dot{q})^T. \tag{7.22}$$

Substituting (7.22) in the dynamics results in the disturbance input

$$d = L_g L_f y(q_d, \dot{q}_d)^{-1} (-L_f^2 y(q_d, \dot{q}_d)) - L_g L_f y(q, \dot{q})^{-1} (-L_f^2 y(q, \dot{q}) + \mu). \tag{7.23}$$

It can be verified that the control law (7.22) is ISS. The formula

$$u^* := L_g L_f y(q_d, \dot{q}_d)^{-1} (-L_f^2 y(q_d, \dot{q}_d)), \tag{7.24}$$

is effectively the torque applied on the robot as if it were on the hybrid zero dynamics. The uncertainty in torque is therefore the deviation of the torque input of the nominal trajectory from the torque input of the actual trajectory.

7.5 Parameter Uncertainty

If the assumed model \hat{D} , \hat{C} and \hat{G} are only uncertain w.r.t. the parameters then we can make use of the fact that these parameters are linear in the EOM of the robot. Therefore,

we can represent the dynamics in the following manner

$$D(q)\ddot{q} + C(q, \dot{q})\dot{q} + G(q) = Y(q, \dot{q}, \ddot{q})\Theta, \quad (7.25)$$

where Θ is the vector of model parameters. With this formulation, we can modify (7.14) to obtain the following

$$\begin{aligned} D(q)\ddot{q} + C(q, \dot{q})\dot{q} + G(q) &= \underbrace{Y(q, \dot{q}, \ddot{q}_d)\Theta - Y(q, \dot{q}, \ddot{q}_d)\hat{\Theta}}_{=:d} \\ &\quad \cdots + D(q)\ddot{q}_d + C(q, \dot{q})\dot{q} + G(q), \end{aligned} \quad (7.26)$$

where $\hat{\Theta}$ is the assumed set of model parameters. This results in the dynamics similar to (7.15) and the control Lyapunov functions can be constructed similar to (7.20). Stability analysis of hybrid bipedal robots under parameter uncertainty is analyzed in Chapter 8. Note that instead of adding and subtracting $Y(q, \dot{q}, \ddot{q}_d)\Theta$ in (7.26), we could have added and subtracted $Y(q, \dot{q}, \ddot{q})\Theta$ (function of the actual acceleration \ddot{q}) and obtained a different formula for the uncertain dynamics d . In fact, this formulation is studied in Chapter 8 and results in no change in the stability properties compared to the original form.

7.6 Phase Uncertainty

Despite all the differences between the different approaches in bipedal walking such as the ZMP based control [81, 82], capture points [83], controlled symmetries [84], SLIP model [85, 86], HZD [62], null space control [87], at a fundamental level, using a set of trajectories (gaits) as reference is still the common universal theme found in them. This is formally called gait planning even though these reference gaits are strictly not adhered to (not strictly tracked) in some approaches. As a direct consequence of using these reference gaits or reference trajectories, comes the issue of modulation of trajectories from start to end. History has shown that smooth and reliable modulation of the trajectories is a really

difficult problem, and there has been a lot of work solely dedicated to finding good candidates for modulation [63]. In the controller of interest, the phase variable τ_v that modulates the desired outputs in (5.2). Due to noisy phase variable (call it $\hat{\tau}_v$, the resulting outputs are

$$\hat{y}_{1,v}(q, \dot{q}) = y_{1,v}^a(q, \dot{q}) - y_{1,v}^d(\hat{\tau}_v, \alpha_v), \quad (7.27)$$

and relative two outputs (pose outputs)

$$\hat{y}_{2,v}(q) = y_{2,v}^a(q) - y_{2,v}^d(\hat{\tau}_v, \alpha_v). \quad (7.28)$$

We have the feedback linearizing controller that drives the outputs $\hat{y}_{1,v} \rightarrow 0, \hat{y}_{2,v} \rightarrow 0$ as

$$\hat{u} = \begin{bmatrix} L_{g_v} \hat{y}_{1,v} \\ L_{g_v} L_{f_v} \hat{y}_{2,v} \end{bmatrix}^{-1} \left(- \begin{bmatrix} L_{f_v} \hat{y}_{1,v} \\ L_{f_v}^2 \hat{y}_{2,v} \end{bmatrix} + \hat{\mu} \right), \quad (7.29)$$

where $\hat{\mu} \in \mathbb{R}^{m_R}$ is the auxiliary control input. The resulting dynamics is

$$\begin{aligned} \dot{x} &= f_v(x) + g_v(x) (\underbrace{\hat{u} - u + u}_d) \\ &= f_v(x) + g_v(x)u + g_v(x)d, \end{aligned} \quad (7.30)$$

where d is explicitly given as

$$d = \begin{bmatrix} L_{g_v} \hat{y}_{1,v} \\ L_{g_v} L_{f_v} \hat{y}_{2,v} \end{bmatrix}^{-1} \left(- \begin{bmatrix} L_{f_v} \hat{y}_{1,v} \\ L_{f_v}^2 \hat{y}_{2,v} \end{bmatrix} + \mu \right) - \begin{bmatrix} L_{g_v} y_{1,v} \\ L_{g_v} L_{f_v} y_{2,v} \end{bmatrix}^{-1} \left(- \begin{bmatrix} L_{f_v} y_{1,v} \\ L_{f_v}^2 y_{2,v} \end{bmatrix} + \mu \right). \quad (7.31)$$

It can be observed that the the nonlinearity of the outputs w.r.t. the phase variable τ_v leads to d attaining large values even for a slight perturbation of the phase variable. This phase uncertainty can be simplified further and the controllers are developed in Chapter 9.

CHAPTER 8

PARAMETER UNCERTAINTY TO STATE STABILITY

There are two main paths for approaching the problem of model parameter uncertainty in mechanical systems: 1. Obtain (usually through exhaustive experimentation) an accurate identification of the model and then adopt a stabilizing controller. 2. Develop a robust controller that renders the system stable despite the uncertainty. For the first approach, many methods have been explored in identifying the model parameters involving state estimation, regression, determination and validation in a systematic manner [88, 89]; this often involves substantial and time consuming experimental validation [90]. By determining an accurate model, model dependent controllers can be applied to realize accurate tracking and control of such systems. Despite its simplistic nature, the success of this tedious approach typically relies on the accuracy of the estimation while accounting for variations of parameters over time. While these model dependent controllers are able to deliver on the performance (exponential convergence, large domains of attraction) promised by the formal controller design process, they are extremely sensitive to changes in the parameters sometimes leading to instability.

There is a significant amount of work in literature that take the second approach, i.e., relax the need for an accurate model [91, 92, 93, 94]. Some of the methods even completely eliminate the requirement of the information of the entire parameter set via adaptive control [95, 77], and via PD and PID regulation and tracking [96, 97, 98, 99, 100, 78, 101]. [102, 103] achieved adaptive control in bipedal robots without the analysis of impact models. L1 adaptive control was implemented in [104, 105] to yield an ultimate bound on the tracking errors. There is also a significant amount of work done on developing controllers that yield a bounded output error for a bounded parameter uncertainty [91, 92]. While all these methods lead to the development of a robust controller that renders the system stable for a

bounded uncertainty, the tracking and regulation performance is sacrificed, which is critical in systems that undergo rapid changes in states—hybrid systems with impulsive effects.

It is important to note that the concept of a bounded error output for a bounded parameter uncertainty has proven to be extremely restrictive on the choice of available controllers. For example, it is a well known fact that the swinging motion of a simple pendulum with zero input (trivial input) is independent of the point mass at its end. This simple example demonstrates that we can always realize a space of unbounded model parameter sets that have the exact same response for the given control input. This motivates the need for a formal framework to understand the relationship between model parameter uncertainty and the resulting tracking/regulation performance—especially in the context of hybrid system models of robotic systems. In order to properly quantify this uncertainty that can be formally related to the resulting stability of the system, a *measure* will be defined and verified in simulation in the robot AMBER1 [106]. After establishing the measure, stability properties are proved by using showing the system is ISS w.r.t. to this measure.

For systems of the form $\dot{x} = f(\Theta; x, u)$, where Θ represents the parameter set, x represents the state and u the control input, the class of controllers that achieve a desired control objective, e.g., driving $x \rightarrow 0$, can be written via the Control Lyapunov Function (CLF) $V(x) > 0$, through the set of control inputs that satisfy the derivative condition that V decreases along solutions:

$$\mathbf{K} = \{u \in \mathbb{U} : L_f V(x, u) \leq 0\}.$$

Therefore model dependent controllers, such as feedback linearization [66] and adaptive control [107] can be reformulated via CLFs, which satisfy the condition: $V \rightarrow 0 \implies x \rightarrow 0$. Since $\dot{V}(x, u) = \frac{\partial V}{\partial x} f(\Theta; x, u)$ is a function of the vector field f , determination of u depends consequently on the parameters Θ . But, if the controller (say CLF) that stabilizes the known model is applied on the imperfect model, the resulting dynamics of this imper-

fect model satisfies the conditions of an ISS-Lyapunov function [10]. The ISS-Lyapunov function is constructed w.r.t. the input that is a function of the uncertainty. Furthermore, for robotic systems, this function can be written as a linear function of the error in parameters Θ . Therefore, by defining a measure that quantifies the parameter uncertainty as a function of the path and the controller, we can construct robust controllers that yield strict ultimate bounds for the specified uncertainty in the model. Further, as an improvement on the performance, we can construct controllers that use a combination of model based and non model based controllers (computed torque+PD) to obtain exponential ultimate bounds for hybrid systems.

The main goal of this chapter is to obtain ISS-CLFs for the uncertain robot model AMBER1. It is assumed that the kinematics of the robot are accurately known. In other words, the unknown parameters are the inertial properties of the robot. We first construct these unknown inertial elements of the robot via spatial vector algebra. The advantage is due to the fact that these parameters are linear in the dynamics of the robot.

8.1 Unmodeled Dynamics and State Stability

Since the parameters are not perfectly known, the equations of motion, (6.22), computed with the given set of parameters will henceforth have $\hat{\cdot}$ over the symbols. Therefore, D_a , C_a , G_a represent the actual model of the robot, and \hat{D} , \hat{C} , \hat{G} represent the assumed model of the robot.

As mentioned in (7.25), it is a well known fact that the inertial parameters of a robot are affine in the EOM (see [108]). Therefore (6.22) can be restated as:

$$Y(q, \dot{q}, \ddot{q})\Theta = Bu, \quad (8.1)$$

where $Y(q, \dot{q}, \ddot{q})$ is the regressor [108], and Θ is the set of base inertial parameters. Accordingly, Θ_a is the actual set of parameters, and $\hat{\Theta}$ is the assumed set of base inertial

parameters. We will only separate the parameters that are difficult to identify, i.e., we will assume that the kinematic parameters, such as link lengths, are accurately known. This reduces the set of unknown parameters to only the inertial elements of the robot.

Computed Torque Redefined. The method of computed torque becomes very convenient to apply if the regressor and the inertial parameters are being computed simultaneously. If \ddot{q}_d is the desired acceleration vector for the robot, the method of computed torque can be defined as:

$$Bu_{ct} = \mathbf{Y}(q, \dot{q}, \ddot{q}_d)\hat{\Theta}. \quad (8.2)$$

It can be observed that (8.2) is just a reformulation of (6.42). For convenience, the mapping matrix B on the left hand side of (8.2) will be omitted, i.e., $Bu_{ct} = u_{ct}$. Note that it is assumed that the mapping matrix B (including its parameterization) is known to the user. Due to the difference in parameters, it can be observed that the dynamics of the robot becomes different, which is shown below:

Lemma 23. Define:

$$\Phi = \hat{D}^{-1}\mathbf{Y}(q, \dot{q}, \ddot{q}), \quad (8.3)$$

where the dependency of Φ on q, \dot{q}, \ddot{q} has been suppressed for notational connivance. Similar to (6.41), if the control law used with the assumed model is:

$$\ddot{q}_d = \begin{bmatrix} \hat{D}_1 \\ J \end{bmatrix}^{-1} \left(\begin{bmatrix} 0 \\ \mu \end{bmatrix} - \begin{bmatrix} \hat{H}_1 \\ J\dot{q} \end{bmatrix} \right), \quad (8.4)$$

combined with the computed torque (8.2), then the resulting dynamics of the robot evolve

as:

$$\ddot{y} = \mu + J\Phi(\hat{\Theta} - \Theta_a). \quad (8.5)$$

Proof. By substituting for Bu in (6.22), we have:

$$D_a(q)\ddot{q} + C_a(q, \dot{q})\dot{q} + G_a(q) = \hat{D}(q)\ddot{q}_d + \hat{C}(q, \dot{q})\dot{q} + \hat{G}(q), \quad (8.6)$$

by adding and subtracting $\hat{D}(q)\ddot{q}$ on the right hand side of (8.6), we have:

$$\hat{D}(q)\ddot{q} - \hat{D}(q)\ddot{q}_d = Y(q, \dot{q}, \ddot{q})(\hat{\Theta} - \Theta_a), \quad (8.7)$$

where by substituting for \ddot{q}_d , the following result is obtained:

$$\begin{bmatrix} \hat{D}_1\ddot{q} + \hat{H}_1 \\ \ddot{y} \end{bmatrix} = \begin{bmatrix} \hat{D}_1\Phi(\hat{\Theta} - \Theta_a) \\ \mu + J\Phi(\hat{\Theta} - \Theta_a) \end{bmatrix}. \quad (8.8)$$

The bottom row is the desired result. The top row shows the dynamics of one of the zero coordinates and its relationship with parameter uncertainty. \square

The dynamics of this uncertain system can be written in the following form:

$$\begin{aligned} \dot{\eta} &= F\eta + G\mu + GJ\Phi\tilde{\Theta} \\ \dot{z} &= \Psi(\Theta_a; \eta, z), \end{aligned} \quad (8.9)$$

where $\tilde{\Theta} = \hat{\Theta} - \Theta_a$. The dependency of the zero dynamics on the true parameter set Θ_a is explicitly shown. If $\tilde{\Theta} = 0$, we could apply (5.27) to drive $\eta \rightarrow 0$. But since the parameters are uncertain, i.e., $\tilde{\Theta} \neq 0$, the resulting nonlinear dynamics will be observed in

the derivative of the Lyapunov function:

$$\begin{aligned}\dot{V}_\varepsilon(\eta, \mu) &= \dot{\eta}^T P_\varepsilon \eta + \eta^T P_\varepsilon \dot{\eta}, \\ &= \eta^T (F^T P_\varepsilon + P_\varepsilon F) \eta + 2\eta^T P_\varepsilon G \mu + 2\eta^T P_\varepsilon G J \Phi \tilde{\Theta},\end{aligned}\tag{8.10}$$

where $\dot{\eta}$ is obtained via (8.9). The next section will establish the relationship between parameter uncertainty and the uncertain dynamics appearing in the CLF through the *parameter uncertainty measure*.

8.2 Parameter Uncertainty Measure

Due to the unmodeled dynamics, applying the controller, $\mu(\eta) \in \mathbf{K}_\varepsilon(\eta)$, does not result in exponential convergence of the controller. The controller will still yield boundedness based on how the unmodeled dynamics affect \dot{V}_ε . The *parameter uncertainty measure*, ν , that quantifies the ultimate bound on the Lyapunov function V_ε is defined as:

$$\nu := Y(q, \dot{q}, \ddot{q}) \tilde{\Theta}.\tag{8.11}$$

It can be observed that: $Y(q, \dot{q}, \ddot{q}) \tilde{\Theta} = Y(q, \dot{q}, \ddot{q}) \hat{\Theta} - Y(q, \dot{q}, \ddot{q}) \Theta_a$, which is the difference between the actual and the expected torque being applied on the robot. Therefore, the *parameter measure* is effectively the difference in torques applied on the robot. It can be observed that the sensitivity and the uncertainty analysis w.r.t. the parameters take a similar approach (see [109]), where the partial derivatives of the controller inputs are computed w.r.t. Θ :

$$\begin{aligned}\text{Control Sensitivity} &= \frac{\partial u}{\partial \Theta} = Y(q, \dot{q}, \ddot{q}), \\ \text{Control Uncertainty} &= \frac{\partial u}{\partial \Theta} (\hat{\Theta} - \Theta_a) = \nu,\end{aligned}\tag{8.12}$$

which justifies the reasoning behind using the nomenclature *parameter uncertainty measure*.

sure. If $\tilde{\Theta}$ is identically a vector of 1's, ν is called *parameter sensitivity measure*. It must be noted that ν was called the *parameter sensitivity measure* in [106], which was changed to the current nomenclature after the review.

8.3 Parameter to State Stability

By (8.3) and (8.11), we have: $\hat{D}^{-1}\nu = \Phi\tilde{\Theta}$. Therefore, (8.10) can be expressed as:

$$\dot{V}_\varepsilon(\eta, \mu) = \eta^T(F^T P_\varepsilon + P_\varepsilon F)\eta + 2\eta^T P_\varepsilon G\mu + 2\eta^T P_\varepsilon GJ\hat{D}^{-1}\nu, \quad (8.13)$$

which is now a function of ν . This provides an important connection with Lyapunov theory, and the notion of parameter uncertainty is motivated by this observation. In other words, if the path of least ν is followed, then the convergence of the Lyapunov function to a value very close to zero can be realized. Therefore, we will define the notion of *Parameter to State Stability* in the following manner:

Definition 50. Assume a ball of radius r around the origin. The system given by (8.9) is locally **parameter to η stable**, if there exists $\beta \in \mathcal{KL}$, and $\iota \in \mathcal{K}_\infty$ such that:

$$|\eta(t)| \leq \beta(|\eta(0)|, t) + \iota(\|\nu\|_\infty), \quad \forall \eta(0) \in \mathbb{B}_r(0), \forall t \geq 0, \quad (8.14)$$

and it is locally **parameter to state stable**, if

$$|(\eta(t), z(t))| \leq \beta(|(\eta(0), z(0))|, t) + \iota(\|\nu\|_\infty), \quad \forall (\eta(0), z(0)) \in \mathbb{B}_r(0, 0), \forall t \geq 0. \quad (8.15)$$

If a suitable controller is applied to (8.13): $\mu(\eta) \in \mathbf{K}_\varepsilon(\eta)$, the stability of the Lyapunov function can be achieved as long as the following equation is satisfied:

$$\dot{V}_\varepsilon \leq -\frac{\gamma}{\varepsilon} V_\varepsilon + 2\eta^T P_\varepsilon GJ\hat{D}^{-1}\nu \leq 0, \quad (8.16)$$

This class of controllers can be explicitly obtained from (5.55), or in terms of the joint actuators as

$$\mathbf{K}_\varepsilon(\eta, z) = \{u \in \mathbb{U} : L_{\hat{f}}V_\varepsilon(\eta, z) + L_{\hat{g}}V_\varepsilon(\eta, z)u + \frac{1}{\varepsilon}V_\varepsilon(\eta) \leq 0\}, \quad (8.17)$$

where $L_{\hat{f}}, L_{\hat{g}}$ are the Lie derivatives of the robot model that we know (note the presence of $\hat{\cdot}$ over f, g). They are nothing but (5.56) with the relabeled f, g . They can be explicitly obtained as

$$\begin{aligned} L_{\hat{f}}V_\varepsilon &= \eta^T P_\varepsilon \frac{\partial \eta}{\partial x} f + f^T \frac{\partial \eta}{\partial x} P_\varepsilon \eta \\ L_{\hat{g}}V_\varepsilon &= 2\eta^T P_\varepsilon G \mathcal{J} \hat{D}^- B. \end{aligned} \quad (8.18)$$

It must be noted that the measure ν is also a function of the control input μ , resulting in an algebraic loop in (8.16). But, by a careful selection of the control input, it is possible to stabilize the dynamics of η by the restriction of ν through the robot model parameters. Therefore, we first assume the bounds on the robot model in the following manner:

$$\begin{aligned} c_4 \leq \|D\| \leq c_5, \quad \|C\| \leq c_6\|\dot{q}\|, \quad \|G\| \leq c_7, \\ \hat{c}_3 \leq \|\hat{D}\| \leq \hat{c}_4, \quad \|\hat{C}\| \leq \hat{c}_5\|\dot{q}\|, \quad \|\hat{G}\| \leq \hat{c}_6. \end{aligned} \quad (8.19)$$

where $c_4 - c_7, \hat{c}_3 - \hat{c}_6$ are constants (see [110, 111]). Since the outputs are degree one functions of q , the Jacobian can also be bounded by the constant: $\|J\| \leq \kappa$. By assuming that ν is bounded over time, we can establish a *parameter to state stable*(PSS)-Lyapunov function for the dynamics (8.13), which is shown in the following Lemma.

Lemma 24. *Given a controller $\mu(\eta) \in \mathbf{K}_\varepsilon(\eta)$, the system (8.9) is parameter to η stable, w.r.t. the parameter input ν .*

Proof. Since $V_\varepsilon(\eta)$ is bounded by the norms of $\|\eta\|$, we have the following:

$$\frac{\gamma}{\varepsilon} \eta^T P_\varepsilon \eta \geq \frac{\gamma}{\varepsilon} c_1 \|\eta\|^2, \quad (8.20)$$

For (8.16) with the bounds on P_ε, G, J and \hat{D} we have the following inequality:

$$\dot{V}_\varepsilon \leq -\frac{\gamma}{\varepsilon} V_\varepsilon + 2 \frac{c_2 \kappa \hat{c}_3^{-1}}{\varepsilon^2} \|\eta\| \|\nu\|. \quad (8.21)$$

The system is 0 stable for $\nu \equiv 0$, and with γ replaced with $\gamma_1 + \gamma_2 = \gamma$:

$$\begin{aligned} \dot{V}_\varepsilon &\leq -\frac{\gamma_1 + \gamma_2}{\varepsilon} V_\varepsilon + 2 \frac{c_2 \kappa \hat{c}_3^{-1}}{\varepsilon^2} \|\eta\| \|\nu\|, \\ \implies \dot{V}_\varepsilon &\leq -\frac{\gamma_2}{\varepsilon} V_\varepsilon, \quad \text{for } \frac{\gamma_1}{\varepsilon} V_\varepsilon(\eta) > 2 \|\eta\| \|\nu\| \frac{c_2 \kappa}{\varepsilon^2 \hat{c}_3}, \end{aligned} \quad (8.22)$$

which implies that V is decreasing exponentially for $\frac{\gamma_1}{\varepsilon} c_1 \|\eta\|^2 > 2 \|\eta\| \frac{c_2 \kappa}{\varepsilon^2 \hat{c}_3} \|\nu\|$. This satisfies the AG property, and from Lemma 2 it implies parameter to η stability w.r.t. ν . \square

It can be observed that due to AG, the exponential ultimate bound for a nonzero $\|\nu\|_\infty$ is given by $\lim_{t \rightarrow \infty} \|\eta(t)\| \leq 2 \frac{c_2 \kappa}{c_1 \varepsilon \hat{c}_3 \gamma_1} \|\nu\|_\infty$. A good way to reduce the ultimate bound is to increase ε , but, this affects the convergence rate, $\frac{\gamma_2}{\varepsilon}$. Consequently Lemma 24 yields a low convergence rate for the output error η . This affects the stability of hybrid periodic orbits as mentioned in Theorem 2 of [28], which requires ε to be sufficiently small for stable walking. In order to retain the original convergence rate, $\frac{\gamma}{\varepsilon}$ without sacrificing the ultimate bound, and to nullify the uncertain dynamics separately, we pick an auxiliary input $\bar{\mu}$ satisfying:

$$B u_{ctn} = \hat{D}(q) \ddot{q}_d + \hat{C}(q, \dot{q}) \dot{q} + \hat{G}(q) + B \bar{\mu}. \quad (8.23)$$

Note that this is not unique and other types of controllers can also be used. Computed torque with linear inputs appended have also been used in [95] in order to realize asymptotic

convergence. The resulting dynamics of the outputs then reduces to:

$$\ddot{y} = \mu + J\hat{D}^{-1}\nu + J\hat{D}^{-1}B\bar{\mu}, \quad (8.24)$$

which can be obtained by adding $B\bar{\mu}$ in (8.6) in the proof of Lemma 23.

By applying (8.24), (8.9) will have an extra input $\bar{\mu}$ that yields:

$$\begin{aligned}\dot{\eta} &= F\eta + G\mu + GJ\hat{D}^{-1}\nu + GJ\hat{D}^{-1}B\bar{\mu} \\ \dot{z} &= \Psi(\Theta_a; \eta, z),\end{aligned}\quad (8.25)$$

Therefore, \dot{V}_ε for the new input can be reformulated as:

$$\dot{V}_\varepsilon(\eta, \mu, \bar{\mu}) = \eta^T(F^TP_\varepsilon + P_\varepsilon F)\eta + 2\eta^TP_\varepsilon G\mu + 2\eta^TP_\varepsilon GJ\hat{D}^{-1}(\nu + B\bar{\mu}). \quad (8.26)$$

Consider the input $\bar{\mu} = -\frac{1}{\bar{\varepsilon}}\Gamma^TG^TP_\varepsilon\eta$, where $\bar{\varepsilon} > 0$, $\Gamma = J\hat{D}^{-1}B$ (should not be confused with the directed graph in (4.1)). Then μ and $\bar{\mu}$ together form the computed torque+PD control on the robot. The end result is a positive semidefinite expression: $\frac{1}{\bar{\varepsilon}}\eta^TP_\varepsilon G\Gamma\Gamma^TG^TP_\varepsilon\eta \geq 0$, which motivates the construction of a positive semidefinite function:

$$\bar{V}_\varepsilon(\eta) = \eta^TP_\varepsilon G\Gamma\Gamma^TG^TP_\varepsilon\eta =: \eta^T\bar{P}_\varepsilon\eta. \quad (8.27)$$

From (8.18) we also have that

$$\bar{V}_\varepsilon = \frac{1}{4}L_{\hat{g}}V_\varepsilon L_{\hat{g}}V_\varepsilon^T. \quad (8.28)$$

Using the property of positive semi-definiteness, we can establish new bounds on the outputs. Let $\mathcal{N}(\bar{P}_\varepsilon)$ be the null space of the matrix \bar{P}_ε . If $\eta \in \mathcal{N}(\bar{P}_\varepsilon)$, then $\bar{V}_\varepsilon(\eta) = 0$.

Otherwise, for some $c_8, c_9 > 0$:

$$c_8 \|\eta\|^2 \leq \bar{V}_\varepsilon(\eta) \leq \frac{c_9}{\varepsilon^4} \|\eta\|^2. \quad (8.29)$$

Note that (8.29) can be used to restrict the uncertain dynamics in (8.26). Utilizing these constructions, we can pick $\bar{\mu}$ from the class of controllers

$$\bar{\mathbf{K}}_{\varepsilon, \bar{\varepsilon}}(\eta) = \{\bar{\mu} \in \mathbf{U} : 2\eta^T P_\varepsilon G J \hat{D}^{-1} B \bar{\mu} + \frac{1}{\bar{\varepsilon}} \bar{V}_\varepsilon(\eta) \leq 0\}, \quad (8.30)$$

inorder to cancel the uncertain dynamics due to ν separately.

We can also define the following class of controllers

$$\mathbf{K}_{\varepsilon, \bar{\varepsilon}}(\eta, z) = \{u \in \mathbb{U} : L_{\hat{f}} V_\varepsilon(\eta, z) + L_{\hat{g}} V_\varepsilon(\eta, z) u + \frac{1}{\varepsilon} V_\varepsilon(\eta) + \frac{1}{\bar{\varepsilon}} \bar{V}_\varepsilon(\eta) \leq 0\}, \quad (8.31)$$

which is nothing but (5.58). Lemma 24 can now be redefined to obtain the new exponential ultimate bound for the new control input (8.23).

Lemma 25. *Given the controllers $\mu(\eta) \in \mathbf{K}_\varepsilon(\eta)$, $\bar{\mu}(\eta) \in \bar{\mathbf{K}}_{\varepsilon, \bar{\varepsilon}}(\eta)$, the system (8.25) is exponential parameter to η stable w.r.t. the parameter input ν .*

Proof. If η is in the null space of the semi definite matrix, as given in (8.27): $\eta \in \mathcal{N}(\bar{P}_\varepsilon)$, then $\eta^T P_\varepsilon G = 0$ and the uncertainty does not affect V_ε giving the desired result. If η does not belong to the null space, then the result can be proved by using the following constraint:

$$\frac{1}{\bar{\varepsilon}} \bar{V}_\varepsilon(\eta) > 2 \frac{c_2 \kappa \hat{c}_3^{-1}}{\varepsilon^2} \|\eta\| \|\nu\|, \quad (8.32)$$

which gives the AG property: $\lim_{t \rightarrow \infty} \|\eta\| \leq 2 \frac{c_2 \kappa}{c_8 \varepsilon^2 \hat{c}_3} \bar{\varepsilon} \|\nu\|_\infty =: b_\eta \|\nu\|_\infty$ implying parameter to η stability. \square

It can be inferred that:

$$\begin{aligned} V_\varepsilon(\eta(t)) &\leq e^{-\frac{\gamma}{\varepsilon}t}V_\varepsilon(\eta(0)) & \forall \|\eta(t)\| > b_\eta\|\nu\|_\infty, \\ \Rightarrow \|\eta(t)\| &\leq \frac{1}{\varepsilon}\sqrt{\frac{c_2}{c_1}}e^{-\frac{\gamma}{2\varepsilon}t}\|\eta(0)\| & \forall \|\eta(t)\| > b_\eta\|\nu\|_\infty. \end{aligned} \quad (8.33)$$

It should be noted that both the main and auxiliary gains $\varepsilon, \bar{\varepsilon}$ affect the measure ν . Therefore, the gain $\bar{\varepsilon}$ and also the measure norm need to be reasonably small to get sufficient ultimate bounds. This is illustrated very well in Fig. 8.3 where an almost constant measure (excluding the impacts), and a decreasing $\bar{\varepsilon}$ results in lowering of V_ε .

Given the locally Lipschitz continuous feedback law $\mu(\eta) = \mathbf{K}_\varepsilon(\eta), \bar{\mu}(\eta) = \bar{\mathbf{K}}_{\varepsilon, \bar{\varepsilon}}(\eta)$, we have the following equation:

$$\begin{aligned} \dot{\eta} &= F\eta + G\mu(\eta) + GJ\hat{D}^{-1}B\bar{\mu}(\eta) + GJ\hat{D}^{-1}\nu \\ \dot{z} &= \Psi(\Theta_a; \eta, z), \end{aligned} \quad (8.34)$$

We can now utilize the ISS notion in under-actuated systems given that the zero dynamics of the robot has a locally exponentially stable periodic orbit for the assumed model.

Zero Dynamics. Let $X \subset \mathbb{R}^{2k}, Z \subset \mathbb{R}^{2(n-k)}$. Let $\varphi_t(\eta, z)$ be the flow of (8.34) with the initial condition $(\eta, z) \in X \times Z$. The flow φ_t is periodic with period $T^* > 0$ and a fixed point (η^*, z^*) if $\varphi_{T^*}(\eta^*, z^*) = (\eta^*, z^*)$. Associated with the periodic flow is the periodic orbit

$$\mathcal{O} = \{\varphi_t(\eta^*, z^*) \in X \times Z : 0 \leq t \leq T^*\}.$$

Similarly, we denote the flow of the zero dynamics given by (8.34) by φ_t^z and for a periodic flow we denote the corresponding periodic orbit by $\mathcal{O}_z \subset Z$. Due to the invariance of the zero dynamics, we have the mapping $\mathcal{O} = \iota_0(\mathcal{O}_z)$, where $\iota_0 : Z \rightarrow X \times Z$ is the canonical embedding.

Without loss of generality, we can use the norm on $X \times Z$ as the sum of the norms

constructed on X and Z separately: $\|(\eta, z)\| = \|\eta\| + \|z\|$. The distance between (η, z) and the periodic orbit \mathcal{O} satisfies:

$$\begin{aligned}\|(\eta, z)\|_{\mathcal{O}} &= \inf_{(\eta', z') \in \mathcal{O}} \|(\eta, z) - (\eta', z')\| \\ &= \inf_{z' \in \mathcal{O}_z} \|z - z'\| + \|\eta - 0\| \\ &= \|z\|_{\mathcal{O}_z} + \|\eta\|.\end{aligned}\tag{8.35}$$

The periodic orbit \mathcal{O} is exponentially stable if there are constants $r, \delta_1, \delta_2 > 0$ such that if $(\eta, z) \in \mathbb{B}_r(\mathcal{O}) = \{(\eta, z) \in X \times Z : \|(\eta, z)\|_{\mathcal{O}} < r\}$ it follows that $\|\varphi_t(\eta, z)\|_{\mathcal{O}} \leq \delta_1 e^{-\delta_2 t} \|(\eta, z)\|_{\mathcal{O}}$. Exponential stability of \mathcal{O}_z can also be similarly defined.

We can introduce a theorem that establishes the parameter to state stability of the periodic orbit \mathcal{O} with the assumption that \mathcal{O}_z is exponentially stable.

Theorem 5. *Assume that the periodic orbit $\mathcal{O}_z \subset Z$ is exponentially stable for the assumed model $\hat{\Theta}$. Given the controllers $\mu(\eta) \in \mathbf{K}_{\varepsilon}(\eta)$, $\bar{\mu}(\eta) \in \bar{\mathbf{K}}_{\varepsilon, \bar{\varepsilon}}(\eta)$ applied on (8.34), that render exponential η stability, then the periodic orbit \mathcal{O} obtained from the canonical embedding is exponential parameter to state stable.*

Proof. Due to the inherent stability of η , 0 stability of the entire dynamics is directly implied. AG property is established by computing the ultimate bound on the state dynamics (η, z) . Since \mathcal{O}_z is exponentially stable, there is a Lyapunov function $V_z : Z \rightarrow \mathbb{R}_{\geq 0}$ such that in a neighborhood $\mathbb{B}_r(\mathcal{O}_z)$ of \mathcal{O}_z (see [112]) it is exponentially stable. Specific bounds is given by the following:

$$\begin{aligned}c_{10} \|z\|_{\mathcal{O}_z}^2 &\leq V_z(z) \leq c_{11} \|z\|_{\mathcal{O}_z}^2, \\ \frac{\partial V_z}{\partial z} \Psi(\hat{\Theta}; 0, z) &\leq -c_{12} \|z\|_{\mathcal{O}_z}^2, \\ \left\| \frac{\partial V_z}{\partial z} \right\| &\leq c_{13} \|z\|_{\mathcal{O}_z},\end{aligned}\tag{8.36}$$

where $c_{10}, c_{11}, c_{12}, c_{13}$ are constants. The zero dynamics of the actual model deviates from the nominal model; we have the following inequality that is inferred from the first row of (8.8):

$$\begin{aligned} \frac{\partial V_z}{\partial z} \Psi(\Theta_a; 0, z) &\leq -c_{12} \|z\|_{\mathcal{O}_z}^2 + \frac{\partial V_z}{\partial z} (\Psi(\Theta_a; 0, z) - \Psi(\hat{\Theta}; 0, z)) \\ &\leq -\frac{c_{12}}{2} \|z\|_{\mathcal{O}_z}^2 - \frac{c_{12}}{2} \|z\|_{\mathcal{O}_z}^2 + c_{13} \|z\| L_z \|\nu\|, \end{aligned} \quad (8.37)$$

for which the exponential upper bound for z can be obtained: $b_z \|\nu\|_\infty := \frac{2c_{13}L_z}{c_{12}} \|\nu\|_\infty$. L_z is the Lipschitz constant.

The combined Lyapunov function of the entire dynamics is given as:

$$V_c(\eta, z) = \sigma V_z(z) + V_\varepsilon(\eta). \quad (8.38)$$

Upper bounds and lower bounds on V_c can be defined as:

$$\begin{aligned} V_c(\eta, z) &\leq \max\{\sigma c_{11}, \frac{c_2}{\varepsilon^2}\} (\|z\|_{\mathcal{O}_z}^2 + \|\eta\|^2), \\ V_c(\eta, z) &\geq \min\{\sigma c_{10}, c_1\} (\|z\|_{\mathcal{O}_z}^2 + \|\eta\|^2), \end{aligned} \quad (8.39)$$

Therefore, taking the derivative:

$$\begin{aligned} \dot{V}_c(\eta, z) &= \sigma \frac{\partial V_z}{\partial z} \Psi(\hat{\Theta}; 0, z) + \sigma \frac{\partial V_z}{\partial z} (\Psi(\Theta_a; \eta, z) - \Psi(\Theta_a; 0, z) \\ &\quad + \Psi(\Theta_a; 0, z) - \Psi(\hat{\Theta}; 0, z)) + \dot{V}_\varepsilon(\eta), \\ &\leq -\sigma c_{12} \|z\|_{\mathcal{O}_z}^2 + \sigma c_{13} \|z\|_{\mathcal{O}_z} (L_q \|\eta\| + L_z \|\nu\|) + \dot{V}_\varepsilon(\eta), \end{aligned} \quad (8.40)$$

where L_q, L_z are the Lipschitz constants for Ψ in (8.9) w.r.t. η and ν respectively. Using (8.10), (8.40) can be modified such that sufficient conditions for boundedness can be

realized. Using (8.32) we have the following expression for the Lyapunov function:

$$\dot{V}_c \leq -\sigma \frac{c_{12}}{2} \|z\|_{\mathcal{O}_z}^2 + \sigma c_{13} L_q \|z\|_{\mathcal{O}_z} \|\eta\| - \frac{\gamma}{\varepsilon} V_\varepsilon, \quad \forall \|(\eta, z)\| > (b_\eta + b_z) \|\nu\|_\infty. \quad (8.41)$$

To ensure negative definiteness of the \dot{V}_c in (8.41), σ is picked such that: $\frac{c_{12}}{2} c_1 \frac{\gamma}{\varepsilon} - \sigma \frac{c_{13}^2 L_q^2}{4} > 0$, giving the desired result. \square

8.4 Hybrid Dynamics

We now extend Theorem 5 to hybrid robotic systems that involve alternating phases of continuous and discrete dynamics. A hybrid system with a single continuous and a discrete event is defined as follows:

$$\mathcal{H} = \begin{cases} \dot{\eta} = F\eta + G\mu(\eta) + GJ\hat{D}^{-1}B\bar{\mu}(\eta) + GJ\hat{D}^{-1}\nu, \\ \dot{z} = \Psi(\Theta; \eta, z), & \text{if } (\eta, z) \in \mathbb{D} \setminus \mathbb{S} \\ \eta^+ = \Delta_\eta(\Theta, \eta^-, z^-), \\ z^+ = \Delta_z(\Theta, \eta^-, z^-), & \text{if } (\eta^-, z^-) \in \mathbb{S} \end{cases} \quad (8.42)$$

It must be noted that the parameter vector Θ can be either Θ_a or $\hat{\Theta}$. Since the parameters Θ_a are not known, the output trajectory design is made for the assumed model $\hat{\Theta}$.

It is assumed that Ψ is Lipschitz in both ν, η . \mathbb{D}, \mathbb{S} are the domain and switching surfaces and are given by:

$$\mathbb{D} = \{(\eta, z) \in X \times Z : h(\eta, z) \geq 0\}, \quad (8.43)$$

$$\mathbb{S} = \{(\eta, z) \in X \times Z : h(\eta, z) = 0 \text{ and } \dot{h}(\eta, z) < 0\},$$

for some continuously differentiable function $h : X \times Z \rightarrow \mathbb{R}$. The reset map

$$\Delta(\Theta, \eta^-, z^-) = (\Delta_\eta(\Theta, \eta^-, z^-), \Delta_z(\Theta, \eta^-, z^-)),$$

represents the discrete dynamics of the system. For the bipedal robot, AMBER, h represents the non-stance foot height and Δ represents the impact dynamics of the system. Plastic impacts are assumed. For $(q^-, \dot{q}^-) \in \mathbb{S}$, being the pre-impact angles and velocities of the robot, the post impact velocity for the assumed model $\dot{\hat{q}}^+$, and for the actual model \dot{q}^+ will be obtained from:

$$\begin{bmatrix} \hat{D} & -\mathcal{J}^T \\ \mathcal{J} & 0 \end{bmatrix} \begin{bmatrix} \dot{\hat{q}}^+ \\ \delta \hat{F}_{imp} \end{bmatrix} = \begin{bmatrix} \hat{D} \dot{q}^- \\ 0 \end{bmatrix}, \quad \begin{bmatrix} D_a & -\mathcal{J}^T \\ \mathcal{J} & 0 \end{bmatrix} \begin{bmatrix} \dot{q}^+ \\ \delta F_{imp} \end{bmatrix} = \begin{bmatrix} D_a \dot{q}^- \\ 0 \end{bmatrix} \quad (8.44)$$

where $\delta \hat{F}_{imp}, \delta F_{imp}$ are the impulsive forces acting from the ground, \mathcal{J} is the Jacobian of the foot where the impulse forces are acting on the robot. By using the Schur complement to get the block matrix inversion we can obtain the post impact velocities as (see [73]):

$$\begin{aligned} \dot{\hat{q}}^+ &= (I - \hat{D}^{-1} \mathcal{J}^T (\mathcal{J} \hat{D}^{-1} \mathcal{J}^T)^{-1} \mathcal{J}) \dot{q}^-, \\ \dot{q}^+ &= (I - D_a^{-1} \mathcal{J}^T (\mathcal{J} D_a^{-1} \mathcal{J}^T)^{-1} \mathcal{J}) \dot{q}^-, \\ \dot{q}^+ - \dot{\hat{q}}^+ &= \tilde{D}(q) \dot{q}^-, \end{aligned} \quad (8.45)$$

where $\tilde{D}(q) \in \mathbb{R}^{n \times n}$ is a long expression obtained after computing the difference between the two post impact velocities. If $D_a = \hat{D}$, $\tilde{D}(q) = 0$, which can be used as a candidate for measuring uncertainty during impacts.

Impact Measure. Using the impact model, measuring uncertainty of post-impact dynamics can be achieved by introducing an *impact measure*, ν_s , for hybrid systems. It is defined

as:

$$\nu_s := \tilde{D}(q)\dot{q}^- . \quad (8.46)$$

It should be noted that the impact equations are Lipschitz continuous w.r.t. the impact measure ν_s . Accordingly, we have the following bounds on the impact map:

$$\begin{aligned} & \|\Delta_\eta(\Theta_a, \eta^-, z^-) - \Delta_\eta(\hat{\Theta}, 0, z^-)\| \\ & \leq \|\Delta_\eta(\Theta_a, \eta^-, z^-) - \Delta_\eta(\hat{\Theta}, \eta^-, z^-) + \Delta_\eta(\hat{\Theta}, \eta^-, z^-) - \Delta_\eta(\hat{\Theta}, 0, z^-)\| \\ & \leq L_1 \|\nu_s\| + L_2 \|\eta^-\|, \end{aligned} \quad (8.47)$$

where L_1, L_2 are Lipschitz constants for Δ_η . Similarly:

$$\|\Delta_z(\Theta_a, \eta^-, z^-) - \Delta_z(\hat{\Theta}, 0, z^-)\| \leq L_3 \|\nu_s\| + L_4 \|\eta^-\|, \quad (8.48)$$

where L_3, L_4 are Lipschitz constants for Δ_z . In order to obtain bounds on the output dynamics for hybrid periodic orbits, it is assumed that \mathcal{H} has a hybrid zero dynamics for the *assumed* model, $\hat{\Theta}$, of the robot. More specifically, we assume that $\Delta_\eta(\hat{\Theta}, 0, z^-) = 0$, so that the surface Z is invariant under the discrete dynamics. The hybrid zero dynamics can be described as:

$$\mathcal{H}|_Z = \begin{cases} \dot{z} = \Psi(\hat{\Theta}; 0, z) & \text{if } z \in Z \setminus (\mathbb{S} \cap Z) \\ z^+ = \Delta_z(\hat{\Theta}, 0, z^-) & \text{if } z^- \in (\mathbb{S} \cap Z) \end{cases} \quad (8.49)$$

Realizing hybrid zero dynamics (desired trajectories in particular) is in itself a difficult problem and requires large scale nonlinear programming toolboxes, which are explained in detail in [64].

Given the hybrid system (8.42), denote the hybrid flow as $\varphi_t(\Theta; \Delta(\Theta, \eta^-, z^-))$ with the initial condition $(\eta^-, z^-) \in \mathbb{S} \cap Z$. For the model estimate $\hat{\Theta}$, we can define the hybrid

flow of (8.49) as $\varphi_t^z(\hat{\Theta}; \Delta_z(\hat{\Theta}, 0, z^-))$ with the initial state $(0, z^-) \in \mathbb{S} \cap Z$. If a periodic orbit \mathcal{O}_z exists in (8.49), then there exists a periodic flow $\varphi_t^z(\hat{\Theta}; \Delta_z(\hat{\Theta}, 0, z^*))$ of period T^* for the fixed point $(0, z^*)$. Through the canonical embedding, the corresponding periodic flow of the periodic orbit \mathcal{O} in (8.42) will be $\varphi_t(\hat{\Theta}; \Delta(\hat{\Theta}, 0, z^*))$. Note that existence of periodic orbits for the assumed model $\hat{\Theta}$ does not guarantee existence for the actual model Θ_a . Associated with the hybrid periodic orbit is the Poincaré map $\mathbb{P} : \mathbb{S} \rightarrow \mathbb{S}$ given by:

$$\mathbb{P}(\Theta; \eta, z) = \varphi_{T(\Theta; \eta, z)}(\Theta; \Delta(\Theta, \eta, z)), \quad (8.50)$$

where Θ can be either Θ_a or $\hat{\Theta}$, and T is the time to impact function defined by:

$$T(\Theta; \eta, z) = \inf\{t \geq 0 : \varphi_t(\Theta; \Delta(\Theta, \eta, z)) \in \mathbb{S}\}. \quad (8.51)$$

The Poincaré map can be divided into η component \mathbb{P}_η , and z component \mathbb{P}_z respectively. Similar to the assumptions made in [28], the implicit function theorem implies that T is well defined in a neighborhood of $(\hat{\Theta}, \eta^*, z^*)$. Therefore, $T(\hat{\Theta}; \eta^*, z^*) = T^*$ and so $\mathbb{P}(\hat{\Theta}; \eta^*, z^*) = (\eta^*, z^*)$. Also, since $\varphi_t(\Theta; \Delta(\Theta, \eta, z))$ is Lipschitz continuous, T is also Lipschitz.

A hybrid periodic orbit \mathcal{O}_Z , of \mathcal{H}_Z can be similarly defined, in which case the corresponding Poincaré map $\vartheta : \mathbb{S} \cap Z \rightarrow \mathbb{S} \cap Z$ is termed the restricted Poincaré map:

$$\vartheta(z) = \varphi_{T_\vartheta(z)}^z(\hat{\Theta}; \Delta_z(\hat{\Theta}, 0, z)), \quad (8.52)$$

where φ^z is the flow of $\dot{z} = \Psi(\hat{\Theta}; 0, z)$ and T_ϑ is the restricted time to impact function, which is given by $T_\vartheta(z) = T(\hat{\Theta}; 0, z)$. Without loss of generality, we can assume that $\hat{\Theta} = 0, \eta^* = 0, z^* = 0$. For ease of notations let $\Theta = \Theta_a - \hat{\Theta} = \Theta_a$ ¹. The following Lemma will introduce the relationship between time to impact, Poincaré functions with the

¹It is safe to assume $\hat{\Theta} = 0$ here because we are interested in capturing the uncertainty in the dynamics (difference) and not the actual dynamics by itself.

state η and the impact measure ν_s .

Lemma 26. *Let \mathcal{O}_Z be the periodic orbit of the hybrid zero dynamics $\mathcal{H}|_Z$ transverse to $\mathbb{S} \cap Z$ for the nominal model $\hat{\Theta}$ ($\Theta = 0$). Given Θ_a ($\Theta \neq 0$), and given the controllers $\mu(\eta) \in \mathbf{K}_\varepsilon(\eta)$, $\bar{\mu}(\eta) \in \bar{\mathbf{K}}_{\varepsilon,\bar{\varepsilon}}(\eta)$ applied on the hybrid system (8.42), then for $r > 0$ such that $(\eta, z) \in \mathbb{B}_r(0, 0)$ and $\|\eta\| > b_\eta \|\nu\|_\infty$, there exist finite constants $A_1, A_2, A_3, A_4 > 0$ such that:*

$$\begin{aligned}\|T(\Theta; \eta, z) - T_\vartheta(z)\| &\leq A_1 \|\eta\| + A_2 \|\nu\|_{\max}, \\ \|\mathbb{P}_z(\Theta; \eta, z) - \vartheta(z)\| &\leq A_3 \|\eta\| + A_4 \|\nu\|_{\max}, \quad \|\nu\|_{\max} = \max\{\|\nu\|_\infty, \|\nu_s\|\}.\end{aligned}\tag{8.53}$$

Proof. (8.53) is proved by constructing an auxiliary time to impact function T_B that is Lipschitz continuous and then relate it to T . Let $\mu_1 \in \mathbb{R}^{2(n-k)}$, $\mu_2 \in \mathbb{R}^{2k}$ be constant vectors and let $\varphi_t^z(\Delta_z(0, 0, z_0))$ be the solution of $\dot{z} = \Psi(0; 0, z)$ with $z(0) = \Delta_z(0, 0, z_0)$. Define:

$$T_B(\mu_1, \mu_2, z) = \inf\{t \geq 0 : h(\mu_1, \varphi_t^z(\Delta_z(0, 0, z)) + \mu_2) = 0\},$$

which is nothing but equation (55) of [28] with the inclusion of model parameters. It follows that $T_B(0, 0, z) = T_\vartheta(z)$. By construction, T_B is Lipschitz continuous. We have,

$$\|T_B(\mu_1, \mu_2, z) - T_\vartheta(z)\| \leq L_B(\|\mu_1\| + \|\mu_2\|),\tag{8.54}$$

where L_B is the local Lipschitz constant. We note that $T(\Theta; \eta, z)$ is continuous and therefore there exists $r > 0$ such that for all $\mathbb{B}_r(0, 0) \cap \mathbb{S}$: $c_{15} T^* \leq T(\Theta; \eta, z) \leq c_{16} T^*$, where $0 < c_{15} < 1$ and $c_{16} > 1$. Let $(\eta_1(t), z_1(t))$ satisfy $\dot{z}_1 = \Psi(\Theta; \eta_1(t), z_1(t))$ with $\eta_1(0) = \Delta_\eta(\Theta, \eta, z)$ and $z_1(0) = \Delta_z(\Theta, \eta, z)$. Similarly let $z_2(t)$ satisfy $\dot{z}_2(t) = \Psi(0; 0, z_2(t))$ such that $z_2(0) = \Delta_z(0, 0, z)$. We can now determine μ_1, μ_2 .

The bounds on the Lyapunov function can be given as $\|\eta_1(0)\| = \|\Delta_\eta(\Theta, \eta, z) -$

$\Delta_\eta(0, 0, z) \leq L_1 \|\nu_s\| + L_2 \|\eta\|$, which is obtained through (8.47). Since $\|\eta_1\| > d$, by using (8.33) we have:

$$\|\eta_1(t)\|_{t=T(\Theta; \eta, z)} \leq \sqrt{\frac{c_2}{c_1}} \frac{1}{\varepsilon} e^{-\frac{\gamma}{2\varepsilon} c_{15} T^*} (L_1 \|\nu_s\| + L_2 \|\eta\|),$$

which yields the value of $\|\mu_1\|$. To obtain $\|\mu_2\|$, we use the Gronwall-Bellman argument (similar to page 8 in [28]). We know that:

$$z_1(t) - z_2(t) = z_1(0) - z_2(0) + \int_0^t \Psi(\Theta; \eta_1(\tau), z_1(\tau)) - \Psi(0; 0, z_2(\tau)) d\tau,$$

and therefore by using (8.48) and using the property of Lipschitz continuity of Ψ :

$$\begin{aligned} \|z_1(t) - z_2(t)\| &\leq L_3 \|\nu_s\| + L_4 \|\eta\| + \int_0^t L_q (\|\eta_1(\tau)\| + \|z_1(\tau) - z_2(\tau)\|) + L_z \|\nu\| d\tau \\ &\leq L_3 \|\nu_s\| + L_4 \|\eta\| + \frac{2}{\gamma} \sqrt{\frac{c_2}{c_1}} L_q (L_1 \|\nu_s\| + L_2 \|\eta\|) + c_{16} T^* L_z \|\nu\|_\infty \\ &\quad + \int_0^t L_q (\|z_1(\tau) - z_2(\tau)\|) d\tau, \end{aligned} \tag{8.55}$$

where (8.55) is integrated and substituted in the above equation. By Gronwall-Bellman inequality,

$$\|z_1(t) - z_2(t)\| \leq (C_2 \|\eta\| + C_3 \|\nu\|_\infty) e^{L_q t} \tag{8.56}$$

$$C_2 = \frac{2}{\gamma} \sqrt{\frac{c_2}{c_1}} L_q L_2 + L_4, \quad C_3 = 2 \max\left\{\frac{2}{\gamma} \sqrt{\frac{c_2}{c_1}} L_q L_1 + L_3, c_{16} T^* L_z\right\}.$$

Therefore, $\|\mu_2\| \leq \|z_1(c_{16} T^*) - z_2(c_{16} T^*)\|$ by substituting for the upper bound on T .

Proof of (8.53) can now be obtained by substituting for $\|\mu_1\|, \|\mu_2\|$.

To prove (8.54), define:

$$C_4 = \max_{c_{15} T^* \leq t \leq c_{16} T^*} \|\Psi(0; 0, z_2(t))\|, \tag{8.57}$$

it then follows that:

$$\begin{aligned} \|\mathbb{P}_z(\Theta; \eta, z) - \vartheta(z)\| &\leq \|z_1(0) - z_2(0)\| \\ &\quad + \int_0^{T(\Theta; \eta, z)} \|\Psi(\Theta; \eta_1(\tau), z_1(\tau)) - \Psi(0; 0, z_2(\tau))\| d\tau \\ &\quad + \int_{T(\Theta; \eta, z)}^{T_\vartheta(z)} \|\Psi(0; 0, z_2(\tau))\| d\tau, \end{aligned}$$

which results in the following inequality:

$$\|\mathbb{P}_z(\Theta; \eta, z) - \vartheta(z)\| \leq \|z_1(c_{16}T^*) - z_2(c_{16}T^*)\| + C_4 \|T(\Theta; \eta, z) - T_\vartheta(z)\|. \quad (8.58)$$

Collecting the terms together yields the desired result. \square

8.5 Main Theorem

We can now introduce the main theorem of the chapter. Similar to the continuous dynamics, it is assumed that the periodic orbit \mathcal{O}_z is exponentially stable in the hybrid zero dynamics.

Theorem 6. *Let \mathcal{O}_z be an exponentially stable periodic orbit of the hybrid zero dynamics $\mathcal{H}|_Z$ transverse to $\mathbb{S} \cap Z$ for the nominal model $\hat{\Theta}$ ($\Theta = 0$). Given the actual model Θ_a ($\Theta \neq 0$) and the controllers $\mu(\eta) \in \mathbf{K}_\varepsilon(\eta)$, $\bar{\mu}(\eta) \in \bar{\mathbf{K}}_{\varepsilon, \bar{\varepsilon}}(\eta)$ for the hybrid system \mathcal{H} given by (8.42), then for the ball of radius $r > 0$ such that $(\eta, z) \in \mathbb{B}_r(0, 0)$, there exists $\delta > 0$ such that for $\|\nu\| < \delta$, $\|\nu_s\| < \delta$ the periodic orbit \mathcal{O} is exponential parameter to state stable.*

Proof. Results of Lemma 26 and the exponential stability of \mathcal{O}_z imply that there exists $r > 0$ such that $\vartheta : \mathbb{B}_r(0) \cap (\mathbb{S} \cap Z) \rightarrow \mathbb{B}_r(0) \cap (\mathbb{S} \cap Z)$ is well defined for all $z \in \mathbb{B}_r(0) \cap (\mathbb{S} \cap Z)$ and $z_{j+1} = \vartheta(z_j)$ is locally exponentially stable, i.e., $\|z_j\| \leq N\xi^j \|z_0\|$ for some $N > 0$, $0 < \xi < 1$ and all $j \geq 0$. Therefore, by the converse Lyapunov theorem for discrete systems, there exists a Lyapunov function V_ϑ , defined on $\mathbb{B}_r(0) \cap (\mathbb{S} \cap Z)$

for some $r > 0$ (possibly smaller than the previously defined r), and positive constants $c_{17}, c_{18}, c_{19}, c_{20}$ such that:

$$\begin{aligned} c_{17}\|z\|^2 \leq V_\vartheta(z) &\leq c_{18}\|z\|^2, \\ V_\vartheta(\vartheta(z)) - V_\vartheta(z) &\leq -c_{19}\|z\|^2, \\ |V_\vartheta(z) - V_\vartheta(z')| &\leq c_{20}\|z - z'\|(\|z\| + \|z'\|). \end{aligned} \quad (8.59)$$

Zero stability (perfect model) is valid by default due to the construction (hybrid zero dynamics and RES-CLF with sufficiently small ε provide exponential convergence to \mathcal{O} , see [28]). To prove AG property it should be first ensured that the region defined by $\overline{\lim}_{t \rightarrow \infty} \|(\eta(t), z(t))\|$ must be within the bounds defined by r . Therefore it is required that the ultimate bound is less than r :

$$(b_\eta + b_z)\|\nu\|_\infty < r, \quad \delta_r := \frac{r}{(b_\eta + b_z)}, \quad (8.60)$$

which gives the allowable upper bound δ_r on $\|\nu\|_\infty$. It is also required that the post impact states are also in $\mathbb{B}_r(0, 0)$. Therefore, a second upper bound δ_I is given as follows:

$$\begin{aligned} \|\Delta(\Theta; \eta, z)\| &\leq L_{\Delta_1}\|\nu_s\| + L_{\Delta_2}\|(\eta, z)\| \leq r, \\ \implies \delta_I &:= \frac{r}{L_{\Delta_1} + L_{\Delta_2}(b_\eta + b_z)}, \end{aligned} \quad (8.61)$$

$L_{\Delta_1}, L_{\Delta_2}$ are Lipschitz constants.

For the RES-CLF V_ε , denote its restriction to the switching surface by

$$V_{\varepsilon, \eta}(\eta) = V_\varepsilon|_{\mathbb{S}}(\eta) = V_\varepsilon(\eta), \quad \eta \in \mathbb{S}. \quad (8.62)$$

With these two Lyapunov functions we define the following candidate Lyapunov function:

$$V_P(\eta, z) = V_\vartheta(z) + \sigma V_{\varepsilon,\eta}(\eta), \quad (8.63)$$

defined on $\mathbb{B}_r(0, 0) \cap \mathbb{S}$. The lower and upper bounds on V_P are:

$$\min\{c_{17}, \sigma c_1\} \|(\eta, z)\|^2 \leq V_P(\eta, z) \leq \max\{c_{18}, \sigma \frac{c_2}{\varepsilon^2}\} \|(\eta, z)\|^2. \quad (8.64)$$

The idea is to show that there exists a bounded region into which the dynamics of the robot exponentially converge. If the outputs enter this region then it stays for all time even through impacts. We know that $\eta_1(0) = \Delta_\eta(\Theta, \eta, z)$. if $\|\eta_1(0)\| < b_\eta \|\nu\|_\infty$, then the boundedness is verified. For the case when the impact map takes the outputs outside the bounded region (by utilizing (8.33)) we pick the lower bound on the time to impact function:

$$\begin{aligned} V_{\varepsilon,\eta}(\mathbb{P}_\eta(\Theta; \eta, z)) &\leq \frac{c_2}{\varepsilon^2} e^{-\frac{\gamma}{\varepsilon} T(\Theta; \eta, z)} \|\Delta_\eta(\Theta, \eta, z)\|^2, \\ &\leq \frac{c_2}{\varepsilon^2} e^{-\frac{\gamma}{\varepsilon} T(\Theta; \eta, z)} (L_1 \|\nu_s\| + L_2 \|\eta\|)^2. \end{aligned} \quad (8.65)$$

Taking $A_5 = \frac{c_2}{\varepsilon^2} e^{-\frac{\gamma}{\varepsilon} c_{15} T^*}$, we have the following:

$$\begin{aligned} V_{\varepsilon,\eta}(\mathbb{P}_\eta(\eta, z)) - V_{\varepsilon,\eta}(\eta) &\leq A_5 (L_1 \|\nu_s\| + L_2 \|\eta\|)^2 - c_1 \|\eta\|^2. \\ &\leq A_5 (L_1 \|\nu\|_{\max} + L_2 \|\eta\|)^2 - c_1 \|\eta\|^2. \end{aligned} \quad (8.66)$$

Since the origin is an exponentially stable equilibrium for $z_{j+1} = \vartheta(z_j)$, we have the fol-

lowing inequalities:

$$\begin{aligned}
\|\mathbb{P}_z(\Theta; \eta, z)\| &= \|\mathbb{P}_z(\Theta; \eta, z) - \vartheta(z) + \vartheta(z) - \vartheta(0)\| \\
&\leq A_3\|\eta\| + A_4\|\nu\|_{\max} + L_\vartheta\|z\| \\
\|\vartheta(z)\| &\leq N\xi\|z\|,
\end{aligned} \tag{8.67}$$

where L_ϑ is the Lipschitz constant for ϑ . Therefore:

$$\begin{aligned}
V_\vartheta(\mathbb{P}_z(\Theta; \eta, z)) - V_\vartheta(\vartheta(z)) &\leq c_{20}(A_3\|\eta\| + A_4\|\nu\|_{\max}) \\
&\quad (A_3\|\eta\| + A_4\|\nu\|_{\max} + (L_\vartheta + N\xi)\|z\|).
\end{aligned} \tag{8.68}$$

It follows that:

$$V_\vartheta(\mathbb{P}_z(\Theta; \eta, z)) - V_\vartheta(z) = V_\vartheta(\mathbb{P}_z(\Theta; \eta, z)) - V_\vartheta(\vartheta(z)) + V_\vartheta(\vartheta(z)) - V_\vartheta(z), \tag{8.69}$$

and the expressions in (8.68) and in (8.59) can be substituted. Combining the entire Lyapunov function we have:

$$V_P(\mathbb{P}(\Theta; \eta, z)) - V_P(\eta, z) \leq - \begin{bmatrix} \|\eta\| \\ \|z\| \\ \|\nu\|_{\max} \end{bmatrix}^T \Lambda_{\mathcal{H}} \begin{bmatrix} \|\eta\| \\ \|z\| \\ \|\nu\|_{\max} \end{bmatrix}, \tag{8.70}$$

where the symmetric matrix $\Lambda_{\mathcal{H}} \in \mathbb{R}^{3 \times 3}$, with the upper triangular entries being:

$$\begin{aligned}
a_1 &= \Lambda_{\mathcal{H}}(1, 1) = \sigma(c_1 - A_5 L_2^2) - c_{20} A_3^2 \\
-a_2 &= \Lambda_{\mathcal{H}}(1, 2) = -\frac{c_{20} A_3}{2} (L_\vartheta + N\xi) \\
-a_3 &= \Lambda_{\mathcal{H}}(1, 3) = -c_{20} A_3 A_4 - \sigma A_5 L_1 L_2 \\
a_4 &= \Lambda_{\mathcal{H}}(2, 2) = c_{19} \\
-a_5 &= \Lambda_{\mathcal{H}}(2, 3) = -\frac{c_{20} A_4}{2} (L_\vartheta + N\xi) \\
-a_6 &= \Lambda_{\mathcal{H}}(3, 3) = -\sigma A_5 L_1^2 - c_{20} A_4^2.
\end{aligned} \tag{8.71}$$

(8.70) is in the form of discrete time ISS-Lyapunov function as specified by (4.70) (input being the parameter uncertainty $\|\nu\|_{\max}$). Similar to the proof of Theorem 2 in [28], we pick a large enough σ to ensure the matrix $\Lambda = \begin{bmatrix} a_1 & -a_2 \\ -a_2 & a_4 \end{bmatrix}$ is positive definite. A specific value for σ is given in page 9 of [28] that yields exponential convergence of hybrid periodic orbits. This is extended to include parameter uncertainty by utilizing (4.70) in (8.70) in the following manner:

$$\begin{aligned}
V_P(\mathbb{P}(\Theta; \eta, z)) - V_P(\eta, z) &\leq -\lambda_{\min}(\Lambda) \|\eta, z\|^2 \\
&\quad + (2a_3\|\eta\| + 2a_5\|z\| + a_6\|\nu\|_{\max})\|\nu\|_{\max}.
\end{aligned} \tag{8.72}$$

Therefore, to compute the limit on $\|\nu\|_{\max}$, we can divide the minimum eigenvalue $\lambda_{\min}(\Lambda)$ by 2 and obtain the following:

$$\begin{aligned}
V_P(\mathbb{P}(\Theta; \eta, z)) - V_P(\eta, z) &\leq -\frac{\lambda_{\min}(\Lambda)}{2} \|\eta, z\|^2 \\
\text{for } -\frac{\lambda_{\min}(\Lambda)}{2} \|\eta, z\|^2 + 2(a_3 + a_5)\|\eta, z\| \|\nu\|_{\max} + a_6\|\nu\|_{\max}^2 &> 0.
\end{aligned} \tag{8.73}$$

Therefore exponential upper bound is obtained from the positive root of the quadratic

equation in (8.73):

$$\overline{\lim}_{t \rightarrow \infty} \|(\eta(t), z(t))\| \leq \frac{2(a_3 + a_5) + \sqrt{4(a_3 + a_5)^2 + 2\lambda_{\min} a_6}}{\lambda_{\min}} \|\nu\|_{\max}, \quad (8.74)$$

and we expect this limit to be less than r , which yields the upper bound, δ_{\max} , on $\|\nu\|_{\max}$:

$$\delta_{\max} := \frac{r\lambda_{\min}}{2(a_3 + a_5) + \sqrt{4(a_3 + a_5)^2 + 2\lambda_{\min} a_6}}. \quad (8.75)$$

Therefore, we take the minimum value for the upper bound from (8.60),(8.61),(8.75) to obtain $\delta = \min\{\delta_r, \delta_I, \delta_{\max}\}$, resulting in exponential parameter to state stability of \mathcal{O} . \square

8.6 Simulation Results

In this section, we will investigate how the uncertainty in parameters affects the stability of the controller applied to the 5-DOF bipedal robot AMBER1 shown in Fig. 6.1. The model, Θ_a , which has 61 parameters is picked such that the error is 30% compared to the assumed model $\hat{\Theta}$.

To realize walking on the robot, the actual and desired outputs are chosen as in [79] (specifically, see (6) for determining the actual and the desired outputs). The result is outputs of the form $y(q) = y_a(q) - y_d(q)$, which must be driven to zero. Therefore, the objective of the controller (8.23) with $\mu(\eta) \in \mathbf{K}_\varepsilon(\eta)$ and $\bar{\mu}(\eta) \in \bar{\mathbf{K}}_{\varepsilon, \bar{\varepsilon}}(\eta)$ is to drive $y \rightarrow 0$. For the nominal model, $\hat{\Theta}$, a stable walking gait is observed. In other words, a stable hybrid periodic orbit is observed for the assumed given model. Since, the actual model of the robot has an error of 30%, applying the controller yields the dynamics that evolves as shown in (8.25). The value of ε chosen was 0.1, and $\bar{\varepsilon}$ was 10. Fig. 8.1 shows the comparison between actual and desired outputs, and Fig. 8.2 shows the Lyapunov function V_ε . It can be observed that V_ε is always within the bound ≈ 0.06 , while $\|\nu\|$ takes large values at the beginning and end of every step (implying that the control effort applied is large during

those points).

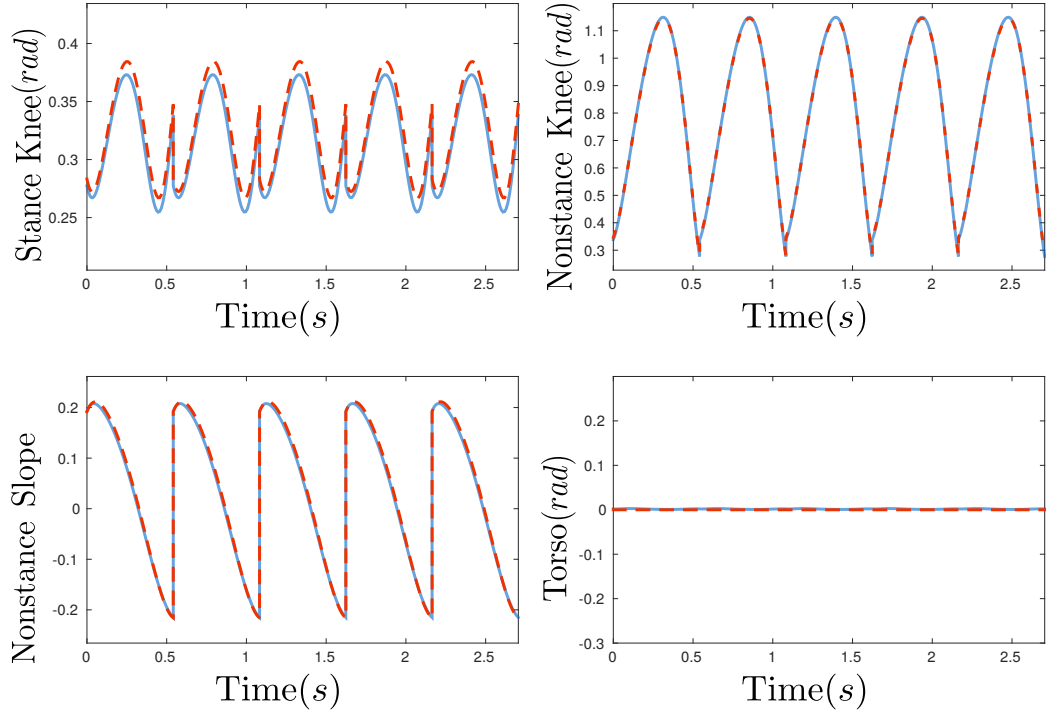


Figure 8.1: Actual (solid lines) and desired (dashed lines) outputs as a function of time are shown here. Each figure corresponds to an output described to the left of the figures.

Fig. 8.3 shows the progression of the CLF over two steps with different values of the auxiliary gain $\bar{\varepsilon}$. Value of ε chosen was 0.05. Plots are shown for the first two steps as opposed to the steady state behavior shown in Fig. 8.2. The measure norm $\|\nu\|_\infty$ remains consistent (except during impacts) for different values of $\bar{\varepsilon}$, resulting in lower ultimate bounds.

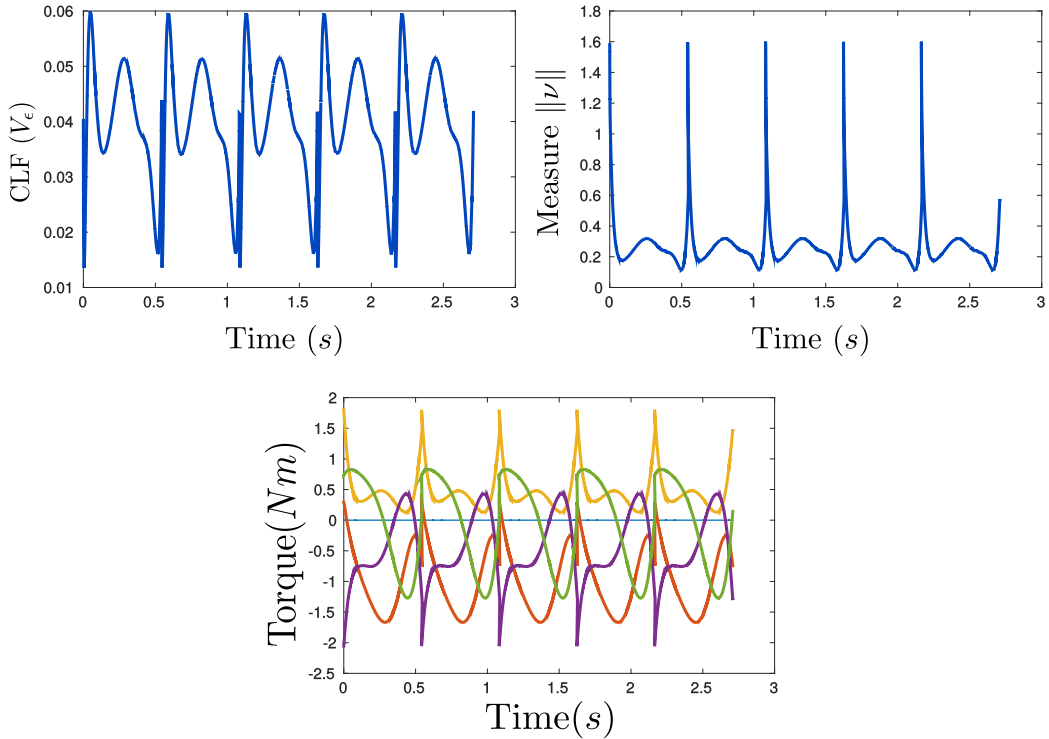


Figure 8.2: The RES-CLF (a), the measure (b) and the torque (c) as a function of time. \dot{V}_ϵ (slope of V_ϵ) crosses 0 in every step, but the CLF is still seen to be ultimately bounded. It can also be observed that $\|\nu\|$ increases when the torque inputs are high.

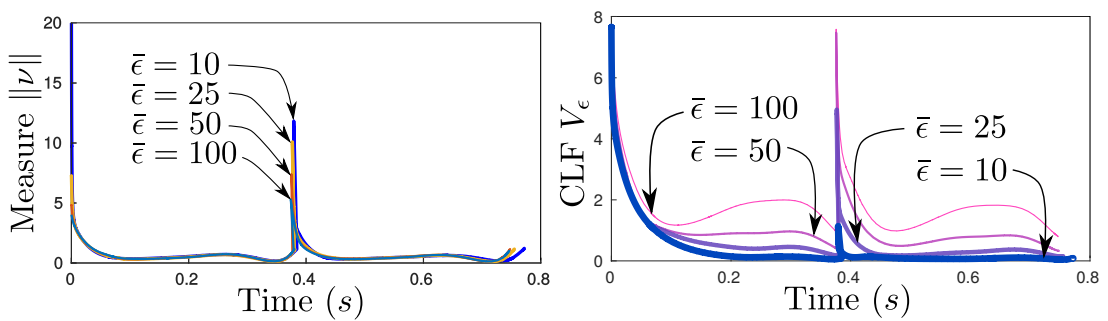


Figure 8.3: Progression of the measure, RES-CLF from the same initial point for different values of the auxiliary gain $\bar{\epsilon}$ is shown in the figure. It appears that the ultimate bound decreases with the auxiliary gain $\bar{\epsilon}$, thereby nullifying the effect of uncertain dynamics.

CHAPTER 9

PHASE UNCERTAINTY TO STATE STABILITY

It is a well known fact that biological bipeds of the natural world emulate a spring loaded inverted pendulum (SLIP) [85]. Robots PETMAN [113] and ATRIAS [86] have realized walking behaviors based on this concept that have been robust to external disturbances. The controllers are developed based on heuristics and involves a lengthy process of a continuous reassessment and tuning of the parameters of the robot until the desired result is achieved. This heuristics based approach is harder to scale and gets more and more difficult as the complexity of the robot increases. The PETMAN that had the most robust walking behavior during its time worked only a few times and has not beeen repeatable. Literature has shown that the Hybrid Zero Dynamics (HZD) based approach [62], that uses a set of **modulated reference** trajectories, is not just robust for a wide class of planar robots [79, 114] but also repeatable. In fact, the success of this approach is backed by the formal stability results, and the experiments are just an outcome of this rigorous analysis. Extension of the HZD based approach from 2D to 3D robots is seamless with a slight alteration of the source of modulation (see [4] for a video of DURUS walking in 3D). It was shown in [115] that a time modulation of same desired trajectories that were constructed for state based trajectory tracking control, also results in stable robotic walking.

Despite all the differences between the different approaches in bipedal walking such as the ZMP based control [81, 82], capture points [83], controlled symmetries [84], SLIP model [85, 86], HZD [62], null space control [87], at a fundamental level, using a set of trajectories (gaits) as reference is still the common universal theme found in them. This is formally called gait planning even though these reference gaits are strictly not adhered to (not strictly tracked) in some approaches. As a direct consequence of using these reference gaits or reference trajectories, comes the issue of modulation of trajectories from

start to end. History has shown that smooth and reliable modulation of the trajectories is a really difficult problem, and there has been a lot of work solely dedicated to finding good candidates for modulation [63]. As a slight deviation, our approach for tackling this problem is by picking a better controller that can handle the noisy, non-smooth nature of this modulation, this chapter will show how to choose robust control Lyapunov functions that can handle this modulation uncertainty for the HZD based reference trajectories. This technique is extended further via a rigorous theoretical and experimental analysis for all kinds of legged locomotion (walking and running).

As the complexity of the robot increases (in terms of both DOF and dynamic behaviors), the state dependency of the controller becomes more of a curse to the stability of the robot. It was observed that in the humanoid robot DURUS (in Fig. 6.7), the uncertainty in the phase variable caused unstable modulation of the desired trajectories leading to frequent failures. It was also observed that a time substitution of the phase $\tau(t)$ caused a smoother modulation of the desired trajectories leading to stable walking in DURUS (more in [115]). The objective of this chapter is to show that a mix of time+state based implementation of the phase variables yields a *less* perturbed modulation of the trajectories by using the notion of ISS.

Stable periodic orbits on the Hybrid Zero Dynamics (HZD) are first constructed for a given bipedal robot model. These orbits on the reduced order dynamics are then embedded into the full order dynamics via the virtual constraints. These virtual constraints are constructed by the desired trajectories that are modulated by what is called a **phase** variable. The phase variable τ is usually a monotonic function of the n -DOF configuration space $q \in \mathbb{R}^n$. Suitable candidates are calf angle, hip position that propagate forward in time. The state dependency of the modulation of the desired trajectories forms the basis for realizing stable periodic orbits in the hybrid zero dynamics (HZD).

We establish the main result by choosing the time based virtual constraints (replacing $\tau(q)$ with $\tau(t)$). By studying both time and state based control Lyapunov functions (CLF)

obtained from these virtual constraints (note that the concept of a time-based CLFs is not a new one, see [116, 117]), we are able to establish stability conditions for a given periodic orbit. Control Lypaunov functions that satisfy the ISS conditions yield an Input to State Stable Lypaunov function, in other words an ISS-CLF. These results are extended to the setting of hybrid dynamical systems—which naturally model bipedal walking robots. With the assumption that there is an exponentially stable periodic orbit in the hybrid zero dynamics, we establish (bounded) stability of a gait under assumptions on the boundedness of the phase uncertainty (which is a function of $\tau(q)$, $\tau(t)$ and their derivatives).

Theorem 21 shows that by picking a RES-CLF, exponentially stable hybrid periodic orbits can be realized. But, due to the difficulty in accurately estimating the phase variable $\tau(q)$ (which is mainly a function of the unactuated degrees of freedom of the robot), an alternative approach is required. Motivated by the time based implementation of the tracking controller in [115], we can construct a controller that uses a time based desired trajectory instead of a state dependent trajectory. The result of using the time based trajectories is the time dependent RES-CLF, which was shown in 5.1 (specifically (5.60)).

9.1 State Based vs. Time Based Control Laws

Given the controller (5.11) that drives the time based outputs $\eta_t \rightarrow 0$, it is important to compare the evolution of the state based outputs η . We will assume no modulation of velocity outputs (constant y_1^d). Picking the input (5.11) on the dynamics of state based

outputs y_1, y_2 , we have

$$\begin{aligned} \begin{bmatrix} \dot{y}_1 \\ \ddot{y}_2 \end{bmatrix} &= \underbrace{\begin{bmatrix} L_f y_1 \\ L_f^2 y_2 \end{bmatrix}}_{\mu} + \underbrace{\begin{bmatrix} L_g y_1 \\ L_g L_f y_2 \end{bmatrix}}_{=:d} u_t \\ \begin{bmatrix} \dot{y}_1 \\ \ddot{y}_2 \end{bmatrix} &= \underbrace{\begin{bmatrix} L_f y_1 \\ L_f^2 y_2 \end{bmatrix}}_{\mu} + \underbrace{\begin{bmatrix} L_g y_1 \\ L_g L_f y_2 \end{bmatrix}}_u u + \underbrace{\begin{bmatrix} L_g y_1 \\ L_g L_f y_2 \end{bmatrix}}_{=:d} (u_t - u) \\ \begin{bmatrix} \dot{y}_1 \\ \ddot{y}_2 \end{bmatrix} &= \mu + d, \end{aligned} \tag{9.1}$$

where d is obtained by substituting for u_t, u (from (5.11),(5.5)). The expression for d can be further simplified to get

$$d(t, q, \dot{q}, \ddot{q}, \mu, \mu_t) = (\mu_t - \mu) + \begin{bmatrix} 0 \\ \ddot{y}_2^d(\tau(t), \alpha) - \ddot{y}_2^d(\tau(q), \alpha) \end{bmatrix}. \tag{9.2}$$

If the time and state based phase variables are closely matching during the duration of the step, then it can be observed that d becomes small. Therefore d can be termed **time-phase uncertainty**, or just **phase uncertainty**.

Going back to (9.1), we can reformulate (5.36) that results in the following representation:

$$\begin{aligned} \dot{\eta} &= F\eta + G\mu + Gd, \\ \dot{z} &= \Psi(\eta, z). \end{aligned} \tag{9.3}$$

From the point of view of the state dependent outputs η , we have the following representa-

tion dynamics of the Lyapunov function:

$$\dot{V}_\varepsilon = \eta^T (F^T P_\varepsilon + P_\varepsilon F) \eta + 2\eta^T P_\varepsilon G \mu + 2\eta^T P_\varepsilon G d. \quad (9.4)$$

By substituting $\mu \in \mathbf{K}_\varepsilon(\eta)$ obtained from (5.55), or by substituting for the joint actuators $u \in \mathbf{K}_\varepsilon(\eta, z)$ obtained from (5.56), the following is obtained:

$$\dot{V}_\varepsilon \leq -\frac{\gamma}{\varepsilon} V_\varepsilon + 2\eta^T P_\varepsilon G d. \quad (9.5)$$

It must be noted that even though time dependent RES-CLF leads to convergence of time dependent outputs $\eta_t \rightarrow 0$, (9.5) extends it to state based outputs η that are driven to an ultimate bound, and this ultimate bound is explicitly derived from d .

We can extend this comparison to a wider class of controllers i.e., (9.5) can be obtained even without using feedback linearization, i.e., by using the time based RES-CLF (5.60),

$$\begin{aligned} \dot{V}_\varepsilon &= L_f V_\varepsilon + L_g V_\varepsilon u_t, & u_t(\eta_t, z_t) &\in \mathbf{K}_\varepsilon^t(\eta_t, z_t) \\ \dot{V}_\varepsilon &= L_f V_\varepsilon + L_g V_\varepsilon u + L_g V_\varepsilon (u_t - u), & u(\eta, z) &\in \mathbf{K}_\varepsilon(\eta, z) \\ &\leq -\frac{\gamma}{\varepsilon} V_\varepsilon + \frac{\partial V_\varepsilon}{\partial \eta} \frac{\partial \eta}{\partial x} g(x)(u_t - u), \end{aligned} \quad (9.6)$$

and picking $V_\varepsilon = \eta^T P_\varepsilon \eta$, we have

$$\dot{V}_\varepsilon \leq -\frac{\gamma}{\varepsilon} V_\varepsilon + 2\eta^T P_\varepsilon G \underbrace{\mathcal{J} D^{-1} B(u_t - u)}_d, \quad \mathcal{J} = \begin{bmatrix} \frac{\partial y_1}{\partial \dot{q}} \\ \frac{\partial y_2}{\partial \dot{q}} \end{bmatrix} \quad (9.7)$$

where the expression for d consists of nonlinear functions of both time and state based τ , \mathcal{J} is the Jacobian matrix. By construction of the outputs it can be assumed that the Jacobian is bounded by a constant. By Bounded Input Bounded Output (BIBO) stability criterion, we know that the outputs y_1, y_2 will remain bounded given that d is bounded for the linear dynamics (9.3). Inorder to extend this observation to a general RES-CLF for

hybrid systems that also includes nonlinear impacts, we use the notion of Input to State Stability (ISS) to establish boundedness of the state based outputs y_1, y_2 given that d is bounded.

9.2 Phase to State Stability

We can now define the notion of *Phase to State Stability* below. A preliminary on Input to State Stability is given in Chapter 2.

Definition 51. Assume a ball of radius r around the origin. The system given by (9.3) is locally **phase to η stable**, if there exists $\beta \in \mathcal{KL}$, and $\iota \in \mathcal{K}_\infty$ such that

$$|\eta(t)| \leq \beta(|\eta(0)|, t) + \iota(\|d\|_\infty), \forall \eta(0) \in \mathbb{B}_r(0), \forall t \geq 0, \quad (9.8)$$

and it is locally **phase to state stable**, if

$$|(\eta(t), z(t))| \leq \beta(|(\eta(0), z(0))|, t) + \iota(\|d\|_\infty),$$

$$\forall \eta(0) \in \mathbb{B}_r(0), \forall t \geq 0.$$

We will first prove phase to η stability, and then include the zero dynamics to show phase to state stability. Based on the asymptotic gain and zero stability property of the system (9.3) w.r.t. the *phase uncertainty* d , we have the following lemma.

Lemma 27. The class of all feedback control laws $u(\eta_t, z_t) \in \mathbf{K}_\varepsilon^t(\eta_t, z_t)$ (time based RES-CLF (5.31)) applied on the system (6.26) yields phase to η stability in the continuous dynamics. Moreover, $\forall \delta > 0, \exists b_\eta > 0$ such that $\|d\| \leq \delta \implies \overline{\lim}_{t \rightarrow \infty} V_\varepsilon(\eta(t)) \leq b_\eta$.

Proof. We will utilize Lemma 2 to prove the stability property here. The Zero Stability (ZS) property is satisfied by construction. The Asymptotic Gain (AG) property is shown below (see Fig. 2.1).

By applying the bounds on (9.5) we have the following constraint:

$$\begin{aligned}
\dot{V}_\varepsilon &= -\frac{\gamma}{\varepsilon}V_\varepsilon + 2\eta^T P_\varepsilon G d \leq -\frac{\gamma}{\varepsilon}V_\varepsilon + 2\|\eta\| \|P_\varepsilon\| \|d\| \\
\frac{\gamma}{\varepsilon}V_\varepsilon &> 2\|\eta\| \frac{c_2\delta}{\varepsilon^2} \implies \dot{V}_\varepsilon < 0 \\
\frac{\gamma}{\varepsilon}c_1\|\eta\|^2 &> 2\|\eta\| \frac{c_2\delta}{\varepsilon^2} \implies \dot{V}_\varepsilon < 0. \\
\|\eta\| &> 2 \frac{c_2\delta}{c_1\varepsilon\gamma} \implies \dot{V}_\varepsilon < 0.
\end{aligned} \tag{9.9}$$

The ultimate bound b_η is obtained when the equality holds (when $\dot{V}_\varepsilon = 0$). Since $V_\varepsilon(\eta) \geq c_1\|\eta\|^2$ from (3.16) we have $\sqrt{V_\varepsilon(\eta)/c_1} \geq \|\eta\|$, b_η is therefore obtained as a function of δ, ε :

$$b_\eta = \frac{4c_2^2\delta^2}{c_1\varepsilon^2\gamma^2}. \tag{9.10}$$

Dependence on ε shows that the ultimate bound gets larger as the desired convergence rate increases. \square

We can also realize **exponential phase to state stability** of the continuous dynamics by appending a state based linear feedback law to the time based feedback linearizing control (5.11):

$$u_{t+q} = u_t + u_q, \tag{9.11}$$

which results in the following output dynamics in the place of (9.1):

$$\begin{bmatrix} \dot{y}_1 \\ \ddot{y}_2 \end{bmatrix} = \mu + d + \begin{bmatrix} L_g y_1 \\ L_g L_f y_2 \end{bmatrix} u_q. \tag{9.12}$$

By the choice of the outputs, the matrix $B_y = \begin{bmatrix} L_g y_1 \\ L_g L_f y_2 \end{bmatrix}$ is invertible. By applying (9.11), (9.3) will have an extra input u_q that yields:

$$\begin{aligned}\dot{\eta} &= F\eta + G\mu + Gd + GB_y u_q \\ \dot{z} &= \Psi(\eta, z).\end{aligned}\tag{9.13}$$

(9.5) then gets reformulated as:

$$\dot{V}_\varepsilon \leq -\frac{\gamma}{\varepsilon} V_\varepsilon + 2\eta^T P_\varepsilon Gd + 2\eta^T P_\varepsilon GB_y u_q.\tag{9.14}$$

By picking a particular control law for the auxiliary input: $u_q = -\frac{1}{2\varepsilon} B_y^{-1} G^T P_\varepsilon \eta$, we have the following simplification of (9.14):

$$\dot{V}_\varepsilon \leq -\frac{\gamma}{\varepsilon} V_\varepsilon + 2\eta^T P_\varepsilon Gd - \frac{1}{\bar{\varepsilon}} \eta^T P_\varepsilon G G^T P_\varepsilon \eta.\tag{9.15}$$

Therefore, by defining the semi-definite Lyapunov function $\bar{V}_\varepsilon(\eta) = \eta^T P_\varepsilon G G^T P_\varepsilon \eta$, we can pick $\bar{\varepsilon}$ small enough to cancel the effect of *phase uncertainty* on the dynamics. Motivated by (9.15), we can realize a class of controllers for the state based linear feedback law u_q as

$$\mathbf{K}_{\varepsilon, \bar{\varepsilon}}^q(\eta, z) = \{u_q \in \mathbb{U} : L_g V_\varepsilon u_q + \frac{1}{\bar{\varepsilon}} \bar{V}_\varepsilon \leq 0\},\tag{9.16}$$

where

$$L_g V_\varepsilon = 2\eta^T P_\varepsilon GB_y.\tag{9.17}$$

Note that $\bar{V}_\varepsilon = \frac{1}{4} L_g V B_y^{-1} B_y^{-T} L_g V^T$. Based on the construction of (5.60) and (5.62), we can realize the classes of controllers that combines both the time and state based imple-

mentations

$$\begin{aligned}
u &= u_t + u_q \\
\mathbf{K}_\varepsilon^t &= \{u_t \in \mathbb{U} : L_f V_\varepsilon^t + L_g V_\varepsilon^t u_t + \frac{\gamma}{\varepsilon} V_\varepsilon^t \leq 0\} \\
\mathbf{K}_{\varepsilon, \bar{\varepsilon}}^q &= \{u_q \in \mathbb{U} : L_g V_\varepsilon u_q + \frac{1}{\bar{\varepsilon}} \bar{V}_\varepsilon \leq 0\},
\end{aligned} \tag{9.18}$$

Lemma 27 can now be redefined to obtain exponential phase to state stability via the new control input (9.11).

Lemma 28. *The class of all time+state based feedback control laws $u_t(\eta_t, z_t) \in \mathbf{K}_\varepsilon^t(\eta_t, z_t)$, $u_q(\eta, z) \in \mathbf{K}_{\varepsilon, \bar{\varepsilon}}^q(\eta, z)$ applied on the system (6.26) yields exponential phase to η stability in the continuous dynamics. Moreover, there exists an exponential ultimate bound b_η such that $\overline{\lim}_{t \rightarrow \infty} V_\varepsilon(\eta(t)) \leq b_\eta$.*

Proof. Denote $\bar{P}_\varepsilon = P_\varepsilon G G^T P_\varepsilon \geq 0$. Since P_ε is symmetric and positive definite, we know that $\eta^T P_\varepsilon G G^T P_\varepsilon \eta = \|\eta^T P_\varepsilon G\|^2$. Therefore, if η falls in the null space of \bar{P}_ε , i.e., $\eta^T \bar{P}_\varepsilon \eta = 0 \implies \|\eta^T P_\varepsilon G\| = 0 \implies \eta^T P_\varepsilon G \equiv 0$.

Therefore, if $\eta \in \mathcal{N}(\bar{P}_\varepsilon)$, the null space, then the exponential stability is established. Otherwise, $\eta^T \bar{P}_\varepsilon \eta > 0$. Therefore we can follow the steps in (9.9) with the semi-definite Lyapunov function $\bar{V}_\varepsilon(\eta)$.

$$\begin{aligned}
\frac{1}{\bar{\varepsilon}} \bar{V}_\varepsilon &> 2\|\eta\| \frac{c_2 \delta}{\varepsilon^2} \implies \dot{V}_\varepsilon < -\frac{\gamma}{\varepsilon} V_\varepsilon \\
\frac{1}{\bar{\varepsilon}} c_1^2 \|\eta\|^2 &> 2\|\eta\| \frac{c_2 \delta}{\varepsilon^2} \implies \dot{V}_\varepsilon < -\frac{\gamma}{\varepsilon} V_\varepsilon. \\
\|\eta\| &> 2 \frac{c_2 \delta \bar{\varepsilon}}{c_1^2 \varepsilon^2 \gamma} \implies \dot{V}_\varepsilon < -\frac{\gamma}{\varepsilon} V_\varepsilon.
\end{aligned} \tag{9.19}$$

The exponential ultimate bound b_η is obtained when the equality holds. Since $\bar{V}_\varepsilon(\eta) \geq c_1^2 \|\eta\|^2$ for $\eta \notin \mathcal{N}(\bar{P}_\varepsilon)$, we have $\sqrt{\bar{V}_\varepsilon(\eta)} / c_1 \geq \|\eta\|$; b_η is therefore obtained as a function

of $\delta, \varepsilon, \bar{\varepsilon}$:

$$b_\eta = \frac{4c_2^2 \delta^2 \bar{\varepsilon}^2}{c_1^2 \varepsilon^4 \gamma^2}. \quad (9.20)$$

□

It must be noted that Lemma 28 \implies Lemma 27 and is a stronger form of stability. Describing the bounds in terms of the coordinates η ,

$$\|\eta(t)\| \leq \frac{1}{\varepsilon} \sqrt{\frac{c_2}{c_1}} e^{-\frac{\gamma}{2\varepsilon}t} \|\eta(0)\|, \quad \forall V_\varepsilon(\eta(t)) \geq b_\eta. \quad (9.21)$$

Stability of Continuous Periodic Orbits. Assume that there is an exponentially stable periodic orbit in the partial (full for running) zero dynamics, as denoted by \mathcal{O}_z (see (5.81) for a formal definition of periodic orbit). For the periodic orbit on the zero dynamics, we have the periodic orbit of the full order dynamics via the canonical embedding $\Pi_0(\mathcal{O}_z) = \mathcal{O}$. Since, the analysis is only for continuous dynamics, the domain notation is ignored. $\|(y_1, z)\|_{\mathcal{O}_z}$, as mentioned in (5.83), represents the distance between z and nearest point on the periodic orbit \mathcal{O}_z . Let Φ^z be the transformation from the partial (full) zero dynamics manifold to the zero coordinates. This means that there is a Lyapunov function $V_z : \Phi^z(\mathbb{PZ}) \rightarrow \mathbb{R}_{\geq 0}$ such that in a neighborhood $\mathbb{B}_r(\mathcal{O}_z)$ of \mathcal{O}_z (by converse Lyapunov theorem [112]) such that

$$\begin{aligned} c_4 \|(y_1, z)\|_{\mathcal{O}_z}^2 &\leq V_z(y_1, z) \leq c_5 \|(y_1, z)\|_{\mathcal{O}_z}^2, \\ \dot{V}_z(y_1, z) &\leq -c_6 \|(y_1, z)\|_{\mathcal{O}_z}^2, \\ \left\| \frac{\partial V_z}{\partial(y_1, z)} \right\| &\leq c_7 \|(y_1, z)\|_{\mathcal{O}_z}. \end{aligned} \quad (9.22)$$

Define the composite Lyapunov function: $V_c(\eta, z) = \sigma V_z(y_1, z) + V_\varepsilon(\eta)$, we can establish boundedness of the dynamics of the robot when $\|d\|$ is bounded. In other words, we have the following theorem, which establishes *phase to state stability* of periodic orbits in

continuous systems.

Theorem 7. *Given that the periodic orbit \mathcal{O}_z of the partial zero dynamics is exponentially stable, and given the controller u_{t+b} as given by (9.11), with $u_t(\eta_t, z_t) \in \mathbf{K}_\varepsilon^t(\eta_t, z_t)$, $u_q(\eta, z) \in \mathbf{K}_{\varepsilon, \bar{\varepsilon}}^q(\eta, z)$ applied on (9.13), that render the outputs η stable w.r.t. d , then the periodic orbit $\mathcal{O} = \Pi_0(\mathcal{O}_z)$ obtained from the canonical embedding is phase to state stable*

.

Proof. Upper bounds and lower bounds on the V_c can be defined as:

$$\begin{aligned} V_c(\eta, z) &\leq \max\{\sigma c_5, \frac{c_2}{\varepsilon^2}\}(\|(y_1, z)\|_{\mathcal{O}_z}^2 + \|\eta\|^2), \\ V_c(\eta, z) &\geq \min\{\sigma c_4, c_1\}(\|(y_1, z)\|_{\mathcal{O}_z}^2 + \|\eta\|^2), \end{aligned} \quad (9.23)$$

Therefore, taking the derivative:

$$\begin{aligned} \dot{V}_c(\eta, z) &= \sigma \frac{\partial V_z}{\partial z} \Psi(y_1, 0, z) + \sigma \frac{\partial V_z}{\partial y_1} \dot{y}_1 \dots \\ &\quad + \sigma \frac{\partial V_z}{\partial z} (\Psi(\eta, z) - \Psi(y_1, 0, z)) + \dot{V}_\varepsilon(\eta), \\ &\leq -\sigma c_6 \|(y_1, z)\|_{\mathcal{O}_z}^2 + \sigma c_7 L_q \|(y_1, z)\|_{\mathcal{O}_z} \|\eta_2\| + \dot{V}_\varepsilon(\eta), \\ &\leq -\sigma c_6 \|(y_1, z)\|_{\mathcal{O}_z}^2 + \sigma c_7 L_q \|(y_1, z)\|_{\mathcal{O}_z} \|\eta\| + \dot{V}_\varepsilon(\eta), \end{aligned} \quad (9.24)$$

where L_q is the Lipschitz constant for Ψ in (9.3). Substituting (9.15) for \dot{V}_ε leads to the following expression for the Lyapunov function:

$$\begin{aligned} \dot{V}_c &\leq -\sigma c_6 \|(y_1, z)\|_{\mathcal{O}_z}^2 + \sigma c_7 L_q \|(y_1, z)\|_{\mathcal{O}_z} \|\eta\| \\ &\quad - \frac{\gamma}{\varepsilon} V_\varepsilon - \frac{1}{\bar{\varepsilon}} \bar{V}_\varepsilon + 2\|\eta\| \|P_\varepsilon\| \|d\| \\ \dot{V}_c &\leq -\sigma c_6 \|(y_1, z)\|_{\mathcal{O}_z}^2 + \sigma c_7 L_q \|(y_1, z)\|_{\mathcal{O}_z} \|\eta\| \\ &\quad - \frac{\gamma}{\varepsilon} V_\varepsilon - \frac{1}{\bar{\varepsilon}} c_1^2 \|\eta\|^2 + 2\|\eta\| \|P_\varepsilon\| \|d\| \end{aligned} \quad (9.25)$$

With $\bar{\varepsilon}$ small enough, the right most expression can be canceled if $V_\varepsilon(\eta) > b_\eta$ (Lemma 28). Therefore, for exponential convergence of V_c , σ is picked such that $c_6 c_1 \frac{\gamma}{\varepsilon} - \sigma \frac{c_7^2 L_q^2}{4} > 0$, giving the desired result.

It is assumed that $(y_1, z) \in \mathbb{B}_r(\mathcal{O}_z) \implies \|(y_1, z)\|_{\mathcal{O}_z} < r$. In other words, $c_5 \|(y_1, z)\|_{\mathcal{O}_z}^2 < c_5 r^2$. Therefore, pick $b_z := \sigma c_5 r^2$. Therefore the ultimate bound for $V_c(\eta, z)$ can be obtained as: $\overline{\lim}_{t \rightarrow \infty} V_c(t) \leq \sigma c_5 \|(y_1, z)\|_{\mathcal{O}_z}^2 + \overline{\lim}_{t \rightarrow \infty} V_\varepsilon(\eta(t)) \leq b_z + b_\eta$, where b_η is obtained from Lemma 28. \square

9.3 Main Theorem

We can now introduce the main theorem of the paper. Note that we will reuse the constants used in Chapter 8 by redenoting. Similar to the continuous dynamics, it is assumed that the periodic orbit \mathcal{O}_z is exponentially stable in the hybrid zero dynamics. We will reintroduce the domain representation for this case. The multi-domain periodic orbit of the hybrid zero dynamics is defined in (5.81). The corresponding periodic orbit of the full order dynamics is \mathcal{O} , which is given by (5.82).

Theorem 8. *Let \mathcal{O}_z be an exponentially stable periodic orbit of the partial hybrid zero dynamics $\mathcal{IHC}_c|_z$ transverse to $\mathbb{S}_c|_z$. Given the controller $u_t + u_q$ applied on the hybrid control system \mathcal{IHC}_c , with $u_t(\eta_{t,v}, z_{t,v}) \in \mathbf{K}_\varepsilon^t(\eta_{t,v}, z_{t,v})$ for each $v \in \mathbb{V}_c$, $u_q(\eta_v, z_v) \in \mathbf{K}_{\varepsilon, \hat{\varepsilon}}^q(\eta_v, z_v)$, and given $r > 0$ such that $(\eta_v, z_v) \in \mathbb{B}_r(\mathcal{O})$, $\exists \delta, \hat{\varepsilon} > 0$ such that whenever $\|d\| < \delta$, $\varepsilon < \hat{\varepsilon}$, the orbit \mathcal{O} is ultimately bounded by $b = b_\eta + b_z$. In other words, the periodic orbit \mathcal{O} is phase to state stable.*

Before proving the main theorem, we will introduce new notations that are required to represent both continuous and discrete transitions as functions of (η_v, z_v) . Based on the construction of the reset map (plastic impacts), it is well known that they are Lipschitz in the state variable x . x are in turn Lipschitz in (η_v, z_v) due to the diffeomorphism Φ_v .

Therefore, by doing the transformation

$$\begin{aligned}\Delta_{y_1,e}(y_{1,v^-}, \eta_{2,v^-}, z_{v^-}) &= \Phi_{1,v^+}(\Delta_e(\Phi_{v^-}^{-1}(\eta_{v^-}, z_{v^-}))), \\ \Delta_{\eta_2,e}(y_{1,v^-}, \eta_{2,v^-}, z_{v^-}) &= \Phi_{2,v^+}(\Delta_e(\Phi_{v^-}^{-1}(\eta_{v^-}, z_{v^-}))), \\ \Delta_{z,e}(y_{1,v^-}, \eta_{2,v^-}, z_{v^-}) &= \Phi_{3,v^+}(\Delta_e(\Phi_{v^-}^{-1}(\eta_{v^-}, z_{v^-}))),\end{aligned}\tag{9.26}$$

where $e = (v^-, v^+)$, we have the following inequality:

$$\begin{aligned}\|\Delta_{y_1,e}(y_{1,v^-}, \eta_{2,v^-}, z_{v^-}) - \Delta_{y_1,e}(0, \eta_{2,v^-}, z_{v^-})\| &\leq L_{1,e}\|y_{1,v^-}\| \leq L_{1,e}\|\eta_{v^-}\|, \\ \|\Delta_{\eta_2,e}(y_{1,v^-}, \eta_{2,v^-}, z_{v^-}) - \Delta_{\eta_2,e}(y_{1,v^-}, 0, z_{v^-})\| &\leq L_{2,e}\|\eta_{2,v^-}\| \leq L_{2,e}\|\eta_{v^-}\|, \\ \|\Delta_{z,e}(y_{1,v^-}, \eta_{2,v^-}, z_{v^-}) - \Delta_{z,e}(y_{1,v^-}, \eta_{2,v^-}, 0)\| &\leq L_{3,e}\|z_{v^-}\|,\end{aligned}\tag{9.27}$$

where $L_{1,e}, L_{2,e}, L_{3,e}$ are the Lipschitz constants. Some of the notations in (9.27) contain the subscripts v^-, v^+, e , to indicate the domain (5.6), and are sometimes suppressed:

$$\begin{bmatrix} y_1 \\ \eta_2 \end{bmatrix} = \begin{bmatrix} y_{1,v} \\ \eta_{2,v} \end{bmatrix} = \eta = \eta_v, \quad z = z_v\tag{9.28}$$

where $v^- = \text{source}(e), v^+ = \text{target}(e)$ based on the domain and range space of the switching map, Δ_e , respectively. Since the surface \mathbb{PZ}_v is invariant under the discrete dynamics, $\Delta_{\eta_2,e}(y_{1,v^-}, 0, z_{v^-}) = 0$, for all e .

For the periodic orbit \mathcal{O}_z , there is also the periodic execution given by (5.4.2). Therefore, for the set of vertices $\mathbb{V}_c = (v_1, v_2, \dots, v_l)$, denote $(\eta_{v_i}^*, z_{v_i}^*) := \Phi_{v_i}(\mathbf{C}_i^z(t_i))$, which is the initial point in every domain. The cycle repeats after l iterations.

Since the number of domains and guards remain the same in a cycle (which also alternate with each other), we will use the same subscripts for both domain and guard representations (in a cycle, every domain has a unique guard associated with it). Associated with the hybrid periodic orbit \mathcal{O} (see (5.82) for the definition of hybrid periodic orbits) is the

time to impact function $T = T_{v_1} + T_{v_2} + \dots + T_{v_l}$, where each T_{v_i} is defined by:

$$T_{v_i}(\eta_{v_i}, z_{v_i}) = \min\{t \geq 0 | \varphi_t^{v_i}(\eta_{v_i}, z_{v_i}) \in \Phi_{v_i}(\mathbb{S}_{v_i})\}, \quad (\eta_{v_i}, z_{v_i}) \in \mathbb{B}(\eta_{v_i}^*, z_{v_i}^*). \quad (9.29)$$

and obtained through the implicit function theorem via the function

$$\mathbb{H}_{v_i}(t, y_{1,v_i}, \eta_{2,v_i}, z_{v_i}) = h(\varphi_t^{v_i}(y_{1,v_i}, \eta_{2,v_i}, z_{v_i})),$$

for which $\mathbb{H}_{v_i}(T_{v_i}, y_{1,v_i}^*, \eta_{2,v_i}^*, z_{v_i}^*) = 0$. $(\eta_{v_i}^*, z_{v_i}^*)$ corresponds to the starting point of the periodic orbit in the domain \mathbb{D}_{v_i} .

Given the initial state (η_v^*, z_v^*) in the guard, \mathbb{S}_v of $v \in \mathbb{V}_c$, the time to impact function is the time taken to reach the same guard (\mathbb{S}_v) the next time. Since, by assumption on \mathbb{S}_v , $\frac{\partial \mathbb{H}_v}{\partial t}(T_v, y_{1,v}^*, \eta_{2,v}^*, z_v^*) < 0$ for every $v \in \mathbb{V}_c$, the implicit function theorem implies that each T_{v_i} is well defined in a neighborhood of $(y_{1,v_i}^*, \eta_{2,v_i}^*, z_{v_i}^*)$. Therefore, $T_v(\eta_v^*, z_v^*) = T_v^*$. Each $\mathbb{H}_v(t, y_{1,v}, \eta_{2,v}, z_v)$ is Lipschitz continuous since it is differentiable in t , h_v is assumed to be continuously differentiable, and $\varphi_t^v(\eta_v, z_v)$ is Lipschitz continuous, and therefore the sum of the time to impact functions T is also Lipschitz.

A hybrid periodic orbit \mathcal{O}_z , of $\mathcal{IH}_c|_z$ has the Poincaré map $\vartheta_v : \mathbb{S}_v|_z \rightarrow \mathbb{S}_v|_z$ is termed the restricted Poincaré map. Therefore, for the point $(y_{1,v_1}, 0, z_{v_1}) \in \mathbb{S}_{v_1}$

$$\vartheta_{v_1}(y_{1,v_1}, z_{v_1}) = \varphi_{T_{\vartheta_{v_l}}}^{z,v_l} \circ \Delta_{v_{l-1}} \circ \dots \circ \varphi_{T_{\vartheta_{v_2}}(y_{1,v_2}, z_{v_2})}^{z,v_2} \circ \Delta_{v_1}(y_{1,v_1}, 0, z_{v_1}), \quad (9.30)$$

where $\varphi_t^{z,v}$ is the flow of the partial hybrid zero dynamics and T_{ϑ_v} is the restricted time to impact function, which is given by $T_{\vartheta_v}(y_{1,v}, z_v) = T(y_{1,v}, 0, z_v)$. Therefore T_{ϑ} is the sum of the individual time-to-impact functions. Without loss of generality, we can assume that the relative degree two outputs $\eta_{2,v}^* = 0$, the zero dynamic coordinates $z_v^* = 0$, but the relative degree one output $y_{1,v}^* \neq 0$. Therefore, we can denote $\zeta_v = (y_{1,v} - y_{1,v}^*, z_v)$, such that the fixed point $(y_{1,v}^*, 0, z_v^*) \implies \zeta_v = 0$. The following Lemma will introduce the

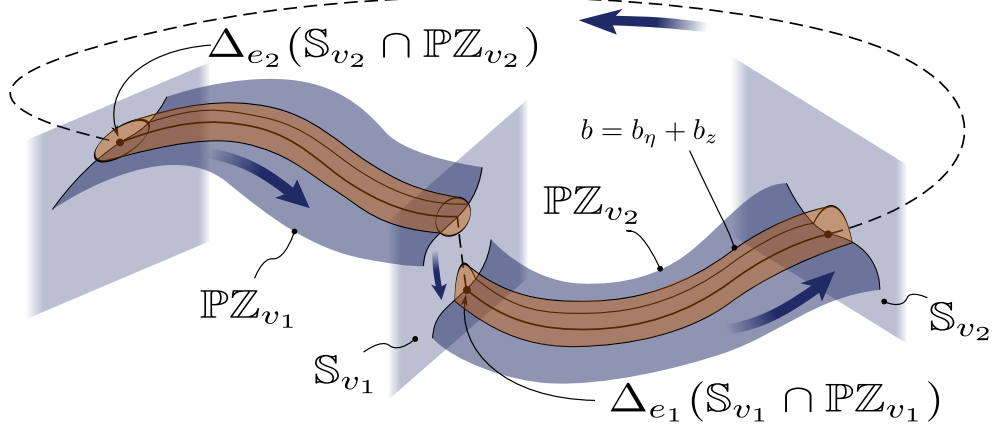


Figure 9.1: Figure showing the bound $b = b_\eta + b_z$ on the periodic orbit for a two domain hybrid system. Phase to state stability ensures that a bounded periodic orbit exists under a bounded uncertainty.

relationship between time to impact, Poincaré functions with the state η_v . We will drop the domain notation, because the Poincaré maps do not change domains.

Lemma 29. *Let \mathcal{O}_z be the periodic orbit of the hybrid zero dynamics $\mathcal{TH}_c|_z$ transverse to $\mathbb{S}_c|_z$. Given the time+state based feedback controller u_{t+q} that render the system η stable, then there exist finite constants A_1, A_2 such that for all $(\eta, z) \in \mathbb{B}_r(\eta^*, z^*) \cap \mathbb{S}$ and $V_\varepsilon(\Delta_\eta(\eta, z)) > b_\eta$:*

$$\|T(\eta, z) - T_\vartheta(y_1, z)\| \leq A_1 \|\eta_2\| \quad (9.31)$$

$$\|\mathbb{P}(\eta, z) - \vartheta(y_1, z)\| \leq A_2 \|\eta_2\| \quad (9.32)$$

Proof. Instead of considering all the domains together, here, we study one domain and obtain bounds on the states till the next impact event. This procedure is repeated l times to yield the final upper bounds on the states of the system as a function of the disturbance input. For each domain, we construct an auxiliary time to impact function T_{B_v} that is Lipschitz continuous and then relate it to T . Let $\mu_{1,v} \in \mathbb{R}^{2n-k_{1,v}-2k_{2,v}}$, $\mu_{2,v} \in \mathbb{R}^{k_{1,v}+2k_{2,v}}$ be constant vectors and let $\varphi_t^{z,v}(y_{1,v}(0), 0, z_v(0))$ be the solution of the partial hybrid zero dy-

namics with the initial condition $z_v(0) = \Delta_{z,v}(\eta_0, 0, z_0), y_{1,v}(0) = \Delta_{y_{1,v}}(\eta_0, 0, z_0)$. Define:

$$T_{B,v}(\mu_{1,v}, \mu_{2,v}, y_{1,v}, z_v) = \inf\{t \geq 0 : h(\mu_{1,v}, \varphi_t^{z,v}(y_{1,v}(0), 0, z_v(0)) + \mu_{2,v}) = 0\}$$

It follows that $T_{B,v}(0, 0, y_{1,v}, z_v) = T_{\vartheta_v}(y_{1,v}, z_v)$. By construction, $T_{B,v}$ is Lipschitz continuous. Hence in the norm $\|(\mu_{1,v}, \mu_{2,v}, y_{1,v}, z_v)\| = \|\mu_{1,v}\| + \|\mu_{2,v}\| + \|y_{1,v}\| + \|z_v\|$,

$$\|T_{B,v}(\mu_{1,v}, \mu_{2,v}, y_{1,v}, z_v) - T_{\vartheta_v}(y_{1,v}, z_v)\| \leq L_{B,v}(\|\mu_{1,v}\| + \|\mu_{2,v}\|), \quad (9.33)$$

where $L_{B,v}$ is the local Lipschitz constant. We note that $T_v(\eta_v, z_v)$ is continuous and therefore there exists $r > 0$ such that for $(\eta_v, z_v) \in \mathbb{B}_r(\eta_v^*, z_v^*) \cap \mathbb{S}_v$: $c_8 T_v^* \leq T_v(\eta_v, z_v) \leq c_9 T_v^*$, where $0 < c_8 < 1$ and $c_9 > 1$. Let $(\eta_{1,v}^s(t), \eta_{2,v}^s(t), z_v^s(t))$ be the time solution that satisfy $\dot{z}^s = \Psi_v(\eta_{2,v}^s(t), \eta_{1,v}^s(t), z_v^s(t)), \dot{\eta}_{1,v}^s(t) = -\frac{1}{\varepsilon} \eta_{1,v}^s(t)$ that includes different domains and switching surfaces. Similarly let $(\eta_{1,v}^{s'}(t), z_v^{s'}(t))$ be the second solution that satisfies $\dot{z}_v^{s'}(t) = \Psi_v(\eta_{1,v}^{s'}(t), 0, z_v^{s'}(t)), \dot{\eta}_{1,v}^{s'}(t) = -\frac{1}{\varepsilon} \eta_{1,v}^{s'}(t)$. We can now determine $\mu_{1,v}, \mu_{2,v}$.

Since $V_\varepsilon(\eta) > b_\eta$, by using (9.21) we have

$$\begin{aligned} \|\eta_{2,v_1}^s(T_{v_1})\| &= \|\eta_{2,v_1}^s(t)\|_{t=T_{v_1}(\eta_{v_1}, z_{v_1})} \leq \sqrt{\frac{c_2}{c_1}} \frac{1}{\varepsilon} e^{-\frac{\gamma}{2\varepsilon} c_8 T_{v_1}} \|\eta_{2,v_1}^s\|, \\ \|\eta_{2,v_2}^s(T_{v_2})\| &= \|\eta_{2,v_2}^s(t)\|_{t=T_{v_2}(\eta_{v_2}, z_{v_2})} \\ &\leq \sqrt{\frac{c_2}{c_1}} \frac{1}{\varepsilon} e^{-\frac{\gamma}{2\varepsilon} c_8 T_{v_2}} L_{2,v_1} \|\eta_{2,v_1}^s(T_{v_1})\|, \end{aligned} \quad (9.34)$$

(9.34) yields $\|\mu_{1,v}\|$ for all v . To obtain $\|\mu_{2,v}\|$, we use the Gronwall-Bellman argument. We know that:

$$\begin{aligned} \begin{bmatrix} \eta_{1,v}^s(t) - \eta_{1,v}^{s'}(t) \\ z_v^s(t) - z_v^{s'}(t) \end{bmatrix} &= \begin{bmatrix} \eta_{1,v}^s(0) - \eta_{1,v}^{s'}(0) \\ z_v^s(0) - z_v^{s'}(0) \end{bmatrix} + \dots \\ &\quad \int_0^t \begin{bmatrix} -\frac{1}{\varepsilon} \eta_{1,v}^s(\tau) + \frac{1}{\varepsilon} \eta_{1,v}^{s'}(\tau) d\tau \\ \Psi(\eta_{1,v}^s(\tau), \eta_{2,v}^s(\tau), z_v^s(\tau)) - \Psi(\eta_{1,v}^{s'}(\tau), 0, z_v^{s'}(\tau)) d\tau \end{bmatrix}, \end{aligned}$$

and therefore by using (9.27) and using the property of Lipschitz continuity of Ψ_v :

$$\begin{aligned}
\zeta_v^s(t) - \zeta_v^{s'}(t) &:= \begin{bmatrix} \eta_{1,v}^s(t) - \eta_{1,v}^{s'}(t) \\ z_v^s(t) - z_v^{s'}(t) \end{bmatrix} \\
\|\zeta_v^s(t) - \zeta_v^{s'}(t)\| &\leq \|\zeta_v^s(0) - \zeta_v^{s'}(0)\| + \int_0^t L_q(\|\eta_{2,v}^s(\tau)\| + \|\zeta_v^s(\tau) - \zeta_v^{s'}(\tau)\|) d\tau \\
&\leq \|\zeta_v^s(0) - \zeta_v^{s'}(0)\| + \frac{2}{\gamma} \sqrt{\frac{c_2}{c_1}} L_q \|\eta_{2,v}^s(0)\| + \int_0^t L_q \|\zeta_v^s(\tau) - \zeta_v^{s'}(\tau)\| d\tau,
\end{aligned} \tag{9.35}$$

where (9.34) is integrated and substituted in the above equation. By Gronwall-Bellman inequality,

$$\begin{aligned}
\|\zeta_{v_2}^s(t) - \zeta_{v_2}^{s'}(t)\| &\leq C_1 \|\eta_{2,v_1}^s(T_{v_1})\| e^{L_q t} \\
C_1 &= \max_{v \in \mathbb{V}_c} \left\{ \frac{2}{\gamma} \sqrt{\frac{c_2}{c_1}} L_q L_{2,v} + 2 \max\{L_{1,v_1}, L_{3,v_1}\} \right\}.
\end{aligned} \tag{9.36}$$

Therefore, we have:

$$\|\mu_{2,v_2}\| \leq \|\zeta_{v_2}^s(T_{v_2}^*) - \zeta_{v_2}^{s'}(T_{v_2}^*)\| \leq C_1 e^{L_q T_{v_2}} \|\mu_{1,v_1}\| \tag{9.37}$$

Proof of (9.31) can now be obtained by substituting for $\|\mu_{1,v}\|, \|\mu_{2,v}\|$ after repeating l times. Total time can now be obtained as: $T_B = T_{B,v_1} + T_{B,v_2} + \dots + T_{B,v_l}$.

To prove (9.32), define:

$$C_2 = \max_{c_8 T_v^* \leq T_v \leq c_9 T_v^*, v \in \mathbb{V}_c} \left\| \begin{bmatrix} -\frac{1}{\varepsilon} \eta_{1,v}^{s'}(t) \\ \Psi_v(\eta_{1,v}^{s'}(t), 0, z_v^{s'}(t)) \end{bmatrix} \right\|, \tag{9.38}$$

also define \mathbb{P}_z as the projection of the Poincaré map to the partial zero dynamic surface. It

then follows that:

$$\begin{aligned} \|\mathbb{P}_z(\eta_{1,v}^s, \eta_{2,v}^s, z_v^s) - \vartheta(\eta_{1,v}^{s'}, z_v^{s'})\| &\leq \|\zeta_v^s(0) - \zeta_v^{s'}(0)\| \\ &+ \sum_{v \in \mathbb{V}_c} \int_0^{T_v(\eta_v, z_v)} \left\| \begin{bmatrix} -\frac{1}{\varepsilon} \eta_{1,v}^s(\tau) + \frac{1}{\varepsilon} \eta_{1,v}^{s'}(\tau) \\ \Psi_v(\eta_{1,v}^s(\tau), \eta_{2,v}^s(\tau), z_{1,v}(\tau)) - \Psi_v(\eta_{1,v}^{s'}(\tau), 0, z_v^{s'}(\tau)) \end{bmatrix} \right\| d\tau \\ &+ \sum_{v \in \mathbb{V}_c} \int_{T_v(\eta_v, z_v)}^{T_{\vartheta_v}(z)} \left\| \begin{bmatrix} -\frac{1}{\varepsilon} \eta_{1,v}^{s'}(\tau) \\ \Psi_v(\eta_{1,v}^{s'}(\tau), 0, z_v^{s'}(\tau)) \end{bmatrix} \right\| d\tau, \end{aligned}$$

which results in the following inequality after a series of substitutions:

$$\|\mathbb{P}_z(\eta_{1,v}^s, \eta_{2,v}^s, z_v^s) - \vartheta(\eta_{1,v}^{s'}, z_v^{s'})\| \leq C_T \|\eta_{2,v}^s\| + C_2 A_1 \|\eta_{2,v}^s\|. \quad (9.39)$$

Collecting the terms together yields the desired result. \square

Proof of Main Theorem. We can now prove the main theorem by using the inequalities obtained from Lemma 29.

Proof of Theorem 8. Results of Lemma 29 and the exponential stability of \mathcal{O}_z imply that there exists $r > 0$ such that $\vartheta : \mathbb{B}_r(0) \cap \mathbb{S}|_z \rightarrow \mathbb{B}_r(0) \cap \mathbb{S}|_z$ is well defined for all $\zeta \in \mathbb{B}_r(0) \cap \mathbb{S}|_z$ and $\zeta_{k+1} = \vartheta(\zeta_k)$ is locally exponentially stable, i.e., $\|\zeta_i\| \leq N\xi^i \|\zeta_0\|$ for some $N > 0, 0 < \xi < 1$ and all $i \geq 0$. Therefore, by the converse Lyapunov theorem for discrete systems, there exists a Lyapunov function V_ϑ , defined on $\mathbb{B}_r(0) \cap \mathbb{S}_c|_z$ for some $r > 0$ (possibly smaller than the previously defined r), and positive constants $c_{10}, c_{11}, c_{12}, c_{13}$ such that :

$$\begin{aligned} c_{10} \|\zeta\|^2 &\leq V_\vartheta(\zeta) \leq c_{11} \|\zeta\|^2, \\ V_\vartheta(\vartheta(\zeta)) - V_\vartheta(\zeta) &\leq -c_{12} \|\zeta\|^2, \\ |V_\vartheta(\zeta) - V_\vartheta(\zeta')| &\leq c_{13} \|\zeta - \zeta'\| (\|\zeta\| + \|\zeta'\|), \end{aligned} \quad (9.40)$$

where ζ consists of z and shifted y_1 as defined before. It must be first ensured that the

region b_η , which is a function of δ must be within the bounds defined by r . For $\|\eta\| = r$, $b_\eta < V_\varepsilon(\eta)$ is ensured through the following condition: $b_\eta < V_\varepsilon(\eta) \leq \frac{c_2}{\varepsilon^2} \|\eta\|^2 \leq \frac{c_2}{\varepsilon^2} r^2$. From Lemma 27 we have: $\frac{4c_2^2 \delta^2}{c_1 \gamma^2 \varepsilon^2} < \frac{c_2}{\varepsilon^2} r^2 \implies \delta < \frac{\sqrt{c_1} \gamma}{2\sqrt{c_2}} r$. We can choose $\delta = \frac{\sqrt{c_1} \gamma}{4\sqrt{c_2}} r$ to leave enough margin for the outputs to rapidly exponentially converge within $\mathbb{B}_r(0, 0)$. By closely matching $\tau(t)$ with $\tau(q)$, the full dynamics of the system can be restricted to the bound b_η .

For the RES-CLF V_ε , denote its reduced Lyapunov function (of only η_2 coordinates) and restriction to the switching surface by V_{ε, η_2} . The domain index $v \in \mathbb{V}_c$ is conveniently picked and fixed. In the walking robot, we pick the end of the single support phase ss as the restriction. With these two Lyapunov functions we define the following candidate Lyapunov function:

$$V_P(\eta, z) = V_\vartheta(\zeta) + \sigma V_{\varepsilon, \eta_2}(\eta_2) \quad (9.41)$$

defined on $\mathbb{B}_r(0, 0) \cap \mathbb{S}_v$. The lower and upper bounds on V_P are $\min\{c_{10}, \sigma c_1\} \|\eta, z\|^2$, $\max\{c_{11}, \frac{\sigma c_2}{\varepsilon^2}\} \|\eta, z\|^2$ respectively. The idea is to show that there exists a bounded region $b = b_\eta + b_z$ into which the dynamics of the robot exponentially converge (see Fig. 9.1). If the outputs enter this region then it stays for all time even through impacts. Picking a point η such that $V_\varepsilon(\eta) = b_\eta$, we have the maximum value for η , which is given by $\|\eta\|_{max} = \sqrt{\frac{b_\eta}{c_1}}$. Also, we know that $\eta_2^s(0) = \Delta_{\eta_2}(\eta, z)$. If $V_\varepsilon(\eta^s(0)) \leq b_\eta$, then the boundedness is verified. For the case when the impact map takes the outputs outside the bounded region (by utilizing (9.21)), we pick the lower bound on the time to impact function. We will ignore the subscript notations for the states (η_v, z_v) . The Poincaré map

\mathbb{P} can be split into two components $\mathbb{P}_{\eta_2}, \mathbb{P}_z$. Therefore

$$\begin{aligned} V_{\varepsilon, \eta_2}(\mathbb{P}_{\eta_2}(\eta, z)) &\leq \underbrace{\dots \frac{c_2}{\varepsilon^2} e^{-\frac{\gamma}{\varepsilon} T_{v_2}} L_{2,v_2}^2 \frac{c_2}{\varepsilon^2} e^{-\frac{\gamma}{\varepsilon} T_{v_1}} L_{2,v_1}^2 \| \eta_2 \|^2}_{A_3} \\ &\leq A_3 \| \eta_2 \|^2. \end{aligned} \quad (9.42)$$

We have the following:

$$V_{\varepsilon, \eta_2}(\mathbb{P}_{\eta_2}(\eta, z)) - V_{\varepsilon, \eta_2}(\eta_2) \leq A_3 \| \eta_2 \|^2 - c_1 \| \eta_2 \|^2$$

Since the origin is an exponentially stable equilibrium for $z_{k+1} = \vartheta(z_k)$, we have the following inequalities:

$$\begin{aligned} \|\mathbb{P}_z(\eta, z)\| &= \|\mathbb{P}_z(\eta, z) - \vartheta(\zeta) + \vartheta(\zeta) - \vartheta(0)\| \\ &\leq A_2 \| \eta_2 \| + L_\vartheta \| \zeta \| \\ \|\vartheta(\zeta)\| &\leq N\xi \| \zeta \|, \end{aligned} \quad (9.43)$$

where L_ϑ is obtained after including the discrete and continuous dynamics and picking the maximum rate or change of ϑ . Therefore:

$$V_\vartheta(\mathbb{P}_z(\eta, z)) - V_\vartheta(\vartheta(\zeta)) \leq c_{13}(A_2 \| \eta_2 \|). (A_2 \| \eta_2 \| + (L_\vartheta + N\xi) \| \zeta \|). \quad (9.44)$$

It follows that:

$$\begin{aligned} V_\vartheta(\mathbb{P}_z(\eta, z)) - V_\vartheta(\zeta) &= V_\vartheta(\mathbb{P}_z(\eta, z)) - V_\vartheta(\vartheta(\zeta)) \\ &\quad + V_\vartheta(\vartheta(\zeta)) - V_\vartheta(\zeta), \end{aligned} \quad (9.45)$$

and the expressions in (9.44) and in (9.40) can be substituted. Combining the entire Ly-

punov function we have:

$$V_P(\mathbb{P}(\eta, z)) - V_P(\eta, z) \leq - \begin{bmatrix} \|\eta_2\| \\ \|\zeta\| \end{bmatrix}^T \Lambda_{\mathcal{H}} \begin{bmatrix} \|\eta_2\| \\ \|\zeta\| \end{bmatrix} \quad (9.46)$$

where the symmetric matrix $\Lambda_{\mathcal{H}} \in \mathbb{R}^{2 \times 2}$, with the upper triangular entries being:

$$\begin{aligned} a_1 &= \Lambda_{\mathcal{H}}(1, 1) = \sigma(c_1 - A_3) - c_{13}A_2^2 \\ a_2 &= \Lambda_{\mathcal{H}}(1, 2) = -\frac{c_{13}A_2}{2}(L_\vartheta + N\xi) \\ a_3 &= \Lambda_{\mathcal{H}}(2, 2) = c_{12} \end{aligned} \quad (9.47)$$

For exponential convergence, it must be shown that :

$$\begin{aligned} V_P(\mathbb{P}(\eta, z)) - V_P(\eta, z) \\ \leq -a_1\|\eta_2\|^2 - 2a_2\|\eta_2\|\|\zeta\| - a_3\|\zeta\|^2, \end{aligned} \quad (9.48)$$

results in a positive definite matrix $\Lambda_{\mathcal{H}}$, which can be ensured by picking ε, σ such that $a_1a_3 - a_2^2 > 0$. $\hat{\varepsilon}$ is picked such that $c_1 - A_1L_1^2 > 0$, and σ such that $a_1a_3 - a_2^2 > 0$. \square

Fig. 9.1 depicts the periodic orbit \mathcal{O} and its tube, which is defined by the bound b . Note that the bound b is defined on the Lyapunov function that is a function of a norm of the distance between the state and the periodic orbit \mathcal{O} . Theorem 8 means that by using a time dependent RES-CLF, any trajectory starting close to the tube will ultimately enter the tube defined by b as long as $\|d\| < \delta$.

9.4 Simulation and Experimental Results

Walking. DURUS consists of fifteen actuated joints throughout the body and one linear passive spring at the end of each leg. The generalized coordinates of the robot are described

in Fig. 6.7 (see [64]). Due to the presence of passive springs, the double-support domain is no longer trivial. Therefore, a two-domain hybrid system model is utilized to model DURUS walking, where a transition from double-support to single-support domain takes place when the normal force on non-stance foot reaches zero, and a transition from single-support to double support domain occurs when the non-stance foot strikes the ground [64]. Since there is no impact while transitioning from double-support to single-support, the discrete map is an identity. The holonomic constraints are defined in such a way that feet are flat on the ground when they are in contact with the ground. In addition, DURUS is supported by a linear boom that restricts the motion of the robot to the sagittal plane. The contacts with the boom are also modeled as holonomic constraints.

The combined outputs of the system are defined as $y^a(q) = [y_1^a, y_2^{aT}]^T$ and $y^d(\tau, \alpha) = [v_{hip}, y_2^d(\tau, \alpha)]^T$, and the feedback control law in (9.18) is applied on the system. Fig. 9.4 shows phase portraits, Fig. 9.2, Fig. 9.3 show the comparison of the phase variable for walking and running respectively, Fig. 9.6 shows the walking tiles. The error between the phase variables is low for simulation $\|d\|_{max} < 9$. See [5] for the corresponding movie.

Running. By utilizing time based feedback linearization + state based PD control law given by (9.11) in simulation, trajectory tracking is achieved that is ultimately bounded to the periodic orbit. For the experimental realization, a variant of time+state based feedback as shown by (9.50) is utilized and the result is sustainable running taking over 150 steps

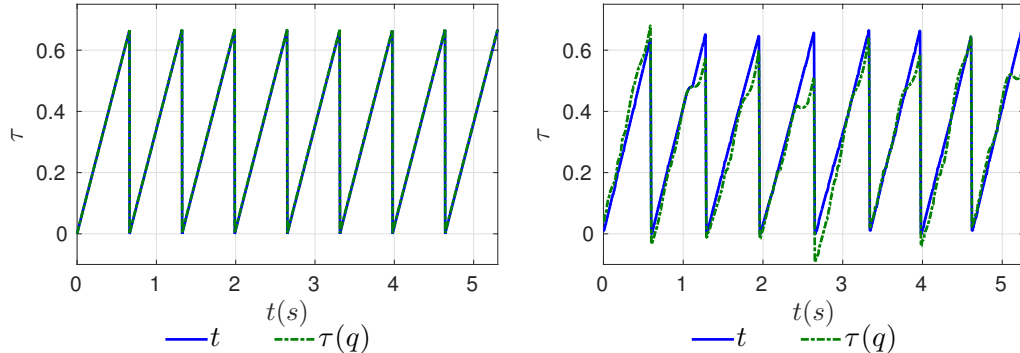


Figure 9.2: Progression of time vs. the phase variable shown for the walking simulation (left) and experiment (right).

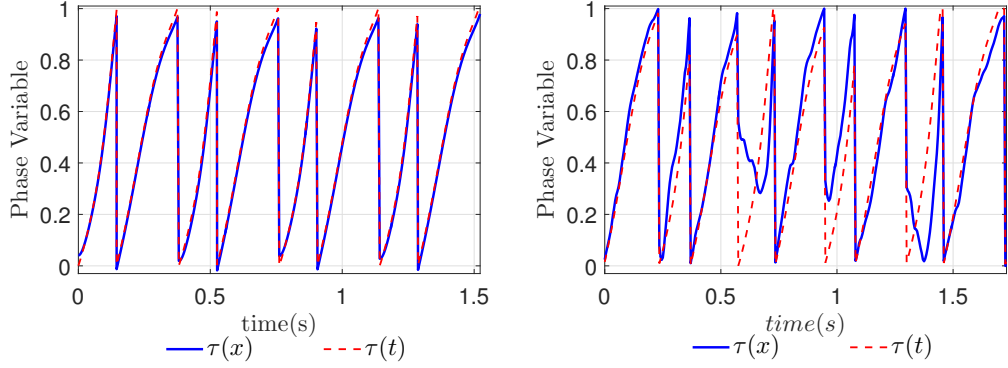


Figure 9.3: Progression of time vs. the phase variable shown for the running simulation (left) and experiment (right).

(see [6] for the video). Multiple views in the video show that the running is repeatable. The phase portrait over 30 steps are shown at Fig. 9.4. The average running speed is 1.75 m s^{-1} . Further, the time based and state based phase variables $\tau(t)$ and $\tau(x)$ are shown together with those from simulation at Fig. 9.3. The running tiles of both simulations and experiment

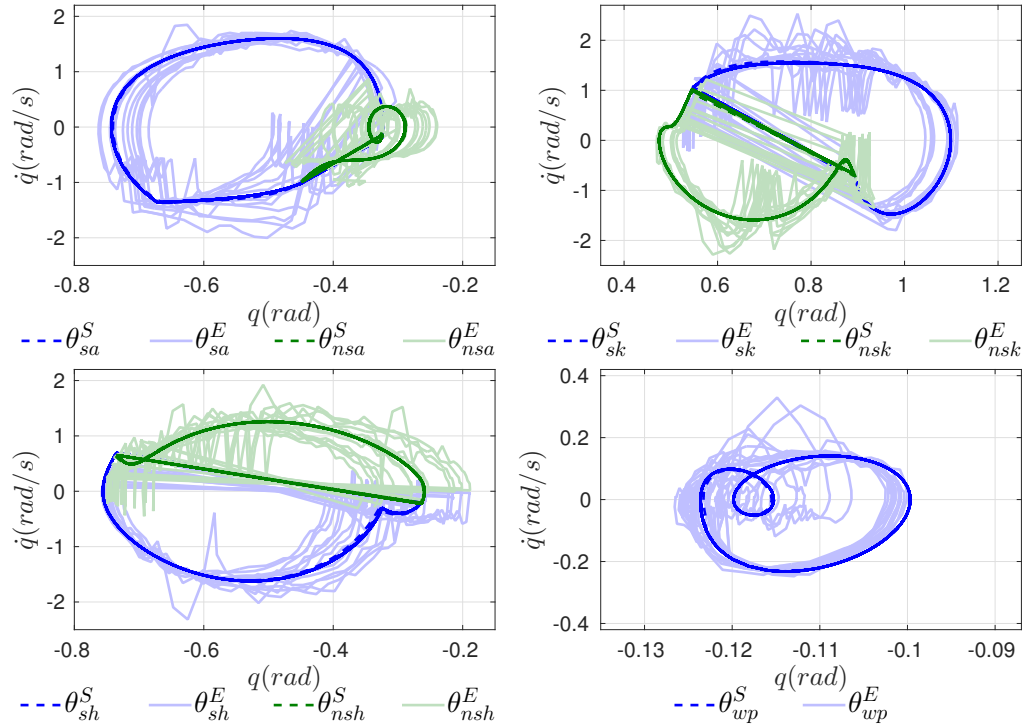


Figure 9.4: Phase portraits of the ankle, knee, hip and waist pitch angles of the robot. Both simulation (S) and experimental (E) results are shown.

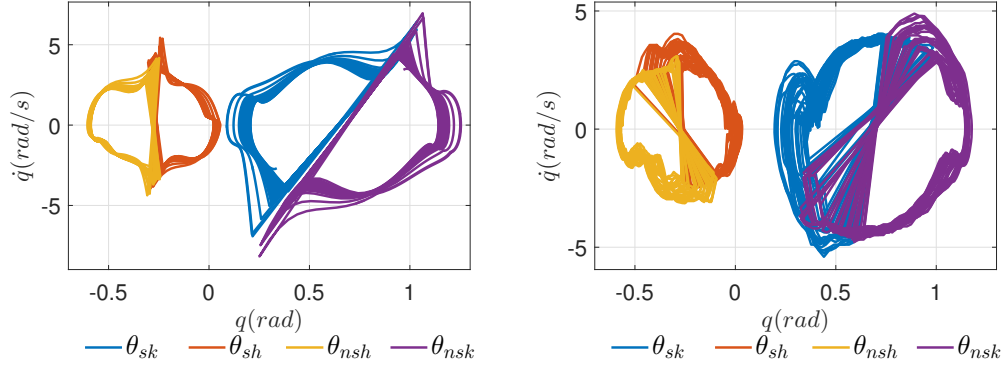


Figure 9.5: Limit cycles of simulations (left) and experiment (right), are shown for the running robot DURUS-2D. Both used the time based desired outputs: $y_2^d(t) = y_2^d(\tau(t), \alpha)$.

are compared at Fig. 9.7.

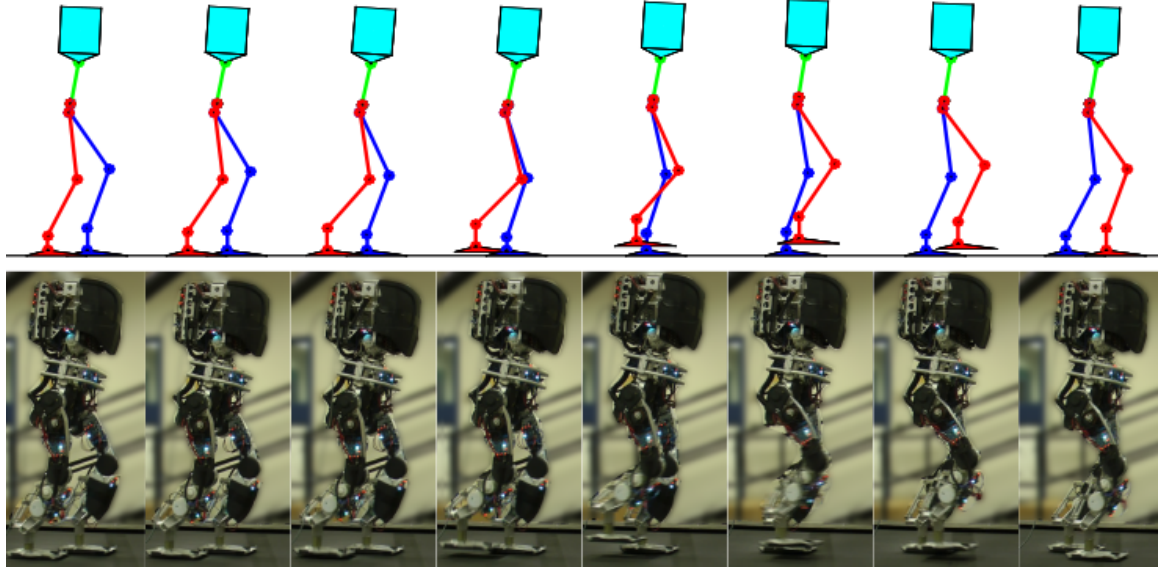


Figure 9.6: Figure showing the walking tiles of DURUS humanoid for one step. Video link to the experiment is given in [5].

Experimental Controller. Motivated by the successful run of the 3D humanoid robot DURUS, the following time+state based controller was implemented in the robot: The linear feedback laws picked are (9.11). For the experimental setup, the time and state based outputs are picked through the inverse diffeomorphism applied (see [67]) to obtain

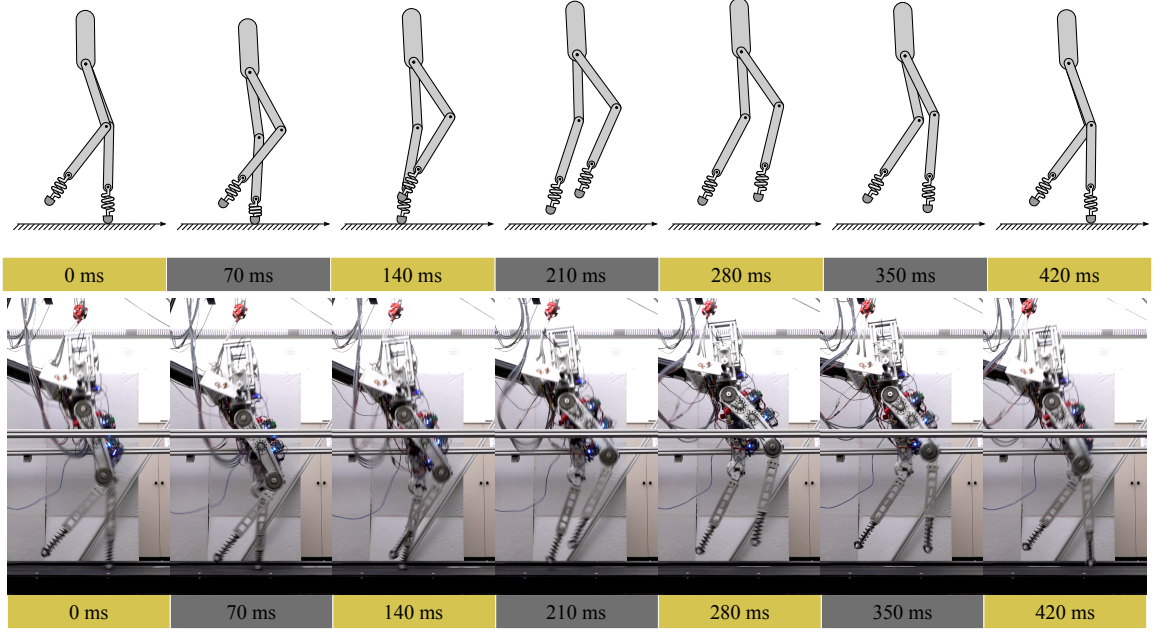


Figure 9.7: Running tiles of simulation vs experiment for the running robot DURUS-2D. Video link to the experiment is given in [6].

the desired configuration angles (q_d) and their derivatives (\dot{q}_d).

$$\begin{bmatrix} q_d \\ \dot{q}_d \end{bmatrix} = \Phi^{-1}(\eta, z), \quad \begin{bmatrix} q_d^t \\ \dot{q}_d^t \end{bmatrix} = \Phi_t^{-1}(\eta_t, z_t) \quad (9.49)$$

A linear feedback law is then applied as the torque input

$$u_W = -\frac{1}{\varepsilon^2} K_P^t (q - q_d^t) - \frac{1}{\varepsilon} K_D^t (\dot{q} - \dot{q}_d^t), \quad (9.50)$$

for the walking robot, and

$$\begin{aligned} u_R = & -\frac{1}{\varepsilon^2} K_P^t (q - q_d^t) - \frac{1}{\varepsilon} K_D^t (\dot{q} - \dot{q}_d^t) \\ & - \frac{1}{\bar{\varepsilon}\varepsilon^2} K_P (q - q_d) - \frac{1}{\bar{\varepsilon}\varepsilon} K_D (\dot{q} - \dot{q}_d), \end{aligned} \quad (9.51)$$

for the running robot. K_P^t, K_D^t, K_P, K_D are constant gain matrices with appropriately tuned values.

CHAPTER 10

APERIODIC SYSTEMS: DYNAMIC DANCING

As a means to show ISS based control implementations for non-periodic systems, this chapter focuses on utilizing time based PD controllers for dynamic dancing. The primary goal is to connect trajectories, i.e., desired outputs y^d , for each motion primitive; that is, we wish to *compose* dynamical systems. To this end, this section will present the notion of *meta-dynamical* systems, which gives a formalism to the notion of composition. We begin by studying different poses of the robot that will be connected through dynamic transitions.

10.1 Basic Definitions

10.1.1 Pose

A *pose* of a robot is a configuration q , which is intended to be realized in the robot. In other words, a pose is just a captured frame of a robot while in motion. For example, a robot with hip forward and low and both feet flat is a crouch, and is called a pose of the robot. There are several possible poses that the robot can assume. The poses are picked from the eight domain representations shown in Fig. 4.3. If the stance toe is always on ground (since jumping is not included), the three remaining points (non-stance toe and heel and stance heel) can be either in contact or not. Therefore, there are eight possible general cases for pose generation. Accordingly, we will include: front heel lift (FHL), front toe lift (FTL), back heel lift (BHL), all feet flat on ground (FF), swing (S) with stance foot being flat on ground, double heel lift (DHL), front toe and back heel lift (FTBH), and under-actuation (UA) with only stance toe in contact with ground.

It is important to note that there could be more than one pose obtained from each domain \mathbb{D} , i.e., more than one type of Back Heel Lift, Front Toe Lift, and other combinations as

well. In other words, there are more than eight types of poses. For example, we could have two different kinds of flat footed poses, where the vertical hip position is high for one and low for the other. This will be discussed further in Section 10.4 where the poses of dancing on AMBER2 are introduced. If a set of poses q_1, q_2, \dots, q_i is used, then dancing is achieved by just executing dynamic transitions between these poses.

10.1.2 Dynamic Transition

Let $x = (q^T, \dot{q}^T) \in \mathbb{R}^{2n}$, and $\dot{x} = f_{cl}(x)$ be a closed loop dynamical system. Let $\varphi(t; x_0)$ be the solution to $\dot{x} = f(x)$ at time $t \in \mathbb{R}$ with initial condition x_0 , and let π_q be the canonical projection $\pi_q(x) = q$.

Definition 52. A *dynamic transition between two poses, q_0 and q_f , is a solution $\varphi(t; x_0)$ to the dynamical system $\dot{x} = f_{cl}(x)$ such that there exists a point $x_0 \in \mathbb{R}^{2n}$ and a time $t_f \geq 0$ with $\pi_q(\varphi(0; x_0)) = q_0$ and $\pi_q(\varphi(t_f; x_0)) = q_f$.*

This transition is achieved by applying a suitable control law on the robot. Note that this transition involves going through multiple domains due to different foot conditions and the impacts. In other words, the transition is piecewise smooth, and is hybrid in nature. For a successful implementation of this transition, we need to ensure that the controllers utilized satisfy the ISS properties required of any stable hybrid transition. This definition allows us to formally introduce meta-dynamical systems.

Definition 53. The meta-dynamical system is defined as a tuple:

$$\text{MD} = (\mathcal{G}, \mathcal{P}, \mathcal{T}), \quad (10.1)$$

- \mathcal{G} is a directed graph given as: $\mathcal{G} = (\mathcal{V}, \mathcal{E})$, where \mathcal{V} is the set of vertices describing desired poses realizable on the robot, and \mathcal{E} represents transitions between these poses. We denote the source and target of an edge $e \in \mathcal{E}$ by $\text{source}(e) \in \mathcal{V}$ and $\text{target}(e) \in \mathcal{V}$.

- \mathcal{P} is the set of poses given by: $\mathcal{P} = \{\mathcal{P}_v\}_{v \in \mathcal{V}}$, where $\mathcal{P}_v = q_v \in \mathbb{R}^n$.
- \mathcal{T} is the set of dynamic transitions: $\mathcal{T} = \{\mathcal{T}_e\}_{e \in \mathcal{E}}$, where $\mathcal{T}_e = \Phi_e$ is the dynamic transition between the poses $q_{\text{source}(e)}$ and $q_{\text{target}(e)}$.

A pictorial representation of a meta-dynamical system for AMBER2 is shown in Fig. 10.1.

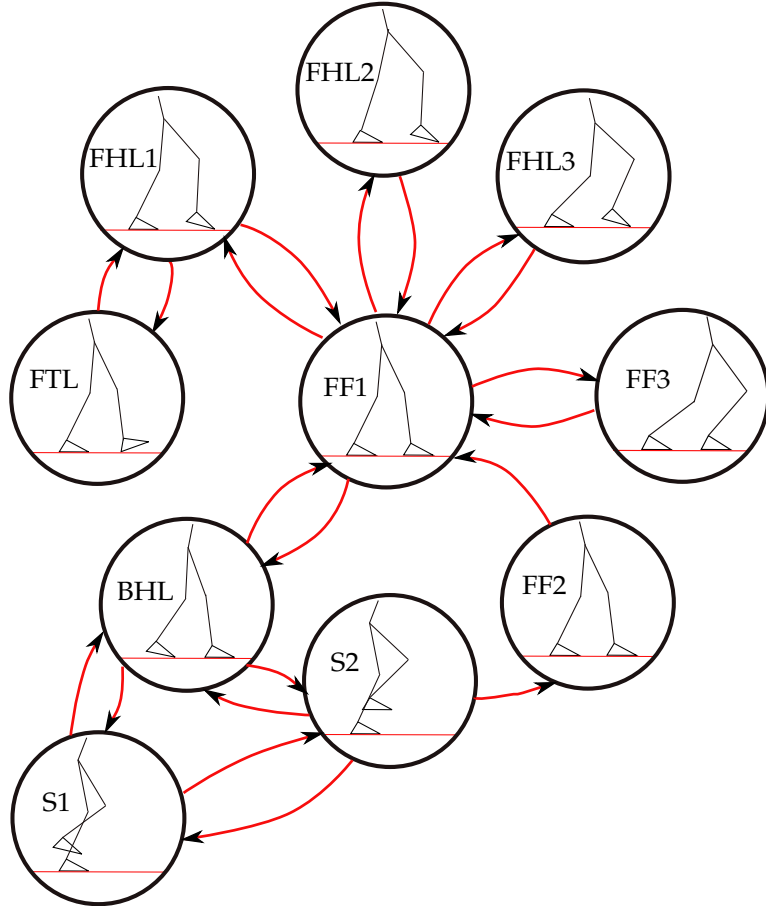


Figure 10.1: Representation of a meta-dynamical system for bipedal robotic dancing. Each vertex represents the pose, and the edges represent the transitions from one pose to another. This is an example of a nonperiodic hybrid system.

Creating dynamic transitions. Suppose we want to construct a meta-dynamical system. Assume we are given a directed graph \mathcal{G} with the set of poses \mathcal{P} . Using the constructions given in 6.1.2, we can construct a set of dynamic transitions \mathcal{T} . Given that the desired outputs y^d are obtained through canonical walking functions as described in (6.23) and (6.25), we propose the following optimization problem for creating a dynamic transition

\mathcal{T}_e for a particular edge $e \in \mathcal{E}$:

$$(v_{\text{hip}}^*, \alpha^*) = \underset{(v_{\text{hip}}, \alpha) \in \mathbb{R}^d}{\operatorname{argmin}} \text{Cost}_D(v_{\text{hip}}, \alpha, v_{\text{hip}}^r, \alpha^r) \quad (10.2)$$

$$\text{s.t. } \begin{bmatrix} y_e^d(0, \alpha) \\ y_e^d(\tau_{\max}, \alpha) \end{bmatrix} = \begin{bmatrix} y^a(q_0) \\ y^a(q_f) \end{bmatrix}, \quad (\text{CZD})$$

where $v_{\text{hip}}^r, \alpha^r$ are the reference parameters, y_e^d denotes whether the desired trajectories designed for each edge, and τ_{\max} is the time at the end of the step that is computed in the following manner:

$$\tau_{\max} = (C_v q_f - C_v q_0) / v_{\text{hip}}, \quad (10.3)$$

with v_{hip} being the hip velocity, as introduced in (6.15). The cost of *dancing* (or objective function), Cost_D , is the least squares error relative to reference data:

$$\text{Cost}_D = \sum_i [y^d(t[i], \alpha) - y^d(t[i], \alpha^r)]^T [y^d(t[i], \alpha) - y^d(t[i], \alpha^r)], \quad (10.4)$$

where the reference used is either obtained from human data that have discrete heel toe behavior, or obtained from the formerly established walking gaits that were provably stable and experimentally realized on robots (see [79],[69]). Note that in some of the transitions for dancing where there were no reference trajectories, a zero cost will be used. The defining aspect of this paper is using the constraints (CZD), which realizes configuration zero dynamics, and is thus instrumental in being able to compose different motion primitives to form a meta-dynamical system. This follows from the fact that the end result of the optimization is a dynamic transition.

Example: Dynamic leg swing. To illustrate meta-dynamical systems, we will examine a simple example consisting of two poses: back heel lift (BHL) and swing (S) (see Fig. 10.2). In particular, we pick a specific example of transition from pose \mathcal{P}_{BHL} to \mathcal{P}_{S2} , i.e., from

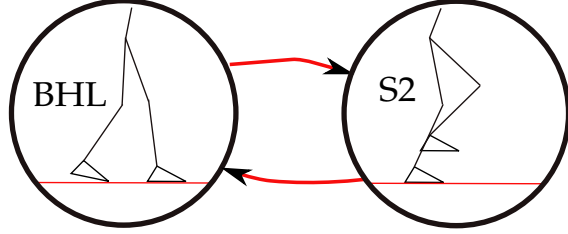


Figure 10.2: Figures showing the initial pose (left) and the final pose (right) for crouch respectively. The red arrows are the edges.

back heel lift to swing. The two poses with the transition is depicted separately in Fig. 10.2.

We can accordingly define the meta-dynamical system in the following manner:

Discrete structure and poses. The graph is given by:

$$\mathcal{G} = (\mathcal{V}, \mathcal{E}), \quad \mathcal{V} = \{S, BHL\}, \quad \mathcal{E} = \{S \rightarrow BHL, BHL \rightarrow S\}. \quad (10.5)$$

The set of poses is given by: $\mathcal{P} = \{\mathcal{P}_v : v \in \mathcal{V}\}$. The set of transitions is given by:

$\mathcal{T} = \{\mathcal{T}_e : e \in \mathcal{E}\}$. The edges are depicted by the arrows shown in Fig. 10.2. Note that the above example can have more than 2 edges depending on the how the transitions between poses are obtained. We will now introduce the optimization problem that realizes the dynamic transitions, \mathcal{T}_e , from one pose to the other.

Dynamic transitions.

The cost for the optimization was evaluated by obtaining the least squares fit with the multi-domain walking trajectory obtained on AMBER2 as found in [69]. The time parameter was picked such that only the swing portion of [69] was chosen for the cost. In other words, the value τ was constrained in the optimization to match the reference trajectories. Additional constraints, such as sufficient foot clearances on ground, were imposed throughout the step. The knee angle was also constrained to be within a certain limit to ensure low

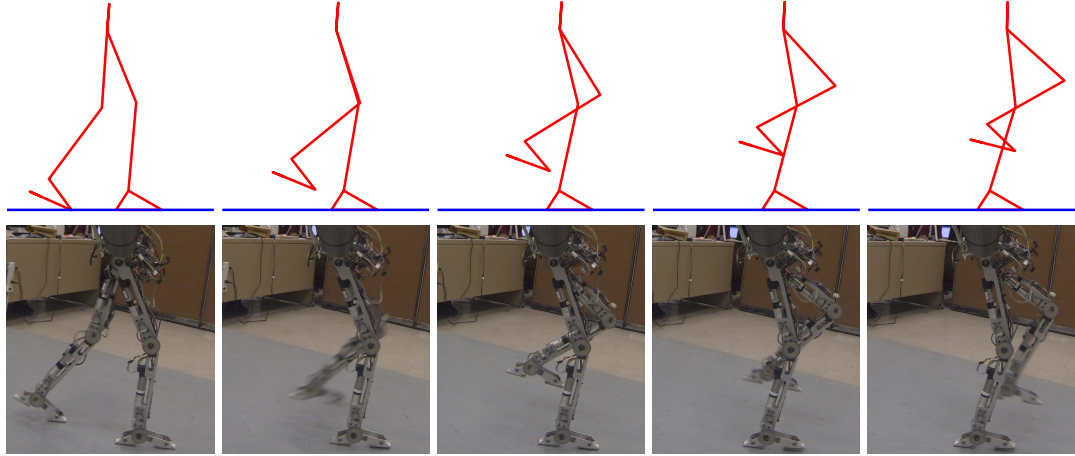


Figure 10.3: Tiles of a leg swing behavior consisting of a transition from back heel lift to swing pose. The top tiles illustrate the behavior of the robot achieved in simulation, and the bottom tiles show the same behavior realized experimentally on AMBER2.

torque is utilized. That is, the final optimization (with physical constraints) is given by:

$$(\nu_{\text{hip}}^*, \alpha^*) = \underset{(v_{\text{hip}}, \alpha) \in \mathbb{R}^{36}}{\operatorname{argmin}} \quad \text{Cost}_D(v_{\text{hip}}, \alpha, v_{\text{hip}}^r, \alpha^r) \quad (10.6)$$

s.t. (CZD)

$$\tau_{\max} < 0.4$$

$$\min(h_{\text{nst}}) > 0$$

$$\min(q_{\text{nsk}}) > 0,$$

where the resulting optimal solution yields the parameters for the desired trajectories represented through the outputs. When this is applied on the robot through trajectory reconstruction (10.12), the swing of the non-stance leg is observed. This was tested in AMBER2, both in simulation and experiment, with tiles of the resulting behavior shown in Fig. 10.3.

10.2 Single and Double Support Controllers

For reducing the number of controllers, there are two types of phases that will be analyzed in the paper, single support ss (when one foot is on ground) and double support ds (when

both the feet are always on ground). Therefore, the transitions from one pose to another are designed such that only type of controller is utilized. Based on Fig. 10.1, it can be observed that each edge (transition) is either a double support or a single support phase. This drastically reduces the number of controllers used, since, in this scenario, each transition occurs in only one domain. It can be represented mathematically as

$$\varphi_v(t; x_0) \in \mathbb{D}_v, \quad t \in [0, t_f], \quad v \in \mathbb{V}. \quad (10.7)$$

Note that the set of vertices \mathbb{V} for the hybrid system, \mathcal{HC} , is different from the set of vertices \mathcal{V} for the meta-dynamical system, MID . Other phases like underactuations where only the stance toe is on the ground are more complex to analyze and are therefore excluded from this study. Depending on the contact conditions being enforced, we get control systems associated with the single support and double support phases, denoted by (f_{ss}, g_{ss}) and (f_{ds}, g_{ds}) , respectively (see [69]).

Single Support. In the single support phase, the foot angle $\psi_0 = 0$, and the non-stance foot is always above ground. Picking only the base coordinates q_b , $k = 5$ desired outputs, $y_{ss}^d : \mathbb{R}^6 \rightarrow \mathbb{R}^5$, and also actual outputs, $y_{ss}^a : \mathbb{R}^6 \rightarrow \mathbb{R}^5$ are chosen (see (6.23)). The desired outputs, $y_{ss}^d : \mathbb{R}_{\geq 0} \times \mathbb{R}^6 \rightarrow \mathbb{R}^5$ are functions of q, τ and $\alpha_{ss} = [\alpha_{sk}, \alpha_{nsk}, \alpha_{hip}, \alpha_{tor}, \alpha_{nsf}]^T$. For the phase τ , instead of using (6.15), we use the time modulation

$$\tau(t, v_{\text{hip}}) = \alpha_{\text{scale}}(t - t_0)/v_{\text{hip}}, \quad (10.8)$$

t_0 is the time at the beginning of every transition. $\alpha_{\text{scale}} = 1$, but can be used to stretch the modulation during a dance sequence, i.e., to match with the beat. It was shown in Chapter 9 that time based modulation still guarantee stability properties for DURUS, DURUS2D (by virtue of ISS). Therefore, the desired trajectories are a function of $(v_{\text{hip}}, \alpha_{ss}) \in \mathbb{R}^{36}$. It is also important to note that the actual output vector y_{ss}^a is a linear function of the angles: $y_{ss}^a = H_{ss}q$, with $H_{ss} \in \mathbb{R}^{5 \times 6}$ being the transformation matrix. Since, $\psi_0 = 0$, $q = [0, q_b^T]^T$

for single support phase.

The objective of the controller is to drive the outputs $y_{ss} = y_{ss}^a - y_{ss}^d$ to zero, i.e., $y_{ss} \rightarrow 0$. This can be achieved by using a simple controller, e.g. PD controller, which does not guarantee convergence to zero, but will ensure convergence to an ultimate bound (as indicated by the ISS properties 7.1). Firstly, we study the hip position from (6.24) for the following¹

$$\delta p_{\text{hip}} = -(L_c + L_t)(q_{sa} + q_{sk}) - L_t q_{sk} = C_{ss} q_b, \quad \psi_0 = 0, \quad (10.9)$$

where $C_{ss} \in \mathbb{R}^{1 \times 6}$ is the row vector of constants. Note that δp_{hip} derived here is the same as (6.24) with ψ_0 omitted. If the controller used is expected to achieve zero tracking error, i.e., $y_{ss}^a - y_{ss}^d = 0$, then the desired joint angles $\dot{q}_{ss}^d \in \mathbb{R}^6$ and velocities $q_{ss}^d \in \mathbb{R}^6$ of the robot for the single support phase that realize this equality can be obtained as

$$y_{ss}^a = y_{ss}^d \implies \begin{bmatrix} C_{ss} \\ H_{ss} \end{bmatrix} q_{ss}^d = \begin{bmatrix} \delta p_{\text{hip}} \\ y_{ss}^d \end{bmatrix}. \quad (10.10)$$

Therefore, the desired angle configuration and the angular velocities are

$$q_{ss}^d = \begin{bmatrix} C_{ss} \\ H_{ss} \end{bmatrix}^{-1} \begin{bmatrix} \delta p_{\text{hip}} \\ y_{ss}^d \end{bmatrix}, \quad \dot{q}_{ss}^d = \begin{bmatrix} C_{ss} \\ H_{ss} \end{bmatrix}^{-1} \begin{bmatrix} 1 \\ \frac{\partial y_{ss}^d}{\partial \tau} \end{bmatrix} \frac{\alpha_{\text{scale}}}{v_{\text{hip}}}. \quad (10.11)$$

The PD controller can thus be defined as

$$u_{ss}^{pd} = -K_{ss}^p(q_b - q_{ss}^d) - K_{ss}^d(\dot{q}_b - \dot{q}_{ss}^d), \quad (10.12)$$

where K_{ss}^p, K_{ss}^d are the proportional and derivative gains respectively.

Double Support. The double support phase adds extra constraints to the robot such as

¹Note that the motivation for this coordinate is given by *partial zero dynamics* as studied in Chapter 5.

friction, pinning conditions (holonomic constraints [72]) and normal forces, which will constrain the dynamics of the robot. The actual and desired outputs for the robot are defined in (6.25). In the double support phase, the stance ankle angle q_{sa} is added in (6.25), where $y_{ds}^a : \mathbb{R}^7 \rightarrow \mathbb{R}^6$, $y_{ds}^d : \mathbb{R}^7 \rightarrow \mathbb{R}^6$, $\alpha_{ds} = [\alpha_{sa}, \alpha_{ss}^T]^T$, with $\alpha_{ds} \in \mathbb{R}^{43}$. The actual outputs can also be written as $y_{ds}^a = H_{ds}q$, with $H_{ds} \in \mathbb{R}^{6 \times 7}$. Since the objective of the controller during the double support phase is to achieve dynamic behaviors in the robot to realize a dancing sequence, the convergence of the outputs to zero is ignored. Similar to (10.9), the following coordinate is defined

$$\delta p_{\text{hip}} = -(L_c + L_t)(\psi_0 + q_{sk} + q_{sa}) - L_t q_{sk} = C_{ds}q, \quad (10.13)$$

where $C_{ds} \in \mathbb{R}^{1 \times 7}$ is the row vector of constant terms. Having obtained the expression for δp_{hip} , the desired joint angles and velocities can be defined as

$$q_{ds}^d = \begin{bmatrix} C_{ds} \\ H_{ds} \end{bmatrix}^{-1} \begin{bmatrix} \delta p_{\text{hip}} \\ y_{ds}^d \end{bmatrix}, \quad \dot{q}_{ss}^d = \begin{bmatrix} C_{ds} \\ H_{ds} \end{bmatrix}^{-1} \begin{bmatrix} 1 \\ \frac{\partial y_{ss}^d}{\partial \tau} \end{bmatrix} \frac{\alpha_{\text{scale}}}{v_{\text{hip}}}. \quad (10.14)$$

With K_{ds}^p , K_{ds}^d as the proportional and derivative matrices, the PD controller is

$$u_{ds}^{pd} = -K_{ds}^p(q - q_{ds}^d) - K_{ds}^d(\dot{q} - \dot{q}_{ds}^d). \quad (10.15)$$

Note that, both these matrices are not square since $u_{ds}^{pd} \in \mathbb{R}^6$. In fact, the first row and column of the gain matrices are zeros.

10.3 Configuration Zero Dynamics

For the single support phase, with the feedback linearizing controller (see [118]) being applied, the outputs y_{ss} are exponentially driven to zero. The closed loop system f_{cl} , after

substituting for u_{ss}^{pd} in (6.22), will exhibit zero dynamics.

$$\mathbb{Z}_{ss} = \{(q, q) : y_{ss}(q_b) = 0, L_f y_{ss}(q_b, \dot{q}_b) = 0, \psi_0 = 0, \dot{\psi}_0 = 0\}. \quad (10.16)$$

This restriction of the dynamics to a surface enables us to connect different motion primitives of the single support phase in such a way that the transition between domains occurs without change of y_{ss} ². In other words, the transition will be smooth. Motivated by the desire to relax the derivative condition in (10.16), we introduce the notion of **configuration zero dynamics** defined to be

$$\mathbb{C}\mathbb{Z}_{ss} = \{(q, \dot{q}) : y_{ss}(q_b) = 0, \psi_0 = 0\}. \quad (10.17)$$

For the double support phase, due to geometric constraints, it is not possible to realize zero dynamics. But, it is possible to connect a motion primitive with the single support phase due to the choice of controller. The concept of configuration zero dynamics plays an important role in the context of dancing, since when switching between a large collection of surfaces, if the configuration zero dynamics constraints are ensured, this allows for a transition without a sudden change in desired angles. Of course, if the zero dynamic constraints are ensured, then it allows for even smoother transitions (jerk free) from one desired trajectory to another. This will be utilized in the next section through the composition of configuration zero dynamic surfaces to allow for minimum jerk transitions between domains. In addition, this constraint will be independent of the speed, in which the transition is executed.

²Note: The construction of the PD controller defined in (10.9) through (10.12) is based on the notion that the desired angles and velocities: $(q_{ss}^d, \dot{q}_{ss}^d) \in \mathbb{Z}_{ss}$.

10.4 Dynamic Robotic Dancing on AMBER2

This section presents the process of realizing dynamic dancing in AMBER2 by using the methods introduced in this chapter. We will not include the domains such as UA, DHL, FTBH from Fig. 4.3 since they require higher torque and are relatively difficult to realize in the robot. Therefore, we will use the remaining five generic cases of the feet behavior for generating the pose. We will use three types of front heel lift: FHL1, FHL2, FHL3, one front toe lift: FTL, three types of flat-footed poses: FF1, FF2, FF3, two types of swing poses: S1, S2, and finally one back heel lift pose: BHL. All ten poses are shown in Fig. 10.1. The end result is an oriented graph $\mathcal{G} = (\mathcal{V}, \mathcal{E})$, where

$$\mathcal{V} = \{\text{FHL1, FHL2, FHL3, FTL, FF1, FF2, FF3, S1, S2, BHL}\}, \quad (10.18)$$

and \mathcal{E} is the set of red arrows in Fig. 10.1.

For generating the dynamic transition between poses, the optimization (10.2) was accordingly solved. Since it was not necessary to optimize trajectories to transition from every pose to every other pose, we used 20 edges (or optimized dynamic transitions) that satisfied **configuration zero dynamic** (CZD) constraints. Therefore, we use the set of edges as shown in Fig. 10.1, with the resulting dynamic transition $\mathcal{T} = \{\mathcal{T}_e : e \in \mathcal{E}\}$, obtained through the optimization in (10.2). Note, additional constraints were also implemented in the optimization to realize different behaviors varying from constraining the angles, to allowing sufficient foot clearance, to constraining the velocities, to constraining final parameterized time: τ_{max} .

Synchronizing with music. The particular method employed to synchronize the behaviors of the robot with the music is to utilize the parameterization of time (10.8). The scaling in τ via α_{scale} causes a corresponding change in desired trajectories of the robot (as represented by the outputs parameterized by τ) resulting in synchronization between the beats of the music and the dynamic transitions. Dynamic programming methods as described in [119]

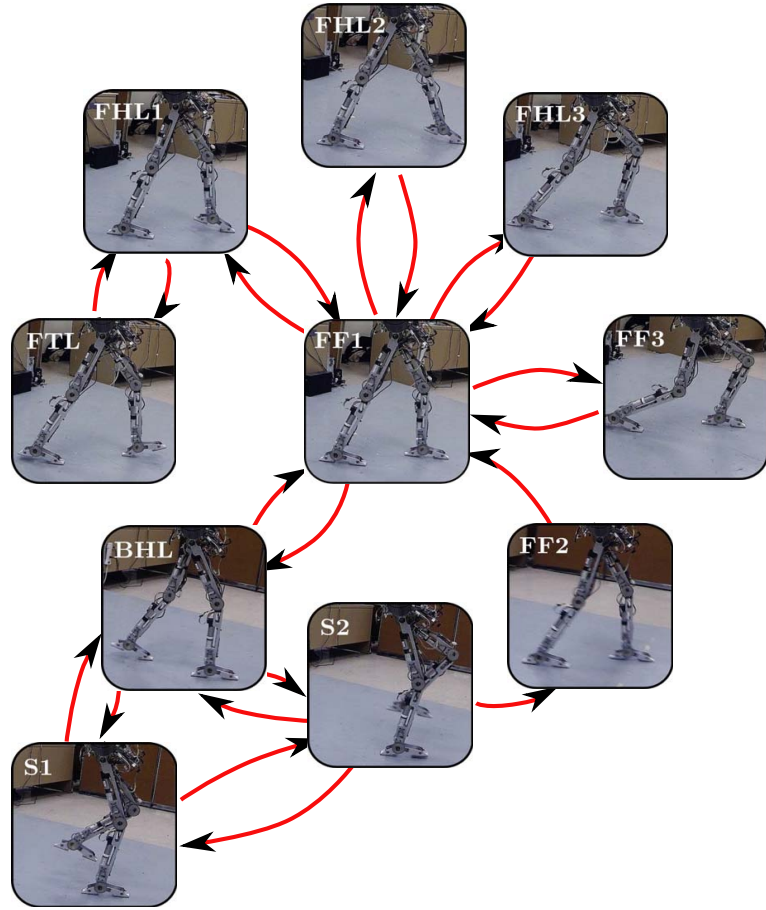


Figure 10.4: Pictorial representation of the results obtained after the implementation of transitions and music synchronization for AMBER2 dancing.

are used to generate music tempo speed for a given song.

10.5 Results

Implementing the transitions in the robot resulted in dynamically stable dancing accurately synchronized with the tempo of the music. Fig. 10.5 shows the comparison between desired and joint angle trajectories, Fig. 10.4 shows the configuration of the robot at different instances of time during the dance sequence. The video of AMBER2 dancing is shown in [7].

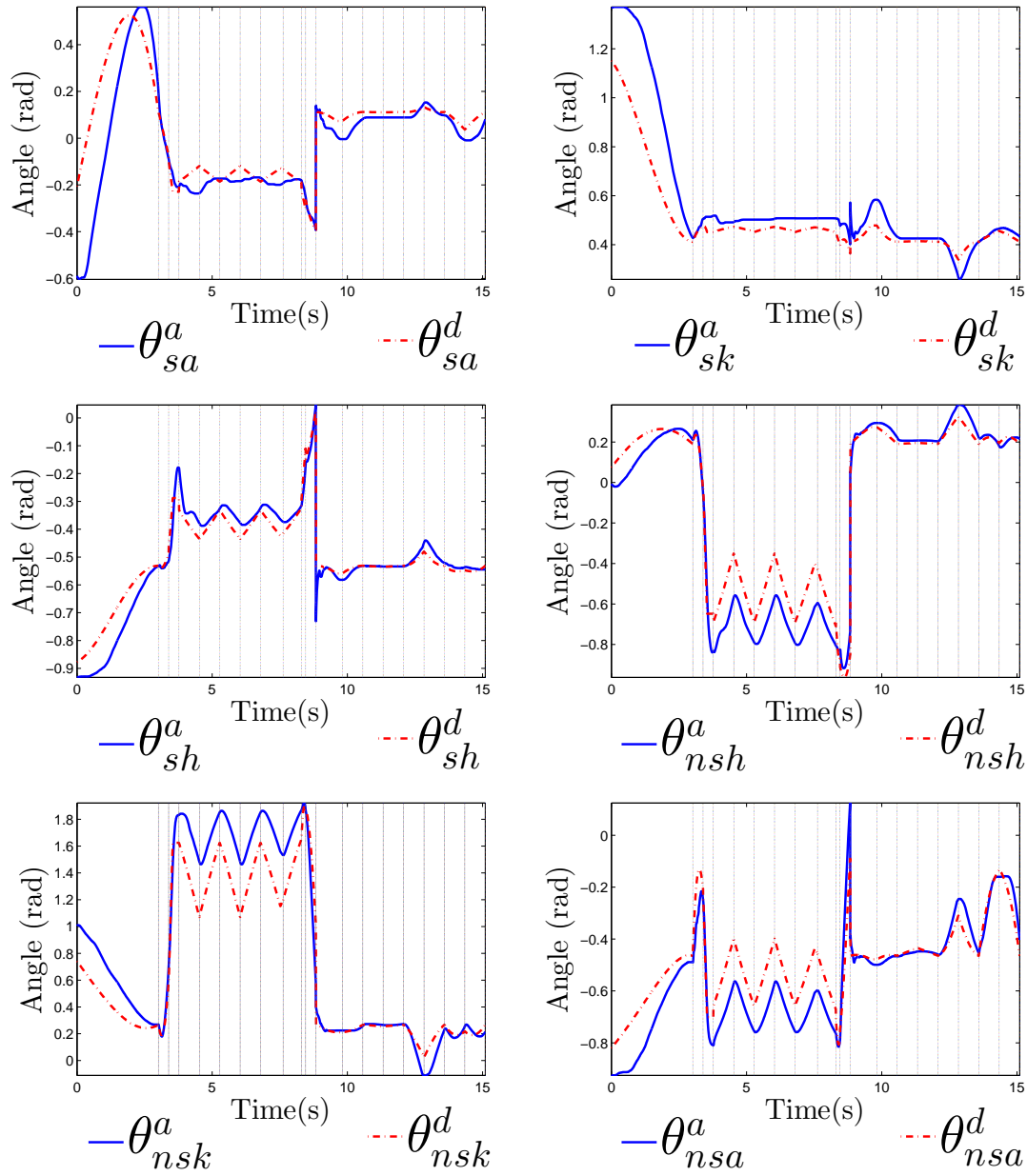


Figure 10.5: Experimental data comparing the actual and desired angles for a sequence of steps extracted from a part of the dance sequence as realized on AMBER2. The vertical dashed lines indicate end points of the transitions.

CONCLUSIONS AND FUTURE WORK

In this work, it was shown how to obtain a class of input to state stabilizing control Lyapunov functions for hybrid systems, given the set of control Lyapunov functions. It was shown in the specific case of the bipedal robots by picking a class of control Lyapunov functions, called the rapidly exponentially stabilizing control Lyapunov functions (RES-CLF). With this construction, we obtained the class of input to state stabilizing controllers that adds robustness to a wide variety of uncertainties. Stabilizing controllers do not always promise stability under uncertainties. The methodology shown in this thesis can be used to realize input to state stabilizing control Lyapunov functions on the fly without any extra analytical effort. Specifically, this was demonstrated for a special class of hybrid systems: systems with impulses. Two kinds of uncertainties were studied in detail: parameter uncertainty and phase based uncertainty, which typically affect bipedal robots.

For parameter uncertainty, the concept of a path dependent measure for evaluating the parameter uncertainty of hybrid systems models of robots was introduced. The main formulation of the proposed work was parameter to state stability that quantifies the effect of parameter uncertainty on the performance of the system. Utilizing this notion, coupled with RES-CLFs, we are able to establish the main results: conditions on parameter to state stability of both continuous and discrete events. Concretely, these results were applied to the case when there is a stable periodic orbit in the zero dynamics, therein implying a stable periodic orbit in the full order dynamics even in the case of parameter uncertainty. This was then verified by realizing a stable walking gait on AMBER having a parameter error of 30%. It is important to observe that while the parameter uncertainty measure yields the difference between the actual and the predicted torque applied on the robot, the impact measure yields the impulsive ground reaction forces acting upon the robot during an impact. Therefore, this can be used as an effective tool to not only design the robot model

more effectively, but also to design the nominal trajectories for the robots that takes the least path of the measure.

For phase based uncertainty, we studied the problem of time dependent CLFs, specifically, those functions that focus on tracking a set of time dependent periodic trajectories. The desired trajectories, typically rendered functions of a phase variable τ , are modulated by variation of time from 0 to the time period T . One of the applications of these trajectories is in generating periodic orbits in hybrid systems, especially in the context of bipedal walking. A comparison was made between the time based and state based control laws and it was formally shown that time dependent CLFs can realize state based tracking with acceptable errors as long as the parameterized time closely matches with the state based phase variable. This was then successfully shown experimentally in two robots DURUS humanoid and DURUS-2D.

Other forms of uncertainties were also studied like unmodeled dynamics, Coriolis and centrifugal effects, gravity effects and also friction based effects. The treatment was not in-depth, but are a natural extension of parameter/phase based uncertainties studied in Chapters 8, 9. It is important to note that the methods developed are applicable to even aperiodic systems; realization of dynamically stable dancing was described in Chapter 10.

Future Work. The merger of control Lyapunov functions and the criterion of input to state stability is just the beginning, and the future work can take numerous directions. The first direction being especially in the area of systems that are not necessarily affine. Several practical systems are non-affine in nature and require an in-depth study. Second direction is in the study of variants of input to state stability such as integral input to state stability, input/output to state stability. The dual of ISS, called the output to state detectability/stability can be widely used for the purposes of optimal state estimation. In other words, we can use these methods to develop dynamic programming approaches to realize optimal estimators that are output to state detectable. Another possible direction is in the construction of ISS versions for robustly stabilizing controllers. For example, adaptive control techniques

can be used in robotic systems to overcome parameter uncertainty. With this stabilizing controller, we can now construct ISS variants that handle other forms of uncertainty.

Given the practical limitations, the goal is to always think of ways to modify a controller such that the resulting closed loop system achieves the desired objective. We could design specifications that yield better performances, we could get a better estimate of the model and the states, or, we could design controllers that are robust to larger disturbances. The theory of input to state stability definitely has its strengths and its weaknesses, and we should find ways to get the best of out the available resources.

REFERENCES

- [8] R. Kline, “Harold black and the negative-feedback amplifier,” *IEEE Control Systems*, vol. 13, no. 4, pp. 82–85, 1993
- [9] G. Zames, “The legacy of george zames,” *IEEE Transactions on Automatic Control*, vol. 43, no. 5, p. 591, 1998
- [10] E. D. Sontag, “Input to state stability: basic concepts and results,” in *Nonlinear and Optimal Control Theory: Lectures given at the C.I.M.E. Summer School held in Cetraro, Italy June 19–29, 2004*, P. Nistri and G. Stefani, Eds. Berlin, Heidelberg: Springer Berlin Heidelberg, 2008, pp. 163–220, ISBN: 978-3-540-77653-6
- [11] E. D. Sontag, “Smooth stabilization implies coprime factorization,” *IEEE Transactions on Automatic Control*, vol. 34, no. 4, pp. 435–443, Apr. 1989
- [12] A. D. Ames, “A categorical theory of hybrid systems,” PhD thesis, Citeseer, 2006
- [13] A. N. Michel and B. Hu, “Towards a stability theory of general hybrid dynamical systems,” *Automatica*, vol. 35, no. 3, pp. 371–384, 1999
- [14] E De Santis, M. Di Benedetto, and G Pola, “Stabilizability of linear switching systems,” *Nonlinear Analysis: Hybrid Systems*, vol. 2, no. 3, pp. 750–764, 2008
- [15] C. Cai and A. R. Teel, “Results on input-to-state stability for hybrid systems,” in *Proceedings of the 44th IEEE Conference on Decision and Control*, Dec. 2005, pp. 5403–5408
- [16] R. Shorten, F. Wirth, O. Mason, K. Wulff, and C. King, “Stability criteria for switched and hybrid systems,” *SIAM review*, vol. 49, no. 4, pp. 545–592, 2007
- [17] M. A. Wicks, P. Peleties, and R. A. DeCarlo, “Construction of piecewise lyapunov functions for stabilizing switched systems,” in *Decision and Control, 1994., Proceedings of the 33rd IEEE Conference on*, vol. 4, Dec. 1994, 3492–3497 vol.4
- [18] R. A. DeCarlo, M. S. Branicky, S. Pettersson, and B. Lennartson, “Perspectives and results on the stability and stabilizability of hybrid systems,” *Proceedings of the IEEE*, vol. 88, no. 7, pp. 1069–1082, 2000
- [19] A. S. Morse, “Supervisory control of families of linear set-point controllers part i. exact matching,” *IEEE Transactions on Automatic Control*, vol. 41, no. 10, pp. 1413–1431, Oct. 1996

- [20] D. Liberzon and A. S. Morse, “Basic problems in stability and design of switched systems,” *IEEE Control systems*, vol. 19, no. 5, pp. 59–70, 1999
- [21] Y. Wang and Z. Zuo, “On quadratic stabilizability of linear switched systems with polytopic uncertainties,” in *2005 IEEE International Conference on Systems, Man and Cybernetics*, vol. 2, Oct. 2005, 1640–1644 Vol. 2
- [22] G. Zhai, “Quadratic stabilizability of discrete-time switched systems via state and output feedback,” in *Decision and Control, 2001. Proceedings of the 40th IEEE Conference on*, vol. 3, 2001, 2165–2166 vol.3
- [23] Z. Artstein, “Stabilization with relaxed controls,” *Nonlinear Analysis: Theory, Methods & Applications*, vol. 7, no. 11, pp. 1163–1173, 1983
- [24] E. D. Sontag, “A ‘universal’ construction of artstein’s theorem on nonlinear stabilization,” *Systems & control letters*, vol. 13, no. 2, pp. 117–123, 1989
- [25] R. G. Sanfelice, “On the existence of control lyapunov functions and state-feedback laws for hybrid systems,” *IEEE Transactions on Automatic Control*, vol. 58, no. 12, pp. 3242–3248, Dec. 2013
- [26] R. Bellman, “On the theory of dynamic programming,” *Proceedings of the National Academy of Sciences*, vol. 38, no. 8, pp. 716–719, 1952
- [27] J. A. Primbs, V. Nevistić, and J. C. Doyle, “Nonlinear optimal control: a control lyapunov function and receding horizon perspective,” *Asian Journal of Control*, vol. 1, no. 1, pp. 14–24, 1999
- [28] A. Ames, K. Galloway, K. Sreenath, and J. Grizzle, “Rapidly exponentially stabilizing control lyapunov functions and hybrid zero dynamics,” *Automatic Control, IEEE Transactions on*, vol. 59, no. 4, pp. 876–891, Apr. 2014
- [29] K. Galloway, K. Sreenath, A. D. Ames, and J. W. Grizzle, “Torque saturation in bipedal robotic walking through control lyapunov function based quadratic programs,” *IEEE Access*, vol. 3, pp. 323–332, 2015
- [30] U. Borrmann, L. Wang, A. D. Ames, and M. Egerstedt, “Control barrier certificates for safe swarm behavior,” *IFAC-PapersOnLine*, vol. 48, no. 27, pp. 68–73, 2015
- [31] Q. Nguyen and K. Sreenath, “Optimal robust control for bipedal robots through control lyapunov function based quadratic programs,” in *Robotics: Science and Systems (RSS)*, Rome, Italy, Jul. 2015
- [32] E. D. Sontag, “Input/output and state-space stability,” in *New Trends in Systems Theory*, Springer, 1991, pp. 684–691

- [33] E. D. Sontag, “Further facts about input to state stabilization,” *IEEE Trans. Automat. Control*, vol. 35, pp. 473–476, 1989
- [34] E. D. Sontag, Y. Wang, *et al.*, “New characterizations of input-to-state stability,” *IEEE Transactions on Automatic Control*, vol. 41, no. 9, pp. 1283–1294, 1996
- [35] E. D. Sontag and Y. Wang, “On characterizations of the input-to-state stability property,” *Systems & Control Letters*, vol. 24, no. 5, pp. 351–359, 1995
- [36] D. Angeli, E. D. Sontag, and Y. Wang, “A characterization of integral input-to-state stability,” *IEEE Transactions on Automatic Control*, vol. 45, no. 6, pp. 1082–1097, 2000
- [37] Z.-P. Jiang and Y. Wang, “Input-to-state stability for discrete-time nonlinear systems,” *Automatica*, vol. 37, no. 6, pp. 857–869, 2001
- [38] D. Liberzon, “Iss and integral-iss disturbance attenuation with bounded controls,” in *Decision and Control, 1999. Proceedings of the 38th IEEE Conference on*, vol. 3, 1999, 2501–2506 vol.3
- [39] D. Liberzon, E. D. Sontag, and Y. Wang, “Universal construction of feedback laws achieving iss and integral-iss disturbance attenuation,” *Systems & Control Letters*, vol. 46, no. 2, pp. 111–127, 2002
- [40] K. Okano, K. Hagino, and H. Oya, “Transformation of clf to iss-clf for nonlinear systems with disturbance and construction of nonlinear robust controller with l2 gain performance,” *J. Control Sci. Eng.*, vol. 2014, 28:28–28:28, Jan. 2014
- [41] A. D. Ames and S. Sastry, “A homology theory for hybrid systems: hybrid homology,” in *Hybrid Systems: Computation and Control: 8th International Workshop, HSCC 2005, Zurich, Switzerland, March 9-11, 2005. Proceedings*, M. Morari and L. Thiele, Eds. Berlin, Heidelberg: Springer Berlin Heidelberg, 2005, pp. 86–102, ISBN: 978-3-540-31954-2
- [42] Y. Or and A. D. Ames, “Formal and practical completion of lagrangian hybrid systems,” in *2009 American Control Conference*, Jun. 2009, pp. 3624–3631
- [43] R. Goebel, J. Hespanha, A. R. Teel, C. Cai, and R. Sanfelice, “Hybrid systems: generalized solutions and robust stability,” in *Proc. 6th IFAC symposium in nonlinear control systems*, 2004, pp. 1–12
- [44] R. Goebel, R. G. Sanfelice, and A. R. Teel, *Hybrid Dynamical Systems: modeling, stability, and robustness*. Princeton University Press, 2012

- [45] K. H. Johansson, J. Lygeros, S. Sastry, and M. Egerstedt, “Simulation of zeno hybrid automata,” in *The 38th IEEE Conference on Decision and Control*, Phoenix, AZ, IEEE, 1999, pp. 3538–3543
- [46] A. D. Ames, “Characterizing knee-bounce in bipedal robotic walking: a zeno behavior approach,” in *Proceedings of the 14th International Conference on Hybrid Systems: Computation and Control*, ser. HSCC ’11, New York, NY, USA: ACM, 2011, pp. 163–172, ISBN: 978-1-4503-0629-4
- [47] A. Lamperski and A. D. Ames, “Lyapunov-like conditions for the existence of zeno behavior in hybrid and lagrangian hybrid systems,” in *Decision and Control, 2007 46th IEEE Conference on*, IEEE, 2007, pp. 115–120
- [48] R. G. Sanfelice, *Robust hybrid control systems*. ProQuest, 2007
- [49] C. Cai, A. R. Teel, and R. Goebel, “Smooth lyapunov functions for hybrid systems part ii: (pre)asymptotically stable compact sets,” *IEEE Transactions on Automatic Control*, vol. 53, no. 3, pp. 734–748, Apr. 2008
- [50] C. Cai, A. R. Teel, and R. Goebel, “Smooth lyapunov functions for hybrid systems — part i: existence is equivalent to robustness,” *IEEE Transactions on Automatic Control*, vol. 52, no. 7, pp. 1264–1277, Jul. 2007
- [51] C. Cai, A. R. Teel, and R. Goebel, “Converse lyapunov theorems and robust asymptotic stability for hybrid systems,” in *Proceedings of the 2005, American Control Conference, 2005.*, Jun. 2005, pp. 12–17
- [52] W. P. Dayawansa and C. F. Martin, “A converse lyapunov theorem for a class of dynamical systems which undergo switching,” *IEEE Transactions on Automatic Control*, vol. 44, no. 4, pp. 751–760, Apr. 1999
- [53] M. Malisoff and F. Mazenc, “On control-lyapunov functions for hybrid time-varying systems,” in *Proceedings of the 45th IEEE Conference on Decision and Control*, Dec. 2006, pp. 3265–3270
- [54] J. P. Hespanha, D. Liberzon, and A. R. Teel, “Lyapunov conditions for input-to-state stability of impulsive systems,” *Automatica*, vol. 44, no. 11, pp. 2735 –2744, 2008
- [55] J. P. Hespanha, D. Liberzon, and A. R. Teel, “On input-to-state stability of impulsive systems,” in *Proceedings of the 44th IEEE Conference on Decision and Control*, Dec. 2005, pp. 3992–3997
- [56] C. Cai and A. R. Teel, “Characterizations of input-to-state stability for hybrid systems,” *Systems & Control Letters*, vol. 58, no. 1, pp. 47 –53, 2009

- [57] H. L. Burmeister, “Bainov, d. d.; simeonov, p. s., systems with impulse effect. stability, theory and applications. chichester, ellis horwood limited/john wiley & sons 1989. 255 pp., 39.95. isbn 0-7458-0457-8/0-470-21437-6 (ellis horwood series in mathematics and its applications),” *ZAMM - Journal of Applied Mathematics and Mechanics / Zeitschrift fr Angewandte Mathematik und Mechanik*, vol. 71, no. 10, pp. 419–419, 1991
- [58] Z. Li, H. Xiao, and J. Song, “A converse lyapunov theorem for the discrete switched system,” in *2011 Chinese Control and Decision Conference (CCDC)*, May 2011, pp. 3947–3951
- [59] J. P. Hespanha, D. Liberzon, and A. R. Teel, “Lyapunov conditions for the input-to-state stability of impulsive systems,” University of California, Santa Barbara, Santa Barbara, Tech. Rep., Dec. 2007
- [60] S. Dashkovskiy and A. Mironchenko, “Input-to-state stability of nonlinear impulsive systems,” *SIAM Journal on Control and Optimization*, vol. 51, no. 3, pp. 1962–1987, 2013
- [61] J. P. Hespanha and A. S. Morse, “Stability of switched systems with average dwell-time,” in *Decision and Control, 1999. Proceedings of the 38th IEEE Conference on*, vol. 3, 1999, 2655–2660 vol.3
- [62] E. Westervelt, J. Grizzle, C. Chevallereau, J. Choi, and B. Morris, *Feedback Control of Dynamic Bipedal Robot Locomotion*, ser. Automation and Control Engineering. CRC Press, 2007, ISBN: 9781420053739
- [63] D. J. Villarreal and R. D. Gregg, “A survey of phase variable candidates of human locomotion,” in *Engineering in Medicine and Biology Society (EMBC), 2014 36th Annual International Conference of the IEEE*, IEEE, 2014, pp. 4017–4021
- [64] A. Hereid, E. A. Cousineau, C. M. Hubicki, and A. D. Ames, “3d dynamic walking with underactuated humanoid robots: a direct collocation framework for optimizing hybrid zero dynamics,” in *2016 IEEE International Conference on Robotics and Automation (ICRA)*, May 2016, pp. 1447–1454
- [65] R. A. Freeman and P. V. Kokotovic, *Robust nonlinear control design: state-space and Lyapunov techniques*. Springer, 2008
- [66] A. D. Ames, K. Galloway, and J. W. Grizzle, “Control lyapunov functions and hybrid zero dynamics,” in *2012 IEEE 51st IEEE Conference on Decision and Control (CDC)*, Dec. 2012, pp. 6837–6842
- [67] A. D. Ames, “Human-inspired control of bipedal walking robots,” *Automatic Control, IEEE Transactions on*, vol. 59, no. 5, pp. 1115–1130, 2014

- [68] C. M. Hubicki, A. Hereid, M. X. Grey, A. L. Thomaz, and A. D. Ames, “Work those arms: toward dynamic and stable humanoid walking that optimizes full-body motion,” in *2016 IEEE International Conference on Robotics and Automation (ICRA)*, May 2016, pp. 1552–1559
- [69] H. Zhao, A. Hereid, W. loong Ma, and A. D. Ames, “Multi-contact bipedal robotic locomotion,” *Robotica*, pp. 1–35, Dec. 2015
- [70] A. D. Ames, “First steps toward automatically generating bipedal robotic walking from human data,” in *Robot Motion and Control 2011*, K. Kozłowski, Ed. London: Springer London, 2012, pp. 89–116, ISBN: 978-1-4471-2343-9
- [71] A. D. Ames, “First steps toward underactuated human-inspired bipedal robotic walking,” in *2012 IEEE Conference on Robotics and Automation*, St. Paul, Minnesota, 2012
- [72] R. M. Murray, Z. Li, and S. S. Sastry, *A Mathematical Introduction to Robotic Manipulation*. Boca Raton: CRC Press, 1994
- [73] J. Grizzle, C. Chevallereau, A. D. Ames, and R. W. Sinnet, “3d bipedal robotic walking: models, feedback control, and open problems,” *IFAC Proceedings Volumes*, vol. 43, no. 14, pp. 505 –532, 2010
- [74] A. D. Ames, E. A. Cousineau, and M. J. Powell, “Dynamically stable bipedal robotic walking with nao via human-inspired hybrid zero dynamics,” in *Proceedings of the 15th ACM International Conference on Hybrid Systems: Computation and Control*, ser. HSCC ’12, Beijing, China: ACM, 2012, pp. 135–144, ISBN: 978-1-4503-1220-2
- [75] S. Kolathaya, W.-L. Ma, and A. D. Ames, “Composing dynamical systems to realize dynamic robotic dancing,” in *Algorithmic Foundations of Robotics XI*, Springer, 2015, pp. 425–442
- [76] E. Cousineau and A. D. Ames, “Realizing underactuated bipedal walking with torque controllers via the ideal model resolved motion method,” in *2015 IEEE International Conference on Robotics and Automation (ICRA)*, May 2015, pp. 5747–5753
- [77] R. Ortega and M. W. Spong, “Adaptive motion control of rigid robots: a tutorial,” *Automatica*, vol. 25, no. 6, pp. 877 –888, 1989
- [78] D. Angeli, “Input-to-state stability of pd-controlled robotic systems,” *Automatica*, vol. 35, no. 7, pp. 1285 –1290, 1999

- [79] S. N. Yadukumar, M. Pasupuleti, and A. D. Ames, “From formal methods to algorithmic implementation of human inspired control on bipedal robots,” in *Algorithmic Foundations of Robotics X: Proceedings of the Tenth Workshop on the Algorithmic Foundations of Robotics*, E. Frazzoli, T. Lozano-Perez, N. Roy, and D. Rus, Eds. Berlin, Heidelberg: Springer Berlin Heidelberg, 2013, pp. 511–526, ISBN: 978-3-642-36279-8
- [80] B. Griffin and J. Grizzle, “Nonholonomic virtual constraints for dynamic walking,” in *2015 54th IEEE Conference on Decision and Control (CDC)*, IEEE, 2015, pp. 4053–4060
- [81] M. Vukobratović, B. Borovac, D. Surla, and D. Stokic, *Biped Locomotion*. Berlin: Springer-Verlag, Mar. 1990
- [82] M. Hirose and K. Ogawa, “Honda humanoid robots development,” *Philosophical Transactions of the Royal Society of London A: Mathematical, Physical and Engineering Sciences*, vol. 365, no. 1850, pp. 11–19, 2007
- [83] J. Pratt, P. Dilworth, and G. Pratt, “Virtual model control of a bipedal walking robot,” in *IEEE Conf. on Robotics and Automation*, Albuquerque, 1997, pp. 193–198
- [84] M. W. Spong and F. Bullo, “Controlled symmetries and passive walking,” *IEEE TAC*, vol. 50, no. 7, pp. 1025–1031, 2005
- [85] H. Geyer, B. Reinhard, and S. Andre, “Natural dynamics of spring-like running: emergence of selfstability,” Suffolk, England: Professional Engineering Publishing Ltd, 2002
- [86] C. Hubicki, J. Grimes, M. Jones, D. Renjewski, A. Spröwitz, A. Abate, and J. Hurst, “Atrias: design and validation of a tether-free 3D-capable spring-mass bipedal robot,” *The International Journal of Robotics Research*, p. 0 278 364 916 648 388, 2016
- [87] M. Mistry and L. Righetti, “Operational space control of constrained and underactuated systems,” in *Proceedings of Robotics: Science and Systems*, Los Angeles, CA, USA, Jun. 2011
- [88] P. K. Khosla, “Categorization of parameters in the dynamic robot model,” *IEEE Transactions on Robotics and Automation*, vol. 5, no. 3, pp. 261–268, Jun. 1989
- [89] A. Goswami, A. Quaid, and M. Peshkin, “Complete parameter identification of a robot from partial pose information,” in *Robotics and Automation, 1993. Proceedings., 1993 IEEE International Conference on*, May 1993, 168–173 vol.1

- [90] H. Park, K. Sreenath, J. Hurst, and J. W. Grizzle, “Identification of a bipedal robot with a compliant drivetrain: parameter estimation for control design,” *IEEE Control Systems Magazine*, vol. 31, no. 2, pp. 63–88, 2011
- [91] S. Gutman and G. Leitmann, “Stabilizing control for linear systems with bounded parameter and input uncertainty,” in *Optimization Techniques Modeling and Optimization in the Service of Man Part 2: Proceedings, 7th IFIP Conference Nice, September 8–12, 1975*, J. Cea, Ed. Berlin, Heidelberg: Springer Berlin Heidelberg, 1976, pp. 729–755, ISBN: 978-3-540-38150-1
- [92] D. M. Dawson and Z. Qu, “On the global uniform ultimate boundedness of a dcsl-like robot controller,” *IEEE Transactions on Robotics and Automation*, vol. 8, no. 3, pp. 409–413, Jun. 1992
- [93] H. Berghuis and H. Nijmeijer, “Robust control of robots via linear estimated state feedback,” *Automatic Control, IEEE Transactions on*, vol. 39, no. 10, pp. 2159–2162, Oct. 1994
- [94] Z. Qu and J. Dorsey, “Robust tracking control of robots by a linear feedback law,” *Automatic Control, IEEE Transactions on*, vol. 36, no. 9, pp. 1081–1084, Sep. 1991
- [95] J.-J. E. Slotine and W. Li, “On the adaptive control of robot manipulators,” *Int. J. Rob. Res.*, vol. 6, no. 3, pp. 49–59, Sep. 1987
- [96] M. Takegaki and S. Arimoto, “A New Feedback Method for Dynamic Control of Manipulators,” *Journal of Dynamic Systems Measurement and Control-transactions of The Asme*, vol. 103, 2 1981
- [97] S. Arimoto, “Stability and robustness of pid feedback control for robot manipulators of sensory capability,” *International Journal of Robotics Research*, pp. 783–799, 1984
- [98] P. Tomei, “Adaptive pd controller for robot manipulators,” *Robotics and Automation, IEEE Transactions on*, vol. 7, no. 4, pp. 565–570, Aug. 1991
- [99] R. Ortega, A. Loria, and R. Kelly, “A semiglobally stable output feedback pi2d regulator for robot manipulators,” *Automatic Control, IEEE Transactions on*, vol. 40, no. 8, pp. 1432–1436, Aug. 1995
- [100] R. Kelly, “Global positioning of robot manipulators via pd control plus a class of nonlinear integral actions,” *Automatic Control, IEEE Transactions on*, vol. 43, no. 7, pp. 934–938, Jul. 1998

- [101] Y. Choi, W. K. Chung, and I. H. Suh, “Performance and h infin; optimality of pid trajectory tracking controller for lagrangian systems,” *Robotics and Automation, IEEE Transactions on*, vol. 17, no. 6, pp. 857–869, Dec. 2001
- [102] R Beerens, H Nijmeijer, and P. van Zutven, “Adaptive control on bipedal humanoid robots,” 2014
- [103] Z. Li and S. S. Ge, “Adaptive robust controls of biped robots,” *IET Control Theory Applications*, vol. 7, no. 2, pp. 161–175, Jan. 2013
- [104] Q. Nguyen and K. Sreenath, “L1 adaptive control for bipedal robots with control lyapunov function based quadratic programs,” in *2015 American Control Conference (ACC)*, Jul. 2015, pp. 862–867
- [105] C. Cao and N. Hovakimyan, “L1 adaptive controller for a class of systems with unknown nonlinearities: part i,” in *2008 American Control Conference*, Jun. 2008, pp. 4093–4098
- [106] S. Kolathaya and A. D. Ames, “Parameter sensitivity and boundedness of robotic hybrid periodic orbits.,” *IFAC-PapersOnLine*, vol. 48, no. 27, pp. 377 –382, 2015
- [107] S. Kolathaya and A. D. Ames, “Exponential convergence of a unified clf controller for robotic systems under parameter uncertainty,” in *2014 American Control Conference*, Jun. 2014, pp. 3710–3715
- [108] M. W. Spong, S. Hutchinson, and M. Vidyasagar, *Robot modeling and control*. John Wiley & Sons Hoboken NJ, 2006
- [109] D. G. Cacuci, M. Ionescu-Bujor, and I. M. Navon, *Sensitivity and uncertainty analysis, volume II: applications to large-scale systems*. CRC press, 2005, vol. 2
- [110] J. Mulero-Martinez, “Uniform bounds of the Coriolis/centripetal matrix of serial robot manipulators,” *Robotics, IEEE Transactions on*, vol. 23, no. 5, pp. 1083–1089, Oct. 2007
- [111] P. J. From, I. Schjlberg, J. T. Gravdahl, K. Y. Pettersen, and T. I. Fossen, “On the boundedness and skew-symmetric properties of the inertia and Coriolis matrices for vehicle-manipulator systems,” *IFAC Proceedings Volumes*, vol. 43, no. 16, pp. 193 –198, 2010
- [112] J. Hauser and C. C. Chung, “Converse lyapunov functions for exponentially stable periodic orbits,” *Systems & Control Letters*, vol. 23, no. 1, pp. 27 –34, 1994
- [113] G. Nelson, A. Saunders, N. Neville, B. Swilling, J. Bondaryk, D. Billings, C. Lee, R. Playter, and M. Raibert, “Petman: a humanoid robot for testing chemical protec-

tive clothing,” *Journal of the Robotics Society of Japan*, vol. 30, no. 4, pp. 372–377, 2012

- [114] J. W. Grizzle, J. Hurst, B. Morris, H. Park, and K. Sreenath, “MABEL, a new robotic bipedal walker and runner,” in *American Control Conference*, St. Louis, MO, USA, 2009, pp. 2030–2036
- [115] S. Kolathaya, A. Hereid, and A. D. Ames, “Time dependent control lyapunov functions and hybrid zero dynamics for stable robotic locomotion,” in *American Control Conference 2016*, 2016
- [116] L. Mazzi and V. Tabasso, “On stabilization of time-dependent affine control systems,” *RENDICONTI DEL SEMINARIO MATEMATICO*, vol. 54, pp. 53–66, 1996
- [117] Z. Jiang, Y. Lin, and Y. Wang, “Stabilization of nonlinear time-varying systems: a control lyapunov function approach,” *Journal of Systems Science and Complexity*, vol. 22, no. 4, pp. 683–696, 2009
- [118] S. Sastry, *Nonlinear systems: Analysis, Stability, and Control*. Springer Science & Business Media, 2013, vol. 10
- [119] D. P. Ellis, “Beat tracking by dynamic programming,” *Journal of New Music Research*, vol. 36, no. 1, pp. 51–60, 2007

VITA

Shishir N. Y. Kolathaya (also known as Shishir Kolathaya) was born in Puttur, a tiny south Indian town located in the state of Karnataka. He was highly inspired by his father, Dr. Yadukumar Nadubettu, who is himself a PhD in agronomy. Highly intrigued by science and engineering, Shishir pursued his undergraduate degree in Electrical Engineering in the National Institute of Technology Karnataka, Surathkal, India. As a part of senior design project, Shishir developed a terrain mapping robot based on SLAM (simultaneous localization and mapping), which was his first exposure to robotics. This inspired him to explore further in the area of robotics. Later, he developed a tiny two-legged robot that could dance to a song. Fascinated by bipedal robots, Shishir started working for Dr. Aaron Ames in robotic locomotion walking research in Texas A & M University. After submitting his M.S. thesis on *Bipedal Walking on AMBER on Rough Terrain*, he got involved more and more in the mathematics of nonlinear control which lead him to pursue his PhD on realizing robust controllers for hybrid systems in the Georgia Institute of Technology.